Title: In-plane Seismic Design of Concrete Masonry Structures
Authors: Voon, Kok Choon
Issue Date: 28-Jun-2007

In-plane Seismic Design of Concrete Masonry Structures

Kok Choon Voon

Supervised by

Assoc. Prof. Jason M. Ingham

Assoc. Prof. John W. Butterworth

Dr. Barry J. Davidson

A thesis submitted in partial fulfilment of the requirements for the degree of Doctor of Philosophy (PhD) in Civil and Environmental Engineering.

The University of Auckland, March 2007.

Abstract

The research presented in this thesis consists of two parts. The first part involved the investigation of concrete masonry shear strength and the second part reports an investigation of the lateral strength of partially grout-filled nominally reinforced perforated concrete masonry walls.

Valuable information about masonry shear strength is reported following the testing of ten full scale concrete masonry walls. It was verified that horizontal shear reinforcement and axial compression load provided additional shear resistance to masonry walls. Consequently, the nominal shear strength of reinforced masonry walls could be evaluated as a sum of contributions from masonry, shear reinforcement and applied axial load. It was also established that masonry shear strength decreases inversely in relation to an increase of the wall aspect ratio.

Criteria relating to codification of the in-plane shear strength of concrete masonry walls when subjected to seismic loading are presented. Particular emphasis is placed on a computational model that is capable of representing the interaction between flexural ductility and masonry shear strength to account for the reduction in shear strength as ductility level increases. The simple method proposed here allows the strength enhancement provided by axial compression load to be separated from the masonry component of shear strength and is considered to result from strut action. In addition, minor modifications are made to facilitate adoption of the method in the updated version of the New Zealand masonry design standard, NZS 4230:2004.

Prediction of shear strength from NZS 4230:2004 and using alternative methods are compared with results from a wide range of test of masonry walls failing in shear. It was established that the shear equation in the former version of the New Zealand masonry standard (NZS 4230:1990) was overly conservative in its prediction of masonry shear strength. The current NEHRP shear expression was found to be commendable, but it does not address masonry shear strength within plastic hinge regions, therefore limiting its use when designing masonry structures in seismic regions. Finally, the new shear equation adopted by NZS 4230:2004 was found to provide significantly improved shear strength prediction with respect to its predecessor, with accuracy close to that resulted from NEHRP.

Test results obtained in the second part of this research indicated that the size of openings and the length of trimming reinforcement significantly affected the lateral strength of perforated masonry walls. The observation of diagonal cracking patterns that aligned well with the load paths by which shear force was assumed to be transferred to the foundation in the strut mechanism supported the use of strut-and-tie analysis as a viable tool to evaluate the flexural strength of walls of this type. Strength prediction using the improved strut-and-tie method and the modified plastic collapse analysis were found to closely match the experimental results of the perforated walls tested in this study. Strength prediction by the simplified strut-and-tie method was found to closely match the test results of masonry walls with a single opening, but significant underestimation of strength by this method was found for walls with double openings. Full plastic collapse analysis was found to significantly over-predict the strength of all perforated walls included in this study.

Finally, the NZS 4229:1999 detail for shrinkage control joints was shown to result in adequate structural performance. In addition, shrinkage control joints constructed in accordance with the NZS 4229:1999 prescription resulted in masonry bracing capacity substantially in excess of the tabulated values in the standard, with gradual strength and stiffness degradation. This increase in strength is due to pier double bending that is not considered by the standard.

Disclaimer

The opinions and conclusions presented herein are those of the author, and do not necessarily reflect those of the University of Auckland or any of the sponsoring parties to this project.

Acknowledgements

The author greatly acknowledges the financial support provided by the Earthquake Commission Research Foundation (EQC). Thanks also go to Firth Industries Ltd., W. Stevenson and Sons Ltd., and Ready Mix Concrete Ltd. for donating the necessary masonry block units, grout and man power in the construction of masonry walls. Their contributions are gratefully appreciated. The author also wishes to thank the contribution by Pacific Steel in providing the necessary reinforcing steel for this project.

Thanks also go to Hank Mooy and Tony Daligan for providing assistance in setting up the test specimens. Thanks go to Professor Guido Magenes of the University of Pavia, and David Barnard and Mike Cathie for their assistance in developing the NZS 4230:2004 shear provisions. Finally, special thanks is given to those who found time to comment on this thesis, particularly my primary supervisor Associate Professor Jason Ingham.

Table of Contents

List of Figures

List of Tables

List of Symbols

A	=	depth of compression
A_h	=	area of single horizontal reinforcing steel
A_n	=	net cross-sectional area
A_r	=	wall aspect ratio
A_s	=	area of vertical reinforcing steel
b	=	width of compressive stress block
a	=	compression block depth
b_f	=	maximum width of ungrouted flue
b_w	=	effective wed width
C_m	=	compression force in masonry
C_1	=	shear strength coefficient in 4.3.1
C_2	=	shear strength coefficient in 4.3.1
C_3	=	shear strength coefficient in 4.3.3
C_d	=	nominal shear strength coefficient
D_{eff}	=	effective depth of section
c	=	neutral axis depth
d	=	distance from end of wall to the extreme wall vertical reinforcement
d'	=	distance between wall edge and outermost wall vertical reinforcing steel
F_{code}	=	code specified wall nominal strength
E	=	elastic modulus of reinforcement
$F_{code,amd}$	=	wall bracing capacity according to proposed amended procedure
$F_{code,no-op}$	=	code specified nominal strength for wall without opening
F_n	=	nominal flexural strength
F_{max}	=	maximum strength recorded during testing
$F_{n,fr1}$	=	nominal wall strength according to modified plastic hinge model
$F_{n,fr0}$	=	nominal wall strength according to full plastic hinge model
$F_{n,no-op}$	=	nominal strength of wall without opening
$F_{n,st1}$	=	nominal wall strength according to improved strut-and-tie model
$F_{n,st0}$	=	nominal wall strength according to simplified strut-and-tie model
F_v	=	shear force applied to masonry wall
f'_m	=	masonry compressive strength
f_v	=	masonry shear stress
f_{vr}	=	masonry shear stress

f_{yh} = yield strength of horizontal reinforcing steel

f_{yv} = yield strength of vertical reinforcing steel

h = wall height

h_e = effective height

h_e/L_w = shear span ratio

jd = lever arm

k = ductility reduction factor

k_p = coefficient of the effect of flexural reinforcement

k_u = reduction factor

L_w = length of masonry wall

M_{bc} = flexural strength for the coupling element section at compression pier end

M_{bt} = flexural strength for the coupling element section at tension pier end

M_c = flexural strength for the compression pier end sections

M_n = nominal bending moment

M_t = flexural strength for the tension pier end sections

N = axial compressive load

P_{ovt} = axial force due to overturning

p_w = $A_s/b_w d$

s_h = spacing of horizontal reinforcement

T = tension force in reinforcing steel

t = thickness of masonry wall

U_b = flexure displacement

U_r = rocking displacement

U_s = shear displacement

V_c = ultimate lateral load capacity of compression pier

V_m = shear strength provided by masonry

V_{max} = maximum lateral strength recorded during testing in positive direction

V_{min} = maximum lateral strength recorded during testing in negative direction

V_n = nominal shear strength

V_p = shear strength provided by axial compressive load

V_s = shear strength provided by shear reinforcement

V_t = ultimate lateral load capacity of tension pier

v_{bm} = basic type-dependent shear strength of masonry

v_m = maximum permitted type-dependent shear stress provided by masonry

v_n	=	total shear stress corresponding to V_n
W_t	=	wall self weight
x	=	depth of masonry block unit
y	=	width of masonry block unit
Δ_y	=	nominal yield displacement
α	=	parameter for compressive stress block
β	=	parameter for compressive stress block
δ	=	factor concerning loading method
ϵ_s	=	reinforcing steel strain
φ	=	wall section curvature
ϕ	=	strength reduction factor
μ	=	ductility level
μ_{av}	=	available ductility
μ_f	=	coefficient of internal friction
μ^*	=	reduced coefficient of friction
ρ_h	=	horizontal reinforcement ratio
ℓ_{dh}	=	development length of reinforcement
ρ_v	=	vertical reinforcement ratio
σ_n	=	axial compressive stress
τ_m	=	shear stress
τ_o	=	shear bond strength
τ_o^*	=	reduced cohesion
τ'_{tb}	=	masonry tensile strength
θ	=	wall section rotation

Chapter 1

GENERAL INTRODUCTION

1.1 MOTIVATION FOR CONCRETE MASONRY WALLS RESEARCH

The research presented in this thesis consists of two parts. The first part reports the investigation of concrete masonry shear strength and the second part reports the investigation of the flexural strength of perforated concrete masonry walls that were nominally reinforced and partially grout-filled. The following sections describe the motivations for each research.

1.1.1 Concrete Masonry Wall Shear Strength

There was general consensus within New Zealand that the former masonry design standard, NZS 4230:1990, was overly conservative in its treatment of masonry shear strength, restricting cost-effective masonry design. The commentary to the former New Zealand Standard for the Design of Masonry Structures (NZS 4230:Part2:1990) noted in clause C7.3.1.6 that "tests on masonry walls of both brick reinforced cavity masonry and concrete reinforced hollow unit masonry have indicated that properly designed and detailed masonry shear walls can sustain average shear stresses well in excess of 2.0 MPa, while exhibiting a ductile flexural failure mode. It is now considered that the limits placed on the total shear stress in NZS 4230P:1985 were unduly conservative". Similar comments regarding uncertainty of the shear strength provided by masonry due to the lack of data were made in clause C7.3.2.1 related to shear and axial compression, C7.3.2.2 related to shear and axial tension, C7.3.3 related to shear strength of prestressed masonry, and C7.5.2 related to masonry shear strength in potential plastic hinge zones. At the time NZS 4230:1990 was released, the scarcity of experimental data related to the shear strength of masonry walls when subjected to in-plane seismic forces prevented the preparation of more accurate criteria. The data sources used in the preparation of the standard were published in 1980 or earlier, such that no data obtained during the last two decades was used in the preparation of the standard.

The masonry design standard was recently revised to accommodate changes since made to the New Zealand Loadings Standard and the New Zealand Building Code. During this revision there was an opportunity to update masonry shear strength criteria based on experimental and

analytical research conducted over the last two decades. Also, there was an opportunity to conduct supplementary experimental testing at the University of Auckland to gain a greater insight into the behaviour of concrete masonry walls when subjected to shear failure under in-plane cyclic loading. In addition, the study reported here compares results derived when using different equations to predict the maximum shear strength of reinforced concrete masonry walls when subjected to different conditions.

1.1.2 Nominally Reinforced Concrete Masonry Walls with Openings

The recent promulgation of alternative construction forms has resulted in the perception within New Zealand that reinforced concrete masonry is an expensive form of construction when compared with competing products and systems. Consequently, a decision was made by the New Zealand concrete masonry industry to develop a non-specific design standard NZS 4229:1999 which, whilst retaining suitable conservatism, was more realistic in its treatment of measured experimental response. In particular, attention was given to permiting the use of partially grout-filled nominally reinforced concrete masonry in the most seismically active regions of New Zealand. Furthermore, efforts were made to simplify use of the standard so that the design of single and double storey masonry structures, not containing crowds and not dedicated to the preservation of human life (such as hospitals), could be effectively conducted by architects and architectural draftspersons with limited, if any, input from consulting structural engineers.

The in-plane lateral strength of a concrete masonry wall panel is specified in NZS 4229:1999 through determination of its “bracing capacity”, with the bracing capacity values being derived from wall tests conducted at the University of Auckland by Brammer (1995) and Davidson (1996), of which only two considered the performance of walls with openings. However, it was subsequently identified that an important trimming reinforcement detail adopted in testing of these two walls differed from that specified in NZS 4229:1999. Hence, a third wall, having an opening and with reinforcement detailing complying with NZS 4229:1999 was tested (Ingham et al., 2001). The experimental result indicated that this wall did not achieve the bracing capacity prescribed in NZS 4229:1999 and subsequent assessment showed that the existing design standard may be non-conservative in its treatment of walls with openings.

In seeking to understand why the third wall did not achieve its predicted strength, it was established that a strut-and-tie analysis of the structure demonstrated that the Standard incorrectly defined the geometry of “bracing panel”, whose geometry is used to establish

lateral wall strength. This analysis is shown diagrammatically in Figure 1.1. Figure 1.1a shows the reinforcement detailing for the test conducted by Davidson (1996). The resultant strut-and-tie analysis is shown in Figure 1.1b, with struts indicated by a broader element thickness. The resultant bracing panels based on the geometry of the diagonal struts of Figure 1.1b are shown in Figure 1.1c. As validated through the discussed analysis procedure, NZS 4229:1999 currently defines the geometry of bracing panels based upon the vertical dimensions of the smallest adjacent openings (see also Figure 6.6 for more details).

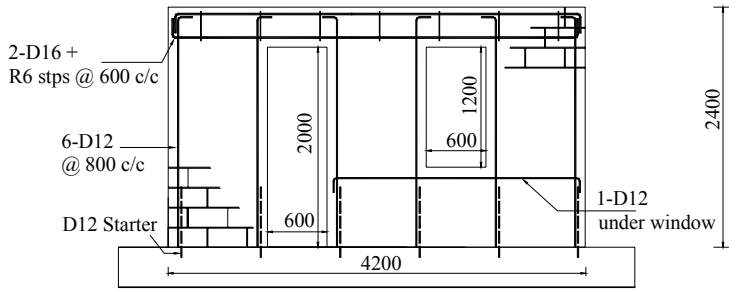

(a) Wall reinforcement detail

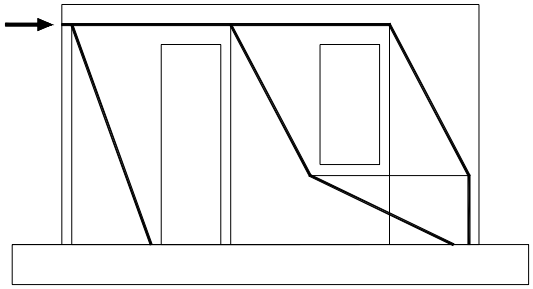

(b) Strut-and-tie model of wall with lintel reinforcement

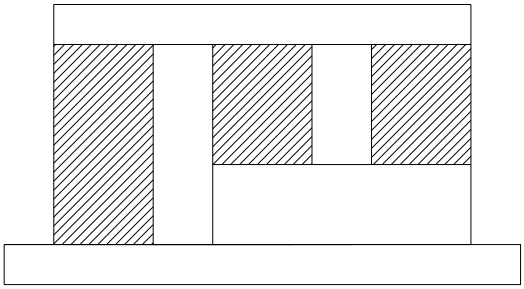

(c) Bracing panels of Figure (b)

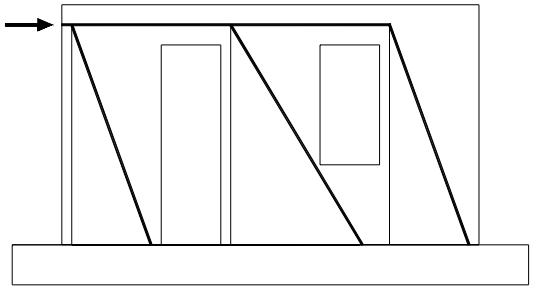

(d) Strut-and-tie model of wall **without** lintel reinforcement

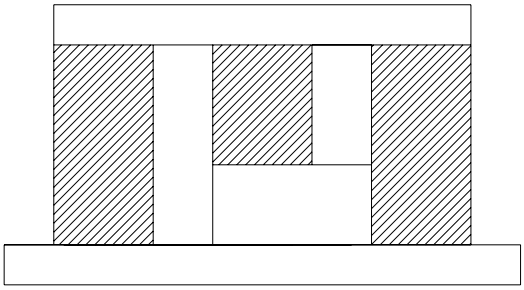

(e) Bracing panels of Figure (d)

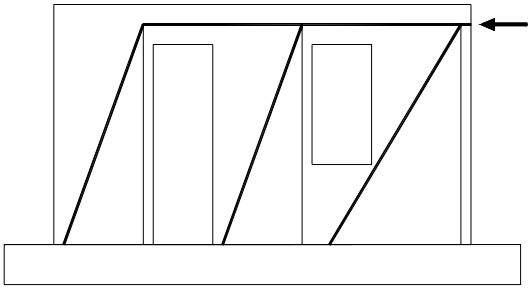

(f) **Reverse** strut-and-tie model of wall **without** lintel reinforcement

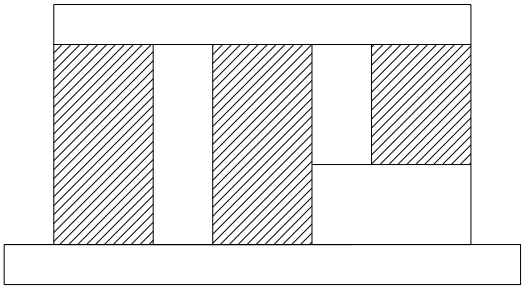

(g) Bracing panels of Figure (f)

Figure 1.1 Strut-and-tie modelling of nominally reinforced concrete masonry walls.

In Figure 1.1d it is shown that when the trimming reinforcement is shortened to comply with the current NZS 4229:1999 specifications, the geometry of the right-most diagonal strut is modified. The corresponding modification to the bracing panel is shown in Figure 1.1e. This effectively shows that the current Standard-defined bracing panel geometry is non-conservative as taller bracing panels have less capacity than shorter bracing panels of the same length. Furthermore, when the wall is instead loaded to the left (see Figure 1.1f), the geometry of the struts is further changed, and an alternative bracing panel distribution is developed as shown in Figure 1.1g.

Possible amendments to the process would be to either adopt bracing panel dimensions based upon the geometry of the largest adjacent wall opening, or to separately analyse the wall for the two direction of loading. Another solution would be to prescribe an extended trimming reinforcement detail as per Figure 1.1a. However, before such actions are taken it was deemed necessary to validate the strut-and-tie analysis through the testing of partially grouted concrete masonry walls with openings. These walls required variations in trimming reinforcement detailing, including that complying to NZS 4229:1999, and also required a range of opening geometries.

1.3 SCOPE AND ORGANISATION OF THESIS

Scope:

This thesis is divided into two parts. The first part presents an experimental study that investigated the in-plane shear strength of ten single storey-height concrete masonry wall panels. The main variables considered in this experimental programme included the amount and distribution of shear reinforcement, level of axial compression stress, type of grouting and wall aspect ratios. This experimental programme supplemented the experimental data already available by specifically investigating the shear strength of walls subjected to low axial compression stresses ($\sigma_n \leq 0.50$ MPa) and low shear reinforcement ratios ($\rho_h \leq 0.062\%$). Experimental studies conducted in both the U.S. and Japan involved masonry walls that were subjected to σ_n and ρ_h of up to 5.9 MPa and 0.67% respectively. Furthermore, this study compares results derived when using different equations to predict the ultimate shear strength of reinforced concrete masonry walls under different conditions, such as different shear reinforcement ratios, shear span ratios, axial compression stresses and masonry strengths. The objective of this study was to establish criteria most suitable for inclusion in the revised New Zealand masonry design standard.

The second part of this thesis describes the results from structural testing of eight single storey-height partially grout-filled concrete masonry walls. The primary objective of this study was to validate the adequacy of NZS 4229:1999 in addressing the bracing capacity of masonry walls containing openings. These eight partially grouted concrete masonry walls had variations in trimming reinforcement detailing, including those complying to NZS 4229:1999, and a range of penetration geometries. A parallel issue was to investigate the influence which shrinkage control joints have on the bracing capacity of partially grouted concrete masonry walls. NZS 4229:1999 prescribed a procedure to account for shrinkage control joints, but this detail had never been verified through structural testing. Consequently, experimental testing on two partially grout-filled concrete masonry walls was conducted to validate the structural adequacy of the shrinkage control joint detail published in NZS 4229:1999.

Organisation:

Chapter 2 of this thesis presents a literature review of currently available research and codification of masonry shear strength. In addition, a brief review of previous studies that attempted to establish the lateral strength of masonry walls containing openings is included in Chapter 2. Two series of structural testing were carried out and interpretation of test results are described in Chapters 3 and 6 respectively. Not only were relevant aspects of these two experimental investigations are reported in comprehensive form in this doctoral dissertation, but they have also been presented in more concise format in Voon and Ingham (2003 and 2006). The principal intent with the ten in-plane wall tests described in Chapter 3 was to investigate the shear strength of concrete masonry walls. Chapter 4 describes a newly proposed NZS 4230:2004 shear expression that is capable of representing the interaction between flexural ductility and masonry shear strength to account for the reduction in shear strength as ductility level increases. The adequacy of the NZS 4230:2004 shear expression and alternative methods in predicting masonry shear strength is described in Chapter 5.

Chapter 6 of this thesis describes the structural testing of ten partially grout-filled nominally reinforced concrete masonry walls. The adequacy of NZS 4229:1999 in addressing the lateral strength of masonry walls containing openings is described in section 6.7.4. This was achieved by comparing the results derived using the NZS 4229:1999 prescribed bracing capacities with those predicted using the modified plastic collapse analysis for perforated masonry walls. Finally, possible amendments to NZS 4229:1999 are presented in Chapter 7.

Chapter 2

LITERATURE REVIEW

2.1 INTRODUCTION

A structural wall carries in-plane horizontal loads, generated by wind or earthquake, which are distributed to the wall primarily via diaphragms such as floors or the roof. Hence, buildings in earthquake-prone regions require adequate seismic shear strength and ductility to complement their vertical load carrying capacity. With the discovery made during the 1950s that the provision of reinforcement provided some ductility to normally brittle masonry, reinforced masonry became a popular and relatively inexpensive means to resist seismic loads in New Zealand.

The contents of this section are arranged so that section 2.2 briefly describes the possible modes of failure that a wall can suffer when being loaded laterally and section 2.3 briefly considers the resistance mechanisms of a masonry wall. Then, of more importance, literature reviews for the shear strength of masonry walls and the strength capacity of perforated masonry walls are comprehensively discussed in sections 2.4 and 2.5 respectively.

2.2 FAILURE OF SHEAR WALLS

Structural walls are required to resist horizontal loads, often termed as “racking loads”. Excluding premature lap-splice or bond failure of reinforcement, a shear wall subjected to horizontal loads may fail in one of three ways: by sliding horizontally, in flexure, or in shear (Park, 1986). The mode of failure is influenced by many factors such as wall aspect ratios, axial compression stress levels, wall boundary conditions and the strength properties of the materials used in wall construction. These types of failure are shown diagrammatically in Figure 2.1. Therefore the name ‘shear wall’ may not be particularly representative since the dominant mode of failure of a shear wall may be other than shear.

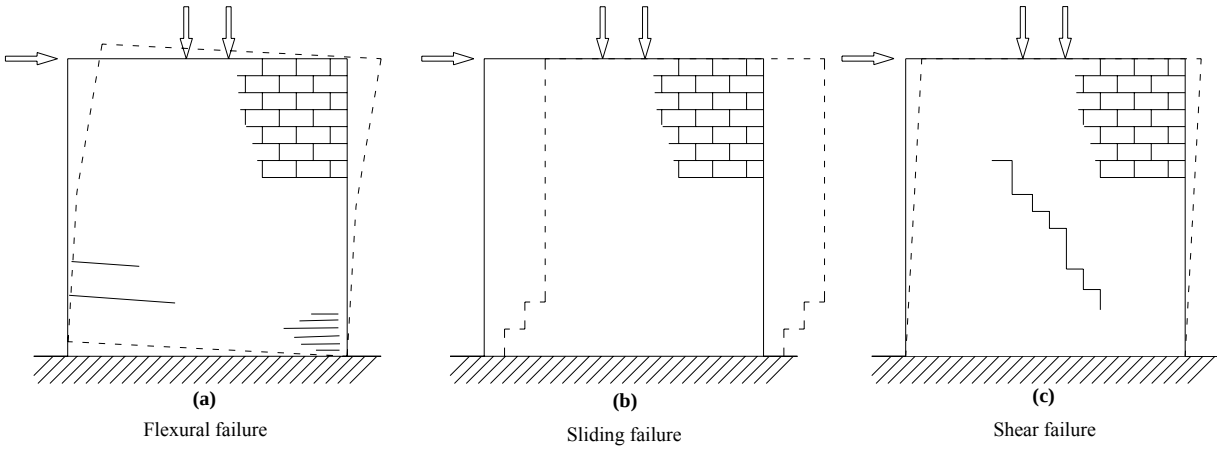

Figure 2.1 Reinforced masonry shear wall failure modes.

2.2.1 Flexural Failure

This type of failure occurs due to yielding of the vertical reinforcement near the wall heel or crushing of the masonry at the wall toe when the wall behaves as a vertical cantilever. Generally this is the preferred mode, as failure is ductile and effectively dissipates energy in conjunction with yielding of the vertical reinforcement anchored into the foundation.

2.2.2 Sliding Failure

Sliding shear is the movement of entire parts of the wall on the base or other mortar bed, and is resisted by dowel action of the vertical reinforcement anchored in the base and by friction on the mortar bed (Priestley, 1976). This type of failure may become significant in any situation where there is a low friction coefficient, such as when using a friction breaker or water proof membrane, or when the wall is positioned on a smooth finished slab. This failure mode may create a problem particularly in unreinforced masonry walls.

2.2.3 Shear Failure

This type of failure is characterised by the initiation of visible diagonal cracking along the shear wall when the principal tensile stresses exceed the tensile strength of the masonry under increasing imposed lateral displacements. Depending on the amount and anchorage of horizontal reinforcement, two types of shear failure are possible: a “ductile shear failure” and a “brittle shear failure” (Sveinsson et al., 1985).

Whenever there is adequate horizontal reinforcement with proper anchorage, redistribution of the stresses across the shear wall will be achieved after the initiation of diagonal cracking. Therefore the initial diagonal cracks do not widen under increasing horizontal loads, but

instead new sets of diagonal cracks form and gradually spread throughout the masonry wall, which resulted in a ductile behaviour that lead to some energy dissipation. Failure occurs gradually in this case as the strength of the masonry wall deteriorates under cyclic lateral loading. Partial localised crushing of the masonry at severely cracked portions of the wall diagonals finally leads to complete loss of strength. This type of failure is described as "ductile shear failure". On the other hand, a "brittle shear failure" occurs when the amount and/or anchorage of the horizontal reinforcement is not adequate to transfer the tensile stresses across the first set of diagonal cracks. These cracks continue to widen extensively and result in a major X-shaped diagonal crack pair, leading to a relatively sudden and destructive failure.

The influence of wall aspect (h_e/L_w) ratio on masonry shear strength was previously investigated by overseas researchers, such as Matsumura (1987) and Okamoto et al. (1987). From these studies, it was observed that masonry walls with smaller aspect ratios exhibited shear strengths at failure that were larger than those for more slender masonry walls. The researchers concluded that this shear strength enhancement was attributed to a more prominent role of arching action in masonry walls with low aspect ratios, in which a significant portion of the shear was resisted by compact regions which transferred large compression stresses, sometimes referred to as compression struts.

Although a flexural mode of failure is sought after, and sliding failure may at least partly occur in well-designed masonry structural walls, the primarily objective of the experimental study presented in Chapter 3 was to consider the shear failure of masonry structural walls. Consequently, of the ten masonry wall specimens presented in Chapter 3, nine of these walls were designed to failure in shear.

2.3 RESISTANCE MECHANISM

Reinforced masonry structure are typically "box like" with shear wall panels potentially subjected to simultaneous gravity and horizontal loads, resulting in overturning moments during seismic excitation. Consequently, the resistance mechanisms of such structural walls are required to have sufficient strength to resist these loads. The following subsections describe briefly the two forms of resistance mechanisms of a masonry shear wall.

2.3.1 Flexural Resistance

The flexural strength of a vertically reinforced masonry wall is usually calculated by means of simple flexural theory, based on the assumption that plane sections remain plane after bending. The nominal flexural strength of a masonry wall can be approximately ascertained using a rectangular compression stress block with a stress level of $0.85f'_m$, and with a depth of "a". The maximum strain, ε_u, allowed by the recently updated New Zealand masonry design standard (NZS 4230:2004) at the extreme compression fibre of an unconfined section is 0.003. These assumptions are shown in Figure 2.2.

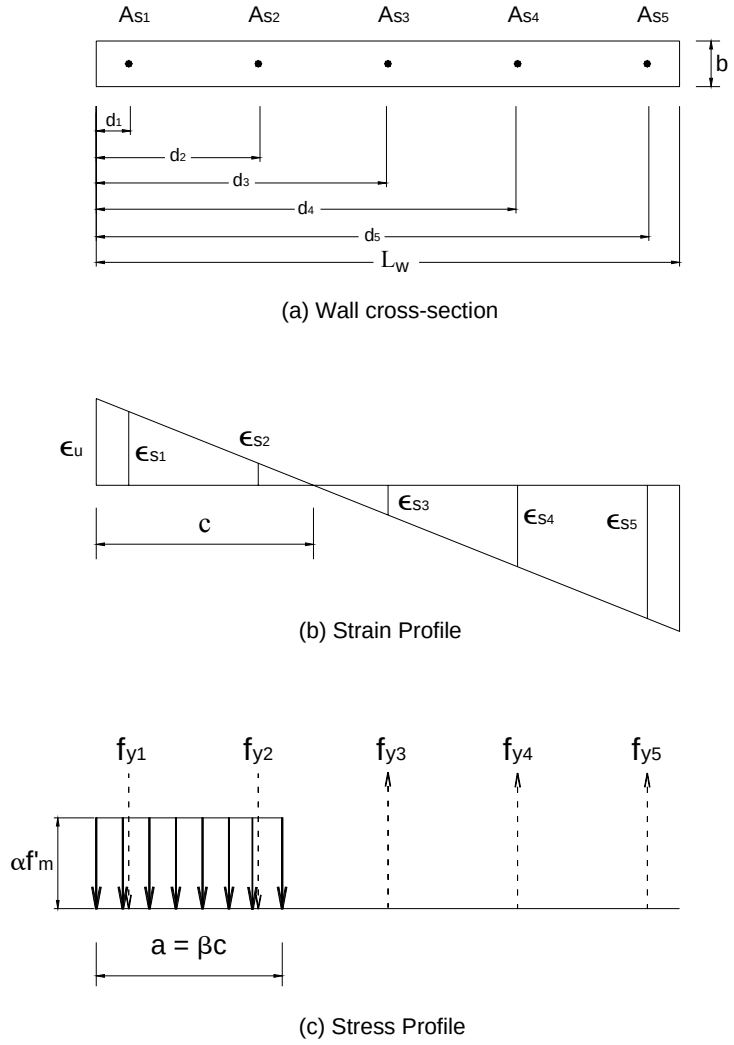

Figure 2.2 Idealised flexural strain and stress.

Based on these assumptions, the nominal moment capacity of a wall section with distributed vertical reinforcement can be evaluated by:

$$M_n = C_m\left(c - \frac{a}{2}\right) + \sum_i^n C_{si}\left(c - d_i\right) + \sum_i^n T_i\left(d_i - c\right) + W_t\left(\frac{L_w}{2} - c\right) \qquad (2\text{-}1)$$

$\sum_i^n C_{si}$ and $\sum_i^n T_i$ are the compressive and tensile strengths of the vertical reinforcement, found from:

$$\sum_i^n C_{si} = \sum_i^n A_{si} E_{si} \varepsilon_{si} \quad \text{and} \quad \sum_i^n T_i = \sum_i^n A_{si} E_{si} \varepsilon_{si} \tag{2-2}$$

where $E_{si}\varepsilon_{si} \le f_y$

The compression force, C_m within the masonry is found by:

$$C_m = W_t + \sum_i^n T_i - \sum_i^n C_{si} \tag{2-3}$$

and the compressive block depth is found by solving the following:

$$a = \frac{C_m}{0.85 f'_m b} \tag{2-4}$$

Hence, the neutral axis depth is as follow:

$$c = \frac{C_m}{0.7225 f'_m b} \tag{2-5}$$

Therefore the nominal strength, F_n of a shear wall with an effective height of H_e can be expressed as:

$$F_n = \frac{M_n}{H_e} \tag{2-6}$$

2.3.2 Shear Resistance

During a shear failure, unreinforced masonry walls behave as brittle structural elements with limited energy dissipation capacity, especially when subjected to high compression stresses (Page, 1989, Shing et al., 1989; Sucuoglu and McNiven, 1991; Tomaževič, 1999). Therefore masonry walls are frequently provided with steel reinforcement, both horizontally and vertically, in order to improve lateral resistance and ductility.

If a masonry wall is reinforced horizontally, the horizontal reinforcement prevents separation of the wall's cracked parts at shear failure, therefore improving the shear resistance and energy dissipation capacity of the wall when subjected to cyclic loading. In the case of unreinforced masonry walls, a single diagonal crack causes severe deterioration in strength and subsequent brittle collapse, see Figure 2.3a. However, if the wall is adequately reinforced horizontally, many smaller cracks will be evenly distributed over the entire surface of the wall, see Figure 2.3b.

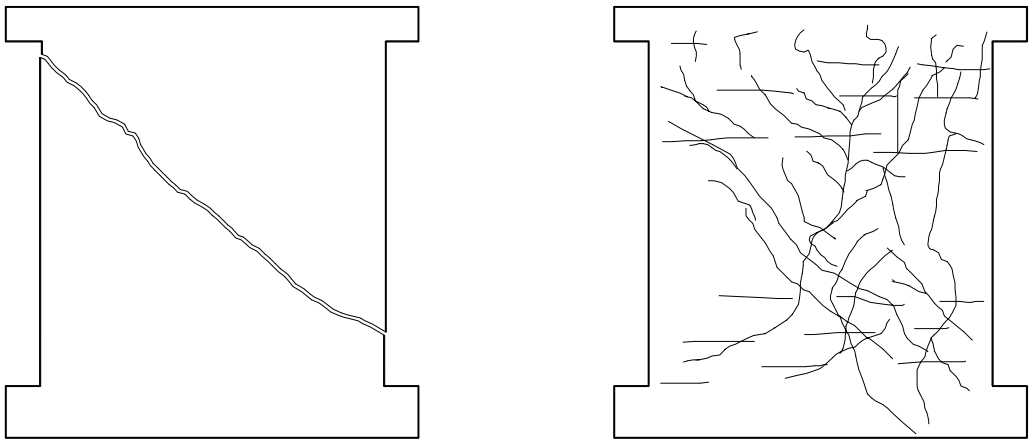

(a) Brittle shear failure (b) Ductile shear failure

Figure 2.3 Modes of shear failure.

2.3.2.1 Unreinforced Masonry Walls

Researchers (e.g. Yokel and Fattal, 1976; Mann and Muller, 1982; Page, 1989) during the past decade have identified two different forms of behaviour for unreinforced masonry shear walls. For low axial compression stresses, the basic form of shear strength expression is based on the Mohr Coulomb shear friction expression, as demonstrated in Equation 2-7 below:

$$\tau_m = \tau_o + \mu_f \sigma_n \tag{2-7}$$

where τ_m and σ_n are the average shear and normal stresses, τ_o is the shear bond strength and μ_f is the coefficient of internal friction. In parametric form, Equation 2-7 can be expressed as:

$$V_n = fn(f'_m, N) \tag{2-8}$$

where V_n represents the nominal shear strength of the masonry wall and N is the axial compression force. As demonstrated from experimental studies, values for the constants τ_o and μ_f vary considerably and are influenced by test method and type of masonry. Paulay and Priestley (1992) recommended a typical range of values of $0.1 \le \tau_o \le 1.5$ MPa and $0.3 \le \mu_f \le 1.2$.

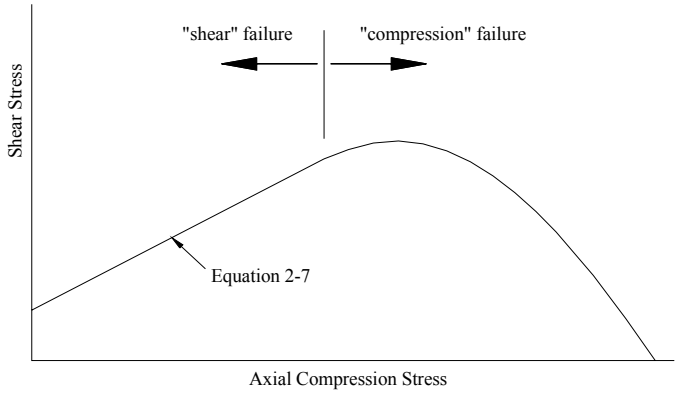

Figure 2.4 Failure criteria for unreinforced masonry shear walls (Page, 1989).

When the axial compression force approaches a sufficiently large stress, the wall reaches peak strength and its behaviour changes, with a failure mode including a combination of shear and crushing of masonry. For even larger compression stresses, shear strength decreases as compression failure of masonry dominates response to loads. Therefore, Equation 2-7 does not apply in these cases. This compression failure corresponds to the second part of the curve shown in Figure 2.4.

2.3.2.2 Reinforced Masonry Walls

For the case when masonry walls are reinforced with distributed vertical and horizontal reinforcement, the basic mechanisms of reinforcement action at shear failure are shown in Figures 2.5a and 2.5b. Past researchers (e.g. Brunner and Shing, 1996; Shing et al., 1988; Tomaževič, 1999) have concluded that the shear resistance of reinforced masonry walls comes from several mechanisms, such as tension of horizontal reinforcement, dowel action of vertical reinforcement, as well as axial compression force that enhances aggregate interlocking between the parts of the walls separated by diagonal cracks.

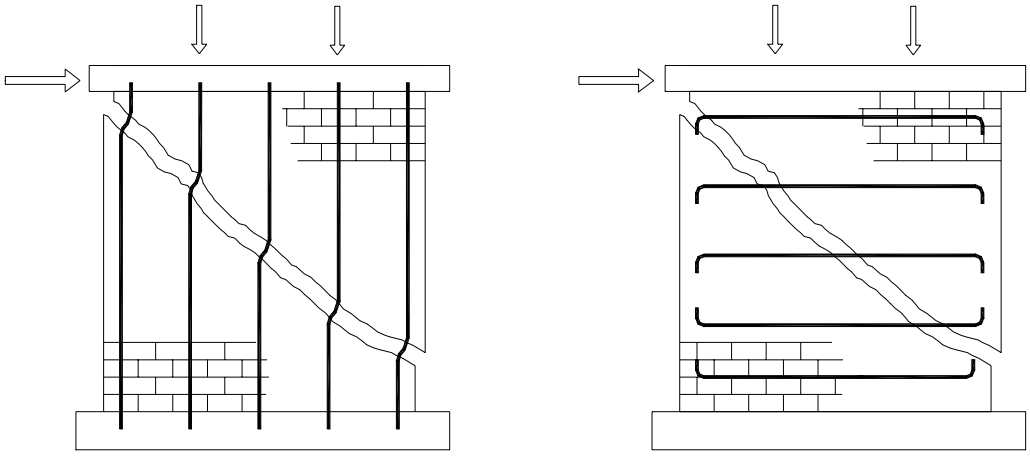

(a) Vertical reinforcement (b) Horizontal reinforcement

Figure 2.5 Role of reinforcement in resisting masonry shear failure.

Due to the complexity of these mechanisms, no effective theoretical models have yet been proposed to predict the shear strength of a masonry wall panel. Therefore, in practical calculation the nominal shear strength, V_n, of reinforced masonry walls is evaluated as the sum of contributions from masonry, reinforcement and applied axial compression load. The three shear resistance mechanisms are incorporated into an equation of the following form:

$$V_n = V_m + V_s + V_p \qquad (2\text{-}9)$$

Where:

V_m is the contribution of masonry to shear strength;

V_s is the contribution of shear reinforcement to shear strength;

V_p is the contribution of applied axial compressive load to shear strength.

As indicated by experimental results (Shing et al., 1988; Sveinsson et al., 1985, Matsumura, 1987), masonry shear strength, V_n is strongly dependent on the masonry compressive strength, f'_m, since there is strong evidence that V_m increases with an increase in f'_m. However, the relationship is not linear, with the increase in V_m diminishing as f'_m increases. Consequently, it is acceptable that V_m increases approximately in proportion to $\sqrt{f'_m}$. Also, in the case where masonry walls are provided with vertical reinforcement, part of the shear resistance capacity can be attributed to dowel action of the vertical reinforcement. Shear forces can be transferred along a well-defined plane (e.g. a diagonal crack) by the shear, flexural and kinking actions which are activated locally in reinforcing bars due to their relative displacement along a crack, see Figure 2.6.

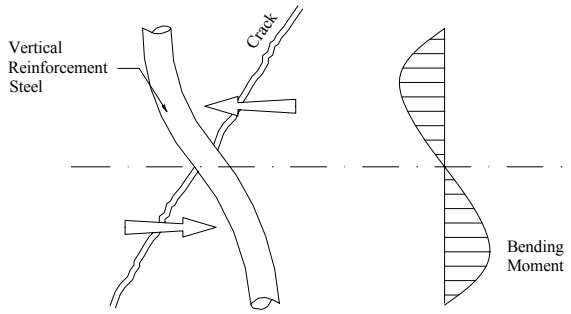

Figure 2.6 Shear carries by dowel action.

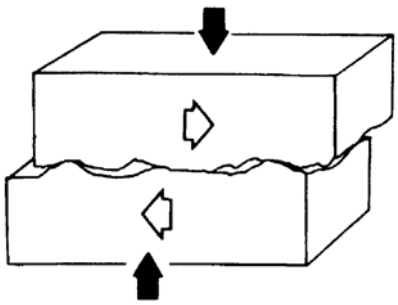

Figure 2.7 Aggregate interlocking across through crack (Hendry, 1991).

In addition, shear reinforcement generally in the form of horizontal steel bars, is placed at right angle to the axis of a masonry wall member (see Figure 2.5b) to provide V_s. Before diagonal cracking occurs, the horizontal reinforcement carries little force. However once diagonal cracks occur, the shear resistance is redistributed among the horizontal steel bars. When adequate shear reinforcement is provided, diagonal cracks do not open excessively but distribute evenly across the wall as shown in Figure 2.3b.

Axial compressive load suppresses the formation of cracking in a masonry wall since the tensile stresses induced by the lateral load must first overcome the compressive field created by the axial compressive load, before diagonal cracks can initiate, see Figure 2.8. In addition, axial compressive load contributes to masonry shear strength by enhancing the aggregate interlocking mechanism. When a crack is developed in a concrete mass, the surfaces of the crack are usually rough and irregular (see Figure 2.7). The majority of the coarse aggregate particles remain embedded in one of the two crack faces. When this crack forms along a continuous plane, a parallel displacement in this plane is possible and projecting particles from one face of the crack come into contact with the matrix of the other face. Further movement is then restricted by bearing and friction of the aggregate particles on the crack surface. Provided that restraint is available to prevent large increases in the crack width, substantial shear forces can be transmitted across the crack interface (Paulay and Loeber, 1974; Hendry, 1991).

The tensile strength of masonry is an important parameter in the behaviour of structural masonry elements such as shear walls, where horizontal forces will produce tension or shear stresses, or both. Initiation of diagonal crack in masonry block takes place when the principal tensile stresses, p_t, exceed the tensile strength of masonry. The Mohr diagram, shown in Figure 2.8b, is employed to evaluate the p_t and p_c (principal compression stress) under the given external loading shown in Figure 2.8a. The principal tensile stress, p_t, can be evaluated according to Equation 2-10:

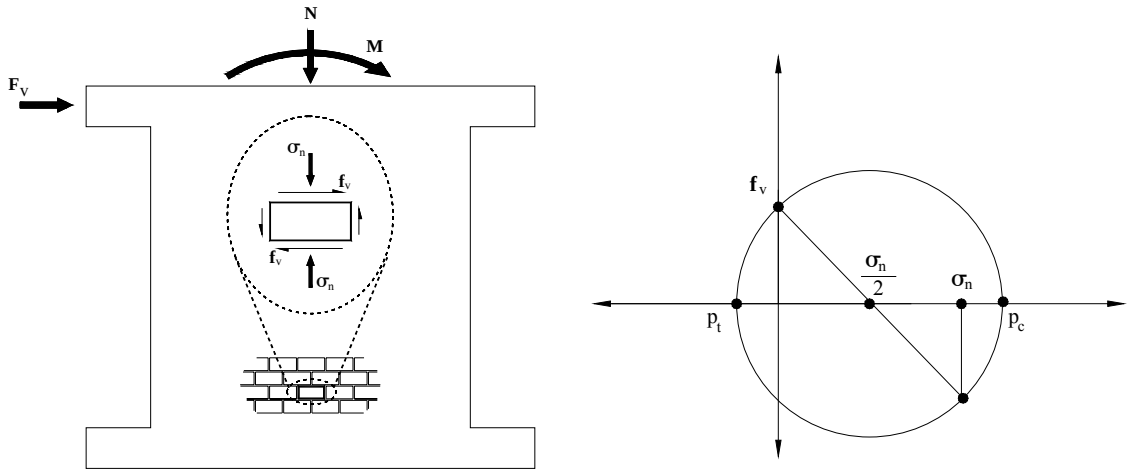

(a) State of stress (b) Mohr diagram

Figure 2.8 Principal stresses acting on masonry.

$$p_t = \frac{\sigma_n}{2} - \sqrt{(f_v)^2 + \left(\frac{\sigma_n}{2}\right)^2} \qquad (2\text{-}10)$$

It is noted that failure hypotheses for homogeneous materials cannot be unrestrictedly applied to masonry. This is because a masonry structure consists of numerous elements, namely the masonry blocks, the grout and the mortar joints, all of which can fail individually. Hence, it is not possible to attribute failure to a single cause, for example, friction failure of the mortar joints. On the contrary, many types of failure are possible. Consequently, failures must be deduced from a small section of masonry, such as that shown in Figure 2.8a, with Equation 2-10 used to evaluate the p_t within that small section of masonry.

2.4 MASONRY SHEAR STRENGTH

A comprehensive literature review indicated that many studies had investigated the behaviour of masonry wall. A large number of these were of full or model scale tests on wall panels (e.g. Priestley, 1976; Sveinsson et al., 1985, Shing et al., 1988, Matsumura, 1988; Larbi and Harris, 1990; Brammer, 1995; Brunner and Shing, 1996). From these test results, equations have been developed to predict the shear strength of masonry walls, usually calibrated to the test results carried out by the particular researchers. These past experimental studies are summarised in section 2.4.1 while section 2.4.2 presents masonry shear expressions that are currently available.

2.4.1 Experimental Research

The data sources used in the preparation of the former New Zealand masonry design standard, NZS 4230:1990, were published in 1980 or earlier. However, significant research relating to masonry shear strength has been conducted in both North America and Japan since 1980. Therefore a considerable amount of additional information is now available. This section of the thesis provides summaries of past experimental studies currently available in the field of masonry shear strength. Reviews are sorted by the date of publication in each category. They cover a brief description of tests performed and the main conclusions from each reference.

Yokel and Fattal (1975) compared failure hypotheses with the results of 32 plain single wythe clay brick masonry walls tested in diagonal compression. Three types of masonry units designated by A, B and S were combined with two types of mortar- conventional and high strength, designated by C and H, to build four types of masonry walls, i.e. AC, AH, BH and SH (eight walls of each type).

The authors concluded the following:

1. Shear failure under diagonal compression and axial load could occur by debonding along mortar joints or splitting of the masonry units.
2. For a given type of wall, failure could occur by joint debonding under low axial load and change to unit splitting under higher axial load. Debonding strength was characterised by a linear relationship and had the function of a Coulomb type relationship:
3. Splitting failure originated at the centre of the walls at a splitting strength governed by a critical relationship between the principal biaxial stresses.

Mayes et al. (1976a and 1976b) tested seventeen concrete block masonry double pier systems coupled with heavily reinforced top and bottom spandrels under cyclic lateral loading at the University of California at Berkeley. The pier system was allowed to rotate at the top under lateral load applied to the top spandrel.

The variables investigated in this study included:

1. The rates of loading, i.e. specimens were tested in identical pairs using a slow and fast rate of loading (0.02 Hz and 3 Hz).
2. Four types of reinforcement arrangement:
    a) None.
    b) Vertical end bars with two reinforcement ratios.
    c) Vertical end bars and horizontal bars with different reinforcement ratios.
    d) Vertical end bars, horizontal bars and toe reinforcement in the form of perforated steel plates in bed joints.
3. Three types of grouting: none, partially and fully grouted.

The authors concluded the followings at the end of the test programme:

1. Sufficient amounts of horizontal reinforcement enhance the ductility of shear mode response significantly.
2. Use of perforated steel plates in the toe area improved flexural mode response.
3. Partial grouting improves the elasto-plastic shear mode response compared with no grouting.
4. Dynamic loading at higher rate increased ultimate strength for the case of shear mode failures and decreased ultimate strength for the case of flexural mode failure compared with strengths obtained from a slow rate of loading.

Priestley (1976, 1977) conducted a comprehensive study on the cyclic behaviour of reinforced concrete masonry walls and established that the maximum shear stresses allowed in the former New Zealand masonry design standard, DZ 4210 were unrealistically low. A total of six heavily reinforced concrete masonry walls were subjected to cyclic shear. Aspects investigated included the influence of vertical and horizontal reinforcement ratios (0.66% and 0.45% vertical steel, 0.66% and 0.34% horizontal steel) and the magnitude of axial compression stress levels on masonry shear strength. Confinement at potential crushing areas by mortar bed confining plates was included to examine their effectiveness in enhancing the performance of masonry shear walls at high ductility levels. Two walls were subjected to axial stress levels of 0.69 MPa (100 psi) and the other four walls were not subjected to axial stresses. Three walls had thin stainless steel confining plates installed in the bottom three mortar courses.

The maximum experimental loads were compared with theoretical and design loads. Priestley analysed the influence of base course slip and compared experimental displacement ductility with code required ductility. The author concluded the following:

1. The maximum allowance for shear stress in the former New Zealand masonry design standard, DZ 4210 was unreasonably low. None of the six walls suffered diagonal shear failure, despite the experimentally obtained shear stresses being 4.2 times the maximum code allowable value of 0.62 MPa.
2. The test results indicated that the former (i.e. 1977) New Zealand design practice overestimated the cracked stiffness of walls by a factor of more than 2.
3. Mortar-bed confining plates did not significantly reduce stiffness degradation of the walls in this study, but substantially reduced damage to the walls at high ductility levels.

Hidalgo et al. (1978, 1979), Chen et al. (1978) and Sveinsson et al. (1985) conducted experiments to evaluate the seismic behaviour of window piers typical of high-rise masonry construction. Principal test parameters considered in the test programme were:

1. The type of masonry construction.
2. The height-to-width ratio.
3. The amount of horizontal reinforcement.
4. The distribution of vertical steel.
5. The effect of different types of anchorage of horizontal reinforcement (90º bend, 180º bend and end plate).
6. The level of axial stress.

Three types of masonry material were used throughout the test programme, namely hollow concrete masonry blocks, hollow clay brick and double wythe grouted core clay brick piers. Out of the ninety-three fixed end piers, twenty-nine of them were constructed of hollow concrete masonry blocks and subjected to cyclic in-plane loads at the Earthquake Research Centre of the University of California. The test-programme included fully and partially grouted single piers with three aspect ratios (h/L_w) of 0.5, 1 and 2.

The studies concluded that the strength associated with shear mode of failure was a function of the compressive strength (f'_m) of the masonry material, the magnitude of gravity stress and of the aspect ratio of the pier. The distribution of vertical reinforcement did not significantly influence the behaviour of piers that failed in shear, and anchorage of horizontal reinforcement with 180º bends was proven to be more effective than any of the other two types of anchorage. It was also observed that the maximum shear strength was approximately the same for fully and partially grouted piers as long as the stress was based on the net area of the cross section of the wall. Among the parameters studied in the test programme, the amount of horizontal reinforcement was found to be the most influential on masonry shear strength, as discussed below.

Horizontal reinforcement was effective in inhibiting the opening of diagonal cracks, but gave diminishing returns as the amount of reinforcing steel was increased. After a certain ratio, increasing the reinforcement content had an adverse effect on the post-cracking deformation capacity. The researchers concluded that when a specified minimum amount of horizontal reinforcement was provided and allowed to yield, a ductile shear failure could be achieved in which diagonal cracks did widen excessively but distributed evenly throughout the panel as shown in Figure 2.3b. Higher amounts of horizontal reinforcement, on the other hand, restrained the post-cracking deformation capacity since the reinforcing steel remained in the elastic range and did not contribute much to the overall lateral deformation. The masonry wall finally reached its maximum lateral deformation capacity due to crushing of masonry at the toes, which were already damaged by the extensions of diagonal cracks. The masonry wall failed when the web slides with respect to the bottom of the spandrel as shown in Figure 2.9.

The findings from this test programme allowed Sucuoglu and McNiven (1991) to propose Equation 2-11 to predict the minimum required horizontal reinforcement ratio for a masonry wall that fails in the shear mode in order to exhibit a ductile post-cracking performance:

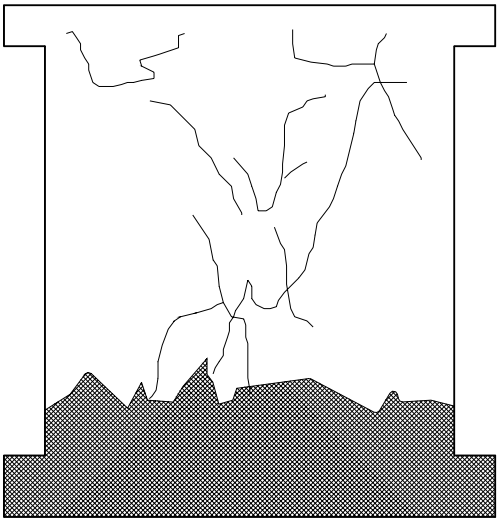

Figure 2.9 Sliding shear failure.

$$\rho_h = 1.41\frac{f'_m}{f_y}\left[-\frac{1}{2}\left(\frac{\sigma_n}{f'_m}\right)+\sqrt{0.0016+0.0128\left(\frac{\sigma_n}{f'_m}\right)+0.2756\left(\left(\frac{\sigma_n}{f'_m}\right)^2\right)}\right] \qquad (2\text{-}11)$$

where

$$\rho_h = \frac{A_h}{t.s}$$

Priestley and Elder (1982) tested three slender concrete block masonry walls under cyclic reversals of in-plane displacements to examine the ductility and strength degradation of such walls. The nominal 200 mm block walls were 6100 mm high and 2440 mm long. Reinforced concrete floor slabs, approximately 1220 mm wide, were cast at the first and second floor levels and a reinforced concrete bond beam was placed at the top to distribute the lateral force and anchor the vertical reinforcement. Steel reinforcement of 16 mm diameter was placed in the vertical cells with a centre to centre spacing of 400 mm. The vertical reinforcement ratio was 0.72% for all walls. The main vertical steel was lapped to starter bars that were anchored in the foundation beam. Two of the walls were subjected to an axial stress of 1.95 MPa and one wall was subjected to an axial stress of 0.74 MPa. Confining plates were placed in the mortar beds in the compression zones of the potential plastic hinge area for one wall. The lap length of vertical reinforcing was 975 mm for two of the walls and 1310 mm for the third wall.

Results from the wall tests indicated that lapping of flexural starter bars in plastic hinge regions at the wall base had a profound influence on wall behaviour. The most important effect was the reduction in equivalent plastic hinge length that resulted from the stiffening and strengthening influence of the doubled reinforcement ratio within the lap. This concentrated the plasticity into a very short region at the wall base, giving a plastic hinge length less than $0.2L_w$ at design ductility levels. A consequence of this action was the high strain in the plastic hinge zone at comparatively low ductility level, inducing premature vertical splitting of the compression zone. A second undesirable effect of the lap was the tensile bond failure induced in tension reinforcement close to the wall end. This was initiated by the vertical splitting caused when the end of the wall had been in compression during a previous loading cycle. Splitting forces associated with transfer of tensile forces from starter to lapped bar propagated the vertical cracks and caused bond failures.

Hirashi (1985) tested nine walls to investigate the flexural behaviour of reinforced masonry walls. Of the nine walls, six were constructed using concrete block and two were constructed of hollow brick units, with the final wall being constructed of reinforced concrete. The horizontal reinforcement used was 0.29% and 1.16%. However, the nine walls had the following common identities:

1. Same geometry (i.e. h/L_w = constant),
2. Fully grouted core,
3. Constant flexural reinforcement in the end cores with confinement at critical compression zones,
4. Constant axial load, and
5. Rotational fixity of top and bottom surfaces.

From the test results, the author was able to conclude the followings:

1. Increasing the amount of horizontal reinforcement (four-fold) had no significant effect on the cracking and maximum shear strengths.
2. Increasing the amount of horizontal reinforcement increased the maximum shear-to-maximum flexural strength ratio and significantly improved deformation capacity: the ability to simultaneously develop large deformations without substantial strength degradation.
3. The ability of a shear wall to develop a large deformation capacity under cyclic load was largely attributed to the presence of confinement at critical compression zones.

4. The ratio of maximum strength-to-cracking shear strength was in the range of 1.3 to 1.8, indicating that substantial post-cracking strength gain is possible in shear mode failures, depending primarily on the effective use, rather than the amount of horizontal reinforcement.

Woodward and Rankin (1985a and 1985b) conducted two studies on masonry walls. The first study was to examine the effect of block and mortar strength on the in-plane shear resistance of concrete masonry walls, while the second study was to examine the influence of aspect ratio on the relationship between lateral in-plane load resistance and vertical in-plane compressive stress.

The first study involved the testing of seventeen 1630 mm high concrete masonry walls with the following variables:

1. Two types of concrete block units with gross area unit strengths of 9.0 MPa and 12.4 MPa.
2. The mortar used in the study was of Type S and Type N.
3. The axial compressive stress varied from 0.69 MPa to 2.76 MPa (based on net cross-sectional area).
4. Of the seventeen walls, thirteen were 1630 mm long, two were 1220 mm long and the remaining two were 2440 mm long.

The conclusions obtained from the first study were as follows:

1. For the lower levels of applied vertical compressive stress, the influence of block and mortar strengths on the maximum shear resistance was negligible. The influence of the component strengths became more significant as the vertical load increased.
2. The interaction effect of block and mortar strength on wall shear strength was greater than the effect of either component's strength taken alone.
3. In general, the linear relationship between maximum shear resistance and applied vertical compressive stress was unaffected by block or mortar strength.
4. The diagonal tensile strain threshold at which diagonal cracking occurred was unaffected by the variation in block and mortar strength. The range of threshold strain was between 110 and 165 microstrain.

The second study involved the testing of seven 1630 mm high, ungrouted and unreinforced concrete masonry walls with fixed-fixed boundary conditions. The aspect ratio was varied by using three different lengths of wall: 1220 mm, 2030 mm and 2440 mm. The axial stress levels for the two 1220 mm long walls were 1.1 MPa and 3.0 MPa. The stress levels for the two 2030 mm long walls were 1.58 MPa and 2.69 MPa respectively, and the remaining three 2440 mm long walls had stress levels of 1.52 MPa, 2.14 MPa and 2.82 MPa.

At completion of the study, the authors concluded the following:

1. There was a relatively weak effect of aspect ratio on the diagonal cracking strength for aspect ratios less than or equal to 1.
2. There was a nearly linear relationship between axial compressive stress and maximum lateral shear resistance.
3. The maximum lateral load resistance was affected by aspect ratio for higher levels of axial compressive stress.

Okamoto et al. (1987) tested eighteen walls constructed from hollow concrete block masonry, hollow clay brick masonry and reinforced concrete. The walls were fully grouted and tested under controlled axial load combined with programmed cyclic lateral loading applied in a manner to keep the top and bottom surfaces rotationally fixed. The parameters investigated in this study included:

1. Aspect ratio: 0.9, 1.6 and 2.3.
2. Axial stress: 2% to 26% of f'_m.
3. Horizontal reinforcement ratio: 0.17% to 0.67% (noted that the vertical reinforcement ratio was kept constant).

The authors concluded the following from this study:

1. Shear cracking load and maximum shear strength increased at decreasing rates with increasing axial load. Gain in shear strength was in the 60% to 66% range with axial load increasing from 2% to 26% of f'_m.
2. Shear strength increased 20% to 30% respectively as the aspect ratio decreased from 2.3 to 1.6 and from 1.6 to 0.9.
3. Specimens that failed in the shear mode had 50% of the deformation capacity of those that failed in a flexure mode.

Matsumura (1985, 1987, 1988 and 1990) presented an empirical formula to predict the shear strength of reinforced masonry walls subjected to in-plane lateral and axial loads, on the basis of the results of testing fifty-seven concrete masonry walls and twenty-three brick masonry walls. The empirical formula developed by Matsumura is described in detail in section 2.4.2. Specimens tested were under different conditions such as various shear reinforcement ratios, shear-span ratios, axial stresses, and strength of materials, as well as two kinds of grouting, namely, partial grouting and full grouting. About 2/3^{rds} of the experimental specimens were partially grouted, with the remainder being fully grouted.

Nominal 200 mm hollow concrete or 150 mm clay brick units were used to construct reinforced, partially grout-filled or fully grout-filled walls of varying sizes. Full size walls ranged in height from 1600 mm to 1800 mm while the lengths ranged from 790 mm (i.e. 31 in) to 2000 mm. There was a set of smaller size walls with dimensions of 610 mm to 1220 mm in height, 400 mm to 500 mm long and 100 mm and 150 mm thick. Two test set-ups were used:

1. Fifty-five full size walls were subjected to horizontal shear loads with a fixed base and the top free to move horizontally (cantilever).
2. Twenty-five of the smaller size walls were laid horizontally and subjected to vertical shear loads like the loading of a restrained deep beam.

From the test results of eighty masonry walls, Matsumura was able to conclude the following:

1. Shear strength of masonry increases nonlinearly with masonry compressive strength, f'_m. The increase in rate of masonry shear strength becomes gradually lower as f'_m increases. Consequently, it may be acceptable that masonry shear strength increases approximately in proportion to $\sqrt{f'_m}$.
2. Masonry shear strength increases in relation to the increase of horizontal shear reinforcement, while it decreases inversely in relation to the shear span ratio $\frac{M}{V.d}$.
3. Axial compressive stress is found to have a beneficial effect on masonry shear strength.

Kaminosono et al. (1988) tested twenty-two walls under double curvature deformation to represent the stress condition due to earthquake motions. Of the twenty-two walls, fourteen were concrete masonry walls, five were clay brick masonry walls and the remaining three were reinforced concrete walls. Eighteen of these walls were “I” shaped, three were “T” shaped wall and one was “+” shaped. The principal objective of this study was to evaluate the effect of

axial stress (0.5 MPa – 6 MPa), shear span ratio (0.452 – 1.139), and amount of shear reinforcement (0.175% - 0.699%) on the wall.

From the test results, the authors concluded the following:

1. For masonry walls that failed in shear, the maximum shear strength increased and the deformation capacity decreased with increase in axial stress, and also with decrease of shear span ratio.
2. Masonry walls with shear span ratio less than 0.8 reached the maximum strength at drift of 0.002 radian, followed by rapid strength deterioration.
3. For walls that failed in flexure, the deformation capacity increased with increase in the amount of shear reinforcement and with increase in the confinement of the compression toe by spiral reinforcement.

Tomaževič et al. (1986, 1987 and 1988) tested two series of sixty concrete block reinforced masonry walls with different geometry (series C with $h/L_w = 1.25$ and series D with $h/L_w = 2.30$) at the Institute for Testing and Research in Materials and Structures (ZRMK) in Ljubljana, Yugoslavia. The walls were constructed in 1:2 scale reduced size with specially manufactured concrete blocks in cement mortar which consisted of 0-2 mm sand and Portland cement in the proportion of 1:3:5. Deformed steel (grade 400) 10 mm diameter bars (ρ_v= 0.26% in series C and $\rho_v = 0.52\%$ in series D) were used as vertical reinforcement, whereas smooth steel (grade 200) 6 mm diameter bars (0.14%) or burned wire, 4.2 mm diameter (0.28%) and 3.1 mm in diameter (0.14%), in the shape of closed stirrups were used as horizontal reinforcement. Stirrups were placed around the vertical bars in each horizontal mortar joint. All walls were tested as simple cantilevers with a constant vertical load of 60 kN and were subjected to cyclic lateral loading.

The study concluded that by reinforcing the masonry walls with vertical and horizontal reinforcement, improved seismic behaviour could be expected. In this respect, the horizontal reinforcement in the bed joint improved the shear and ductility capacity of the walls by causing yielding of the vertical reinforcement and the development of full flexural capacity of the wall's section.

In 1996, Tomaževič et al. conducted 32 more tests on identically reinforced masonry walls to further investigate the influence of different testing procedure: monotonic loading, two

different loading histories, and a simulated displacement seismic response. From these test results, the authors noted that higher resistance and larger ultimate displacement were measured in the case of monotonic loading than in the case of cyclic loading of any type. Tomaževič et al. noted that strength and stiffness degradation took place when the walls were subjected to repeated cyclic lateral load reversals. Consequently, a significantly higher resisting force was measured when monotonic loading was applied than for the corresponding displacement when testing using cyclic loading. It was also observed from the experimental study that the maximum lateral resistance attained by monotonic loading was much higher than corresponding values attained in the case of cyclic loading. It was therefore concluded that at the same amplitude of lateral displacement, less severe stiffness degradation could be obtained in the case of monotonic loading than in the case of cyclic loading.

Shing et al. (1988, 1989, 1990a, 1990b, 1991, 1993) conducted comprehensive experimental testing on sixteen squat concrete masonry walls at the University of Colorado in order to examine the flexural and shear strength of reinforced masonry shear walls. The main variables considered in the experimental study included the amount of vertical and horizontal reinforcement, and the magnitude of applied axial stress. All test specimens were 1.8 m high and 1.8 m long, and 140 mm wide. All specimens were fully grouted, with uniformly distributed vertical and horizontal reinforcement.

The study found that simple flexure theory based on the plane-section assumption could be applied to square wall panels with good accuracy. However, the actual flexural strength of a shear wall subjected to seismic loads could be slightly higher than that predicted by flexure theory due to strain hardening under cyclic loads. In addition, the flexural strength of the shear wall increased with the magnitude of the applied axial load. Nevertheless, it was also found that the axial compressive load had the detrimental effect in reducing the ductility capacity of the shear walls since high axial compressive stress could lead to more severe toe crushing. However, proper toe confinement was found to substantially improve the flexural ductility of shear walls.

Shing et al. concluded from experimental results that specimens that failed in shear tended to exhibit a more brittle behaviour than those failing in flexure. The shear strength of reinforced masonry depends on the tensile strength of masonry as well as on several other mechanisms, such as aggregate interlocking, the dowel action of vertical steel, and the action of horizontal

shear reinforcement. It was found that the occurrence of the first major diagonal crack depends primarily on the tensile strength of masonry and the applied load condition, but not on the amount of reinforcement present. However, the post-cracked shear resistance depends on the amount of vertical and horizontal reinforcement.

Larbi and Harris (1990) conducted a series of ten 1/3rd scale model low rise masonry wall tests to determine the effect of the amount of vertical and horizontal reinforcement on shear and flexural strength. However, the main objective of the study was to assess the effectiveness of the modelling technique used to duplicate the component materials at 1/3rd scale.

In order to demonstrate the effectiveness of the 1/3rd scale model, the results obtained from this study were presented along with the corresponding results attained by Shing et al. at the University of Colorado at Boulder, on similar full scale masonry wall panels. Based on the overall correlation obtained, it was concluded that the modelling technique was efficient and that it represented a good alternative to full scale testing.

Crisafulli et al. (1995) conducted finite element analysis to determine the shear strength of unreinforced brick masonry panels. The researchers concluded that the shear strength of a masonry panel could be evaluated according to the properties of the masonry and its constitutive materials: the tensile strength of the brick, the shear strength of the mortar joints and the compressive strength of masonry. It was also concluded that three modes of failure may occur in masonry panels depending on the magnitude of axial compressive stress levels.

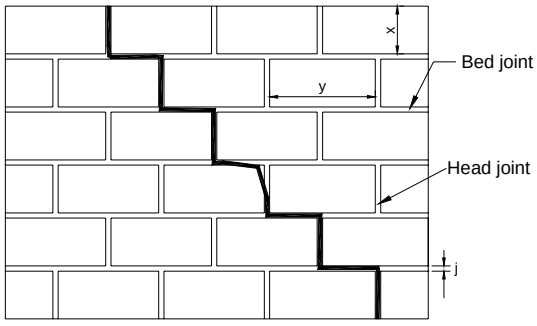

Figure 2.10 Crack develops at low axial compressive stress.

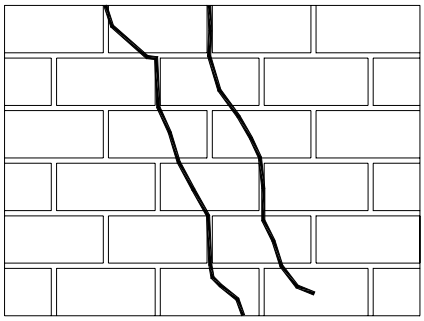

Figure 2.11 Cracks develop in the bricks during diagonal tension failure.

The first type of failure is caused by debonding of the mortar bed at low axial compressive stress. Cracks develop in stepped form as shown in Figure 2.10. For low axial compressive stress, the shear strength resulted from the combination of bond strength and friction resistance between the mortar joint and bricks. Hence, shear strength is a function of normal stress at the bed joint σ_n and has the form of a Coulomb type equation:

$$\tau_m = \tau_o^* + \mu^* \sigma_n \tag{2-12}$$

$$\tau_o^* = \frac{\tau_o}{1 + 2\mu\frac{x}{y}} \qquad \mu^* = \frac{\mu}{1 + 2\mu\frac{x}{y}} \tag{2-13}$$

where x and y are the height and length respectively of the brick as shown in Figure 2.10 and the stresses τ_o and σ_n are considered in absolute value.

Crisafulli et al. concluded that for medium to high axial compressive stress, a diagonal tension failure of the bricks occurs, as shown in Figure 2.11. The shear strength of the bricks increases due to the effect of compressive normal stress and cracks develop in the bricks instead of the bed joint. It is therefore assumed that failure occurs when the principal tensile stress (caused by the combined effect of compressive and shear stresses) in the brick is equal to its tensile strength, τ'_{tb} and Equation 2-14 has been proposed:

$$\tau_m = \frac{\tau'_{tb}}{C_s}\sqrt{1 + \frac{\sigma_n}{\tau'_{tb}}} \tag{2-14}$$

$$\text{where} \quad C_s = \frac{\frac{x}{j} + 1}{\frac{x}{2j} + 1}$$

Brunner and Shing (1996) undertook an experimental study in which walls of low aspect ratio were tested in order to investigate the influence of aspect ratio on the strength and failure mechanism of a reinforced masonry wall. Therefore, a series of three fully grout-filled masonry wall panels was built with aspect ratios (h/L_w) of 0.929, 0.722 and 0.591. A high vertical steel ratio was chosen for all three walls to increase the flexural strength and force the walls to fail in shear.

All walls exhibited shear failure in this study. It was found that wall panels with lower aspect ratios had higher stiffness and reached their maximum resistance at smaller displacement.

Schultz (1996) explored the potential benefits and advantages of partially-grouted masonry shear walls. A total of six partially-grouted masonry shear walls were constructed according to Figure 2.12. Only the outermost vertical cells and a single course bond beam at the mid-height of the wall were reinforced and grouted. All walls were constructed to a height of 1422 mm, but varied in length. Two horizontal reinforcement schemes were used for the bond beams to define reinforcement ratios of 0.05% and 0.12%, based on gross dimensions.

The test observations suggested that partially grouted masonry is a viable lateral load resisting system for regions of moderate and low seismic risk. Decrease in the height-to-length (h/L_w) ratio was observed to have a beneficial effect on the ultimate shear stress, but a detrimental effect on the strength deterioration, deformation capacity and energy dissipation capacity. Increasing the horizontal steel ratio had a modest effect on the maximum shear stress. Finally, it was concluded that the resisting mechanism of partially grouted masonry walls is vastly differently from that of reinforced masonry walls. Vertical cracks arising from stress concentrations between ungrouted and grouted masonry appear to dominate wall behaviour, and sliding friction between masonry panels and concrete surfaces contributes to the resistance mechanisms.

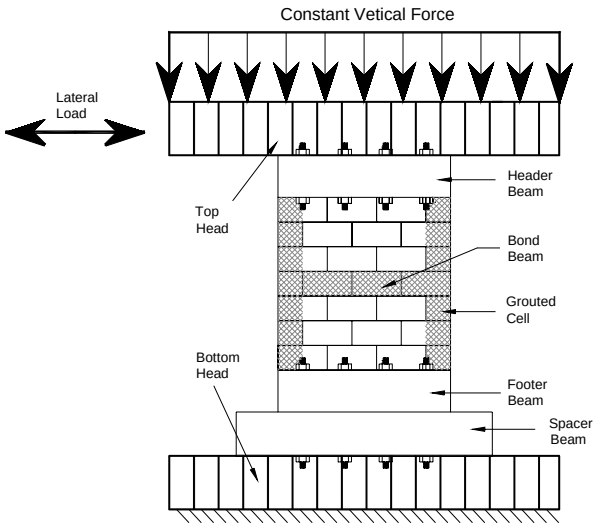

Figure 2.12 Typical tests set-up (Schultz, 1996).

Hansen et al. (1998) used the test set-up shown in Figure 2.13 to conduct twenty-six deformation controlled shear tests to determine the shear strength and shear stiffness as well as

the post peak behaviour of bed joints, including mode II fracture energy (which is the fracture energy related to shear failure and joint dilatancy). The tests were carried out with three types of mortar and four types of bricks: Danish clay solid and perforated, Finnish calcium silicate solid and clay perforated, and three levels of precompression of 0.1 MPa, 0.2 MPa and 0.5 MPa.

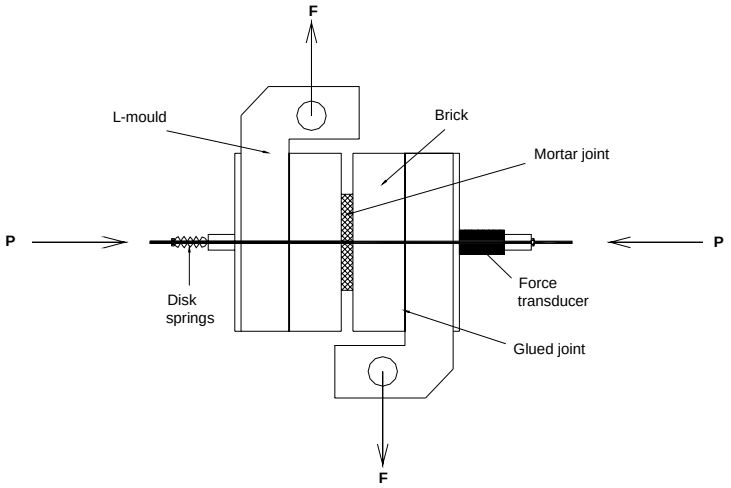

Figure 2.13 Test set-up to determine the shear strength of bed joint.

Based on the test observations, the researchers noted the following points:

- The use of strong mortars does not generally improve the shear properties of bed joints. However, the consequence of using strong mortars is a decrease in the mode II fracture energy of the bed joints that leads to a more brittle masonry with many cracks in the bricks in the ultimate limit state.
- With respect to the mode II fracture energy for bed joints, perforated bricks produce significantly higher values than solid bricks, especially when relatively weak mortars were used.

Cavalheiro and Pedroso (2000) tested triplet specimens to investigate the bond shear strength of masonry with and without precompression forces perpendicular to the bed joints. The loading and support arrangement for the triplet test is shown in Figure 2.14.

The experiments were carried out on two types of masonry, namely hollow clay and concrete masonry, and two types of mortar mixes at the ages of seven, twenty-eight and ninety days. Precompression forces of 0.57 MPa and 1.14 MPa were taken to represent the vertical loads induced by four and eight storey building.

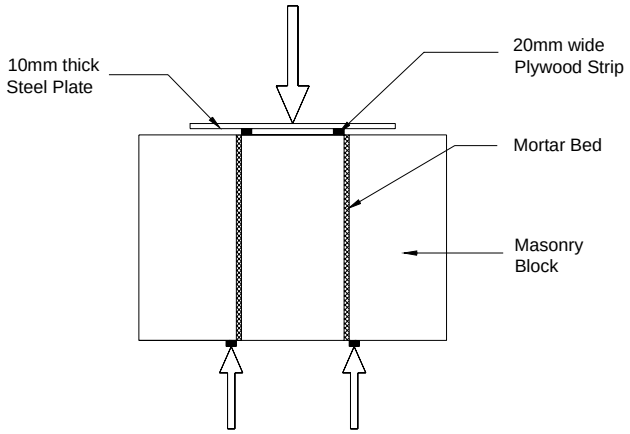

Figure 2.14 Loading and support arrangement.

Cavalheiro and Pedroso observed that the shear strength of masonry in general increased with age, but the increase in shear strength was more significant in specimens without precompression. The results showed strong effect of the precompression in increasing the bond shear strength. However, this bond shear strength was strongly dependent on the vertical forces up to a certain precompression level. Cavalheiro and Pedroso predicted this level to be about 0.6 MPa based on the materials tested in their study.

Laursen and Ingham (2000a and 2000b) conducted a series of eight laboratory tests to explore the in-plane wall response of post-tensioned concrete masonry. The main variables considered in this experimental study included the wall dimensions, prestressing steel content, prestress force and types of grouting: full grouting, partial grouting and ungrouted wall.

Laursen and Ingham concluded that fully grouted unbonded post-tensioned concrete masonry is a competent material combination for ductile structural wall systems. Despite the absent of shear reinforcement, the prestressed masonry walls exhibited a near non-linear response dominated by rocking behaviour. Limited damage of the lower wall corners were observed at large displacement capacities beyond drifts of 1.4%.

It was also concluded from this study that the prestressed partially and ungrouted concrete masonry walls are vulnerable to shear dominated behaviour, which ultimately led to diagonal shear cracking failure mode. However, the tests indicated that the partially and ungrouted prestressed concrete masonry walls are capable of developing significant strength, exceeding the predicted wall flexural strength. Hence, it was concluded that the prestressed partially and ungrouted concrete masonry walls maybe suitable for use in non-ductile strength design.

2.4.2 Existing Masonry Shear Expression

For most reinforced masonry wall panels, it is normally required that the plastic hinges be located at the wall bases. Special care is needed within the plastic hinge zones since the shear strength is a function of flexural ductility. As plastic hinge rotations increase, the widening of flexure-shear cracks reduces the capacity for shear transfer by aggregate interlock, and the shear strength reduces. Examination of the seismic response of reinforced concrete bridge columns by Priestley et al. (1994 and 1996) enables a clear distinction to be made between brittle shear failure, occurring before the flexural strength is reached, and ductile shear failure, where a degree of flexural ductility develops before shear failure occurs. This is acknowledged in the conceptual model for concrete shear strength proposed by the Applied Technology Council (1981) and illustrated in Figure 2.15, where shear strength is assumed to decrease in a linear fashion as the displacement ductility increases. If the lateral force corresponding to flexural strength is less than the residual shear strength (V_r), ductile flexural response is ensured. If it is greater than the initial shear strength (V_i), a brittle shear failure results. If the lateral force corresponding to flexural strength is between the initial and residual shear strength, then shear failure occurs at a ductility corresponding to the intersection of the strength and force-deformation characteristic as shown in Figure 2.15.

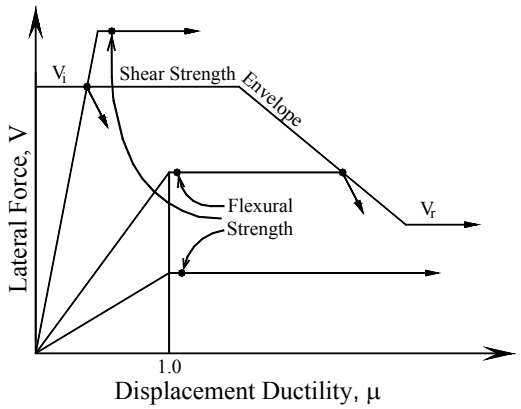

Figure 2.15 Interaction between shear strength and ductility, ATC-6 Model.

Due to the complexity of shear mechanisms that occur in masonry, no effective theoretical models have yet been proposed to accurately establish the shear strength of a masonry wall panel. Consequently, during practical calculation the nominal shear strength of reinforced masonry walls (V_n) is commonly evaluated as the sum of contributions from masonry, applied axial compression load and shear reinforcement. The three shear resistance mechanisms are incorporated into an equation of the following form:

$$V_n = V_m + V_p + V_s \qquad (2\text{-}15)$$

in which the term V_m represents the contribution to shear strength provided by the masonry, V_p represents the contribution of the axial load and V_s represents the contribution of shear reinforcement. A selection of existing masonry shear strength predictive equations are presented in this thesis. The original formats of some of the presented equations have been modified to introduce common notation and consistent units. All expressions are reported in SI units.

Matsumura (1988) shear equation

Matsumura developed a masonry shear strength equation by utilizing his test results, as well as test results reported by other researchers in Japan. Similar to Shing et al., Matsumura employed regression analysis to determine the appropriate functional forms of the parameters:

$$V_n = \left[k_u k_p \left(\frac{0.76}{(h/d)+0.7} + 0.012 \right) \sqrt{f'_m} + 0.2\sigma_n + 0.18\gamma\delta\sqrt{\rho_h f_{yh} f'_m} \right] (0.875td) \qquad (2\text{-}16)$$

where:

k_u = 1.0 for fully grouted masonry
= 0.64 for partially grouted masonry
k_p = $1.16\rho_{ve}^{0.3}$
γ = 1.0 for fully grouted masonry
= 0.6 for partially grouted masonry
δ = 1.0 for loading resulting in inflection point at mid-height of walls (double bending)
= 0.6 for loading of cantilever type (single bending)

This equation also includes a masonry term, along with axial load and shear reinforcement terms. As illustrated by Equation 2-16, the effect of aspect ratio (h/d) is included in the V_m term. Unlike Shing's equation (see Equation 2-17), only the vertical reinforcement provided by the edge bars is considered to be effective in providing shear resistance. Also, the form of the shear reinforcement term does not seem to be derived from any logical mechanisms.

Shing et al. (1990) shear equation

Shing et al. carried out tests on 22 masonry walls and developed the following shear strength equation:

$$V_n = \left(0.166 + 0.0217\rho_v f_{yv}\right)\sqrt{f'_m}A_n + \left(0.0217\sigma_n A_n\right)\sqrt{f'_m} + \left(\frac{L_w - 2d'}{s_h} - 1\right)A_h f_{yh} \quad (2\text{-}17)$$

This equation was developed to fit Shing's data using regression analysis. It follows the customary form in that there is a masonry component, an axial load component and a shear reinforcement component and provides good agreement with Shing's data. Shing et al. observed during their experimental study that the post-cracking strength of masonry increases in proportion to vertical steel content and the magnitude of axial compression load, mainly through resistance at the compression face due to aggregate interlocking and dowel action. These contributions to V_n are represented by the first and second terms of Equation 2-17, respectively. The V_s term of Equation 2-17 takes into account the ineffectiveness of the top and bottom layers of horizontal shear reinforcement due to insufficient embedment length to develop their yield capacity following diagonal shear cracking.

NZS 4230:1990

At the time the former New Zealand masonry design standard NZS 4230:1990 was released, it was recorded in the associated commentary that the shear strength provisions in this standard were overly conservative. This conservatism was mostly due to the scarcity at that time of relevant data on the shear strength of masonry when subjected to in-plane seismic forces. As mentioned earlier in section 2.4, the data sources used in the preparation of this standard were published in 1980 or earlier, such that no data obtained in the US and Japan during the late 1980s was available for the preparation of more accurate criteria.

NZS 4230:1990 adopted Equation 2-18 to calculate the shear strength of reinforced masonry walls. The shear strength is obtained by adding two terms; one term for the strength provided by the masonry component and the other for strength provided by the horizontal shear reinforcement:

$$V_n = v_m b_w d + A_h f_{yh} \, d/s_h \quad (2\text{-}18)$$

where v_m is equal to the greater of 0.30 MPa or $0.3\left(0.1f'_m + \sigma_n\right)$, except that $\left(0.1f'_m + \sigma_n\right)$ shall not be taken to exceed 2.4 MPa with f'_m not to be taken greater than 16 MPa, and the maximum permitted total shear stress shall be taken as $v_{n(max)} = V_n/\left(b_w d\right) = 0.2f'_m \le 2.4$ MPa. As shown in Figure 2.16, d is the effective depth and shall be taken as $0.8L_w$ for masonry walls subjected to in-plane loading.

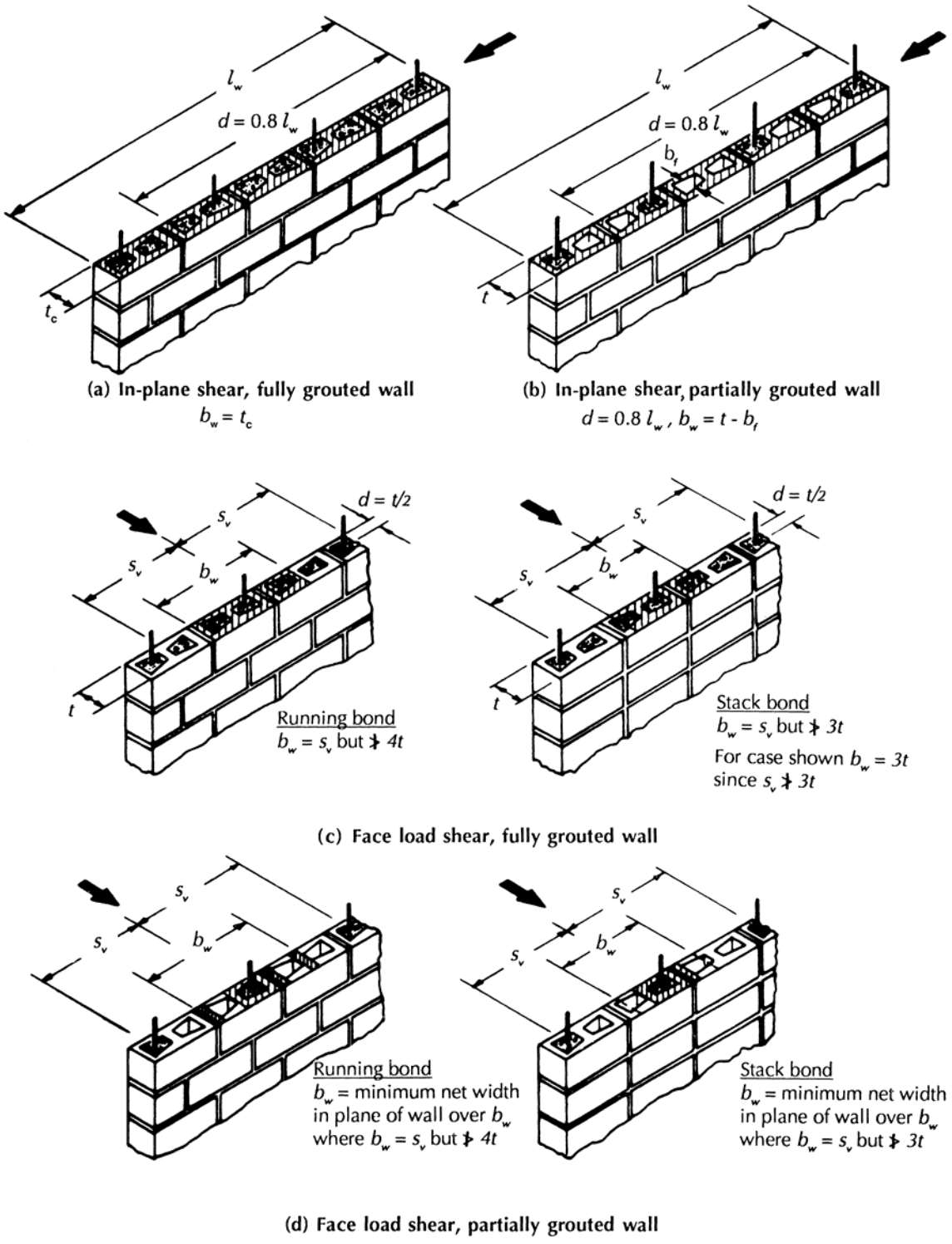

Figure 2.16 Effective areas for shear (NZS 4230:1990).

It is noted that the conceptual model illustrated in Figure 2.15 for concrete shear strength was adopted by NZS 4230:1990 in significantly simplified form. NZS 4230:1990 stated that the just mentioned v_m and $v_{n(max)}$ are only valid for walls that are not subject to cyclic loads into the inelastic range, i.e. no plastic hinges forming. For masonry shear strength within plastic hinge regions, v_m, shall be taken as zero, except for masonry structures of limited ductility ($\mu = 2.0$)

where v_m shall be assumed to be 0.15 MPa. Furthermore, $v_{n(max)}$ is reduced to the lesser of $0.15f'_m$ or 1.8 MPa within plastic hinge regions.

Anderson and Priestley (1992) shear equation

After reviewing Shing's and Matsumura's shear equations, Anderson and Priestley developed a significantly simplified equation to predict the ultimate shear strength of masonry walls tested by Sveinsson et al. (1985), Matsumura (1988) and Shing et al. (1990). This equation takes into account the degradation of shear strength when the wall is subjected to cyclic loading into the inelastic range, represented by the ductility coefficient factor, k, included in Equation 2-19. Anderson and Priestley proposed that within plastic hinge zones, the k factor shall be equal to 1.0 up to a flexural ductility ratio of 2, and then decrease linearly to zero at a ductility ratio of 4. The C_{ap} term is to account for the type of masonry used in construction, and shall be taken as 0.24 and 0.12 for concrete and clay brick masonry respectively.

$$V_n = C_{ap} A_n k \sqrt{f'_m} + 0.25\sigma_n A_n + 0.5 A_h f_{yh}\, d/s_h \qquad (2\text{-}19)$$

Equation 2-19 was developed from statistical data fitting and shows that the contribution from shear reinforcement to be half of that adopted for reinforced concrete members. In addition, Equation 2-19 did not include shear resistance attributed to the dowel action of vertical reinforcement.

NEHRP (1997)

One of the primary goals of the Federal Emergency Management Agency (FEMA) and the National Earthquake Hazards Reduction Program (NEHRP) is to encourage US design and building practices that address earthquake hazard and minimise the resulting damage. NEHRP adopted a masonry shear equation similar to that proposed by Anderson and Priestley (1992). However, the v_m term shown in Equation 2-20 was modified to include the parameter h_e/L to account for the effect of wall aspect ratio on masonry shear strength:

$$V_n = 0.083\left[4.0 - 1.75\frac{h_e}{L_w}\right] A_n \sqrt{f'_m} + 0.25\sigma_n A_n + 0.5 A_h f_{yh}\, L_w/s \qquad (2\text{-}20)$$

where h_e/L_w need not be taken greater than unity. It is noted here that the NEHRP expression does not address masonry shear strength within the plastic hinge regions for masonry structures that are subjected to inelastic response. Similar to Anderson and Priestley (1992), NEHRP did not consider shear resistance attributed to dowel action of longitudinal reinforcement. Depending on the magnitude of h_e/L_w, the maximum total shear strength $V_{n(max)}$ is limited as follows:

$$V_{n(max)} = 0.5A_n\sqrt{f'_m} \qquad \text{for } \frac{h_e}{L_w} \le 0.25 \text{ or}$$

$$V_{n(max)} = 0.33A_n\sqrt{f'_m} \qquad \text{for } \frac{h_e}{L_w} \ge 1.00$$

with straight line interpolation to be used for $\frac{h_e}{L_w}$ values between 0.25 and 1.00.

Uniform Building Code (1997)

The Uniform Building Code (UBC) contains an empirical formula, shown in Equation 2-21, for calculating the shear strength of reinforced masonry walls. The nominal shear strength is obtained by adding two terms: the first term is for strength provided by the masonry and the second term accounts for the strength provided by the shear reinforcement. The UBC presents several design assumptions that are essential when using the formula to calculate the nominal shear strength:

1. The nominal shear strength of an individual reinforced masonry wall cross-section is based on applicable conditions of equilibrium and strain compatibility;
2. Strains in the reinforcement and masonry are assumed to be directly proportional to the distance from the neutral axis;
3. Maximum usable strain at the extreme masonry compression fibre is assumed to be 0.003;
4. Stress in the reinforcement below the specified yield strength, f_{yh}, is taken as the elastic modulus, E_s, times the steel strain;
5. For strains greater than the yield strain the stress in the reinforcement is equal to the yield stress, f_{yh}.

$$V_n = 0.083C_dA_n\sqrt{f'_m} + A_hf_{yh}\frac{L_w}{s_h} \le 0.33A_n\sqrt{f'_m} \qquad (2\text{-}21)$$

Depending on the h_e/L_w, the nominal shear strength coefficient, C_d, is evaluated as follows:

for $\frac{h_e}{L_w} < 0.25$, $C_d = 2.4$;

for $0.25 \le \frac{h_e}{L_w} \le 1.0$, $C_d = 2.8 - 1.6\frac{h_e}{L_w}$;

for $\frac{h_e}{L_w} > 1.0$, $C_d = 1.2$.

AS 3700-1998

The Australian masonry standard (AS 3700-1998) provides an empirical formula, as shown in Equation 2-22, for calculating the in-plane shear strength of reinforced masonry walls:

$$V_n = f_{vr}A_n + 0.8f_{yh}A_s \qquad (2\text{-}22)$$

where:

$$f_{vr} = \left(1.50 - 0.5\frac{h_e}{L_w}\right) \text{MPa; and}$$

A_s = the cross-sectional area of reinforcement, as follows:

(i) If $\frac{h_e}{L_w} > 1.0$; A_s = area of horizontal reinforcement.

(ii) If $\frac{h_e}{L_w} \leq 1.0$; A_s = the total cross-sectional area of horizontal reinforcement, or total cross-sectional area of vertical reinforcement, whichever is less.

The Australian masonry design standard states that the following requirements are essential when using the above formula to calculate the masonry shear strength:

1. The reinforcement shall be located symmetrically in the cross-section.
2. Vertical reinforcement shall be spaced at centres not exceeding 0.75h and in any case not greater than 200 mm horizontally. Horizontal reinforcement shall be spaced at centres not exceeding $0.75L_w$ and in any case not greater than 3000 mm vertically.
3. The vertical reinforcement shall be such that $A_s \geq 0.0013A_n$ and the horizontal reinforcement be such that $A_s \geq 0.0013A_n$. If the reinforcement does not meet these requirements then the wall shall be designed as an unreinforced masonry wall.

2.5 STRENGTH CAPACITY OF PERFORATED MASONRY WALL

Because of their role as lateral load resisting elements, masonry shear walls have attracted the attention of many researchers. However, most of this research was carried out to study the behaviour of solid masonry shear walls, despite the fact that masonry walls are commonly constructed with openings. Introducing openings in a wall alters its behaviour and adds complexity and difficulties in analysis and design. An extensive literature review by Voon and Ingham (2003) verified the earlier finding by Brammer (1995) that there exists little data from outside New Zealand that is directly relevant to the performance of nominally reinforced

masonry walls that were constructed according to the specifications contained in NZS 4229:1999. This section of the report provides a brief review of those studies that are direct relevance towards the issues discussed in Section 1.2.2.

2.5.1 Experimental Research

Brammer (1995) performed quasi-static in-plane cyclic load tests on twelve nominally reinforced concrete masonry walls. Nine of these walls were partially grout-filled, where only those cells containing vertical reinforcement were grouted, and the remaining three walls were solid grout-filled. All walls were constructed to a common height of 2400 mm with horizontal reinforcement placed in a bond beam within the top two courses, but varied in wall length and thickness (see Figure 2.17 for typical reinforcement of a nominally reinforced concrete masonry wall). None of the walls had applied axial load. The main objective of this study was to compare the attained test behaviour with that assumed and predicted by the New Zealand design standards NZS 4229 and NZS 4230:1990, and to examine the response of nominally reinforced masonry walls when subjected to cyclic loading. Attention was given to maximum strength, stiffness, ductility, modes of failure, force-displacement characteristics, base course slip, and also the shear and flexural components of displacement.

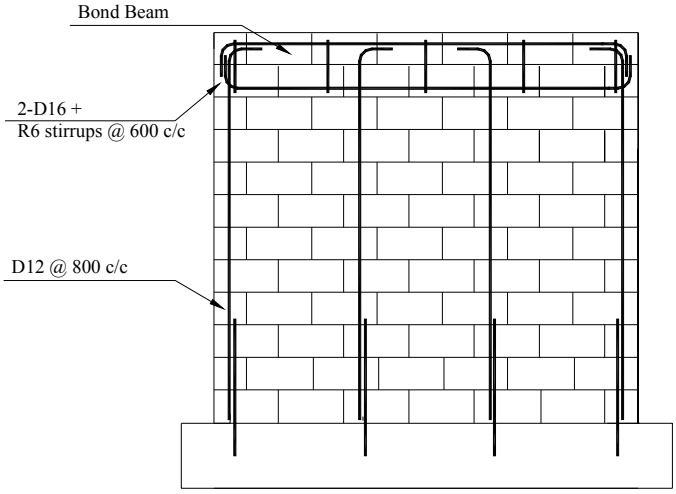

Figure 2.17 Typical reinforcement details of nominally reinforced concrete masonry wall.

Due to the lack of horizontal shear reinforcement in the walls of Brammer's study, it was observed that most walls failed in diagonal tension with failure characterized by the development of early flexural cracking which was later exaggerated by diagonal cracking that extended throughout the whole masonry wall. Figure 2.18 shows the force-displacement response derived from two typical wall tests, for partially grout-filled walls with lengths of 2600 mm and 4200 mm respectively. In both cases, the walls were constructed of 15 series

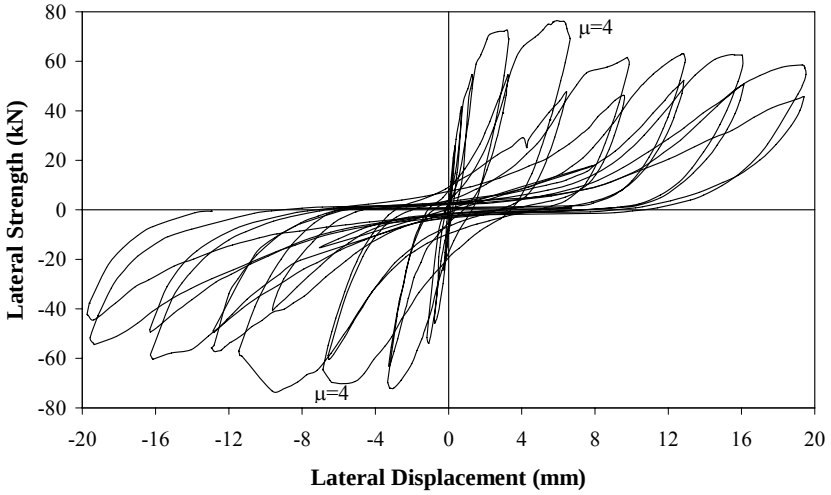

(a) 2600 x 2400 x 140

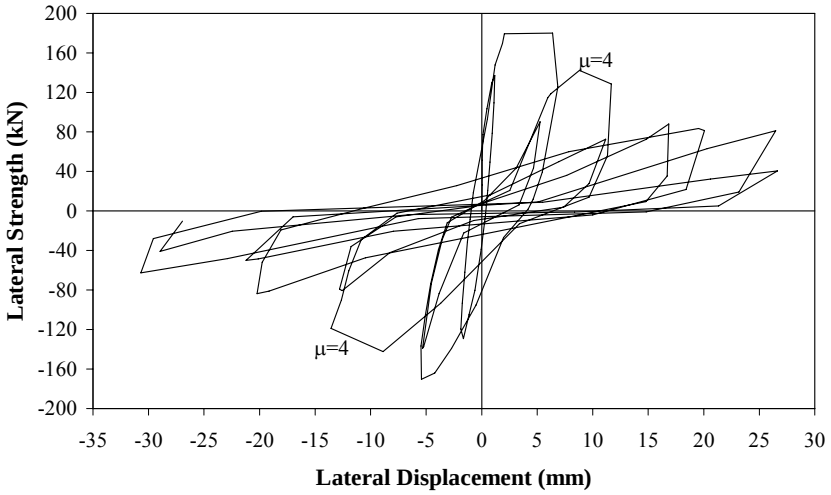

(b) 4200 x 2400 x 140

Figure 2.18 Force-displacement histories of partially grout-filled concrete masonry walls.

concrete masonry precast units, therefore resulted in wall thickness of 140 mm. From Figure 2.18 a number of general characteristics of partially grout-filled concrete masonry walls can be identified:

1. The maximum strength was typically developed during the first excursion to $\mu = 4$. Following this, cracking became significant and strength degraded.
2. Less hysteretic energy was expended during the second cycle to any displacement level, when compared with the first displacement cycle. This is illustrated by the more pinched hysteresis loops on the second cycle.
3. None of the tests exhibited a sudden failure, as is typically with conventional shear failure. Instead, strength degraded in a gradual manner.

4. Lateral displacements mostly arose from both flexure and shear modes of deformation. The presence of shear deformation is implied in Figure 2.18 through the pinched nature of the inelastic hysteresis loops.
5. The absence of damage in the solid grout-filled bond beam and the general geometry of the deformed walls supported the notion of frame-type action being developed at later stages of testing.

An important finding concluded from this study was that the ductile diagonal tension mode developed even in the case when the dependable shear strength predicted using NZS 4230:1990 shear expressions was less than the wall nominal flexural strength. This indicated that the predicted shear strength using NZS 4230:1990 was of limited relevance for concrete masonry structures having a reinforcement distribution as indicated by Figure 2.17 and supporting little axial compressive load. It was concluded that this was partially because NZS 4230:1990 was conservative in shear prediction, but more importantly due to the frame action generated by the use of a bond beam and the shear friction generated between blocks during lateral deformation. The information collected from Brammer's study was then used to develop the bracing capacity tables presented in NZS 4229:1999.

Davidson (1996) extended Brammer's research to investigate the behaviour of walls with openings and applied axial compression stress. Two nominally reinforced concrete masonry walls having the same geometry (4200 mm long x 2400 mm high x 190 mm wide) were constructed so that they had an identical arrangement of a 2000 mm x 600 mm 'doorway' and a 1200 mm x 600 mm 'window' (see Figure 1.2a), with the only difference being the magnitude of the applied axial compressive load. The 'doorway' and 'window' were arranged in a manner enabling the vertical reinforcement to be placed at 800 mm centres. Note that the reinforcement used in this study was of f_y = 275 MPa.

The force-displacement response of the 4200 mm long perforated concrete masonry wall with axial compressive load is shown in Figure 2.19. A comparison of this test result with those obtained by Brammer (1995) illustrated that the capacity of the masonry wall with openings, tested by Davidson, was approximately half that of the complete wall. Furthermore, the test results successfully showed that compression stress was effective in increasing the lateral strength of the perforated masonry wall. Consequently, it was concluded from this study that openings have a detrimental effect on the lateral strength of masonry walls while axial compression stress is beneficial. Furthermore, it was successfully illustrated that a plastic hinge

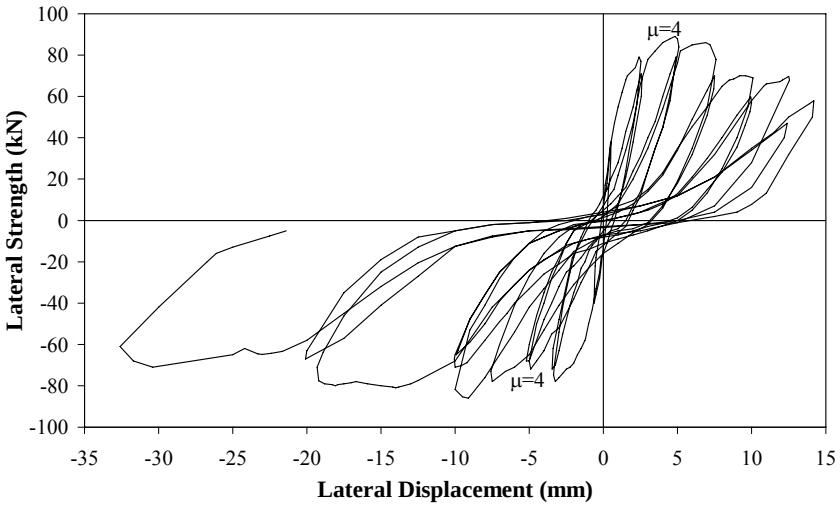

Figure 2.19 Force-displacement history of partially grout-filled concrete masonry wall with openings.

model which assumed flexural hinges forming at the bases of all piers, at the top of the central pier and in the lintels was able to represent the bracing capacity of the partially grout-filled masonry walls included in this study.

Singh (1998) investigated the serviceability and strength performance of a full-scale reinforced concrete masonry wall with Ribraft^{TM} floor. The wall was C-shaped in plan and was partially grouted. The results showed that masonry wall behaved in a ductile manner, and that response remained elastic to an out-of-plane load of approximately 6 kPa. The wall reached the ultimate limit state deflection criterion of 2% drift at a load of 7.6 kPa. The crack and deflection patterns were as predicted by the yield-line theory, which however provided a conservative estimate of the out-of-plane failure load of 5.0 kPa. The test was halted at a load of 10.7 kPa at which the main wall did not collapsed but were supported by the return walls.

Zhang (1999) investigated the out-of-plane performance of partially grouted, reinforced concrete masonry walls that were subjected to simulated seismic loading. Three full-scale walls, with and without openings, were constructed from 190 mm thick concrete masonry blocks and were 9.0 m long and 2.4 m high with two 2.5 m long return walls. A minimum quantity of reinforcement permitted by NZS 4229 was used, and additional diagonal bars were added to the corners of the bond beam at wall top. The test results showed that the specimens exhibited ductile behaviour with pinched shape of hysteresis response and that the ultimate out-of-plane strengths of the walls were considerably greater than the demands calculated according to the New Zealand concrete and masonry standards. The test results indicated that the location and size of openings influenced the wall strength significantly. Yield line theory

gave a safe but conservative prediction of the out-of-plane strength of these three masonry walls.

Elshafie et al. (2002) conducted experimental testing on thirteen single storey-height $^{1}/_{3}^{rd}$-scale solid grout-filled masonry walls with openings. The primary objective of this study was to develop a simple analysis approach employing plastic hinge failure mechanisms to predict failure mechanism and lateral load carrying capacity. The test specimens in this study were designed to behave mainly in a flexural mode by forming plastic hinges at the member ends (i.e. enough shear reinforcement was provided to suppress shear failure in different wall elements). Experimental results from this study showed that the plastic hinge model developed by Leiva at al. (1990a, 1990b and 1994) provided a good estimate for the lateral load capacity of masonry shear walls containing openings. Consequently, the following failure mechanisms may develop, depending on the relative strength of the wall sections:

a) Strong pier/weak beam mechanism in which the wall fails by forming plastic hinges (shaded areas) at both ends of the coupling beam(s), then plastic hinges at the pier bases as shown in Figure 2.20a;
b) Strong beam/weak pier mechanism in which the wall fails by forming plastic hinges at both ends of all piers as shown in Figure 2.20b;
c) Mixed mechanism in which a combination of mechanisms (a) and (b) develops as shown in Figure 2.20c.

The experimental results of Elshafie et al. (2002) indicated that a simple model proposed by Hart et al. (1988) provided a good estimate for the post-cracking stiffness of the test specimens. Also, it was observed in this study that for shear walls with similar overall dimensions and flexural reinforcement arrangements, the effects of openings on the reduction of the wall strength and stiffness were proportional, i.e. the ratio of reduction in stiffness due to openings is equal to the ratio of reduction in strength.

2.5.2 NZS 4229:1999 Codification of Wall Capacity

The in-plane lateral strength of a concrete masonry wall panel is specified in NZS 4229:1999 through determination of its bracing capacities, where such bracing capacities were calculated considering the masonry performance once the nominal shear strength had been exceeded. As demonstrated by Brammer (1995), it was established that nominal lateral strength was satisfactorily evaluated based on a rectangular masonry compression stress block using

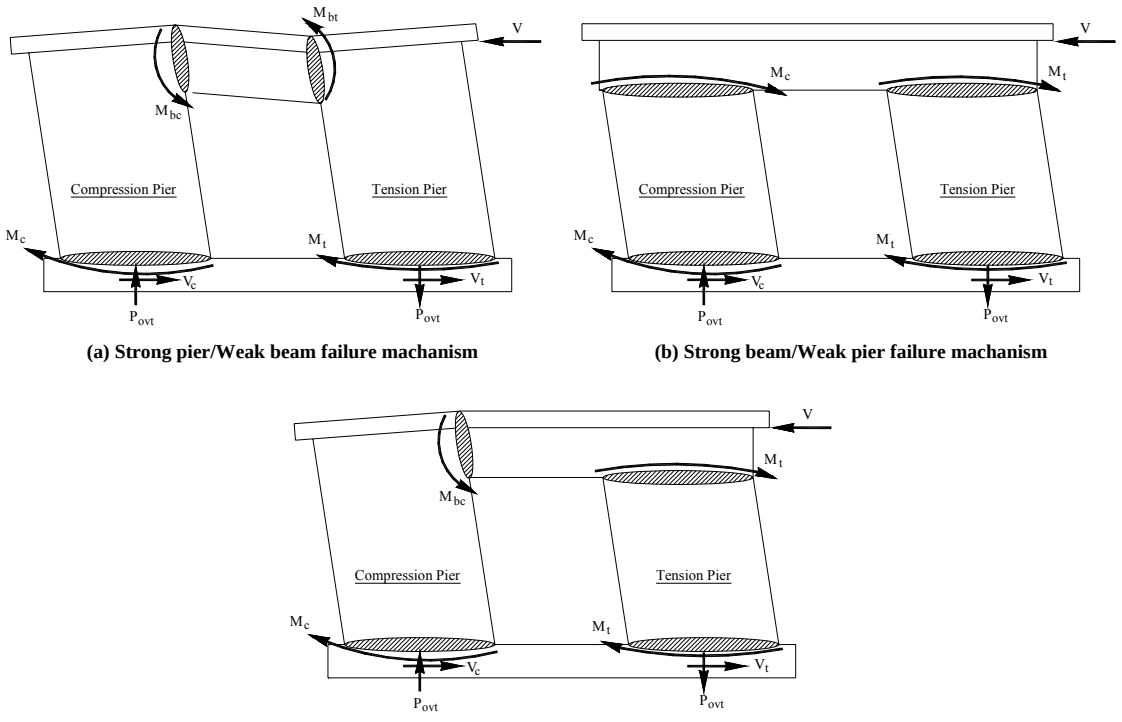

Figure 2.20 Failure mechanisms for wall with opening.

Equation 2-6, assuming $f_y = 300$ MPa and $f'_m = 8$ MPa, and treating the walls as vertical flexural cantilevers with a height measured to the centre of the fully grouted bond beam. Bracing capacities are reported in NZS 4229:1999 in tabular form for various wall thickness and grout-fill options, as illustrated in Table 2.1 for partially grouted 15 Series (140 mm thick) concrete masonry, where 100 bracing units corresponds to 5 kN. It is necessary to point out that conservatism of the NZS 4229:1999 evaluated bracing capacities with respect to the experimental results (Brammer, 1995 and Davidson, 1996) was primarily attributed to the actual material strengths being significantly greater than specified, the adoption of a flexural strength reduction factor of $\phi = 0.8$, and a further reduction to 80% of the evaluated capacity for walls having a length greater than 3.0 m. Also, in all cases the calculation assumed the vertical reinforcement of ∅ 12 mm to be distributed at a maximum spacing of 800 mm (where possible) or for bars to be spaced in the least favourable positions, resulting in the most conservative flexural strength.

Recalling that NZS 4229:1999 is primarily intended for use by architects and draftspersons, rather than structural engineers, a simplified procedure was adopted for the assessment of bracing capacity. The strategy employed in NZS 4229:1999 for proportioning bracing capacity is primarily dependent on wall geometry. The assumption was that the bracing capacity of a

masonry wall having penetrations could be determined based on the geometry of individual bracing panels, as demonstrated by the shaded areas shown in Figure 6.6, where the geometry of each bracing panel is based upon the vertical dimension of the smallest adjacent opening. The total bracing capacity is then assumed to be the sum of the capacities provided by the individual bracing panels of the wall. From Table 2.1 it is evident that the wall bracing capacity increases as the panel length increases, but diminishes as the panel height increases. This prompted some observers to comment on the influence which a small wall opening would have, as this would effectively generate two bracing panels with a small height, rather than a single panel that is taller and longer, such that it is conceivable that the addition of a small wall opening might result in the evaluated capacity of the wall to increase.

Table 2.1 Bracing capacities* for 15 series partially grouted concrete masonry

Panel height (m)	**Panel length (m)**										
	0.8	**1.2**	**1.6**	**2.0**	**2.4**	**2.8**	**3.2**	**3.6**	**4.4**	**5.2**	**6.0**
0.8	385	650	1005	1425	1935	2505	2525	3110	4455	6040	7870
1.0	330	560	865	1230	1670	2165	2185	2690	3855	5225	6810
1.2	275	470	730	1035	1405	1825	1840	2265	3250	4415	5750
1.4	245	420	650	930	1260	1635	1650	2030	2920	3960	5160
1.6	215	370	575	820	1115	1445	1460	1800	2580	3505	4575
1.8	195	335	525	750	1020	1325	1340	1650	2370	3220	4200
2.0	180	305	480	680	925	1205	1220	1500	2155	2930	3825
2.2	165	280	445	635	860	1120	1335	1400	2005	2730	3565
2.4	155	260	410	585	800	1040	1050	1295	1860	2530	3305
2.6	145	245	385	550	750	980	985	1220	1755	2385	3115
2.8	130	230	360	515	705	915	925	1140	1645	2240	2920
3.0	125	215	340	490	665	870	880	1085	1560	2125	2780

* 100 Bracing Units corresponds to 5 kN

2.5.3 Shrinkage Control Joint

Differential movement creates cracking in masonry construction when excessive stress is allowed to develop. Control joints are one method used to relieve horizontal tensile stresses due to shrinkage of the concrete masonry units, mortar, and when used, grout. They are essentially vertical separations built into the wall at locations where stress concentrations may occur. Control joints are typically only required in exposed concrete masonry walls, where shrinkage cracking may detract from the appearance of the wall. Shrinkage cracks in concrete

masonry are an aesthetic, rather than a structural concern (Beck et al., 1988). In many cases, horizontal reinforcement is used to control shrinkage cracking, but strategically located control joints will further assist in the elimination of random cracks, and prevent moisture penetration which might otherwise occur.

The placing of control joints in walls is a matter of judgement by the designers with consideration being given to the type of construction, shape of walls (accounting for features such as openings), the amount of reinforcement in the walls and exposure to weather. In the case of nominally reinforced concrete masonry walls, NZS 4229:1999 requires shrinkage control joints to be provided at no more than 6 m centres. In addition, NZS 4229:1999 requires that vertical control joints be located:

a) Within 600 mm of return angles in T and U-shape structures;
b) Within 600 mm of L shaped corners or by restricting the spacing to the next control joint to 3.2 m maximum;
c) At changes in wall height exceeding 600 mm;
d) At changes in wall thickness.

NZS 4229:1999 requires that the non-structural reinforcement, such as the horizontal reinforcement that is used for crack control only, should be discontinuous through a control joint, since this will otherwise restrict horizontal movement. However, structural reinforcement, such as bond beam and lintel reinforcement at the floor and roof diaphragms that resists diaphragm cord tension, must be continuous through the control joint.

Chapter 3

STRUCTURAL TESTING – SERIES A

3.1 INTRODUCTION

A total of ten concrete masonry cantilever walls were tested in the Civil Engineering Test Hall at the University of Auckland. The primary objective of this experimental programme was to investigate the shear strength of masonry walls constructed of materials locally available in New Zealand and to supplement worldwide experimental data currently available. A description of this wall testing programme is followed by a presentation of results from the structural testing of eight fully grout-filled walls and two partially grout-filled walls. Discussion of the results is concerned with wall structural response in term of shear strength.

The main variables being considered in Series A were as follows:

1. The amount of horizontal reinforcement,
2. Distribution of horizontal reinforcement,
3. The level of axial compression stress,
4. The type of grouting,
5. The influence of h_e/L_w ratios on masonry shear strength.

3.2 CONSTRUCTION DETAILS

3.2.1 Wall Specifications

The dimensions and reinforcement details for the ten walls are summarised in Table 3.1 and Figure 3.1. All walls (except Walls A5 and A6) were fully-grouted and had vertical reinforcing steel spaced at 400 mm centres, but varied in the quantity and positioning of horizontal shear reinforcement. The horizontal shear reinforcing steel was uniformly distributed evenly up the height of the walls and was hooked (180^o bend) around the outermost wall vertical reinforcing bars. Walls A5 and A6 were partially grout-filled with no horizontal shear reinforcement and their vertical reinforcement was spaced at 400 mm and 800 mm respectively. For the two partially grout-filled walls, only cells containing reinforcing bars were filled with grout. Walls A1 to A6 were tested without externally applied vertical axial compression load. Walls A7 and A8 were duplicates of Wall A1, but with externally applied axial compression stress of 0.5

MPa and 0.25 MPa, providing an average compressive load of 126 kN and 63 kN respectively to the two walls. Walls A9 and A10, which were constructed to h_e/L_w ratios of 2.0 and 0.6, were both subjected to axial compression stress of 0.25 MPa, providing an average compressive load of 63 kN and 105 kN in each wall. All test walls (except Wall A3) were designed to have a dominant shear type of failure. Wall A3 was designed to fail in flexure.

The walls tested at the University of Auckland supplemented existing experimental data by providing new data for masonry walls with low shear reinforcement ratios ($\rho_h \leq 0.0625\%$) and low axial compression stress levels ($0 \leq \sigma_n \leq 0.5$ MPa). Experimental studies reported in Chapter 2 investigated shear strength of masonry walls with higher shear reinforcement ratios ($0 \leq \rho_h \leq 0.668\%$) and higher axial compression stress levels ($0 \leq \sigma_n \leq 5.87$ MPa).

Table 3.1 Masonry wall specimens

Wall	H	L_w	Effective width	h_e	h_e/L_w	Reinforcement		ρ_h	Grouting	Axial stress
						Vertical	Horizontal			
A1	1800	1800	140	1800	1.0	5-D20	5xR6	0.05	Full	---
A2	1800	1800	140	1800	1.0	5-D20	1-R6	0.01	Full	---
A3	1800	1800	140	1800	1.0	5-D20	5-D10	0.14	Full	---
A4	1800	1800	140	1800	1.0	5-D20	2-D10	0.06	Full	---
A5	1800	1800	60	1800	1.0	5-D20	---	---	Partial	---
A6	1800	1800	60	1800	1.0	3-D20	---	---	Partial	---
A7	1800	1800	140	1800	1.0	5-D20	5-R6	0.05	Full	0.50
A8	1800	1800	140	1800	1.0	5-D20	5-R6	0.05	Full	0.25
A9	3600	1800	140	3600	2.0	5-DH25	9-R6	0.05	Full	0.25
A10	1800	3000	140	1800	0.6	8-D20	5-R6	0.05	Full	0.25
Units	mm	mm	mm	mm	---	---	---	%	---	MPa

3.2.2 Construction Materials

All walls were constructed by experienced masons under supervision, and employed a running bond pattern of standard production 15 series (140 mm wide) precast concrete masonry units (CMUs). 140 mm wide CMUs were adopted for the tests to ensure that high shear stresses

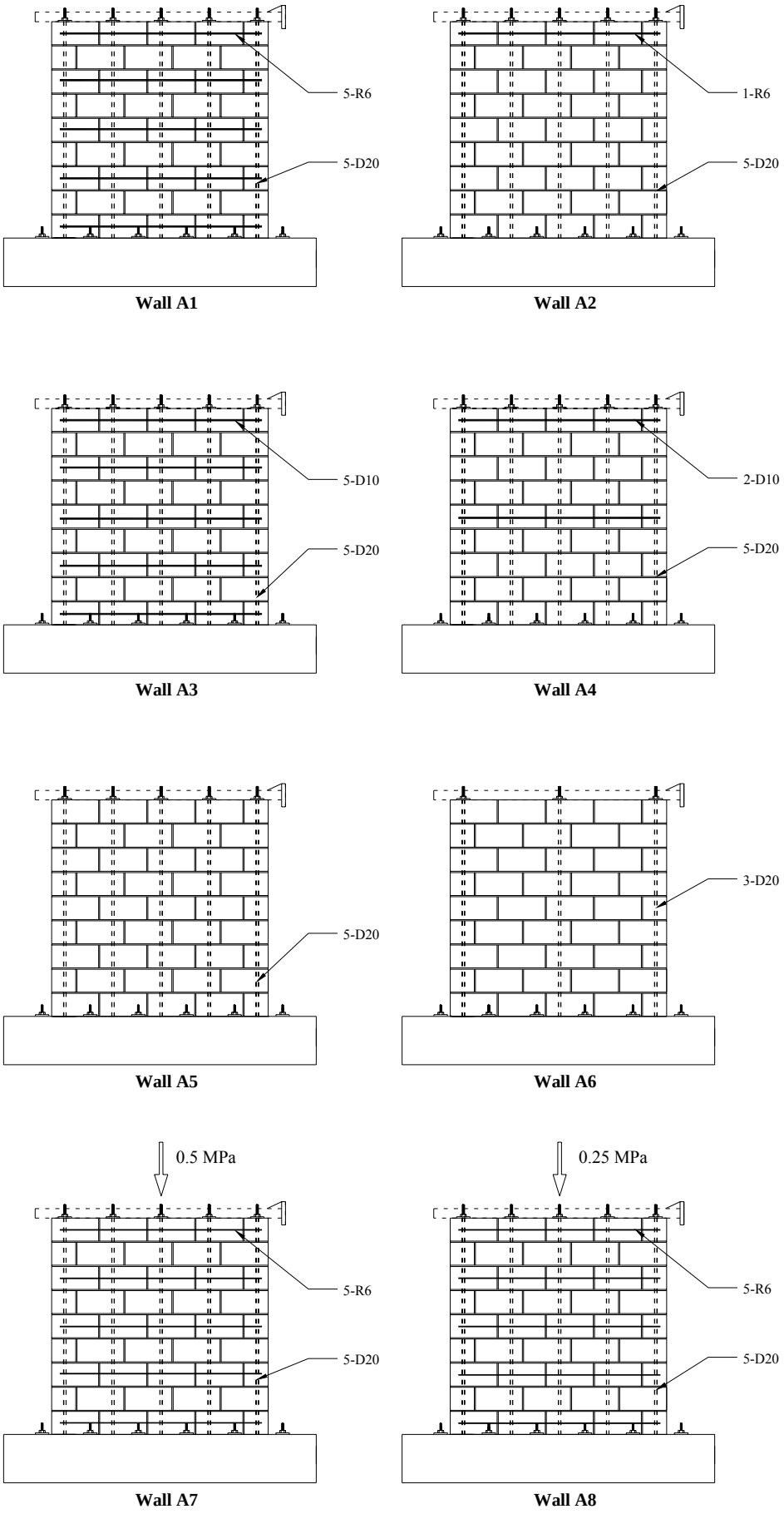

Figure 3.1 Series A-Wall reinforcing details.

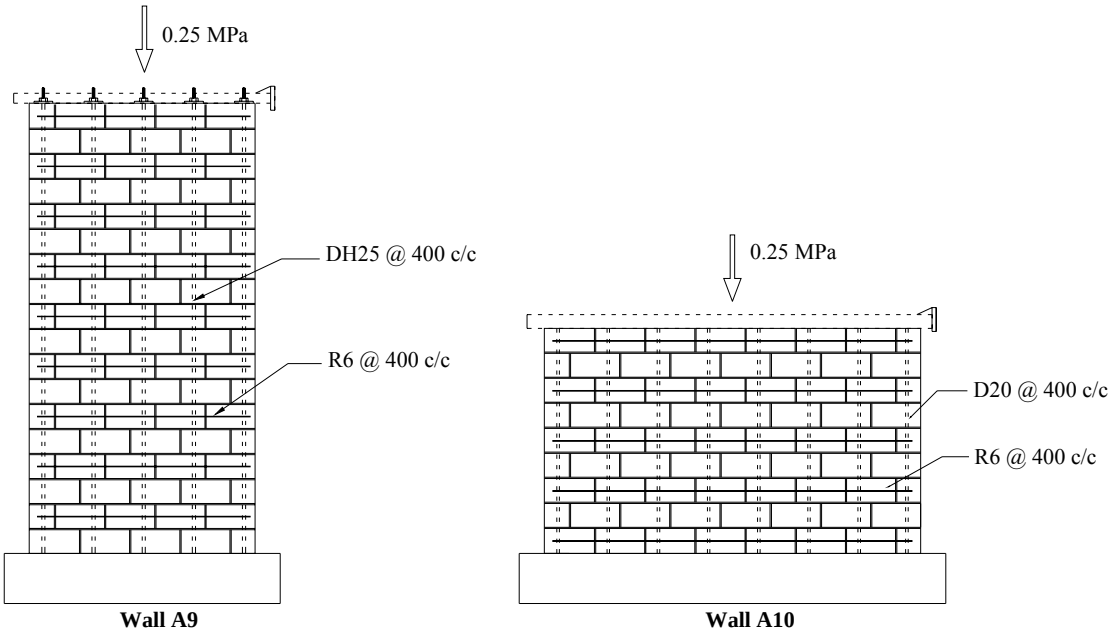

Figure 3.1 Series A-Wall reinforcing details (continued).

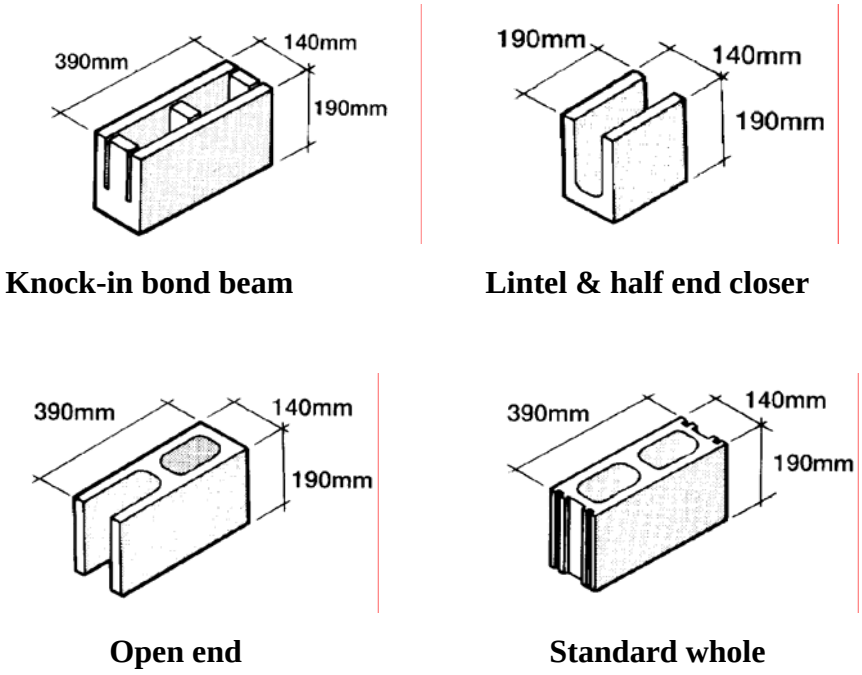

Figure 3.2 15-Series concrete masonry units.

could be applied within the maximum load restrictions of the hydraulic actuators available at the University of Auckland. Open-end bond beam CMUs having a depressed web were used throughout the wall height to allow the horizontal shear reinforcement to be positioned at all levels and to enhance the continuity of grout.

Dricon^{TM} trade mortar, being a bagged 1:4 portions of Portland cement and sand by volume, was used throughout. High slump ready-mix grout using small aggregate (7 mm) was employed for filling the cavities within the test walls and a common commercially used expansive chemical additive was added to the grout to avoid formation of voids caused by high shrinkage of the grout.

All reinforcing steels used was grade 300 MPa (except Wall A9), consisting of D20 for the vertical reinforcement, and R6 or D10 for the horizontal reinforcement. The detailing of vertical reinforcement is discussed in section 3.3, while the horizontal shear reinforcement was hooked around (180^{o} bend) the extreme vertical reinforcement. Wall A9 was the only specimen that used grade 500 MPa steels for its longitudinal reinforcement.

3.2.3 Material Properties

Masonry prisms were built at the completion of laying each wall (see Figure 3.3), using the same mortar and CMUs used in the wall. These prisms were built of three CMUs stacked on top of each other using the same construction technique as was used for the wall. The prisms were then filled at the same time as the walls, using the same grout. The prisms were tested using an Avery Testing Machine as shown in Figure 3.4. This type of test specimen provided the most accurate estimate of masonry compressive strength, f'_m . It was noted that f'_m for concrete masonry walls constructed of regular materials, found by prism testing at the University of Auckland, has consistently been above the f'_m = 12 MPa specified by NZS 4230:2004 for Type B Observation masonry.

Samples were taken from steel reinforcement used as flexural and shear reinforcement in the wall panels. The samples were subjected to tensile testing using the Avery Universal Testing Machine at the University, see Figure 3.5. Each type of reinforcing steel used in the walls was from the same batch. Consequently, the average yield strengths for the R6, D10 and D20 reinforcing steel were established to be 325 MPa, 320 MPa and 318 MPa respectively. An illustration of the tensile test results is presented in Figure 3.6.

Figure 3.3 Masonry prism grouting.

Figure 3.4 Masonry prism subjected to compression test.

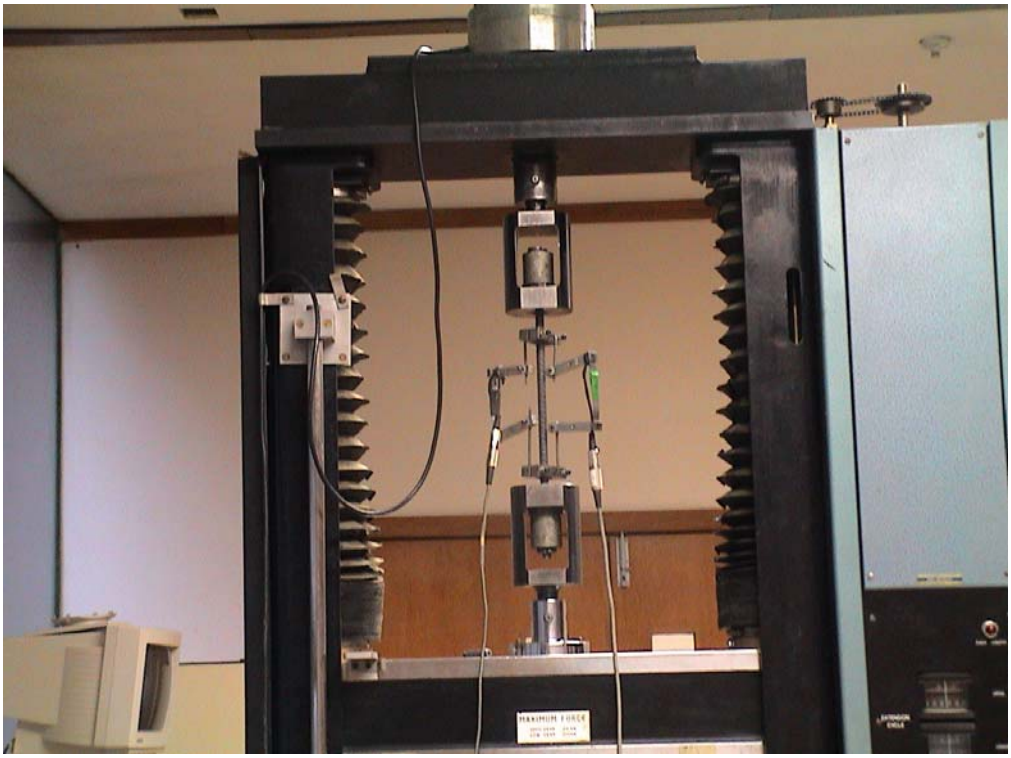

Figure 3.5 Reinforcing steel subjected to tensile test.

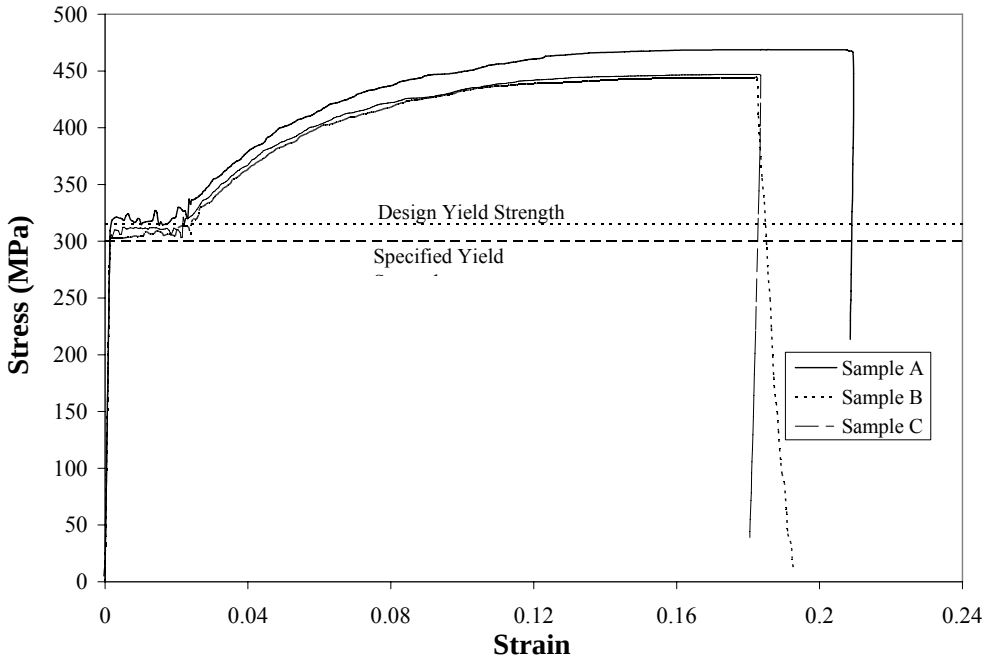

Figure 3.6 Stress-strain curve for D20 reinforcing bars.

3.3 TESTING DETAILS

3.3.1 Test Setup

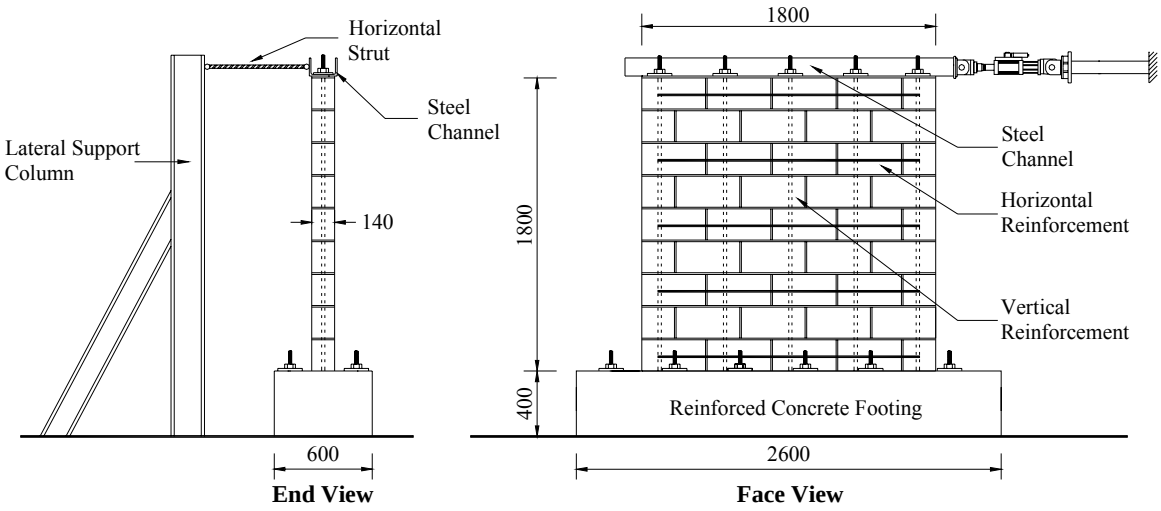

Figure 3.7 Typical test setup, Series A.

The typical test set-up is shown in Figure 3.7, primarily consisting of a reinforced concrete footing and a horizontally mounted hydraulic actuator providing a horizontal shear force to the top of the wall through a 150 x 75 steel channel section (herein called the loading beam). The wall was stabilised from moving in its out-of-plane direction by two parallel horizontal struts which were positioned perpendicular to the wall and hinged to the channel and a reaction frame. The test specimens were designed based upon the limiting capacity of the hydraulic actuators at the University of Auckland, from which it was established that a maximum test design force, when using a single hydraulic jack, of 275 kN and 370 kN in the respective pulling and pushing directions would be appropriate. As shown in Figure 3.7, the dimensions of the walls were such that the block size was sufficiently small compared to the panel size. It is recognised that this type of horizontal force transfer is of a cantilevered wall type and therefore may not be representative of all structures. Additional detailed description of the test setup is reported in Voon and Ingham (2003).

All walls, except Wall A9, were constructed on re-usable reinforced concrete footings. The concrete footing shown in Figure 3.8 had DH32 starter bars spaced at 400 mm centres that were drilled and tapped to accommodate D20 vertical reinforcement. The concrete footing was stressed down to the laboratory floor with high strength steel rods, each loaded to approximately 300 kN so that sufficient shear friction was provided to eliminate any slip between the footing and the floor. Each of the wall vertical reinforcement bars was first tapped at both ends, then threaded into the DH32 starters that protruded from the reinforced concrete

base. Once the loading beam was placed on top of the concrete masonry wall using a pack of trade mortar for best possible shear force transfer between the wall and the loading beam, the vertical reinforcement was tightened. Wall A9 was the only specimen that was constructed on a purpose-built reinforced concrete footing with cast-in DH25 vertical reinforcement spaced at 400 mm centres.

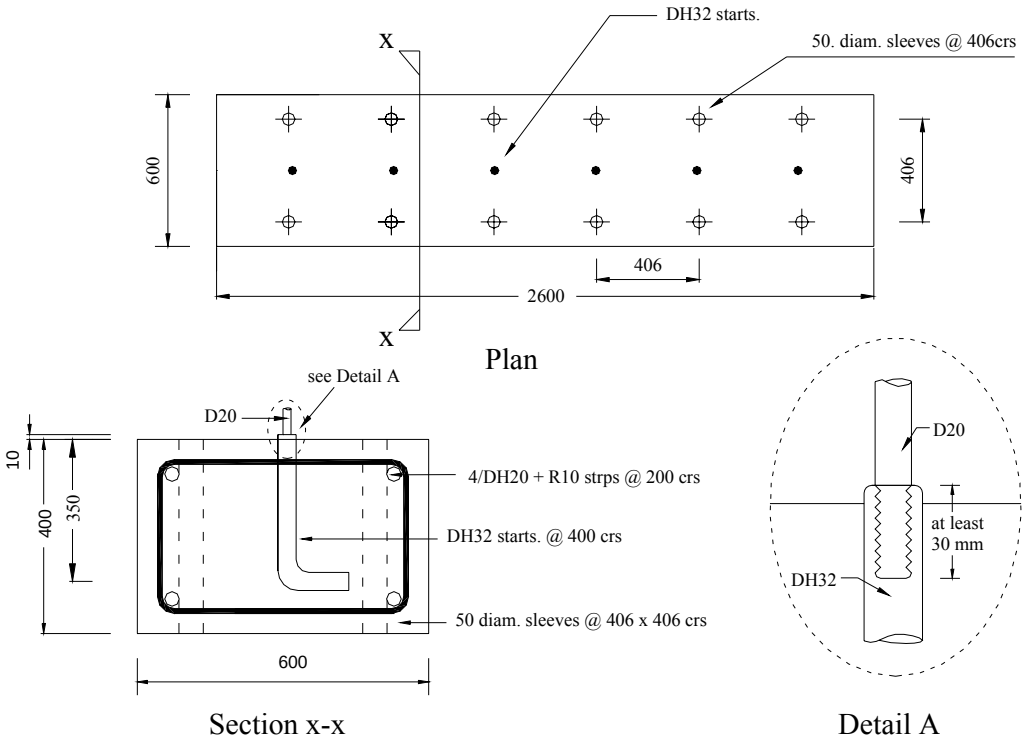

Figure 3.8 Details of concrete footing.

In order to determine the effect of threading on the yield strength of D20 reinforcing bar, two types of bar were subjected to tensile test. Figure 3.9 compares test results of the threaded and unthreaded D20 reinforcing bars. It is clearly illustrated in the figure that threading had negligible effect on the yielding strength of D20 but the figure also shows that the threading significantly reduces the post elastic performance of the D20 reinforcing steel. However, such reduction in the post elastic performance of the D20 reinforcing steel would have negligible effect on the performance of the masonry walls presented in this study since these masonry walls were designed to exhibit shear failure mode. Consequently, failure of the walls was expected to be reached at low drift ratio.

For the testing of Walls A7 to A10, the test set-up was similar to that shown in Figure 3.7, but with two 250 x 90 steel channels (tightly fastened together) set on top of the loading beam in order to provide proper transfer of axial compressive stress into the entire wall. The axial compression force was applied to the wall through the action of 2 pairs of high strength 23 mm

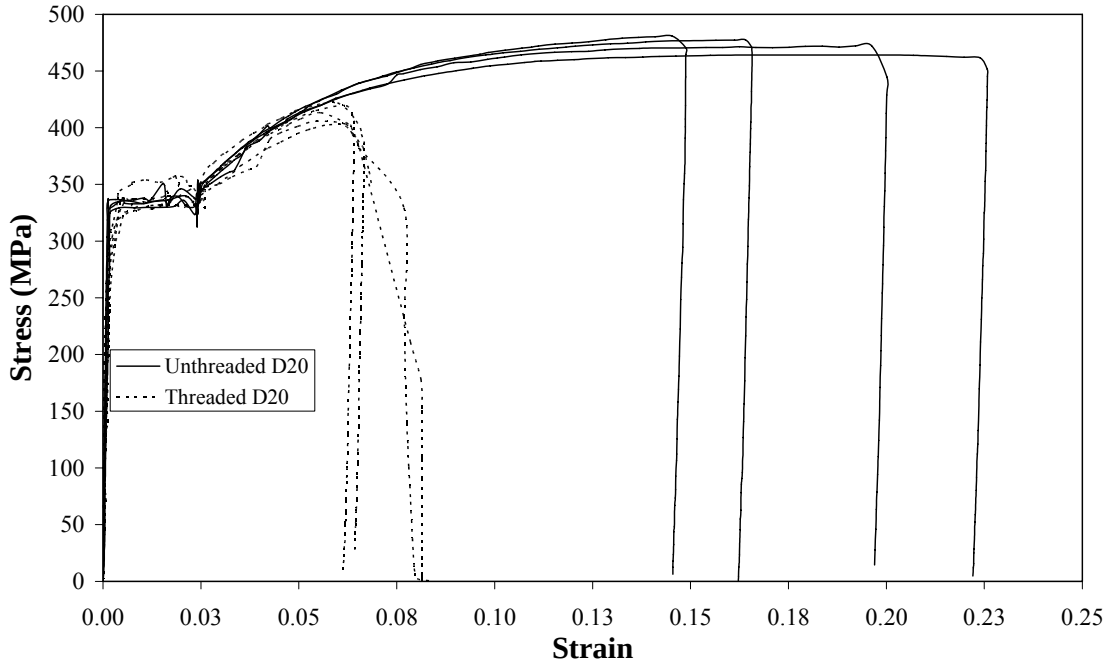

Figure 3.9 Stress-strain curve for the threaded and unthreaded D20 reinforcing bars.

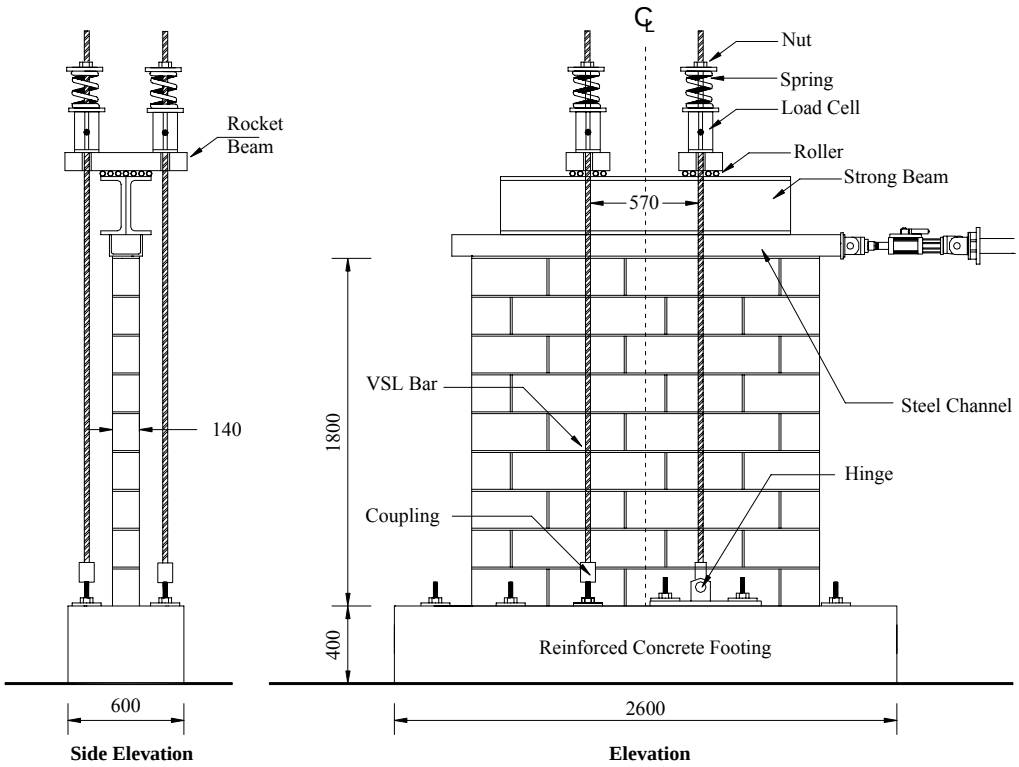

Figure 3.10 Test set-up for wall with applied axial load.

diameter VSL prestressing bars incorporated at the locations similar to those shown in Figure 3.10. The rocker beam which was balanced across the strong beam ensured that the pull down force in the prestressing bars on either side of the wall were equal. Each prestressing bar passed through a 1 kN/mm coil spring placed between the rocker beam and a load cell. The

load cells enabled the magnitude of tension forces in the prestressing bars to be monitored throughout the test. The prestressing bars were tensioned by tightening nuts above the load cells. The primary objective of using the coil springs in the test set-up was to maintain an approximately constant vertical force during the test, when the wall was displaced horizontally.

3.3.2 Instrumentation

The wall instrumentation included two types of instruments: load cell and portal displacement transducer. Both types of devices were calibrated on a regular basis. At various stages of testing, all displacement transducers and the load cell were scanned by a data logger and the measured displacement from the transducer and force magnitudes from the load cell were recorded by a computer.

A load cell is a device that measures the magnitude of applied force from the hydraulic actuator. It consists of a steel cylinder with strain gauges attached to the outer surface. Any deformation of the cylinder due to applied force causes a change in voltage output in the strain gauges. The portal displacement transducers consisted of a strain gauge attached to a spring steel strip between two rigid portal legs. This type of instrument is capable of measuring relative movement between the legs. Any axial movement causes the steel strip to be subjected to flexure, and the transducer is calibrated so that the resulting strain in the strain gauge correlates to the axial displacement. This type of device is capable of measuring displacement of about ± 50 mm with acceptable accuracy.

The arrangement for the measuring instrumentation is shown in Figure 3.11. A load cell to measure the magnitude of the lateral force was placed between the actuator and the steel channel, denoted as [0] in the figure. Portal displacement transducers, denoted as [1] and [2], measured lateral displacement at the top of the wall. The base uplift was monitored by portal displacement transducers [44] and [45] installed very close to the base joint while relative sliding displacement between the wall and footing was measured by transducers [42] and [43]. Any slip in the steel channel was measured by transducer [6]. Finally, the wall flexural and shear deformations were monitored by transducers [3]-[14] and [15]-[41] respectively.

Measuring points were formed by drilling into the masonry and epoxy grouting 10 mm diameter mild steel studs that were threaded to accept aluminium rosettes. Steel rods of 4 mm diameter were fixed to the rosettes in a formation of ‘spider webs’ that triangulated the wall between the measuring points, as shown Figure 3.11.

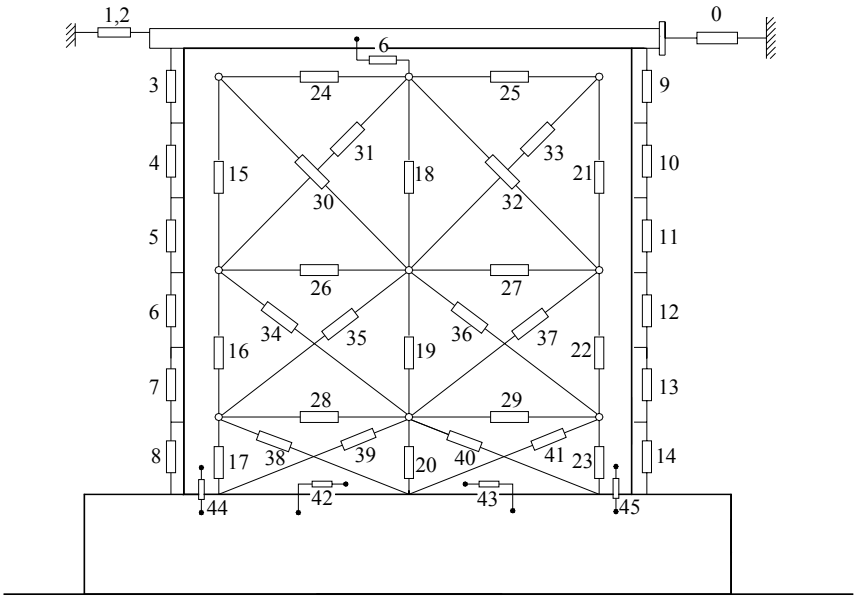

Figure 3.11 Instrumentation of test wall.

3.4 WALL STRENGTH PREDICTION

The nominal flexural and shear strengths of the tested walls were calculated before experimental testing was conducted. The wall nominal flexural strength was calculated according to the procedure outlined in section 2.3.1 and the evaluated wall flexural strength is represented as F_n in Table 3.2. A preliminary study presented by Voon and Ingham (2001) found that the NEHRP (1997) masonry shear provisions have the ability to predict the shear strength of fully grout-filled masonry walls with accuracy superior to that of NZS 4230:1990. Consequently, it was decided to use Equation 2-20 to determine the predicted shear strength of the masonry walls described in section 3.2.1. Table 3.2 presents the estimated flexural and shear strength for each masonry wall according to the measured rather than specified material strengths. Shear strength predicted by NZS 4230:1990 was included in Table 3.2 for comparison purpose as discussed at a later stage of this thesis. The shear strengths of the two partially grouted walls listed in Table 3.2 were calculated using a common New Zealand approach where the effective section width for shear was assumed to be the net thickness of the face shells only (see Figure 2.16). This limitation was to satisfy the requirements of continuity of shear flow and to avoid the possibility of vertical shear failure up a continuous ungrouted flue. This resulted in an effective width of 60 mm for the partially grout-filled concrete masonry walls.

All walls, except Walls A1 and A3, were designed to have a dominant shear type of failure. Wall A3 was designed to have a predominantly flexural type of failure. Although Wall A1 had $F_n/V_n > 1.0$, this wall was expected to fail in a flexure/shear mode due to the arrangement of shear reinforcement and the absence of axial stress.

Table 3.2 Prediction of wall strengths, based upon measured material properties

Wall	f'_m	F_n	V_n		Expected Failure Mode
			NEHRP (1997)	NZS 4230:1990	
A1	17.6	229	219	142	Flexure/Shear
A2	17.6	229	195	105	Shear
A3	17.0	229	250	191	Flexure
A4	17.0	229	219	152	Shear
A5	18.5	229	91	50	Shear
A6	18.5	142	91	50	Shear
A7	18.8	282	256	176	Shear
A8	18.8	256	240	161	Shear
A9	24.3	272	268	178	Shear
A10	24.3	672	558	297	Shear
Units	MPa	kN	kN	kN	---

Note: no strength reduction factor applied to F_n and V_n.

3.5 TESTING PROCEDURE

Before any masonry wall was tested, prism testing was carried out on the day of testing to determine f'_m. The cyclic loading sequence adopted for all tests was that shown in Figure 3.12, and consisted of a series of displacement–controlled components. Each stage of loading consisted of two cycles to the selected tip displacement. In each case, wall testing was terminated when sufficient strength degradation was evident. This usually coincided with a marked change in the slope of the force-displacement curve. This thesis defines failure as the point on the loading curve at which the wall strength has reduced to 80% of the maximum strength recorded in whichever direction this occurs first, see Figure 3.13. The displacement capacity, $d_{u,}$ is the point at which failure occurs, see Figure 3.13.

There were two reasons for applying this testing procedure: (1) To avoid a high level of dependency on instrument readings during the process of testing, in this case only the readings

of overall wall displacement (i.e. instruments [1] and [2] in Figure 3.11) were used in the load excursion. Hence, the test could proceed without knowledge of the actual strength or maximum displacement capacity of the test specimen. (2) The non-ductile nature (shear type of failure) of the test specimens mean small displacement increments are necessary to avoid the specimen being loaded to failure at an early stage of testing.

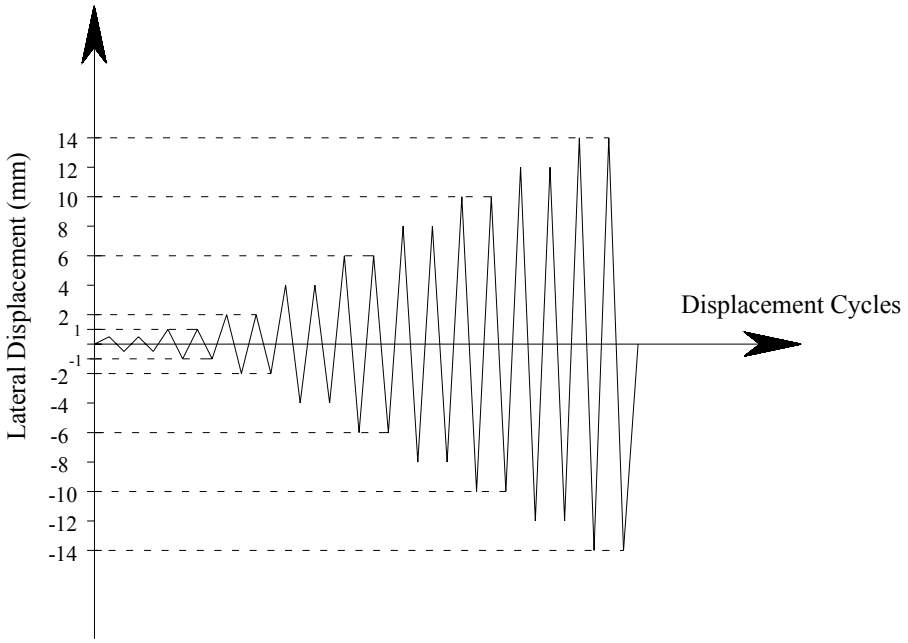

Figure 3.12 Imposed displacement history.

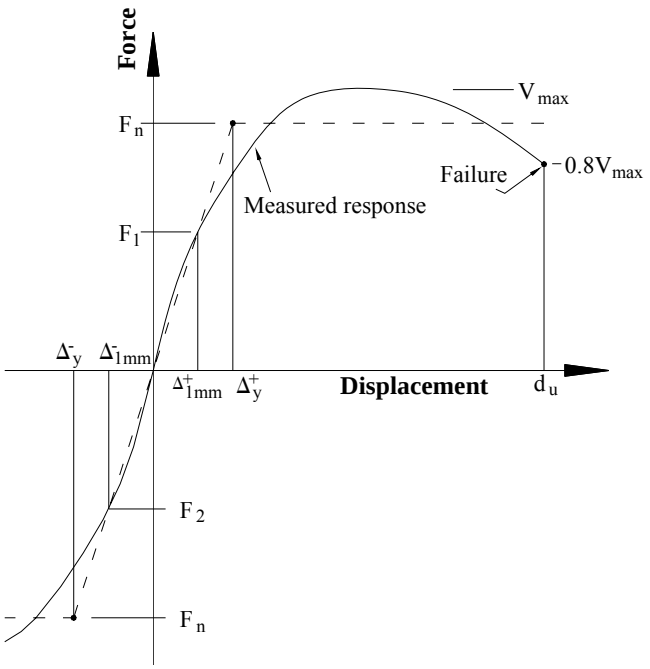

Figure 3.13 Nominal yield displacement.

The procedure for calculating the nominal yield displacement Δ_y is illustrated in Figure 3.13. This procedure involves the measurement of lateral forces F_1 and F_2 when the wall is being loaded to the first cycle of ± 1 mm displacement (i.e. Δ_{1mm}), and Δ_y (in mm units) is calculated according to Equation 3-1:

$$\Delta_y = \Delta_{1mm}\left(\frac{F_n}{1/2(F_1 - F_2)}\right) \qquad (3\text{-}1)$$

3.5.1 Miscellaneous

Precondition

Prior to initiation of the loading procedure, the specimens were inspected for any pre-test cracking or damage, to avoid confusion with any damage attributed to the applied loading.

Crack marking

During testing, visual observations were carefully noted along with key force and displacement readings at the extreme of each load excursion. Cracks due to applied loading in the push directions were marked in red and cracks due to pull excursions were marked in black. Also, photos were taken of any significant structural event during testing. In reporting, the term "compression toe" was used to describe the end of the wall by the base in compression due to flexural action, and the term "heel" described the opposite end of the wall that was experiencing decompression/uplift. The position of "compression toe" and "heel" depended on loading direction, the two terms reversed in position when the loading direction was reversed.

3.5.2 DATA REDUCTION

It was determined that the displacement of the wall consisted of four components: rocking and sliding deformation, flexural deformation, and shear deformation. As described earlier in section 3.3.2, instrumentation was attached to the wall as shown in Figure 3.11 to allow the deformation components to be isolated.

Rocking deformation:

The rocking (uplift) deformation was recorded by the two portal displacement transducers placed at the two ends of the wall-foundation base interface. At a given wall state, the rocking displacement component was calculated by extrapolating the rotation measured between the

wall ends. This is demonstrated in Figure 3.14. Hence, the rotation, θ_r of the wall due to rocking on its base was:

$$\theta_r = \frac{d_{r1} - d_{r2}}{L_w + 2\ell_s} \tag{3-2}$$

where d_{r1} and d_{r2} are the deformations measured by the portal displacement transducer, noting that elongation is represented by positive displacement, and ℓ_s is the distance between the wall end and the transducer. Therefore, the resulting rocking displacement recorded was evaluated as:

$$U_r = \theta_r h_e \tag{3-3}$$

Flexural deformation

Instrumentation mounted on both ends of the wall allowed the calculation of flexural deformation. Assuming that plane sections remain plane, the wall rotation, θ_i at height (x_i) above the base could be evaluated by Equation 3-4.

$$\theta_i = \frac{d_{b1} - d_{b2}}{L_w + 2\ell_s} \tag{3-4}$$

where d_{b1} and d_{b2} were the displacement measured by the pair of instruments shown in Figure 3.15. The resulting displacement u_{bi} at the top of the wall due to θ_i could be evaluated as:

$$u_{bi} = \theta_i(h_e - x_i) \text{ and } U_b = \sum_i u_b \tag{3-5}$$

Shear deformation

The method used in this report for calculating the shear deformation component was based on Hiraishi (1984) and Brammer (1995), with more detailed description provided in Appendix C. The mentioned method utilised the measured relative displacements between points on the wall face (transducers mounted diagonally on the wall, as shown in Figure 3.11) to evaluate the shear component of deformation.

Walls of Series A had at least six panel sections attached to the wall face in a 3x2 pattern. The dimensions of each panel section were defined by the length, L, the height, h, and the diagonal length, d. The following formula was used to calculate the shear deformation component (u_s) for each panel:

$$u_s = \frac{d(\delta_1 - \delta_2)}{2L} - \frac{h^2}{6(2d_u + h)}(\delta_{v1} - \delta_{v2}) \tag{3-6}$$

and $U_s = \sum u_s$

where δ's were the measured relative deformation within each panel section, and d_u was the distance between the two upper points of each panel section and the top of the wall. The sum of u_s from one side of the panel section was necessary to evaluate U_s, if two sides of a panel section were considered, then the results of the two may be averaged.

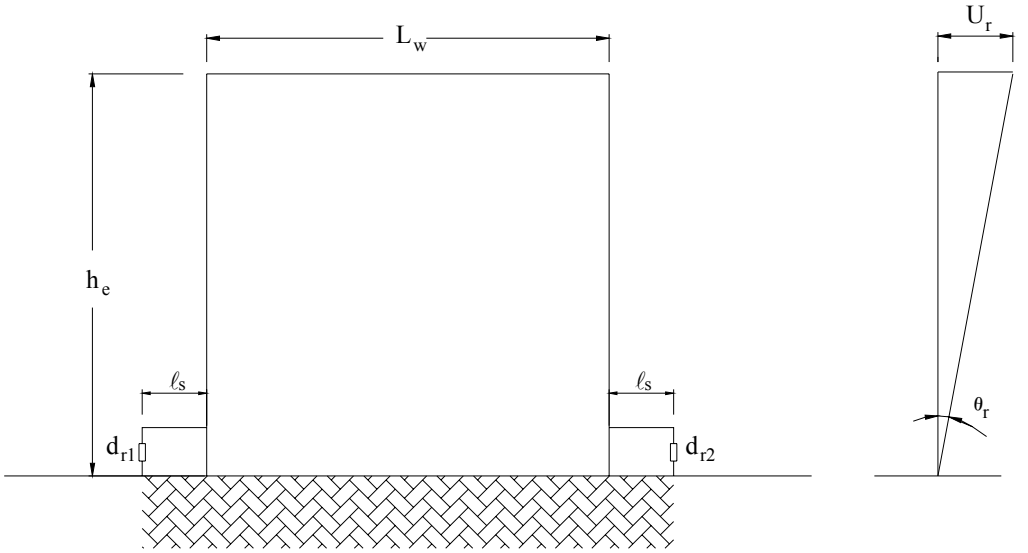

Figure 3.14 Rocking displacement

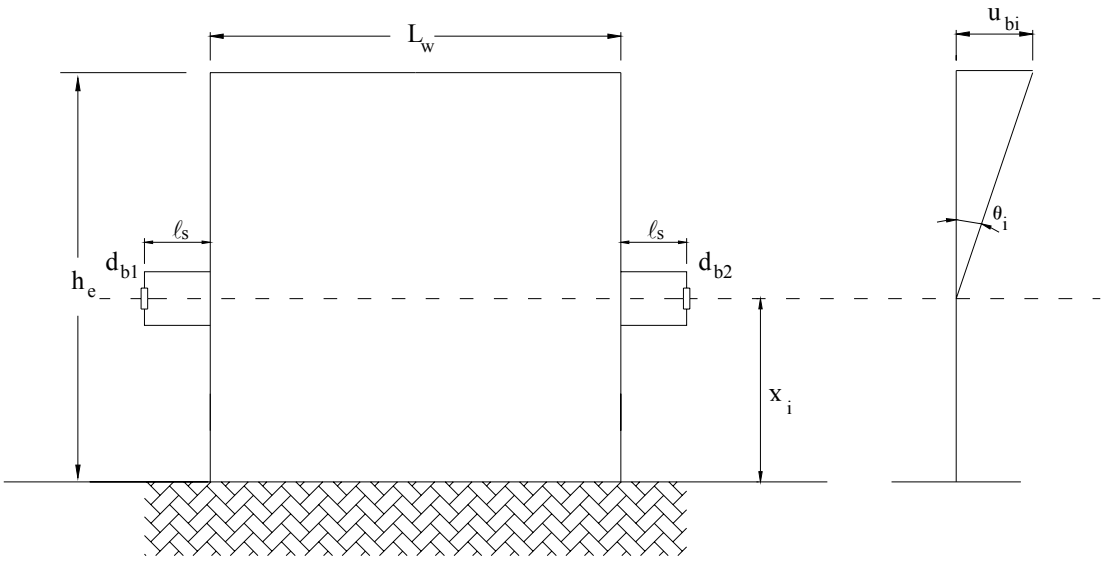

Figure 3.15 Flexural displacement.

Sliding deformation

This component was used to measure the slip between the wall and the base. Sliding may become significant when there is a low friction coefficient, such as when using a friction breaker or water proof membrane, or when the wall is positioned on a smooth finished slab. All

walls reported here were built on a purposely roughened concrete surface in order to reduce the magnitude of sliding.

3.6 TEST RESULTS

This section summarises the behaviour of the ten walls and presents the measured force-displacement responses. General wall behaviour is summarised in Table 3.3, where V_{max} is the maximum lateral force recorded and d_{vmax} is the corresponding displacement. The ultimate displacement capacity, d_u, is defined as the point at which the lateral wall strength had degraded to below 80% of V_{max}. For detailed description of the experimental results, refer to Voon and Ingham (2003). The nominal strengths, F_n and V_n, shown in Table 3.3 and Figure 3.16 are without strength reduction factor (i.e. $\phi = 1.0$). This thesis defines loading in the push direction as positive and loading in the pull direction as negative.

3.6.1 Force-Displacement Response

The experimentally obtained force-displacement curves for the ten walls are presented in Figure 3.16, depicting the lateral displacement at the top of the walls as a function of applied lateral shear force. Test results indicated that all walls, except for Walls A1 and A3, exhibited shear dominated response. This type of response was characterised by the development of early horizontal flexural cracks which were then superceded by wide open diagonal cracks that extended throughout the masonry walls. These diagonal cracks were initiated by tension splitting of masonry in the compression strut that formed in the walls. Rapid strength degradation was observed for walls that failed in the shear dominated mode (e.g. Figures 3.16(b) and (g)), attributed to the widening of diagonal cracks and crushing of masonry. Equation 2-10 was used to establish the principal tensile stresses within the masonry walls during the initiation of the first diagonal crack. Test results showed that principal tensile stresses of 0.52-0.73 MPa were reached when diagonal cracks were first observed in masonry walls that had no axially applied load. For the four masonry walls that had axially applied load, principal stresses of 0.56-0.60 MPa were reached during the initiation of first diagonal crack. These observed stress values corresponded well with the allowable masonry tensile stress of 0.55 MPa specified by the ACI 530-02.

A selection of experimentally measured displacement component plots is presented in Figure 3.17. These are plots that decomposed the total lateral displacement of each wall into four different displacement components according to the procedure outlined in section 3.5.2. From

Figures 3.17(c) and (d), it is shown that for masonry walls that failed in a shear mode, the shear component of deformation was the most dominant displacement mode when the masonry walls were pushed/pulled to large displacement levels. It is indicated in Figure 3.17(c) and (d) that the influences of sliding and rocking modes of deformation were mostly negligible once the tested walls were loaded beyond ±4.0 mm displacement. The results presented in Figures 3.17(c) and (d) confirm the observations, at the later stage of testing, of significant widening of diagonal shear cracks on walls that exhibited shear failure mode.

Although Wall A1 (see Figure 3.16a) was expected to fail in shear, it did not exhibit sudden strength degradation after reaching maximum wall strength, therefore indicating possible yielding of vertical reinforcement during testing. This notion is supported by the displacement component plot presented in Figure 3.17a to indicate significant magnitude of rocking and flexural displacement component developed by this wall (compared to negligible flexural response as illustrated in Figures 3.17(c) and (d)). Consequently, it was classified as having a flexure/shear type of failure. This type of failure mode was possible due to the absence of axial load and the adoption of closely distributed shear reinforcement using small size reinforcing bars (i.e. R6). Accordingly, the initial diagonal cracks did not widen significantly under increasing lateral force, but instead new sets of diagonal cracks formed and gradually spread over the wall diagonals, accompanied by higher energy dissipation and ductile behaviour. Failure occurred gradually in this case as the strength of the wall deteriorated under cyclic horizontal loading. Finally, partially crushing at the compression toe and at severely cracked portions of the wall diagonals took place at larger imposed displacement. Due to the presence of closely distributed diagonal shear cracking and the absence of abrupt strength degradation, Wall A1 could also be classified as exhibiting a "ductile shear failure".

Although Wall A3 was designed to fail in flexure, Figure 3.16c shows that this wall failed to reach F_n. The maximum strength developed by Wall A3 was about 94% of the calculated flexural strength of 229 kN. This lower than expected wall strength was due to significant sliding at the wall base where sliding component of displacement contributed about 20% of the wall lateral displacement at end of testing (see Figure 3.17b). Consequently, a portion of the shear force was transferred by dowel action of vertical reinforcement. This in turn led to a reduction in wall lateral strength.

The test results of Figure 3.16 confirm that the NZS 4230:1990 shear expression significantly under-predicted the in-plane shear strength of masonry walls. It is also observed from the same

Table 3.3 Summary of test results

Wall specimen	Prediction			Test result							
	F_n	V_n *	$\frac{F_n}{V_n}$	Δ_y	d_{vmax}	V_{max}	$\frac{V_{max}}{V_n}$	$\frac{V_{max}}{F_n}$	d_u	$\mu^{**}_{v\,max}$	Failure mode
A1	229	219	1.05	3.0	10 -6	215 -205	0.96	0.92	12 -14	2.67	Flexure/ Shear
A2	229	195	1.17	2.3	6 -6	177 -195	0.95	0.81	8 -8	2.61	Shear
A3	229	250	0.92	2.5	8 -6	215 -203	0.84	0.91	10 -10	2.80	Sliding/ Flexure
A4	229	219	1.05	2.7	8 -6	223 -201	0.97	0.93	10 -10	2.59	Shear
A5	229	91	2.52	4.7	8 -8	143 -134	1.57	0.62	10 -10	1.70	Shear
A6	142	91	1.56	5.1	8 -10	93 -93	1.02	0.65	14 -14	1.76	Shear
A7	282	256	1.10	2.2	6 -6	263 -261	1.02	0.93	8 -8	2.73	Shear
A8	256	240	1.07	2.2	6 -6	244 -250	1.03	0.96	6 -6	2.73	Shear
A9	272	268	1.01	7.0	20 -20	204 -207	0.77	0.76	24 -24	2.86	Shear
A10	672	568	1.18	3.0	4 -4	572 -598	1.03	0.87	4 -4	1.33	Shear
Units	kN	kN	---	mm	mm	kN	---	---	mm	---	---

* V_n is the calculated masonry shear strength, based on net cross-sectional area using NEHRP (1997) recommendations; no strength reduction factor (ϕ) applied.

** $\mu_{v\,max} = \frac{d_{v\,max}}{\Delta_y}$.

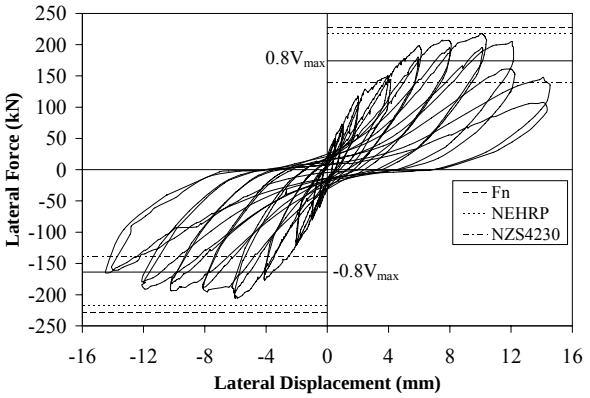

(a) Wall A1

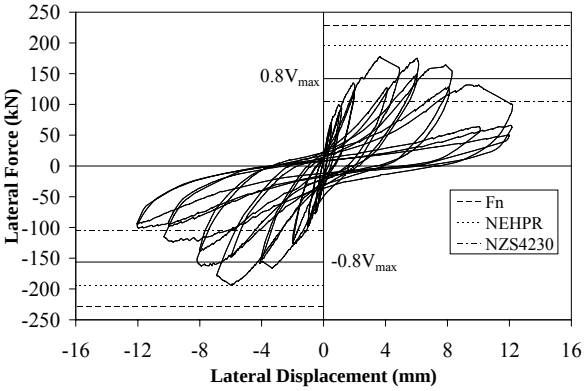

(b) Wall A2

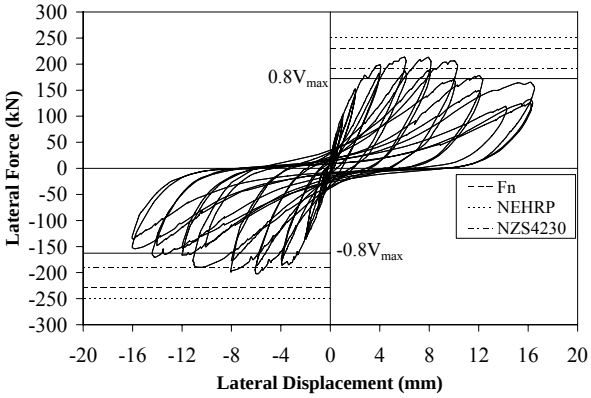

(c) Wall A3

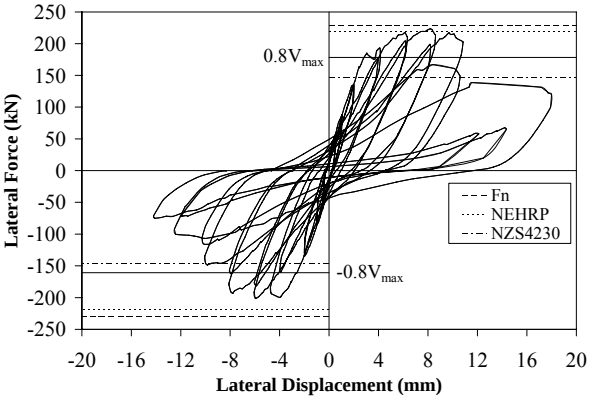

(d) Wall A4

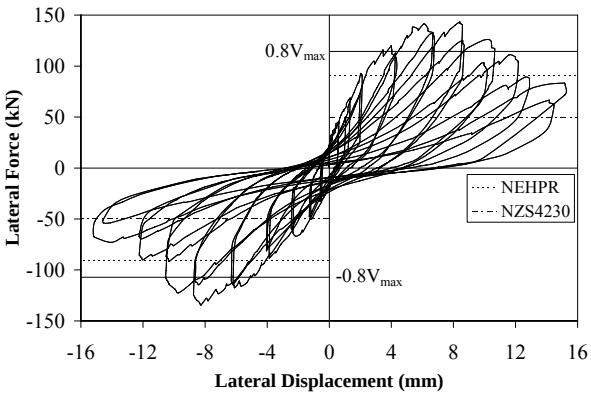

(e) Wall A5 (F_n = 229 kN)

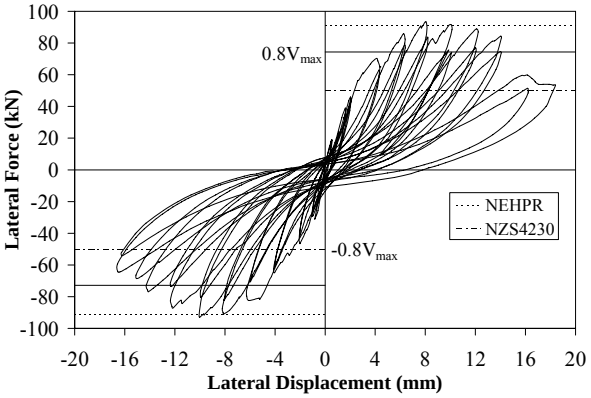

(f) Wall A6 (F_n = 142 kN)

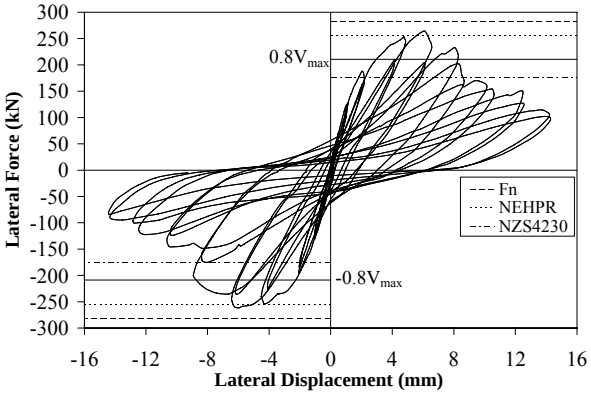

(g) Wall A7

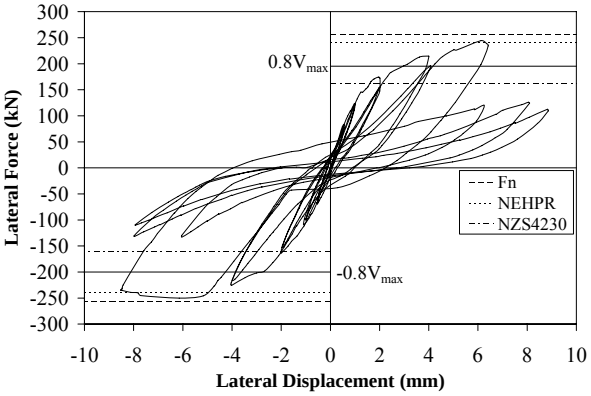

(h) Wall A8

Figure 3.16 Series A, force-displacement histories.

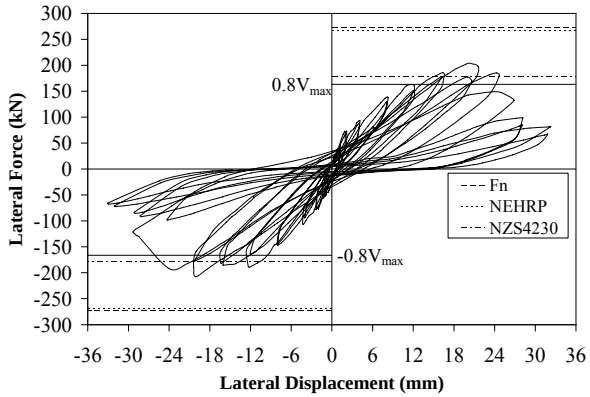

(i) Wall A9

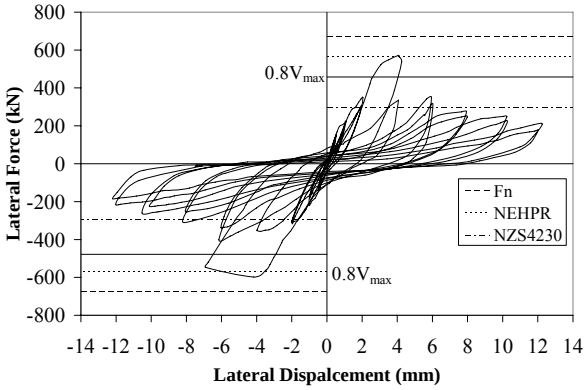

(j) Wall A10

Figure 3.16 Series A, force-displacement histories (continued).

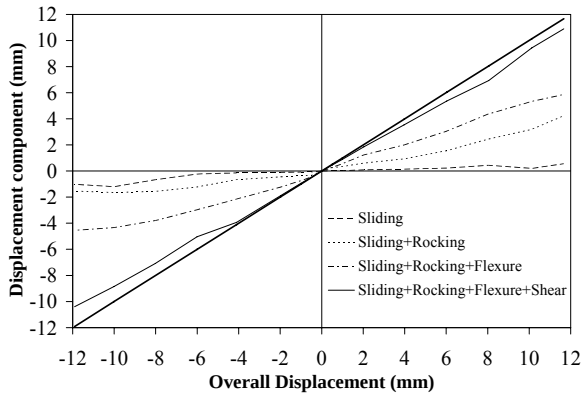

(a) Wall A1

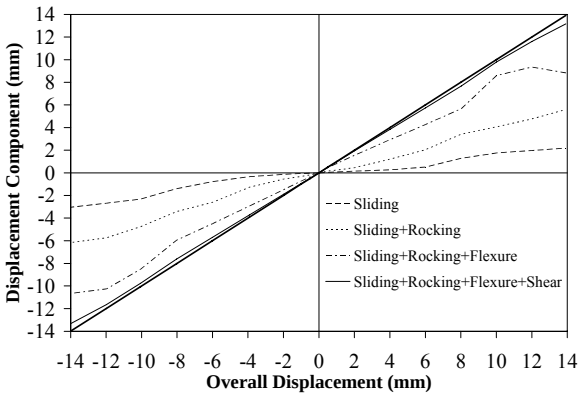

(b) Wall A3

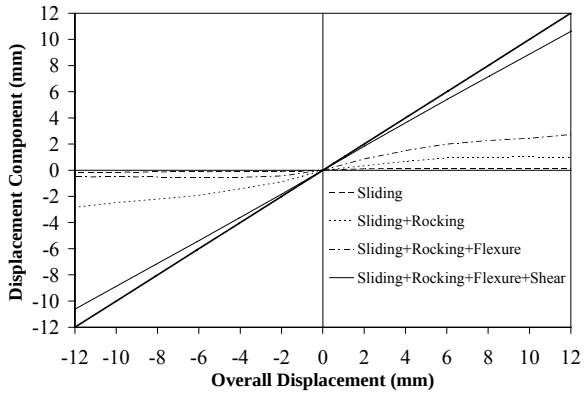

(c) Wall A6

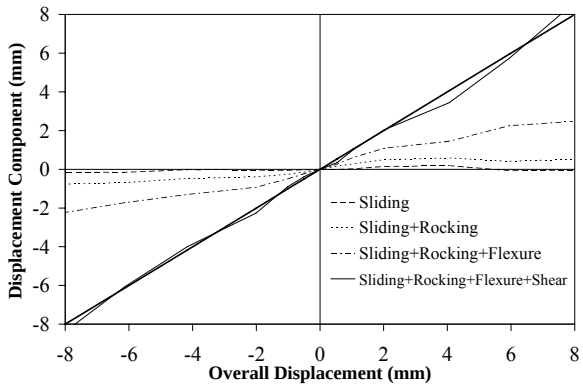

(d) Wall A10

Figure 3.17 Series A, plots of displacement component.

figure that shear prediction using the NEHRP shear expression provided a better match for walls that had $h_e/L_w \leq 1.0$. However, Figure 3.16i illustrates that the NEHRP expression over-predicted the shear strength of Wall A9 by about 23%. This over-prediction of shear strength was due to the substantial increase in diagonal shear cracking (compared to other walls) that developed before the maximum wall strength was reached, and also due to the fact that the NEHRP shear expression does not address the reduction in masonry shear strength within

potential plastic hinge regions. Experimental results indicated that a displacement ductility level of 2.9 was recorded when Wall A9 developed its maximum strength.

3.6.2 Damage Pattern

Rapid strength degradation was observed for masonry walls that exhibited a shear mode of failure. This rapid degradation of strength was due to the development of wide open diagonal cracks, initiated by tension splitting of masonry in the compression strut forming in the walls. Figures 3.18-3.21 present a selection of photographs to illustrate the condition of some tested wall at the end of testing, with Figure 3.22 schematically depicting the cracking patterns of all walls after failure. The shaded areas shown in Figure 3.22 indicate masonry crushing.

3.7 DISCUSSION

This section discusses how design parameters, such as the amount of shear reinforcement, distribution of shear reinforcement, magnitude of axial compression load, wall h_e/L_w ratio and type of grouting affect the shear strength of masonry walls. The figures in this section are limited to force-displacement envelopes, arranged in groups to show the effect of a particular parameter.

3.7.1 Effect of Shear Reinforcement

In this study both the amount of shear reinforcement and the distribution of reinforcing bars throughout the height of the wall were varied. It was observed that a change in the quantity of shear reinforcement had a direct influence on V_n. This is clearly illustrated in the experimental results shown in Figure 3.23, where the maximum shear strength increased from 195 kN for Wall A2 to 215 kN for Wall A1, resulted in a strength increase of 10% when the shear reinforcement increased from 1-R6 to 5-R6. However, this increase in the maximum shear strength with increasing amount of horizontal shear reinforcement was not observed in Wall A3. In this case, significant sliding along the wall-foundation base interface resulted in a portion of shear force being transferred by the dowel action of vertical reinforcement, which subsequently led to a reduction in wall lateral strength. Consequently, the average maximum shear strength attained by Wall A3 was about the same as those recorded for Walls A1 and A4 although the horizontal shear reinforcement employed in Wall A3 was about 2.5 times the shear reinforcement used in the other two walls.

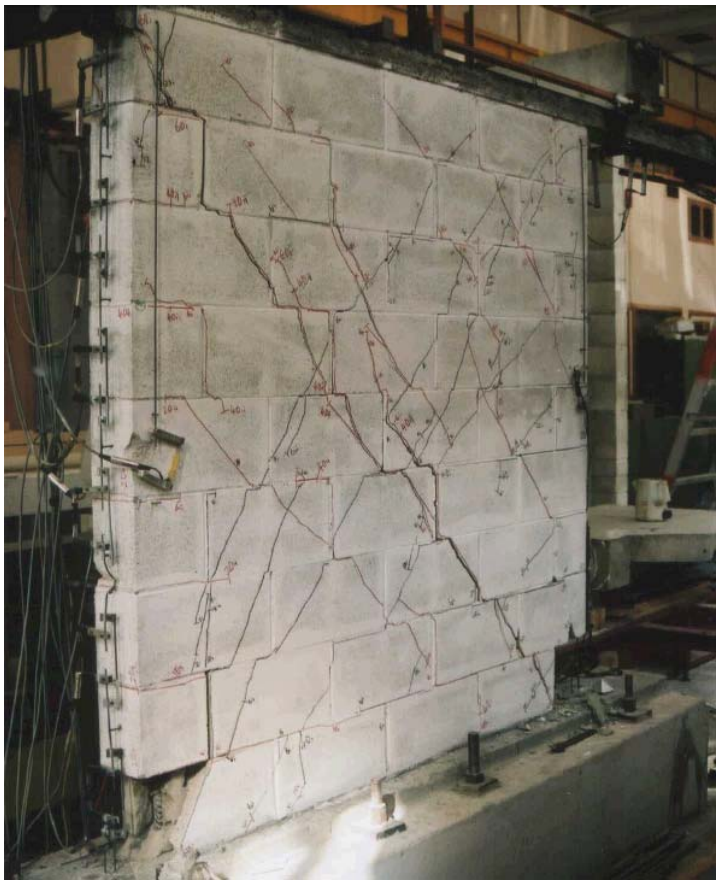

Figure 3.18 Series A, condition of Wall A1 at end of testing.

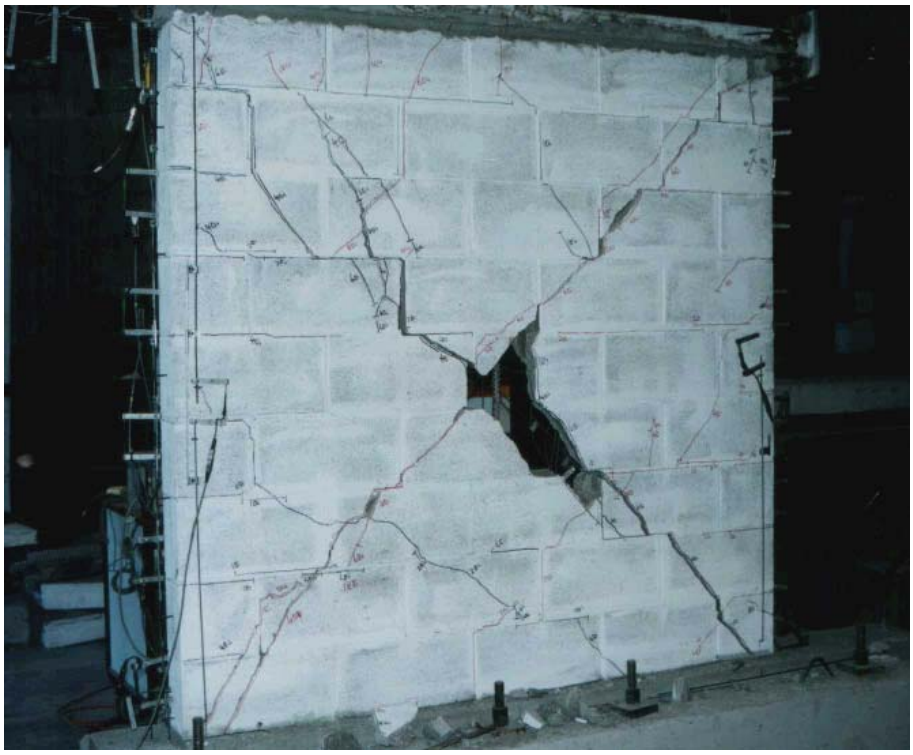

Figure 3.19 Series A, condition of Wall A2 at end of testing.

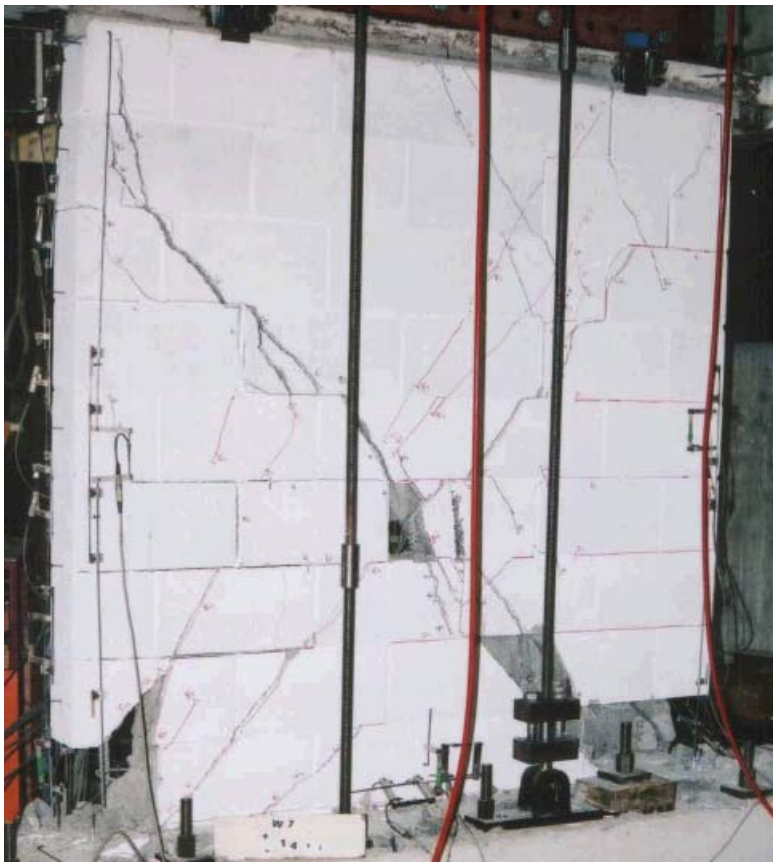

Figure 3.20 Series A, condition of Wall A7 at end of testing.

Figure 3.21 Series A, condition of Wall A9 at end of testing.

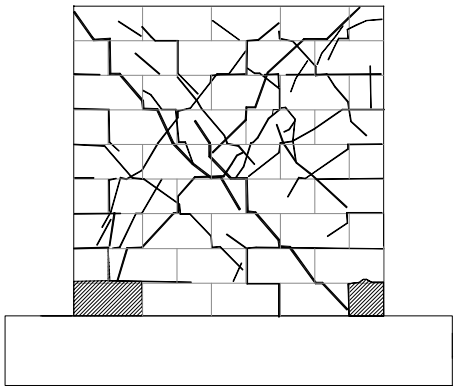

(a) Wall A1

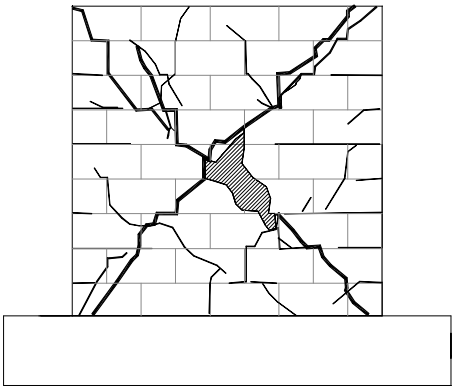

(b) Wall A2

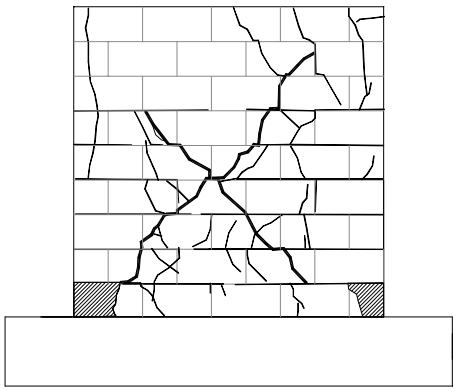

(c) Wall A3

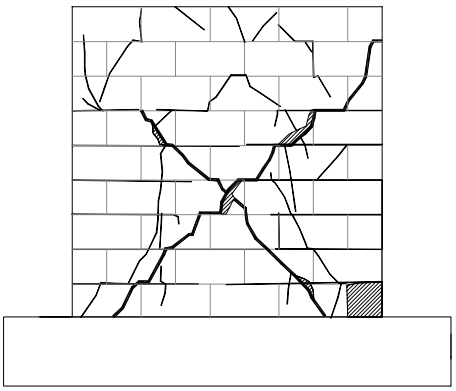

(d) Wall A4

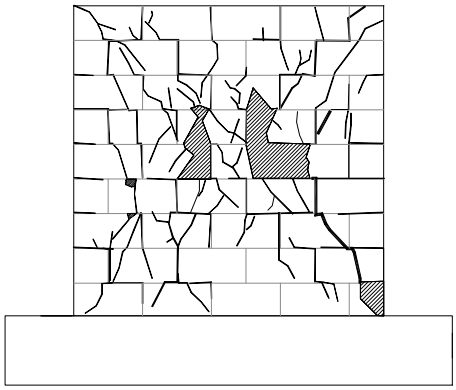

(e) Wall A5

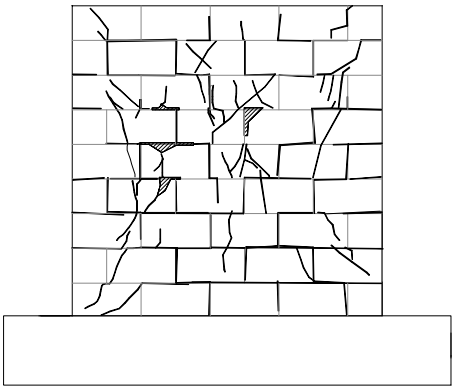

(f) Wall A6

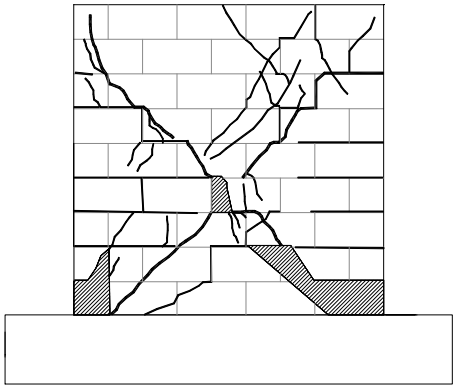

(g) Wall A7

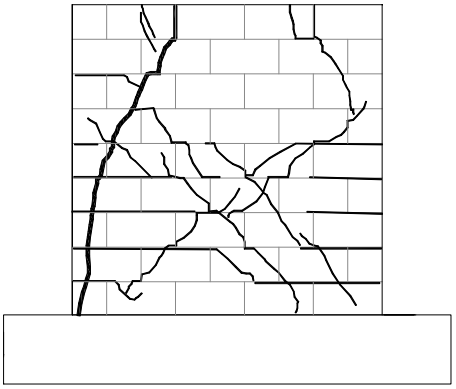

(h) Wall A8

Figure 3.22 Series A, masonry wall cracking patterns.

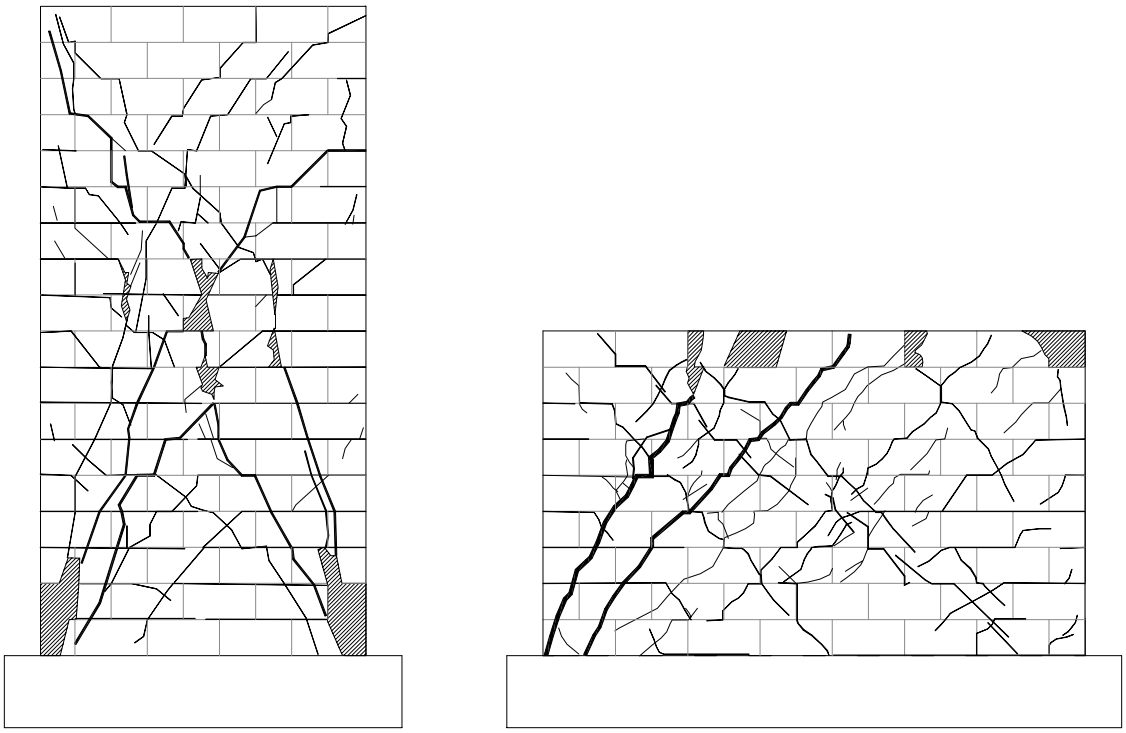

(i) Wall A9 **(j) Wall A10**

Figure 3.22 Series A, masonry wall cracking patterns (continued).

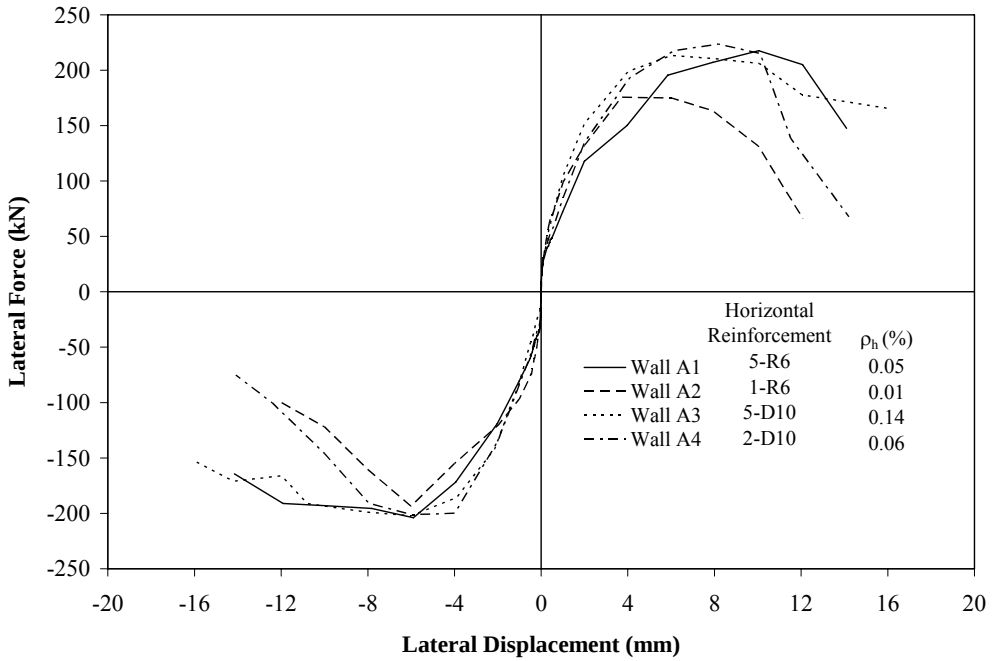

Figure 3.23 Effect of shear reinforcement on masonry shear strength.

Figure 3.24 shows the effectiveness of horizontal reinforcement in enhancing the post-cracking performance of masonry walls. It can be seen that the deformability of walls improved when the amount of shear reinforcement increased from 1-R6 to 5-R6 reinforcing bars for the case of

Walls A2 and A1, and when the horizontal reinforcement increased from 2-D10 to 5-D10 reinforcing bars for the case of Walls A4 and A3. The advantage of distributing shear reinforcement (using a greater number of reinforcing bars of smaller diameter) up the height of the wall can be clearly observed by comparing the force-displacement envelopes of Walls A1 and A4. These two walls contained approximately the same total cross-sectional area of shear reinforcement, but the shear reinforcement was distributed differently according to Figure 3.1. Figure 3.24 shows that Wall A4 exhibited abrupt strength degradation after the peak wall strength was attained, whereas Wall A1 exhibited a more gradual strength degradation. This type of failure was made possible for Wall A1 due to the adoption of 400 mm spaced R6 horizontal reinforcement. The closely spaced shear reinforcement enabled the distribution of stresses throughout the wall diagonals after the initiation of shear cracking. According, the initial diagonal cracks did not widen significantly under increasing lateral displacements, but instead new sets of diagonal cracks formed and gradually spread over the wall diagonals, accompanied by higher energy dissipation and more ductile behaviour. It was therefore possible to classify Wall A1 as having a flexure/shear type of failure or "ductile shear failure". Conversely, Wall A4 exhibited a "brittle shear failure". This type of shear failure was expected since Wall A4 was constructed without the closely distributed shear reinforcement. This prevented the tensile stress due to applied shear force from being adequately transferred across the diagonal cracks. Hence the cracks opened extensively, resulting in a major x-shaped diagonal crack pair (see Figure 3.22d for wall crack pattern), which led to a relatively sudden and destructive failure.

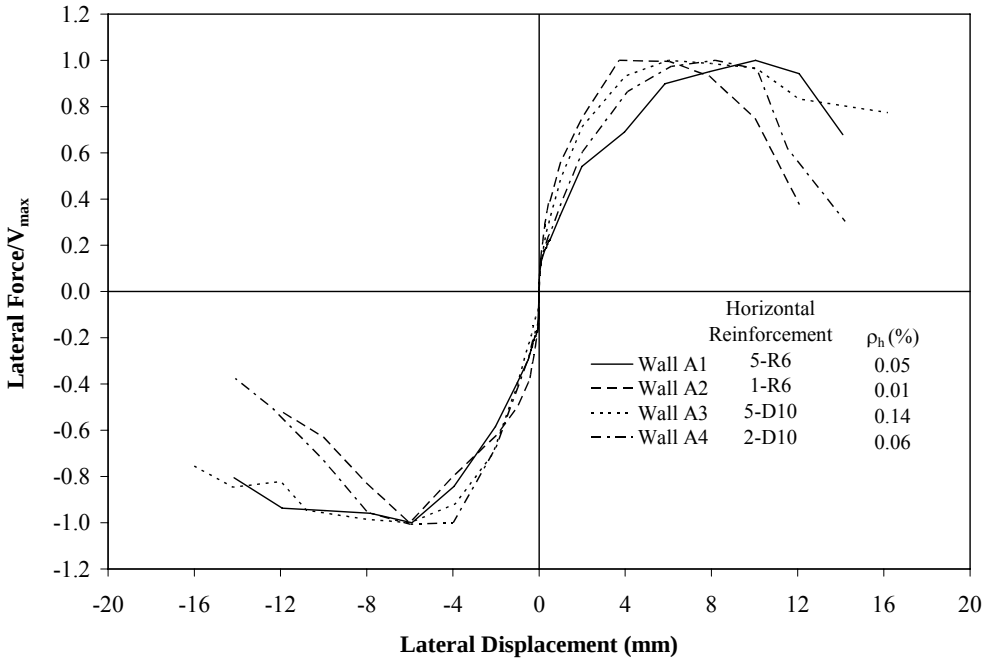

Figure 3.24 Force-displacement envelopes normalised with V_{max}.

3.7.2 Effect of Axial Compression Stresses

The positive influence of axial compression stress on masonry shear strength is illustrated in Figure 3.25. This figure shows the performance of the three masonry walls that had the same dimensions and reinforcement details, but were subjected to varying levels of axial compression stress. The maximum shear strength increased from 215 kN for Wall A1 to 244 kN (Wall A8) and 263 kN (Wall A7) when the axial compression stress was increased from zero to 0.25 MPa and 0.50 MPa, resulting in an increase of about 13% and 22% respectively. Also observed from the same figure is reduction of the post-cracking deformation capacity of Walls A7 and A8. This was because the failure type became more brittle as the axial compression stress increased.

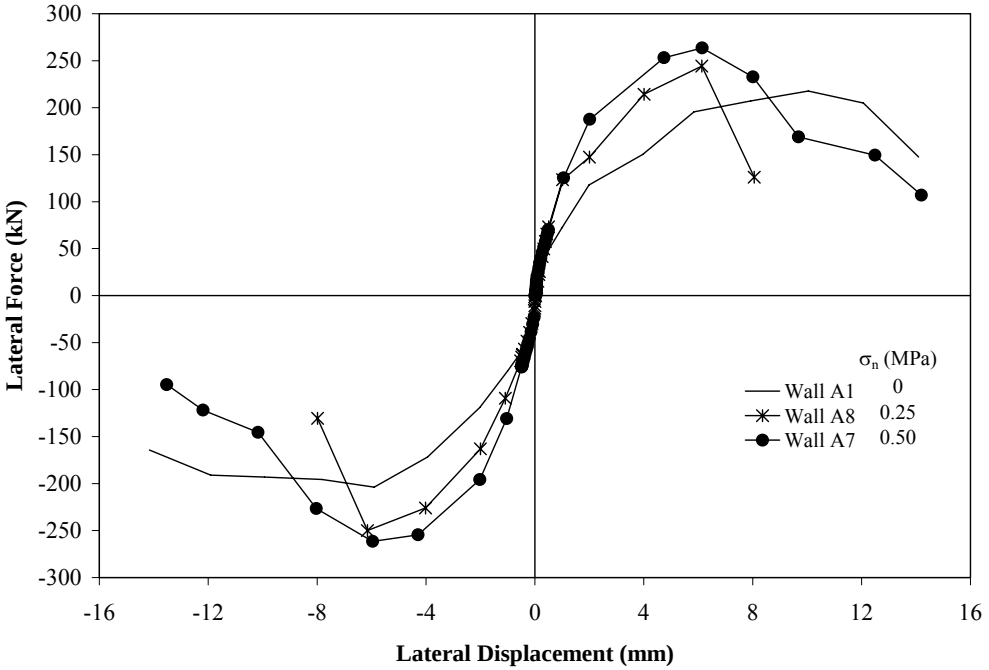

Figure 3.25 Effect of axial compression stress on masonry shear strength.

It was also noted from observations made during the experimental process that an increase in axial compression stress delayed the initiation of cracking until larger lateral force was applied. This can be explained from principal stresses: a larger lateral force is required to exceed the compressive field resulting from the larger axial load. This compressive field must first be overcome before cracking can initiate.

3.7.3 Effect of Grouting

Experimental results presented in Table 3.3 illustrate the significant reduction of shear strength when the masonry walls were partially grouted. For the two partially grouted masonry walls, it was also shown that Wall A5 with five grouted flues had about 50% higher strength than the

corresponding Wall A6, which had only three grouted flues. However, the effect of grouting method becomes less significant when the net shear stress is calculated by considering the cross-sectional area of both the CMUs and the grouted cells. This is shown in Figure 3.26, where force-displacement envelopes of both fully (without axial load) and partially grouted walls (Walls A5 and A6) are presented. It is shown that Wall A5 had similar net shear stress as those illustrated by the fully grout-filled masonry walls.

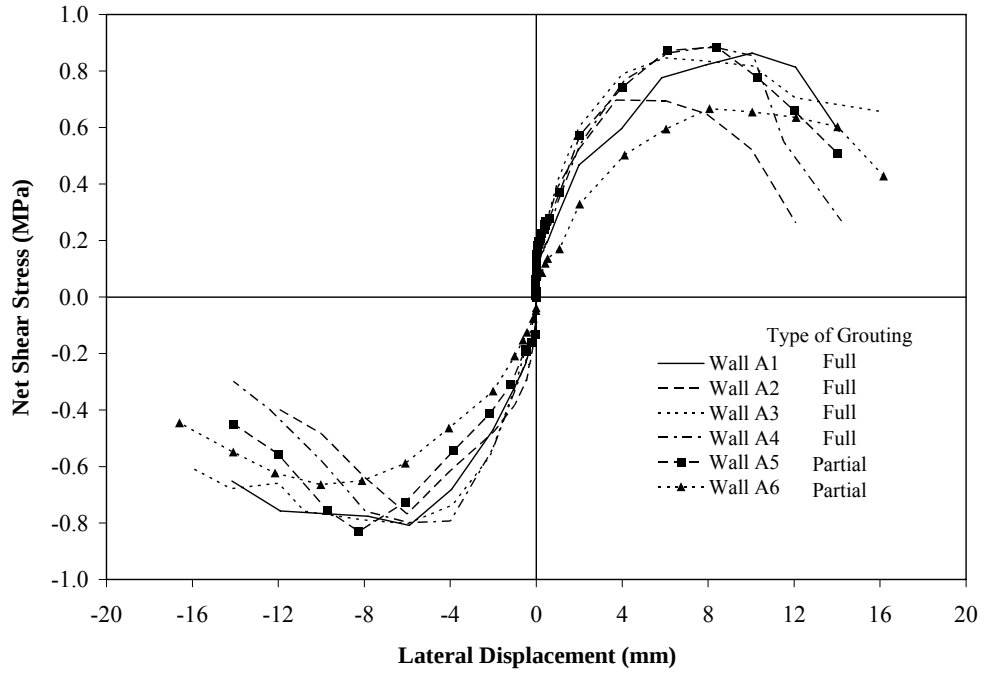

Figure 3.26 Effect of grouting on masonry shear stress.

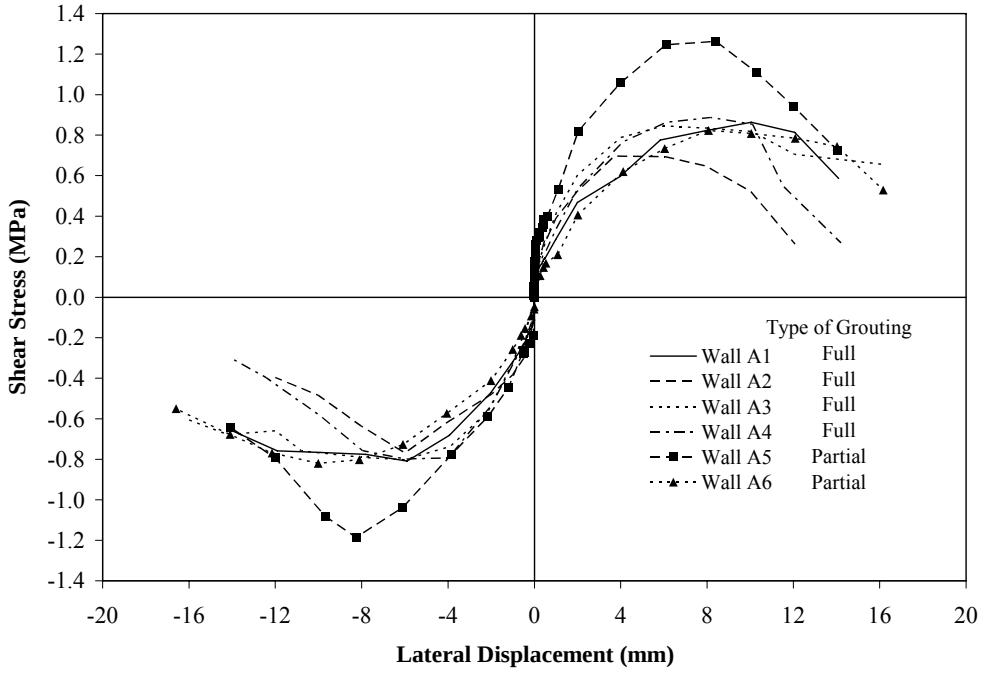

Figure 3.27 Shear stress calculated according to New Zealand approach.

However, the just mentioned approach of considering the cross-sectional area effective for shear in a partially grout-filled wall is different from that currently used in New Zealand. The common New Zealand approach (see Figure 2.16b) considers the effective section width for shear as the net thickness of face shells only. This limitation is to satisfy the requirements of continuity of shear flow and to avoid the possibility of vertical shear failure up a continuous ungrouted flue. Consequently, this resulted in an effective width of 60 mm for the two partially grouted masonry walls included in this study. The information presented in Figure 3.26 is reproduced in Figure 3.27 to incorporate the New Zealand method for interpreting the effective shear area in a partially grout-filled masonry wall. As expected, significantly increased shear stress is observed when the face shells are considered as the only shear resisting element. From the information illustrated in Figures 3.26 and 3.27, it is concluded that the shear stress (v_n) resisted by any partially grout-filled masonry wall is similar to that of its fully grout-filled counterpart.

3.7.4 Effect of Wall h_e/L_w Ratio

The influence of wall h_e/L ratio on masonry shear strength was included in this study and the results are discussed in this subsection. It is illustrated in section 3.6.1 that the wall h_e/L_w ratio affects the wall ultimate strength considerably. Figure 3.28 shows the force-displacement envelopes for Walls A8, A9 and A10. These three walls had the same axial compression stress and similar reinforcement details (although Wall A9 had a higher vertical steel ratio), but were built to varying h_e/L_w ratios. A higher longitudinal reinforcement ratio of $\rho_v f_{yv} = 4.82$ MPa was necessary in Wall A9 to increase the flexural strength in order to generate shear failure.

It is illustrated in Figure 3.28 that shear strength decreased from a maximum of 250 kN for Wall A8 ($h_e/L_w = 1.0$) to 207 kN when the h_e/L_w ratio was increased to 2.0 in the case of Wall A9, resulting in a decrease of 17%. Figure 3.28 also shows that the maximum shear strength of Wall A10 was 598 kN for an h_e/L_w ratio of 0.60, therefore resulting in a strength increase of 139%. This indicates that masonry shear strength increases as the h_e/L_w ratio decreases, while it decreases inversely in relation to an increase in h_e/L_w ratio. In addition, Figure 3.28 illustrates that wall panels with lower aspect ratios would have higher stiffness and reached their maximum resistance at smaller displacements, but abrupt strength degradations take place immediately after peak strengths are reached.

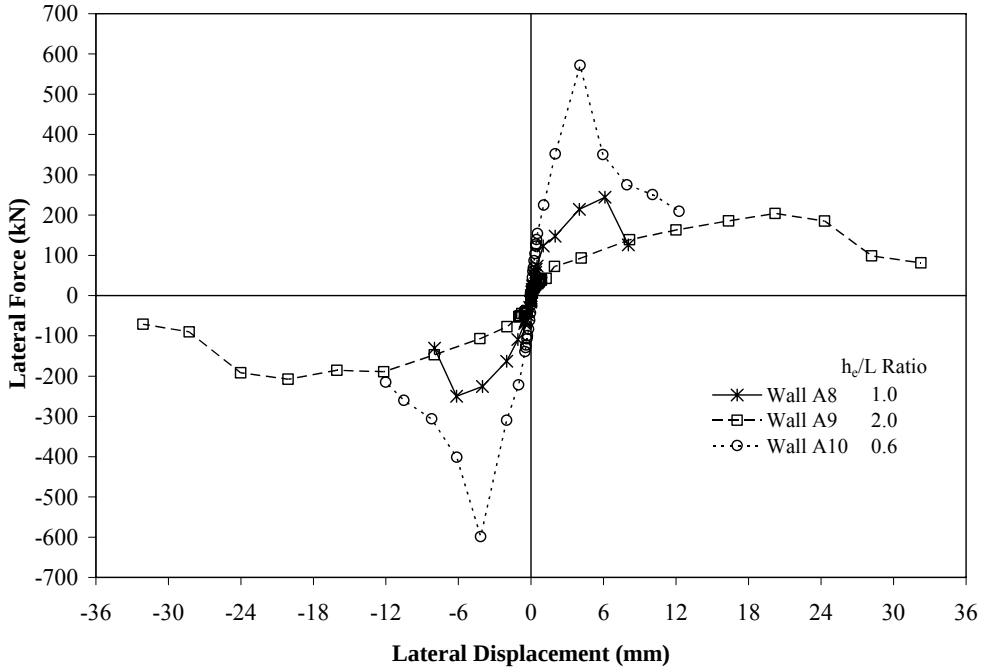

Figure 3.28 Effect of h_e/L_w on masonry shear strength.

It is however realised that the different shear strength in Walls A8, A9 and A10 could have been due to the variations in A_n and f'_m. In order to meaningfully observe the relation between masonry shear strength and h_e/L_w ratio, the influence of A_n and f'_m must be excluded from the test results. Consequently, a plot of $v_n/\sqrt{f'_m}$ is presented in Figure 3.29. As anticipated, Figure 3.29 produced results similar to those presented in Figure 3.28, but the strength difference between the three walls was significantly reduced. Tendency similar to that observed in Figure 3.28 is evident. Consequently, it is concluded that h_e/L_w has an inverse effect on $v_n/\sqrt{f'_m}$ since the figure shows that $v_n/\sqrt{f'_m}$ decreases when the h_e/L_w ratio is increased.

3.7.5 Masonry Compressive Strength

All tests conducted in this study used standard material, and resulted in only minor variations in masonry compression strength (f'_m) between various test, as shown in Table 3.2, and therefore the effect of f'_m was not considered in this study. However, it is expected that masonry shear strength will increase with masonry crushing strength, as suggested by the various shear equations described in section 2.4.2. In addition, the wall masonry shear strength is dependent on wall dimensions, in particular the wall cross-sectional area defined by the wall length, L_w, and wall thickness, t. Therefore, an increase in both L_w and t results in an increase of shear strength.

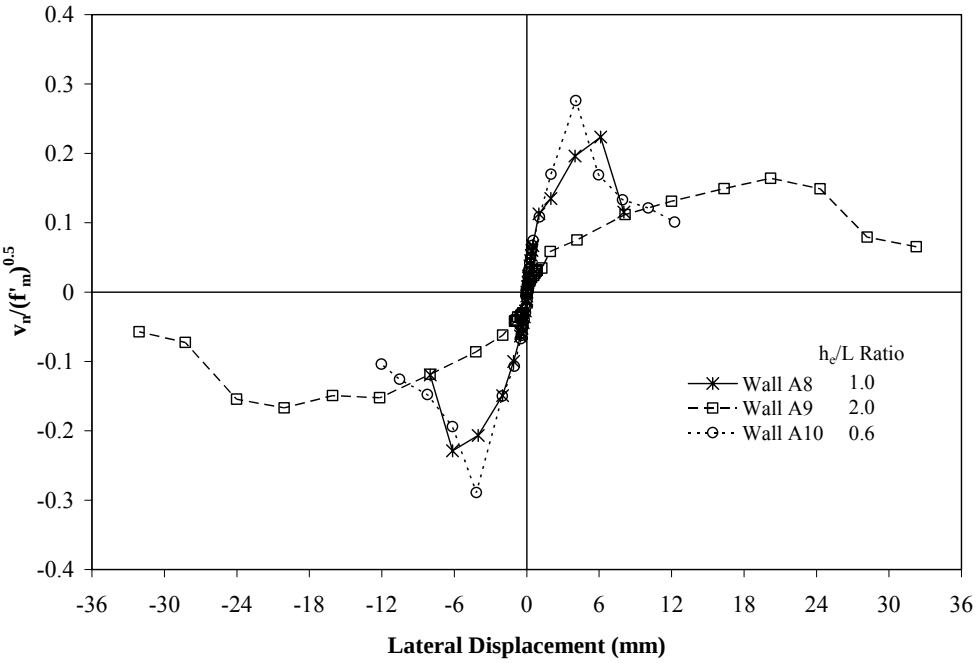

Figure 3.29 Effect of h_e/L_w on $v_n / \sqrt{f'_m}$.

Chapter 4

SHEAR EQUATION IMPROVEMENT

4.1 INTRODUCTION

An analytical study by Voon and Ingham (2001) established that the NZS 4230:1990 shear expression was conservative in its evaluation of the maximum shear strength for the range of parameters represented by the masonry walls considered. The significant conservatism of NZS 4230:1990 was further confirmed in the test results presented in section 3.6. This conservatism was partly because the beneficial effects of axial compression and vertical reinforcement on masonry shear strength were not properly considered by this standard, but also because the codified shear strength expression of NZS 4230:1990 was intended to provide a conservative and safe lower bound to strength. However, the same analytical study revealed a decrease in conservatism of NZS 4230:1990 when the horizontal shear reinforcement ratio increased, therefore indicating the possibility of over-predicting the contribution of shear reinforcement. Of the seven shear equations presented in section 2.4.2, the NEHRP shear expression, despite its simple form, was found to be most capable of predicting masonry shear strength with significantly improved accuracy (with respect to NZS 4230:1990). Also, it has an advantage over the Anderson and Priestley equation because the wall aspect ratio is included when calculating v_m. Nevertheless, there are still some deficiencies in the NEHRP shear equation as it does not address masonry shear strength within potential plastic hinge regions and the use of $0.5\rho_h f_{yh}$ in its v_s term is contrary to the well established split beam analogy (Mörsch, 1912) to account for the contribution of shear reinforcement. Consequently, a new shear equation was developed by the authors and is presented in the following section.

Aspects relating to codification of the in-plane shear strength of concrete masonry walls when subjected to seismic loading are presented in this chapter. Particular emphasis is placed on a model that is capable of representing the interaction between flexural ductility and masonry shear strength to account for the reduction in shear strength as ductility level increases. The simple method proposed in section 4.2 allows the strength enhancement provided by axial compression load to be separated from the masonry component of shear strength and is considered to result from strut action. In addition, minor modifications are made in section 4.3

to facilitate adoption of the method in the updated version of the New Zealand masonry design standard, NZS 4230:2004.

4.2 PROPOSED MASONRY SHEAR EQUATION

4.2.1 Modification to V_m

It is proposed that for practical design calculations, the ultimate shear strength of a masonry structure is calculated using Equation 2-15:

$$V_n = V_m + V_p + V_s$$

where

$$V_m = v_m b_w d$$

and $$v_m = k(C_a + C_b)\sqrt{f'_m} \qquad (4\text{-}1)$$

where $C_a = 0.022\rho_v f_{yv}$ and $C_b = 0.083\left[4 - 1.75\frac{h_e}{L_w}\right]$, and $0.25 \le \frac{h_e}{L_w} \le 1.0$

As shown in Equation 4-1, the v_m term proposed here closely matches the NEHRP expression, but this new equation additionally includes the effects of longitudinal reinforcement and displacement ductility on masonry shear strength. Also, the V_m term of Equation 4-1 differs from the NEHRP equation as A_n is replaced by $b_w d$. The k factor adopted here is more conservative than that proposed by Anderson and Priestley (1992) as it assumes that negligible shear strength degradation occurs prior to a member ductility ratio of 1.25, followed by a linear decrease until $v_m = 0$ at a ductility ratio of 4, as illustrated in Figure 4.1.

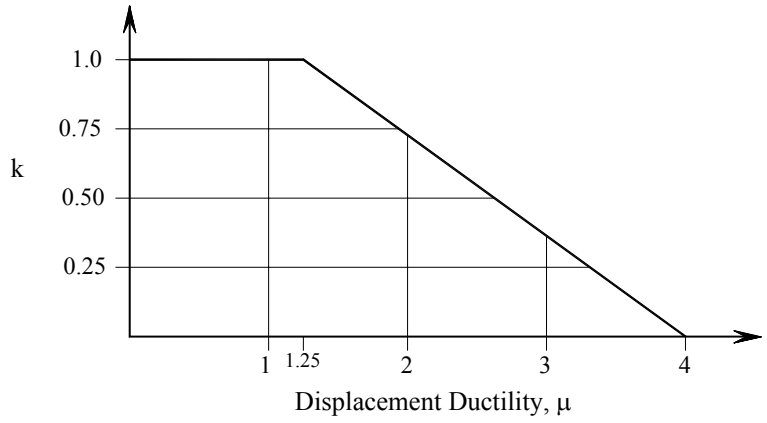

Figure 4.1 Relationship between ductility and masonry shear resisting mechanism.

The C_a term in Equation 4-1 is that proposed by Shing et al. (1990) to account for the contribution of vertical reinforcement towards masonry shear strength. During dowel action of the vertical reinforcing bar, shear force can be transferred along a diagonal crack by the shear, flexural and kinking actions which are activated locally in reinforcing bars due to their relative displacement along a crack. In addition, by helping to control the diagonal cracks, the friction along these cracks is enhanced, therefore resulting in an increase in shear capacity due to vertical reinforcement. However, at the onset of yielding of the longitudinal reinforcement, the effectiveness of these bars inside an unconfined masonry structure would be significantly affected. Consequently, a conservative approach is to consider the resistance provided by the longitudinal reinforcement to diminish at the onset of yielding of these bars. This effect is represented by the k factor presented in Equation 4-1. Similar to the NEHRP shear equation, the C_b term in Equation 4-1 accounts for the effect of wall aspect ratio on masonry shear strength and the limits on h_e/L_w are identical to that shown in Equation 2-20.

4.2.2 Modification to V_p

The shear strength enhancement resulting from axial compression is considered as an independent component of shear strength, resulting from a diagonal compression strut (Priestley et al., 1994) as shown in Figure 4.2, given by Equation 4-2:

$$V_p = 0.9N^* \tan\alpha \qquad (4\text{-}2)$$

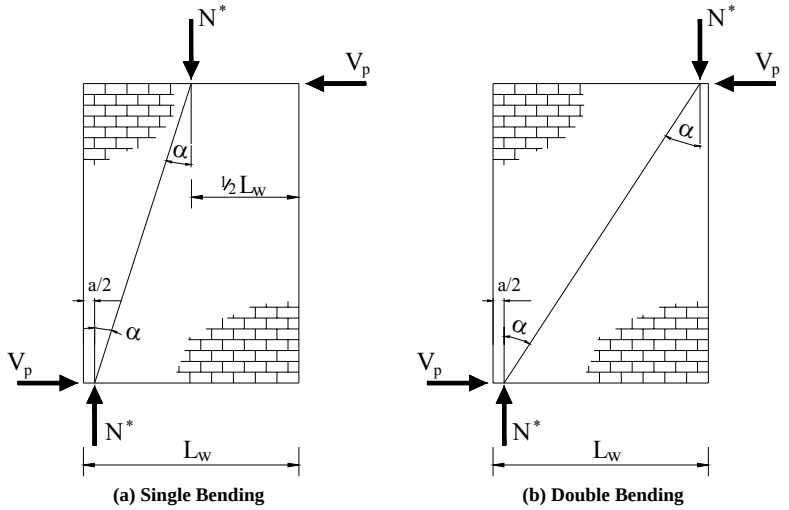

Figure 4.2 Contribution of axial force to masonry shear strength.

For a cantilever wall, α is the angle formed between the wall axis and the strut from the point of load application to the centre of the flexural compression zone at the wall plastic hinge critical section. For a wall in double bending, α is the angle between the wall axis and the line joining the centres of flexural compression at the top and bottom of the wall (see Figure 4.2).

Justification for the abovementioned approach is the simple observation that the axial load must effectively form a compression strut at an angle to the wall axis since it must be transmitted through the flexural compression zone, and that the horizontal component of the strut force resists the applied shear force (Priestley et al., 1994). This method implies that the shear strength of squat axially loaded walls should be greater than that of more slender walls. It also implies that as the axial load increases, and hence the depth "a" of the flexural compression zone increases, the increase in shear strength will become less significant. Note that the 0.9 term in Equation 4-2 has been incorporated to provide a degree of conservatism when applying the theoretical model of Figure 4.2.

4.2.3 Modification to V_s

It has been observed by some researchers that shear reinforcement has limited efficiency in masonry walls. For example, Anderson and Priestley (1992) observed through statistical data fitting that the efficiency of shear reinforcement on masonry shear strength is approximately half of that assumed in a reinforced concrete member. An explanation by Anderson and Priestley is as follows: upon initial loading of a wall, all shear is carried by the masonry and the shear reinforcement is essentially unstressed. When diagonal cracking occurs the reinforcing steel at the crack must go into tension, but because of crack opening the shear carried by the masonry across the crack is reduced. As the crack widens the tension in the shear reinforcement increases, the shear carried across the crack by the masonry decreases. Hence, as deformation increases, the rate at which the reinforcement influences shear capacity may be less than the rate at which the masonry loses strength, and so a maximum capacity is reached.

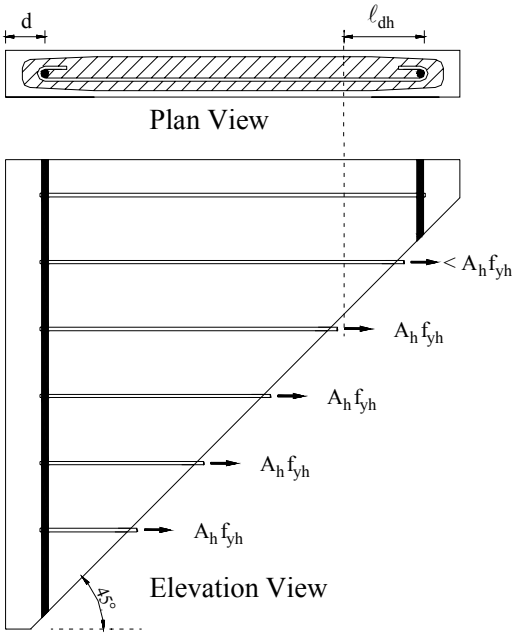

Figure 4.3 Reduced efficiency of shear reinforcement in masonry wall.

In addition to the explanation presented above, it was observed that the data sources used by Anderson and Priestley (1992) included walls that had shear reinforcement with various end anchorage arrangements. While some of the test walls had 180 degree hooks on the ends of the horizontal shear reinforcement, others had 90 degree bends, and some of the walls had end plates welded onto the horizontal reinforcement. Also, several walls in the data sources had rather short length, suggesting that in those walls, because of the anchorage details and development length of the horizontal shear reinforcement, it was unlikely that there was a sufficient length of shear reinforcement to fully develop their yield strength, see Figure 4.3.

Taking account of the above explanations, a new equation is proposed to account for V_s. Equation 4-3 is proposed based on the hypothesis that the reduced efficiency of shear reinforcement due to anchorage efforts could be evaluated by defining a shear reinforcement "dead zone" at each end of the wall, where the reinforcement is not able to develop greater than $0.5f_y$. Consequently, a reduced effective depth of the section, D_{eff} (similar to the V_s term developed by Shing et al.) is proposed to account for cover to the longitudinal reinforcement, depth of masonry compression zone and development of the shear reinforcement:

$$V_s = A_h f_{yh} \frac{D_{eff}}{s_h} \qquad (4\text{-}3)$$

where $D_{eff} = L_w - (d' + c) - \ell_{dh}$. The c presented here accounts for the depth of neutral axis as reinforcement within compression zone is ineffective to be used as anchorage. The ℓ_{dh} accounts for the development length of shear reinforcement that has 90^o hook and shall be taken as $20d_b$ and $35d_b$ for reinforcement with f_y of 300 MPa and 500 MPa respectively.

Adding the modified V_m, V_p and V_s terms, a new shear expression is developed and shown in Equation 4-4. Finally, the lesser $V_{n(max)}$ value of $0.33\sqrt{f'_m}A_n$ imposed by NEHRP is chosen as the only upper limit to Equation 4-4 to prevent this shear equation being less conservative than the NEHRP shear expression.

$$V_n = 0.8k(C_a + C_b)A_n\sqrt{f'_m} + 0.9N^* \tan\alpha + A_h f_{yh}\frac{D_{eff}}{s_h} \quad \le 0.33A_n\sqrt{f'_m} \qquad (4\text{-}4)$$

4.3 MASONRY SHEAR EQUATION FOR NZS 4230:2004

With the primary purpose of facilitating use of the standard, some changes to Equations 4-1 to 4-4 were implemented in order to simplify the shear equations adopted in the recently updated

version of the New Zealand masonry design standard, NZS 4230:2004, for calculating the shear strength of reinforced concrete masonry components such as walls, beams and columns. Unlike the proposed Equation 4-4, the NZS 4230:2004 governing equation for shear strength is presented in the form of stress:

$$V_n = v_n b_w d = \left(v_m + v_p + v_s\right) b_w d \qquad (4\text{-}5)$$

For masonry beams and columns, d shall be taken as the distance from the extreme compression fibre to the centroid of longitudinal tension reinforcement. For masonry walls, d shall be taken as $0.8L_w$. The v_n term shown in Equation 4-5 is the total nominal shear stress and is limited to a maximum stress of $0.45\sqrt{f'_m}$ regardless of loading condition, being reproduced from the maximum stress implemented in Equation 4-4 to account for the replacement of A_n by $b_w d$ (i.e. $0.33\sqrt{f'_m}/0.8 = 0.41\sqrt{f'_m}$) and then being slightly relaxed to give $0.45\sqrt{f'_m}$. It is noted that the $v_{n(max)} \le 0.45\sqrt{f'_m}$ implemented in NZS 4230:2004 is more conservative than that permitted in NZS 4230:1990 for a masonry structure subjected to seismic loading, and having $f'_m < 16$ MPa.

4.3.1 Shear Stress provided by Masonry

Similar to Equation 4-1, NZS 4230:2004 requires the shear stress provided by masonry, v_m, to be dependent on masonry tensile strength, represented by the $\sqrt{f'_m}$ term, and is evaluated using the basic shear stress for masonry, v_{bm}, as defined in Table 4.1. The v_{bm} term shown here is evaluated according to Equation 4-1 for a concrete masonry wall that is assumed to have the most unfavourable wall aspect ratio of $h_e/L_w \ge 1.0$ and reinforced longitudinally using f_y = 300 MPa reinforcing steel with the minimum ratio of ρ_v = 0.07% specified by NZS 4230:2004. This produces $v_{bm} = 0.192k\sqrt{f'_m}$, but was then rounded up to give $0.2k\sqrt{f'_m}$ for convenience. The k factor adopted here is identical to that proposed in section 4.2.1 in that the NZS 4230:2004 assumes that negligible strength loss occurs up to a component ductility of 1.25, followed by a gradual decrease until v_{bm} = 0 at a ductility ratio of 4. This behaviour is presented in tabular form in Table 4.1 which specifies three grades of masonry dependent on the degree of inspection of construction work. Consequently it is conservative to adopt v_{bm} as the type-dependent shear stress provided by masonry, v_m. For masonry components that have aspect ratios of $0.25 \le h_e/L_w \le 1.0$ and/or ρ_v greater than 0.07%, NZS 4230:2004 permits the optional additional use of the C_1 and C_2 terms included in Equation 4-6 to provide an increased value of v_m above that given in Table 4.1.

Table 4.1 Type dependent nominal strengths (MPa)

Type of stress	**Observation type of masonry***		
	C	***B***	***A***
Compression; f'_m	4	12	12**
Basic shear provided by masonry, General conditions, v_{bm}	0.30	0.70	$0.2\sqrt{f'_m}$
Basic shear provided by masonry in potential plastic hinges of limited ductile structures, v_{bm}	N/A	0.50	$0.15\sqrt{f'_m}$
Basic shear provided by masonry in potential plastic hinges of ductile structures, v_{bm}	N/A	0	0
Maximum total shear, $v_{n(max)}$	0.80	1.50	$0.45\sqrt{f'_m}$

* Observation requirement:

Type C: no construction observation by design engineer or nominated representative

Type B: inspection required to establish that work is carried out generally as specified

Type A: in addition to inspection required by Type B, Type A observation of masonry shall require construction supervision at all critical stages

** A higher f'_m may be used if substantiated through prism testing

$$v_m = (C_1 + C_2)v_{bm} \qquad (4\text{-}6)$$

where

(a) $C_1 = 33p_w \frac{f_y}{300}$;

(b) and C_2 is evaluated as follows:

(i) for walls:

$$\text{for } \frac{h_e}{L_w} < 0.25,\ C_2 = 1.5;$$

$$\text{for } 0.25 \le \frac{h_e}{L_w} \le 1.0,\ C_2 = 0.42\left[4 - 1.75\frac{h_e}{L_w}\right];$$

$$\text{for } \frac{h_e}{L_w} > 1.0,\ C_2 = 1.0;$$

(ii) $C_2 = 1.0$ for beams and columns.

The C_1 and C_2 terms presented in Equation 4-6 were obtained by dividing the C_a and C_b terms presented in Equation 4-1 by the v_{bm} of $0.2\sqrt{f'_m}$. The C_1 term allows longitudinal reinforcement other than f_y = 300 MPa to be included when considering the dowel effect towards masonry shear strength.

4.3.2 Shear Stress provided by Axial Load

Since NZS 4230:2004 addresses masonry shear strength in the form of stress, a $b_w d$ term is introduced to Equation 4-2 to produce Equation 4-7. A limitation to the magnitude of axial compression that could be assumed to assist in providing shear strength, $N^* \leq 0.1 f'_m A_n$, was included to prevent the occurrence of brittle shear failure, as it was observed during experimental studies (e.g. Matsumura, 1987; Shing et al., 1990; Sveinsson et al., 1985) that post-cracking deformation capacity of masonry walls were significantly reduced with increasing axial compression load. A final limitation of $v_p \leq 0.1 f'_m$ was included to prevent excess dependence on v_p in a relatively squat masonry wall.

$$v_p = 0.9 \frac{N^*}{b_w d} \tan \alpha \qquad (4\text{-}7)$$

4.3.3 Design of Shear Reinforcement

The method of calculating the shear contribution from shear reinforcement was simplified by replacing the D_{eff} term in Equation 4-3 with a d term:

$$V_s = C_3 A_h f_{yh} \frac{d}{s_h} \qquad (4\text{-}8)$$

The C_3 coefficient was included in Equation 4-8 to represent the limited efficiency of shear reinforcement in masonry walls due to bar anchorage effects. Consequently, C_3 shall be taken as 0.8 for masonry walls, or taken as 1.0 for beams and columns that have shear reinforcement comprised of closed hoops. Note that Equation 4-8 matches Equation 4-3 for a 1740 mm long masonry wall reinforced with 12 mm diameter shear reinforcement of f_{yh} = 500 MPa (ρ_v = 0.2%, σ_n = 0). For masonry walls of greater length and reinforced with shear bars of smaller diameters and lower reinforcement yield stress, Equation 4-8 is more conservative with respect to Equation 4-3. Finally, Equation 4-8 is divided by the $b_w d$ term to produce the v_s required by Equation 4-5:

$$v_s = \frac{V_s}{b_w d} = C_3 \frac{A_v f_y}{b_w s_h} \qquad (4\text{-}9)$$

4.4 MODIFICATION TO SHEAR REDUCTION FACTOR

In addition to the changes described in section 4.3, the masonry shear strength reduction factor has also been updated in NZS 4230:2004. The strategy adopted in NZS 4230:1990 was to consider the value of strength reduction factor for shear that was used in NZS 3101, but to then add additional conservatism based on the perception that masonry material strength characteristics and construction practices were less consistent than their reinforced concrete equivalent.

In NZS 4230:2004, a masonry shear strength reduction factor of $\phi = 0.75$ has been adopted. This new shear strength reduction factor is the same as that used in NZS 3101 and is less stringent than its predecessor because:

1. The manufacture of masonry constituent materials and the construction of masonry structures are governed by the same regulatory regimes as those of reinforced concrete.
2. There is no measured data to form a basis for adoption of strength reduction values other than those employed in NZS 3101 for concrete structures, and the adoption of corresponding values will facilitate designers interchanging between NZS 4230 and NZS 3101.
3. The masonry standard joint committee (MSJC) for the United State, composed of representatives from the American Society of Civil Engineers (ASCE), the American Concrete Institute (ACI) and The Masonry Society (TMS) have adopted $\phi = 0.8$ for shear in the recently released document ACI 530-05/ASCE 5-05/TMS 402-05.

4.5 SHEAR DESIGN ILLUSTRATIONS

4.5.1 Masonry Wall

This section illustrates two simple examples of shear design using NZS 4230:2004, of a nominally ductile (i.e. $\mu = 1.25$) single-storey cantilevered concrete masonry wall that is subjected to (a) $V^* = 150$ kN and (b) $V^* = 275$ kN respectively. The Observation Type B concrete masonry wall is 2600 mm long, 1800 mm high and 140 mm wide. As shown in Figure 4.4, the wall is reinforced vertically with D16 spaced at 400 mm c/c and is of fully grout-filled construction. In both cases, the masonry wall is subjected to an axial load of $N^* = 50$ kN. Note that a more comprehensive masonry wall design example is presented in Appendix A.

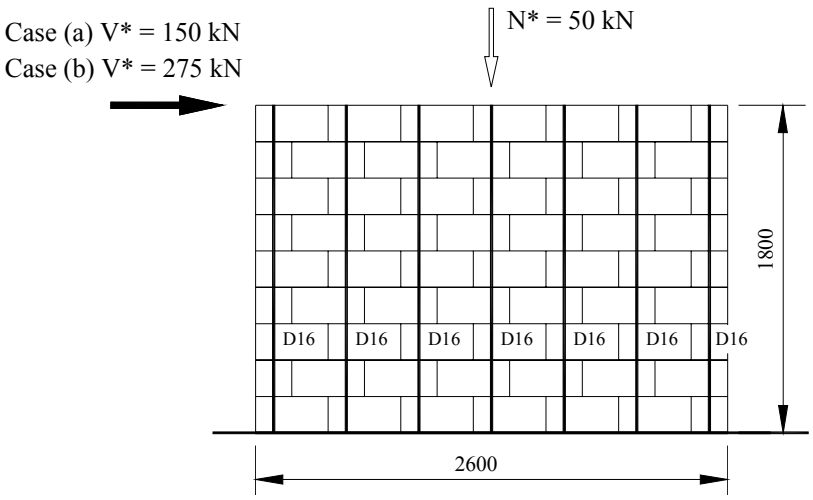

Figure 4.4 Forces acting on masonry wall

Case (a)

V* = 150 kN

Require $\phi V_n \geq V^*$

Therefore $V_n \geq \dfrac{V^*}{\phi}$ and $v_n = \dfrac{V_n}{b_w d}$

$\geq \dfrac{150}{0.75}$ $= \dfrac{200.0 \times 10^3}{140 \times 0.8 \times 2600}$

≥ 200.0 kN $= 0.69$ MPa $< v_{bm}$

Since the required v_n is less than the v_{bm} of 0.70 MPa (see Table 4.1) for a nominally ductile structure, it is unnecessary to consider Equation 4-6 since this equation will provide a v_m above 0.70 MPa as the wall has $p_w > 0.07\%$ and a geometry of $h_e/L < 1.0$. Also, it is unnecessary to consider the contribution of shear resistance provided by the axial load component (v_p) in this loading case because the masonry wall has sufficient strength to resist the applied shear force using the v_m alone. Consequently, shear reinforcement is only required to satisfy the minimum requirement of 0.07% specified by NZS 4230:2004.

Case (b)

V* = 275 kN

Require $\phi V_n \geq V^*$

Therefore $V_n \geq \frac{V^*}{\phi}$ and $v_n = \frac{V_n}{b_w d}$

$\geq \frac{275}{0.75}$ $= \frac{366.7 \times 10^3}{140 \times 0.8 \times 2600}$

≥ 366.7 kN $= 1.26$ MPa

For this loading case, the beneficial effect of C_1 and C_2 terms are not considered at this stage to give a more conservative value of v_m, i.e. $C_1 + C_2$ is assumed to be equal to 1.0, therefore $v_m = v_{bm} = 0.70$ MPa.

Shear strength contributed by the axial load component is evaluated using Equation 4-7. The depth of the compression stress block **a** (see Figure 4.2) is established to be about 246.5 mm according to the principle of force equilibrium. Therefore, $\tan\alpha = (L_w - \mathbf{a})/2h_e = (2600 - 246.5)/(2 \times 1800) = 0.65$. Hence,

$$v_p = 0.9 \times \frac{50 \times 10^3}{140 \times 0.8 \times 2600} \times 0.65 = 0.10 \text{ MPa.}$$

Assuming that the shear reinforcement consists of D10 ($A_v = 78.5$ mm^2) spaced at 400 mm c/c, this will give $v_s = \frac{V_s}{b_w d} = C_3 \frac{A_v f_y}{b_w d} \times \frac{0.8h}{s_h} = 0.8 \times \frac{78.5 \times 300 \times 0.8 \times 1800}{140 \times 0.8 \times 2600 \times 400} = 0.23$ MPa. Note that as shown in Figure 4.5b, this equation differs slightly from Equation 4-9 in order to account for the fact that the critical 45^o crack intersects the wall top when $h/L_w < 1.0$ (Priestley, 1980), therefore giving $V_s = C_3 A_v f_y \frac{0.8h}{s_h}$. The shear reinforcement ratio is $\rho_h = \frac{A_v}{b_w s}$

$= \frac{78.5}{140 \times 400} = 0.0014$.

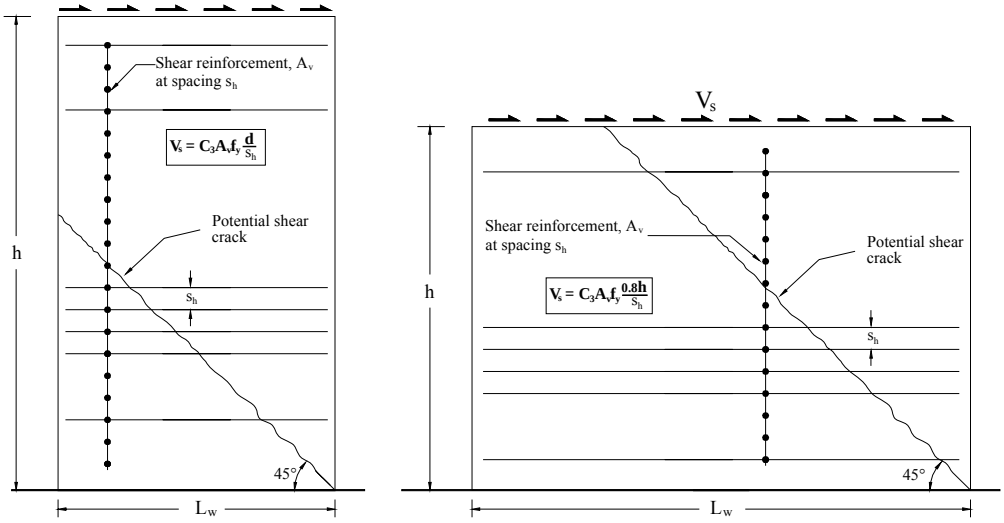

(a) Slender wall ($h/L_w \geq 1.0$) **(b) Squat wall ($h/L_w < 1.0$)**

Figure 4.5 Shear reinforcement for cantilever walls (Priestley, 1980).

Therefore, $v_n = v_m + v_p + v_s = 0.70 + 0.10 + 0.23 = 1.03$ MPa. This is less than the required v_n of 1.26 MPa. Consequently, it is now appropriate to consider the $C_1 + C_2$ terms to provide an increased value of v_m above the v_{bm} specified in Table 4.1.

The p_w and h_e/L_w values are required, where $p_w = A_s/b_w d$ = (6 x D16)/(140 x 0.8 x 2600) = 0.0041 (note that only 6-D16 are in tension) and $h_e/L_w = 1800/2600 = 0.69$. Therefore, according to Equation 4-6, $C_1 = 33 p_w f_y/300 = 0.14$ (where $f_y = 300$ MPa) and $C_2 = 0.42$ x [4 – $1.75 h_e/L_w$] = 1.17. Hence, the new $v_m = (C_1 + C_2) v_{bm}$ = (0.14 + 1.17) x 0.70 = 0.92 MPa. Consequently, the updated prediction of v_m provides an increase value of the design shear strength $v_m + v_p + v_s$ to 1.25 MPa, which is about 1.0% less than the required v_n. Note that if further shear strength had been required, it would have been necessary to provide additional horizontal shear reinforcement and/or to increase the wall thickness if f'_m is to remain 12 MPa.

4.5.2 Masonry Beam

This section demonstrates the shear design of a nominally ductile concrete masonry beam that is subjected to V* = 35 kN. As shown in Figure 4.6, the masonry beam is longitudinally reinforced with 2-D16 and is of Observation Type B construction. The masonry beam described here is not subjected to axial compression load.

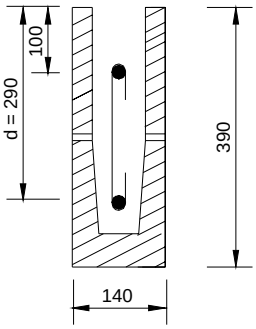

Figure 4.6 Masonry beam dimensions and reinforcement arrangement

V* = 35 kN

Require $\phi V_n \geq V^*$

Therefore $V_n \geq \dfrac{V^*}{\phi}$ and $v_n = \dfrac{V_n}{b_w d}$

$\geq \dfrac{35}{0.75}$ $= \dfrac{46.7 \times 10^3}{140 \times 290}$

≥ 46.7 kN $= 1.15$ MPa

Similar to the previous calculation, the beneficial effect of the C_1 and C_2 terms are not considered at this stage to give a more conservative value of v_m, i.e. $C_1 + C_2$ is assumed to be equal to 1.0, therefore $v_m = v_{bm} = 0.70$ MPa. Since the beam is not subjected to axial load, $v_p = 0$.

Now, assuming that the shear reinforcement consists of R6 ($A_v = 28.3$ mm^2) spaced at 150 mm c/c, this will give $v_s = 1.0 \times \dfrac{28.3 \times 300}{140 \times 150} = 0.40$ MPa.

Therefore, $v_n = v_m + v_s = 0.70 + 0.40 = 1.10$ MPa. This is less than the required v_n of 1.15 MPa. Consequently, it is now appropriate to consider the $C_1 + C_2$ terms to provide an increased value of v_m above the v_{bm} specified in Table 4.1.

Now, $p_w = A_s/b_w d = (1 \text{ x D16})/(140 \text{ x } 290) = 0.0050$. Therefore, according to Equation 4-6, $C_1 = 33 p_w f_y/300 = 0.16$ (where $f_y = 300$ MPa) and $C_2 = 1.0$ for a masonry beam. Hence, the new $v_m = (C_1 + C_2)v_{bm} = (0.16 + 1.0) \text{ x } 0.70 = 0.81$ MPa. Therefore, the updated prediction of

v_m provides an increased value of the design shear strength to $v_m + v_s$ = 1.21 MPa, which is above the required v_n of 1.15 MPa. Note that if further shear strength had been required, it would have been necessary to provide additional shear reinforcement and/or to increase the f'_m value if the beam dimensions were unchanged.

4.5.3 NZS 4230:2004 vs NZS 4230:1990

To illustrate the effects of the revised shear provisions, the theoretical shear strength of two typical wall elements using the updated and former standard shear equations is given in Table 4.2. The two Type A observation category ($f'_m = 12$ MPa) 190 mm thick masonry wall elements are 1.8 m and 4.2 m long respectively, at a common height of 3.0 m. Both walls carry a nominal design axial compression load of 20 kN/m and act in single bending. The walls have D12@400 mm c/c (f_y = 300 MPa) in both orthogonal directions and are assumed to be designed to the limited ductility, μ = 2, provisions. The results in Table 4.2 are presented as nominal strength in terms of stress units.

Table 4.2 Shear strength comparison

		Outside Potential Plastic Hinge Zone			**Within Potential Plastic Hinge Zone**		
		NZS 4230:1990	Equation 4-4	NZS 4230:2004	NZS 4230:1990	Equation 4-4	NZS 4230:2004
1.8 m long wall	v_m(MPa)	0.39	0.68	0.74	0.15	0.50	0.53
	v_p (MPa)	---	0.03	0.03	---	0.03	0.03
	v_s (MPa)	0.45	0.41	0.36	0.45	0.41	0.36
	v_n (MPa)	0.84	1.12	1.13	0.60	0.94	0.92
4.2 m long wall	v_m(MPa)	0.39	0.82	0.85	0.15	0.61	0.61
	v_p (MPa)	---	0.08	0.08	---	0.08	0.08
	v_s (MPa)	0.32	0.33	0.26	0.32	0.33	0.26
	v_n (MPa)	0.71	1.23	1.19	0.47	1.02	0.95

It can be seen that the shear strengths of the short wall, calculated using NZS 4230:2004 equation, both within and outside the potential plastic hinge zones, are increased by 35% and 51% when compared to NZS 4230:1990. Due to the lower wall aspect ratio in the 4.2 m long wall, the masonry and axial shear components both increase when calculated using Equation 4-4 and NZS 4230:2004. From Table 4.2, it is established that the shear strengths of the 4.2 m masonry wall, within and outside the potential plastic hinge zones, are increased by at least 68% and 102% when the new proposed shear equations are used to calculate v_n.

Chapter 5

ACCURACY OF SHEAR EXPRESSIONS

5.1 INTRODUCTION

Probably no issue in masonry research has been more investigated over the last two decades than that of masonry shear strength. Factors that were considered include the type of masonry, mortar and grout used, whether the wall was unreinforced, reinforced or prestressed, whether the wall was ungrouted, partially-grouted or fully-grouted and whether the code was written in permissible stress or limit state format. Recently, considerable experimental research, particularly by those conducted in the U.S. and Japan, has been directed towards better understanding of masonry shear strength. From these test results have come equations to predict the shear strength of masonry walls, usually calibrated to the test results carried out by the particular researchers (e.g. Matsumura 1988 and Shing et al. 1990).

This chapter compares results derived when using the nine masonry shear expressions presented in Table 5.1 to predict the maximum in-plane shear strength of reinforced masonry walls under different conditions, such as different reinforcement ratios, shear span ratios, axial compression stresses and masonry compressive strength. These expressions are correlated with a comprehensive data base of test results to establish their accuracy. Wall characteristics from various test specimens are used as input to the predictive equations and the predicted shear strength are then compared to the actual measured strength of each test result. Fattal and Todd (1991) and Anderson and Priestley (1992) had previously compared predictions using different equations with test results obtained from U.S.A and Japanese experimental studies. Supplementary test results conducted in New Zealand (see Chapter 3) are also included in this study, with the primary interest of establishing the effectiveness of Equation 4-4 and NZS 4230:2004 in predicting masonry shear strength. The definitions of symbols used in the shear expressions presented in Table 5.1 are available in sections 2.4.2, 4.2 and 4.3.

Table 5.1 Masonry shear strength equations

Source	Equation	
Matsumura (1987)	$\left[k_u k_p\left(\frac{0.76}{(h/d)+0.7}+0.012\right)\sqrt{f'_m}+0.2\sigma_n+0.18\gamma\delta\sqrt{\rho_h f_{yh} f'_m}\right](0.875 b_w d)$	(2-16)
Shing et al (1990)	$(0.166+0.0217\rho_v f_{yv})A_n\sqrt{f'_m}+(0.0217\sigma_n A_n)\sqrt{f'_m}+\left(\frac{L_w-2d'}{s_h}-1\right)A_h f_{yh}$	(2-17)
NZS 4230:1990	$v_m b_w d + A_h f_{yh}\, d/s_h$	(2-18)
Anderson and Priestley (1992)	$C_{ap} A_n k\sqrt{f'_m}+0.25\sigma_n A_n+0.5A_h f_{yh}\, d/s_h$	(2-19)
NEHRP (1997)	$0.083\left[4.0-1.75\frac{h_e}{L_w}\right]A_n\sqrt{f'_m}+0.25\sigma_n A_n+0.5A_h f_{yh}\, L_w/s_h$	(2-20)
UBC (1997)	$0.083 C_d A_n\sqrt{f'_m}+A_h f_{yh}\, L_w/s_h$	(2-21)
AS 3700-1998	$f_{vr} A_n + 0.8 f_{yh} A_s$	(2-22)
Equation 4-4	$k(C_a+C_b)b_w d\sqrt{f'_m}+0.9N^*\tan\alpha+A_h f_{yh}\, D_{efff}/s_h$	(4-4)
NZS 4230:2004	$(C_1+C_2)v_{bm} b_w d+0.9\sigma_n A_n\tan\alpha+C_3 A_h f_{yh}\, d/s_h$	(4-5)

5.2 CORRELATION OF SHEAR EQUATIONS

Correlation between the nine shear equations are investigated under different conditions, with the results presented in Figures 5.1 to 5.3. The parameters selected were based on a 140 mm thick concrete masonry wall being 2.4 m high and 1.8 m long. The wall is reinforced longitudinally with 20 mm diameter reinforcement bars space at 400 mm centres. In each figure, only a single parameter is varied with other conditions unchanged. Hence, Figure 5.1 examines the influence of f'_m, and Figures 5.2 and 5.3 examine the influence of $\rho_h f_{yh}$ and σ_n respectively. It is considered that f'_m = 30 MPa, $\rho_h f_{yh}$ = 2.0 MPa and σ_n = 4.0 MPa are deemed to be realistic upper limits to the magnitude to these parameters.

Figure 5.1 shows that the conservatism of NZS 4230:1990 increases as f'_m increases. This is partly because the beneficial effect of axial compression load is not properly considered by this standard. More significantly, the conservatism of NZS 4230:1990 shown in Figure 5.1 is mostly due to the overly conservative assumption regarding the contribution of v_m since the

standard restricted $v_m \leq 0.72$ MPa. Equation 4-4 and NZS 4230:2004 show significantly improved correlation with other shear equations. Of the two codified masonry shear expressions of U.S. origin, it is clearly shown that the UBC is significantly more conservative than the NEHRP expression. This is partly because of the more conservative assumption of the v_m term by the UBC and partly because of the omission by this standard of the beneficial effect of axial compression load towards masonry shear strength.

Figure 5.2 shows the influence of horizontal shear reinforcement on masonry wall shear strength. Matsumura considered the rate of increase in shear resistance to be associated with $\sqrt{f'_m}$. Consequently, he proposed that the effect of shear reinforcement be approximately proportional to $\sqrt{f'_m \rho_h f_{yh}}$. Figure 5.2 shows zero increase in shear resistance beyond $\rho_h f_{yh}$ = 0.50 MPa for the NEHRP (and UBC) and NZS 4230:2004, due to limit for $v_{n(max)}$ of $0.33\sqrt{f'_m}$ and $0.45\sqrt{f'_m}$ imposed by these two codes. Similar to the just mentioned observations, no increase in shear strength for Equation 4-4 when the calculated v_n reaches $v_{n(max)}$. As for the Matsumura, Shing et al., Anderson and Priestley, and the AS 3700-1998 shear expressions, the absence of $v_{n(max)}$ in these four shear expressions had resulted in the almost linear increase in masonry shear strength with $\rho_h f_{yh}$ as shown in Figure 5.2.

Figure 5.3 illustrates the disadvantage of NZS 4230:1990 when strength enhancement provided by axial compression load was not considered separately from the masonry component. The low shear strength of NZS 4230:1990 illustrated in Figure 5.3 is again due to the restriction of $v_m \leq 0.72$ MPa, where NZS 4230:1990 specified $v_m = 0.3(0.1f'_m + \sigma_n)$. The revised masonry shear equation of NZS 4230:2004 is shown to have an improved correlation with the other shear equations. The figure shows zero shear resistance increase beyond σ_n = 1.2 MPa, due to the restrictions of $\sigma_n \leq 0.1f'_m$ and $v_p \leq 0.1f'_m$ imposed by NZS 4230:2004 for preventing excessive dependence on v_p in masonry structures. Similarly, the low masonry shear strength predicted by the UBC was due to overlooking of the beneficial effect of axial compression load by this standard.

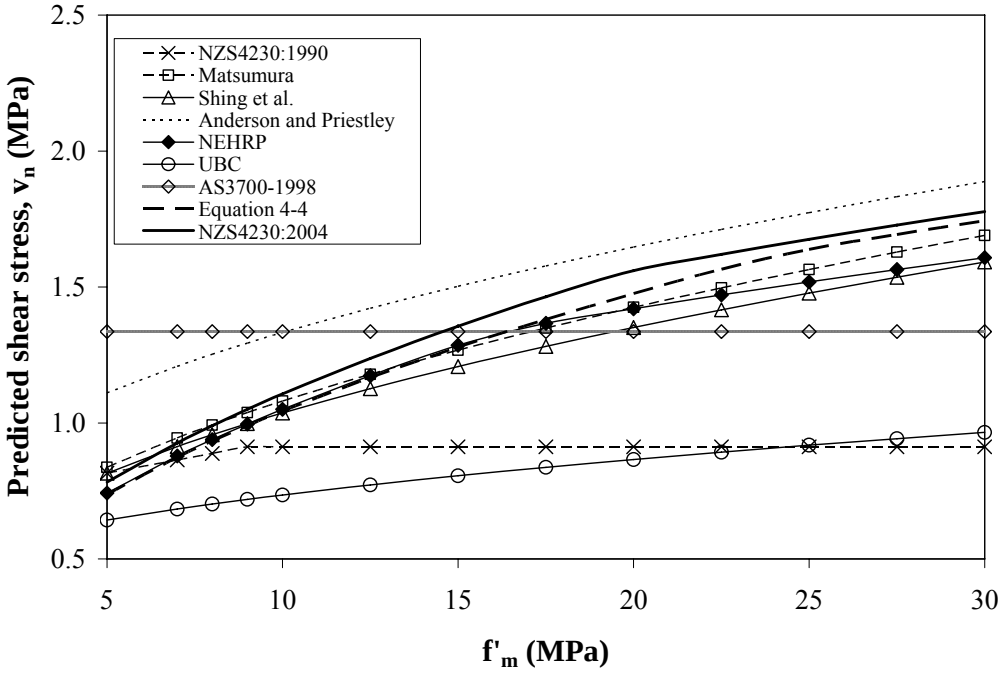

Figure 5.1 Effect of masonry compressive strength on masonry shear strength.

(σ_n = 1.50 MPa, $\rho_h f_{yh}$ = 0.42 MPa, $\rho_v f_{yv}$ = 1.90 MPa)

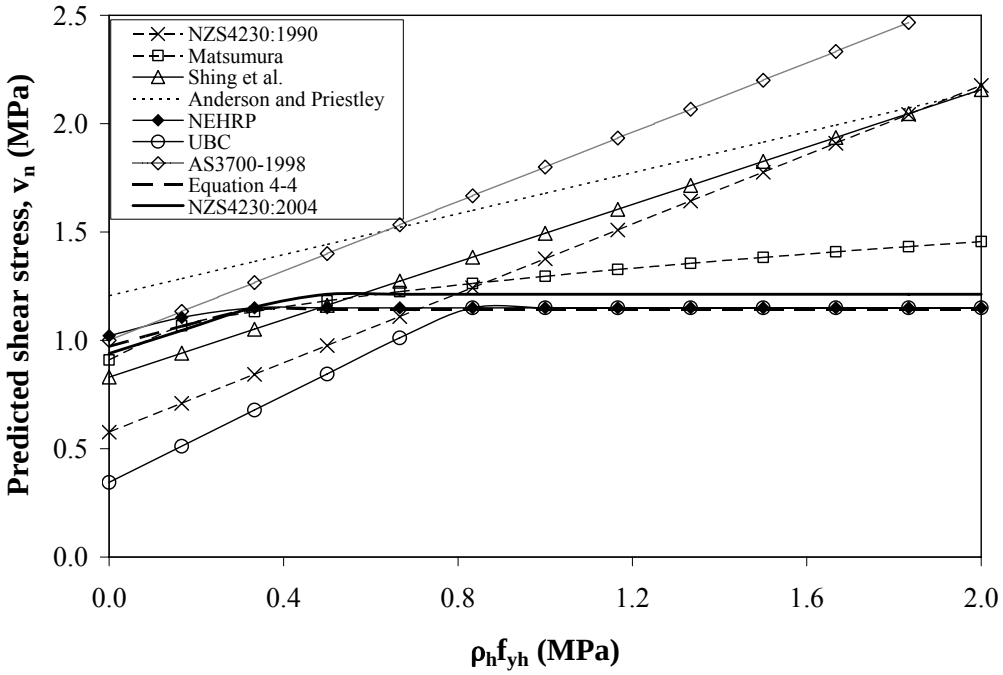

Figure 5.2 Effect of shear reinforcement on masonry shear strength.

(f'_m = 12 MPa, σ_n = 1.5 MPa, $\rho_v f_{yv}$ = 1.90 MPa)

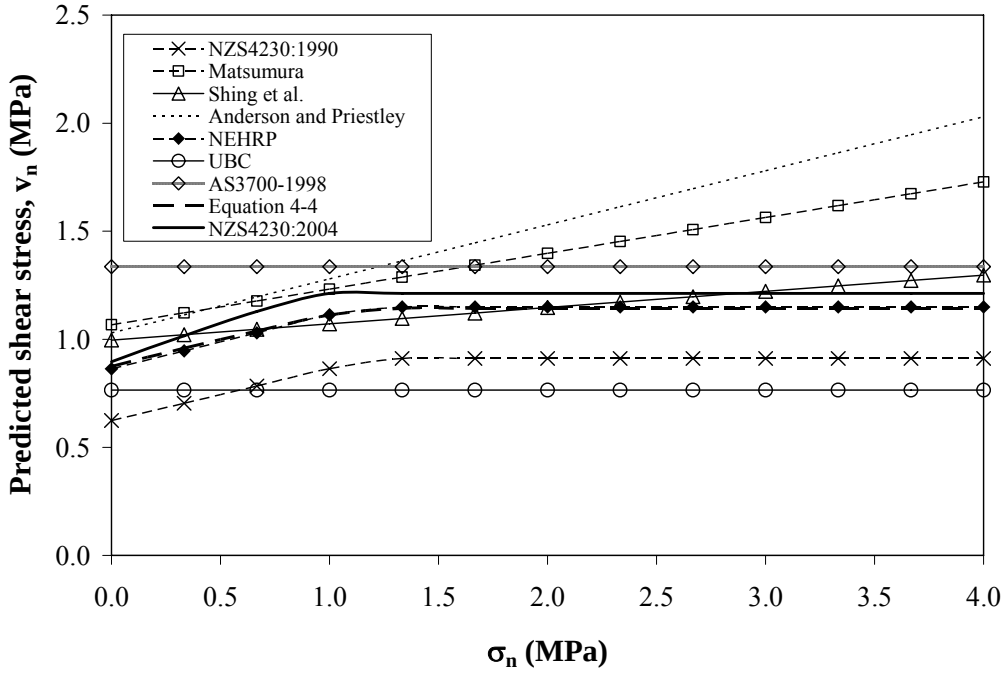

Figure 5.3 Effect of axial compressive stress on masonry shear strength.

(f'_m =12 MPa, $\rho_h f_{yh}$ = 0.42 MPa, $\rho_v f_{yv}$ = 1.90 MPa)

5.3 COMPARISON WITH AVAILABLE TEST RESULTS

5.3.1 Experimental Data Sets

The experimental data sets used as part of the study are those of fully-grouted concrete and clay brick masonry walls that were subjected to reverse cyclic lateral load and failed in shear. The test results selected are from the following experimental programmes:

1. Test conducted by Sveinsson et al. (1985) at the University of California at Berkeley;
2. Test conducted by Matsumura (1988) at Japan's Building Research Institute, Ministry of Construction;
3. Test conducted by Shing et al. (1990) at the University of Colorado;
4. Test conducted by Voon and Ingham (2003) at the University of Auckland.

The first two data sets were obtained from tests in which the top and bottom surfaces were rotationally fixed, while the remaining two were of cantilever type tested at the University of Colorado and University of Auckland. All experimental studies employed displacement controlled testing procedures consisting of multiple cycles of reversed loading. The loading procedures are described in detail in the cited references, which consisted of predefined load-displacement histories characterised by increasing amplitude until failure. The use of a common loading procedure and similar loading rates in each study produced comparable

experimental data. Of the various wall tests conducted at the University of California at Berkeley, only tests reported by Sveinsson et al. (1985) are included here because in some of the other tests there is doubt about the magnitude of axial compression load at failure, which had a tendency to increase during the tests because of the test set-up arrangement.

The maximum shear strength of each wall is defined as the average of the two peak shear forces achieved in the two opposite directions of cyclic loading. Shear strength is calculated using the net cross-sectional area based on actual dimensions (length x wall thickness). Only data from specimens that were reported to have failed in shear were selected, while others that were reported to have failed in bending or sliding were eliminated. Consequently, a total of fifty six test results are included here for comparison. The data subsets finally selected from the studies listed above are identified in the text by the letters B, M, S and A, corresponding to 1-4 respectively. Relevant properties of the specimens are listed in Appendix B. Of the fifty six specimens presented in Table B.1, there are 10S, 18M, 21B and 7A. Seventeen of these specimens were single-wythe walls constructed of hollow brick units, see shaded rows in Table B.1. As shown in Table B.1, experimental testing conducted at the University of Auckland was intended to investigate the shear strength of concrete masonry walls when subjected to low axial compression stresses ($0 \leq \sigma_n \leq 0.5$ MPa) and low shear reinforcement ratios ($\rho_h \leq 0.062\%$). Experimental studies conducted in U.S. and Japan involved masonry walls that were constructed with higher shear reinforcement ratios ($\rho_h \leq 0.668\%$) and subjected to higher axial compression stress levels ($\sigma_n \leq 5.87$ MPa).

The masonry compressive strength, f'_m, listed in Table B.1 was obtained from prism tests. Shing et al. and Matsumura used three course prism tests. Sveinssion et al. used two types of prism test: three course prisms with h/t ratios of 2 and six course prisms with h/t ratios of 4, and the average values of the two were used as the masonry compressive strength for the Sveinsson et al. specimens. The U.S. customary units adopted by Shing et al., and Sveinsson et al. are converted to SI units for convenience.

5.3.2 Correlation between Predicted and Measured Response

Experimental results are compared to shear strength predictions using the shear expressions listed in Table 5.1, accurately accounting for the correct parameters appropriate for each test result. In all cases, predicted strengths are based on measured material properties rather than nominal values. The predicted strength (v_m, v_p, v_s and the sum v_n) and the actual shear strength

(v_{max}) determined from the experimental results of the fifty six specimens are listed in Table B.2 in Appendix B.

Normalised plots (experimentally obtained shear strength, v_{max}, versus predicted shear strength, v_n) are presented in Figures 5.4-5.12 to investigate the accuracy of each individual equation with respect to the different parameters. For example, Figure 5.4(a) examines the accuracy of Equation 2-18 when variation is set on f'_m appropriate to each test result. The line of unity represents perfect correlation. The spread of points above and below the line of unity demonstrates the tendency to over- or under-predict the shear strength of masonry walls, as well as the scatter in the test results. It is emphasised that strength reduction factors or partial safety factors have not been applied when compiling the data shown in Figures 5.4-5.12. The NZS 4230:2004 recommended shear strength reduction factor is represented by the lines of ϕ = 0.75 shown in the figures.

Figure 5.4 presents masonry shear prediction using NZS 4230:1990. The v_n of each masonry wall was evaluated as if the masonry wall was within the elastic range of response. Consequently, a higher value of v_n was obtained than if the wall strength was evaluated according to the experimentally measured ductility level. Figure 5.4 illustrates that, generally, the NZS 4230:1990 approach for masonry shear strength is significantly conservative, as shown by the widely spread data scatter. The figure shows v_{max}/v_n varies from 1.00 to 3.78, with an average of v_{max}/v_n of 1.69. It is shown that NZS 4230:1990 under-predicts the shear strength of 36 specimens by more than 50% of their measured strengths (i.e. $v_{max}/v_n \geq 1.50$). Figure 5.4b indicates a gradual reduction in v_{max}/v_n as the shear reinforcement ratio ($\rho_h f_{yh}$) increases. Although these values are also affected by a simultaneous change in other parameters, Figure 5.4b indicates the likelihood of NZS 4230:1990 to over-predict the contribution of $\rho_h f_{yh}$. In addition, the scatter of results in Figures 5.4(c) and (d) show the deficiency of NZS 4230:1990 when the beneficial effects of axial compression and longitudinal reinforcement on masonry shear strength are not properly considered. Figure 5.4e shows that there is no obviously discernible trend of v_{max}/v_n with increasing displacement ductility μ, but the scatter is rather large, particularly for the Sveinsson's data, making the trend hard to identity.

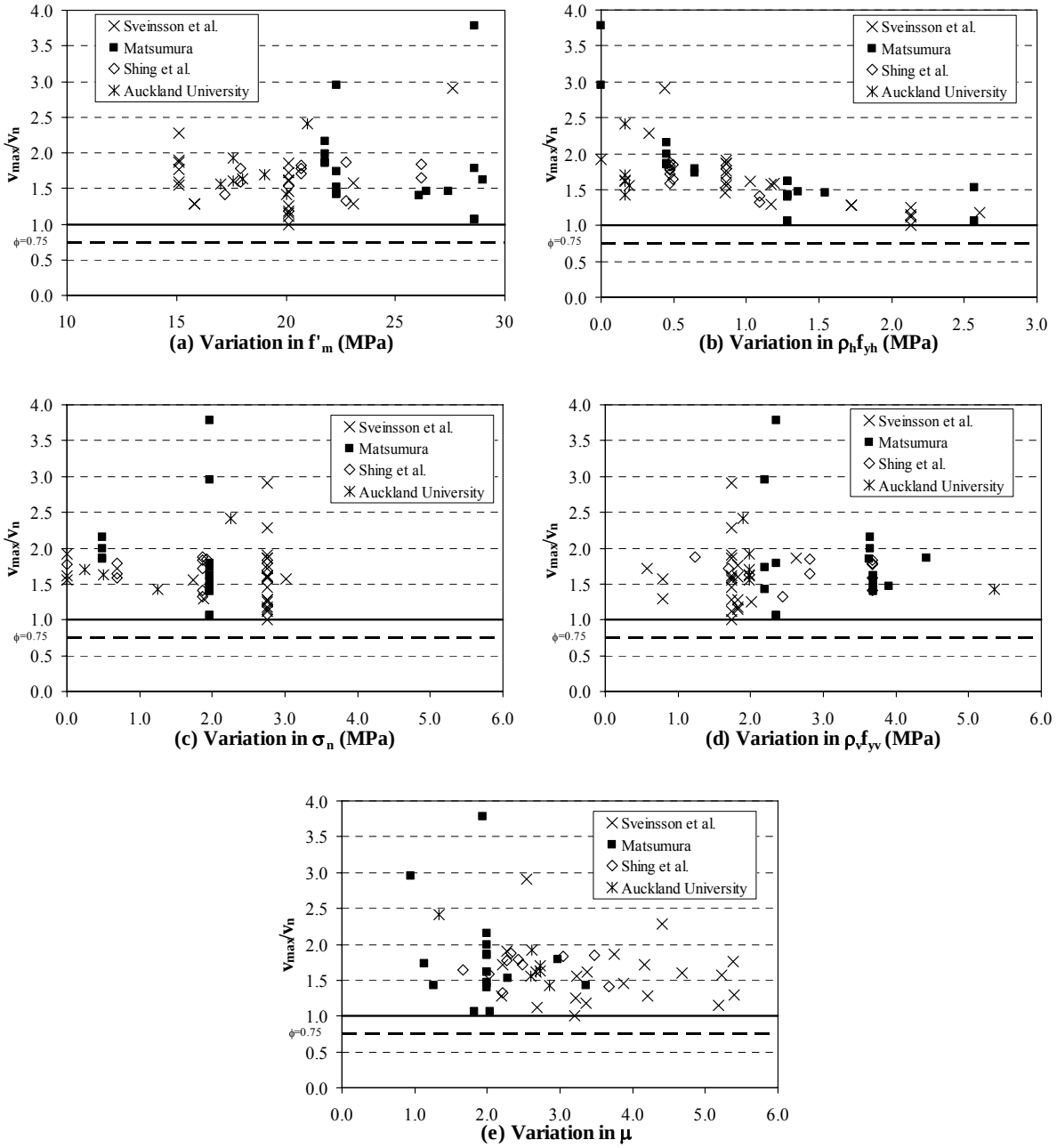

Figure 5.4 Experimental results versus prediction by NZS 4230:1990.

Matsumura developed Equation 2-16 by utilising his test results as well as test results reported by other researchers in Japan. He used regression analysis to determine the appropriate functional forms of the parameters. Overall, Matsumura's equation is more successful than NZS 4230:1990 by narrowing the scatter of points, as illustrated in Figure 5.5. However, this equation does not lend itself to codification due to its complexity and the fact that this equation over-predicted the shear strength of 37% of the tested masonry walls, which includes all seven experimental results recorded at the University of Auckland. The normalised plots show masonry shear prediction using Matsumura's equation resulted in v_{max}/v_n that varies from 0.75 to 1.55, with a mean v_{max}/v_n of 1.03.

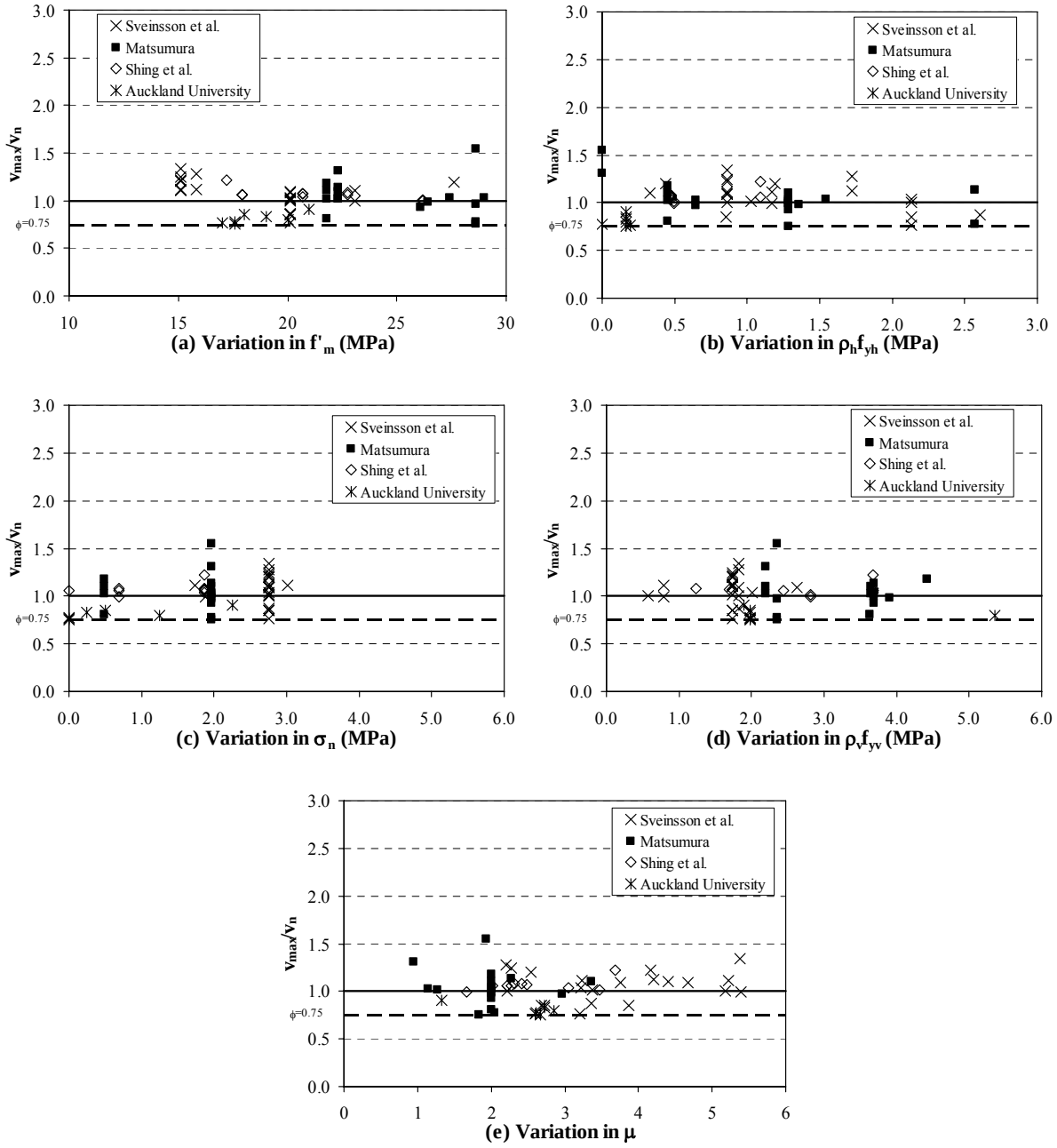

Figure 5.5 Experimental results versus prediction by Matsumura.

Figure 5.6 shows masonry shear prediction using the Shing's shear expression. Shing et al. concluded from their experimental testing that masonry shear strength depends on the tensile strength of masonry as well as on several other mechanisms, such as aggregate interlock, dowel action of longitudinal reinforcement and the truss action of horizontal shear reinforcement. Due to the complexity in predicting the shear strength of reinforcing masonry walls, a semi-empirical design formula based on the mentioned mechanisms was proposed by Shing et al. This formula was developed to fit the test data recorded at the University of Colorado. Consequently, the Colorado test results are better predicted by Equation 2-17 than any of the other experimental data. Figure 5.6 shows that v_{max}/v_n varies from 0.54 to 1.67, with

a mean v_{max}/v_n of 1.12. Similar to that shown in Figure 5.4b, a gradual reduction in the v_{max}/v_n ratio is evident in Figure 5.6b therefore indicating the possibility of Equation 2-17 to over-prediction the contribution of shear reinforcement at high $\rho_h f_{yh}$. The decreasing conservatism of the Shing's equation in prediction the Matsumura's data can be observed in Figure 5.6e when μ increases, with several data points of the Matsumura's tests falling below $v_{max}/v_n = 1.0$. Overall, Shing's shear equation over-predicted the shear strength of 18 specimens, of which 4 specimens had their measured strength less than $0.75v_n$.

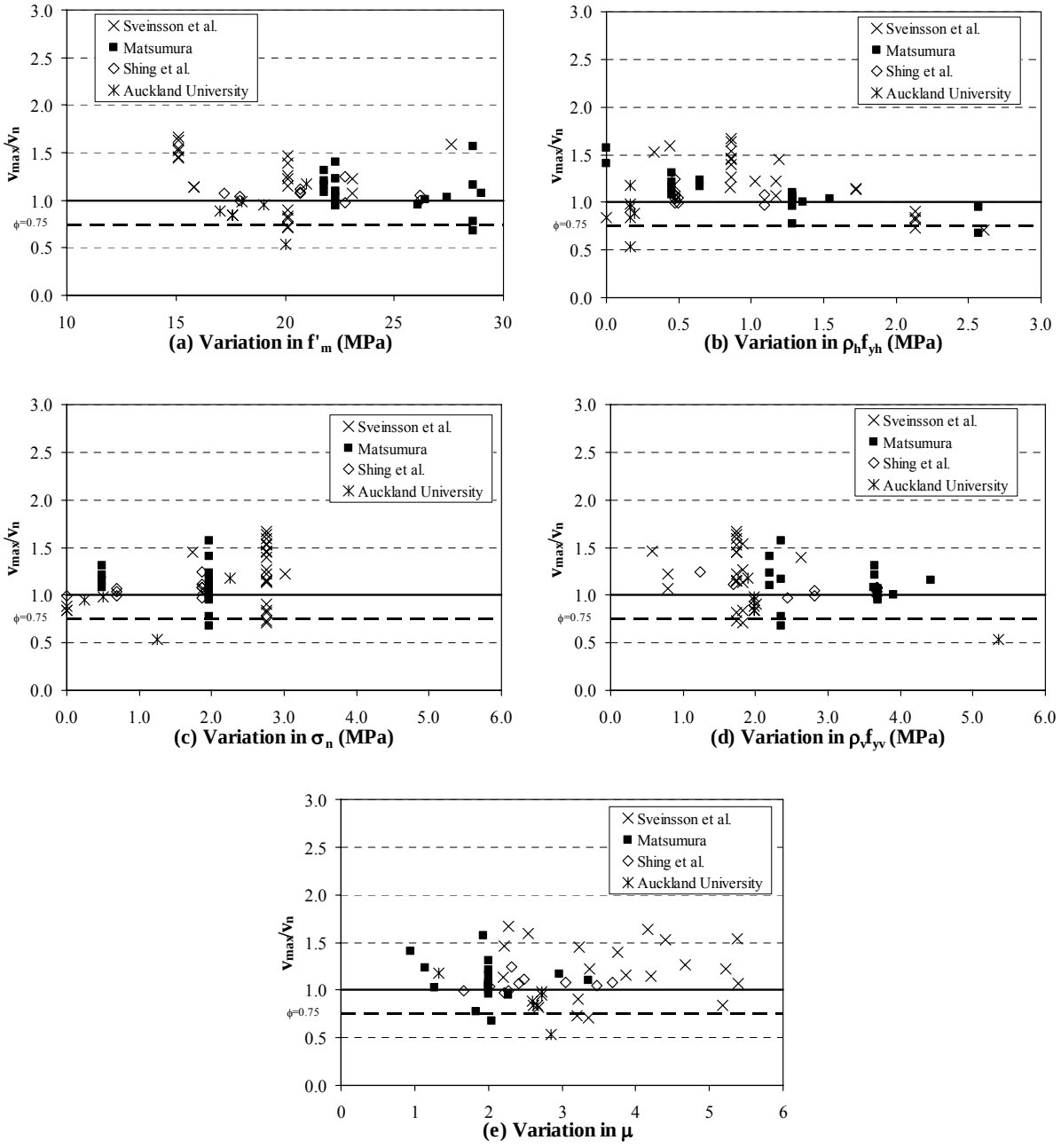

Figure 5.6 Experimental results versus prediction by Shing et al.

Anderson and Priestley developed a simple equation to account for the degradation of masonry shear strength when the wall is subjected to cyclic loading into the inelastic range. The displacement ductility used here to evaluate the k value was based on the measured yield displacement, extrapolating the line from the origin through the displacement at first yield, to the theoretical flexural strength, based on measured material properties. In the absence of defined flexural ductility capacity, a value of $\mu = 2.0$ was assumed for some masonry walls. The accuracy of the Anderson & Priestley shear equation is presented in Figure 5.7. Although the reduction of masonry shear strength ($\mu > 2.0$) is considered in the results presented in

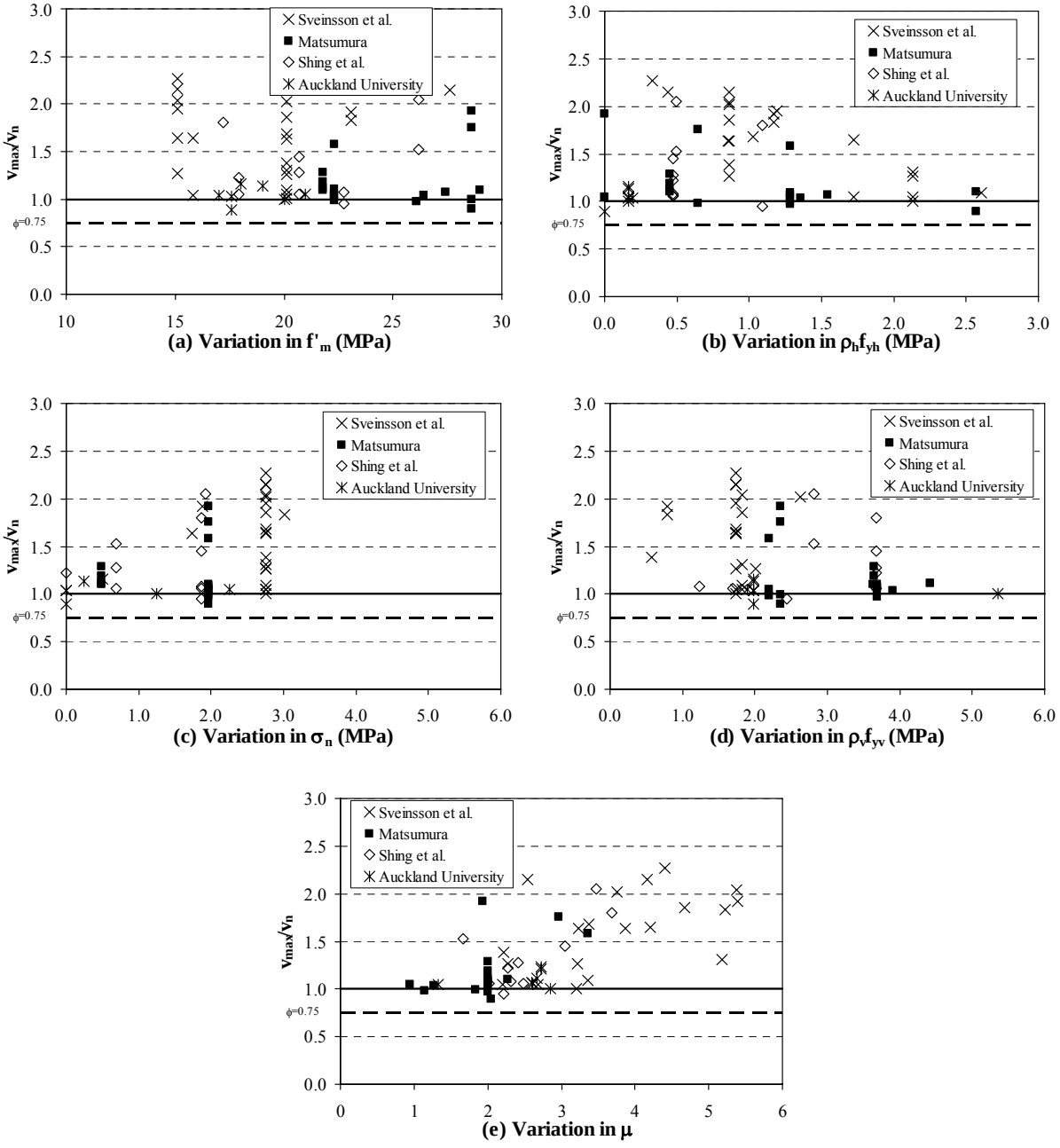

Figure 5.7 Experimental results versus prediction by Anderson and Priestley.

Figure 5.7, it is demonstrated that shear predictions using Equation 2-19 resulted in better accuracy than that predicted according to the NZS 4230:1990 shear expression, therefore further suggesting the excessive-conservatism of NZS 4230:1990. The Anderson & Priestley equation over-predicts the shear strength of 8 specimens, of which 2 had their measured shear strength less than $0.9v_n$. The normalised plots show that v_{max}/v_n varies from 0.89 to 2.27 of which the shear strength of 19 specimens is under-predicted by Equation 2-19 by more than 50% (i.e. $v_{max}/v_n \geq 1.50$). Shear strength prediction using the Anderson and Priestley equation resulted in a mean v_{max}/v_n of 1.36.

Despite the simple form of Equation 2-20, the NEHRP expression is capable of providing significantly improved shear strength prediction (with respect to NZS 4230:1990), as shown by

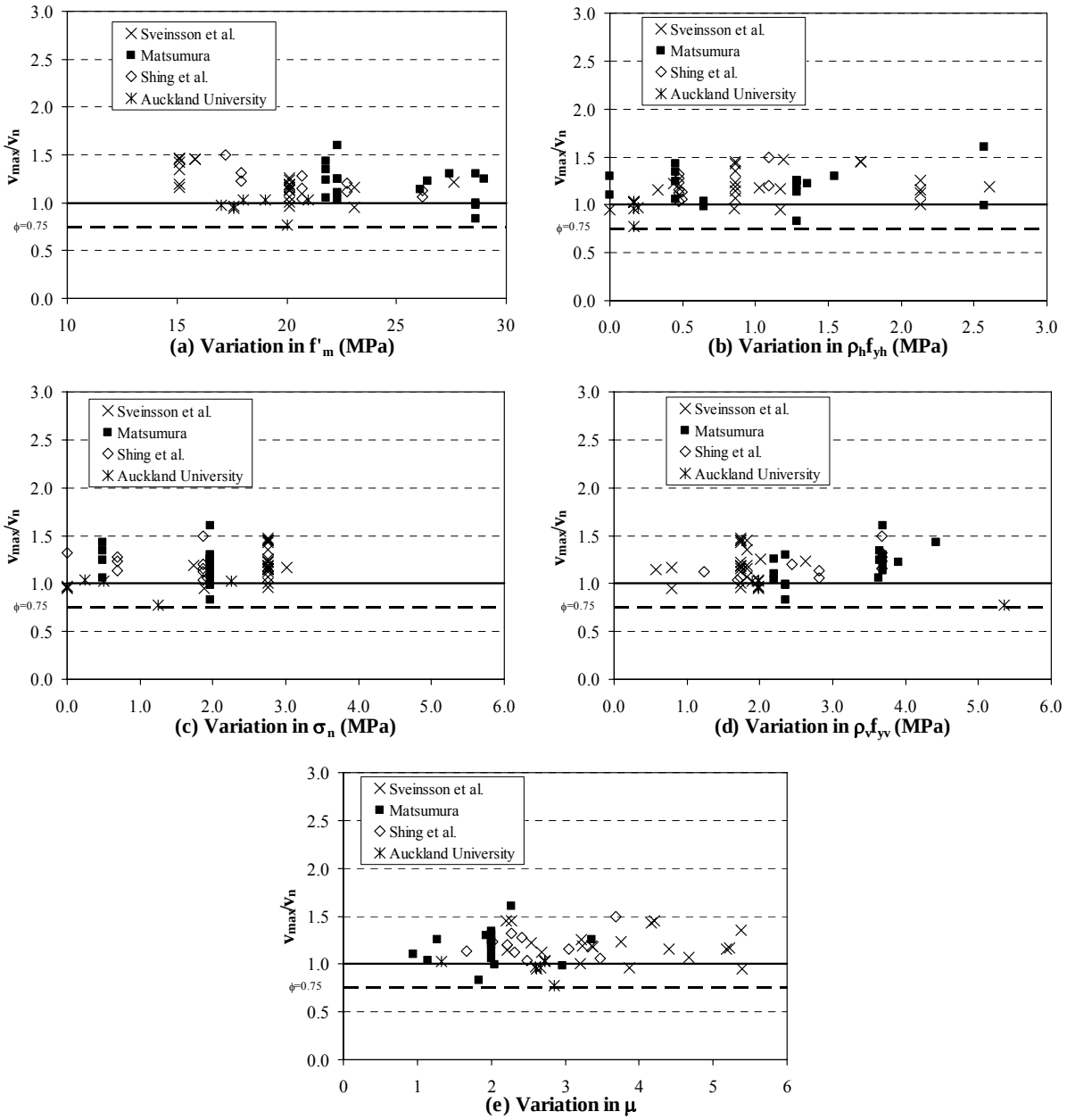

Figure 5.8 Experimental results versus prediction by NEHRP.

the spread of points within v_{max}/v_n of 0.77 and 1.6 in Figure 5.8. The NEHRP shear expression has an advantage over the Anderson & Priestley equation because the wall aspect ratio is included when calculating the masonry component of shear strength, v_m. Figure 5.8e shows the trend of decreasing conservatism of the NEHRP for $2 \le \mu \le 3$, therefore indicating the deficiency in the NEHRP shear equation for not addressing masonry shear strength within the potential plastic hinge regions. In addition, the use of $0.5\rho_h f_{yh}$ in its v_s term is contrary to the well established split beam analogy to account for the contribution of shear reinforcement. Shear strength prediction using the NEHRP shear equation resulted in a mean v_{max}/v_n of 1.18.

Figure 5.9 clearly shows that the UBC shear expression is significantly less successful than the NEHRP in predicting masonry shear strength. This is shown by the spread of points within

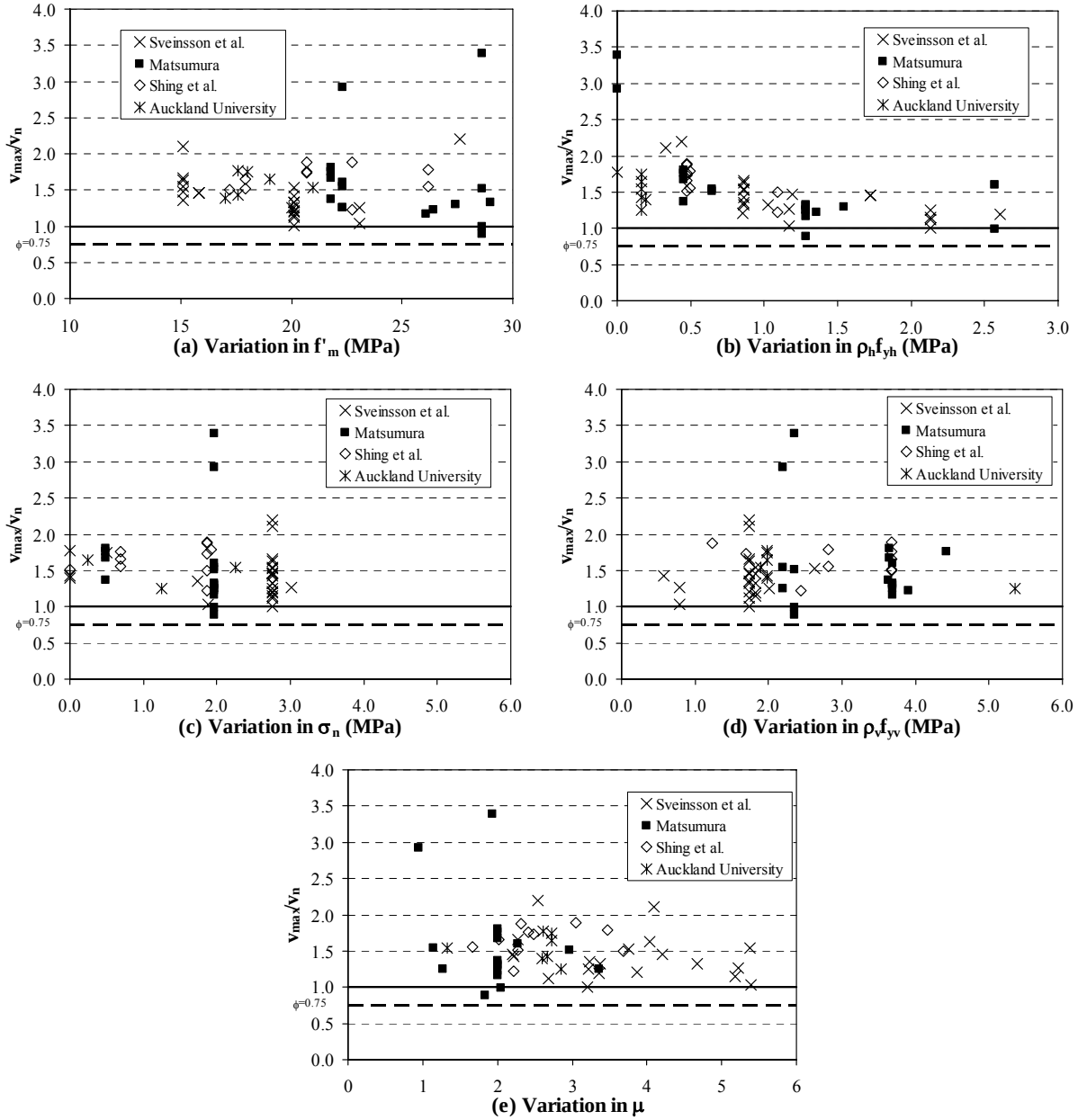

Figure 5.9 Experimental results versus prediction by UBC.

v_{max}/v_n of 0.89 and 3.39 in the figure. The scatter shown in the figure is mostly due to the neglection of shear contributions resulting from the axial compression load and the dowel effect of longitudinal reinforcing steel. Also shown in Figure 5.9b is the reduction of v_{max}/v_n when the $\rho_h f_{yh}$ increases, therefore suggesting that the UBC over-predicting the contribution of shear reinforcement. In addition, Figure 5.9e clearly illustrates the decreasing conservatism of UBC when the displacement ductility level increases. This behaviour is expected based on the prediction model of Figure 2.15 since the strength/ductility degradation is not included in the UBC approach. Shear strength prediction using the UBC masonry shear expression resulted in a mean and standard deviation v_{max}/v_n of 1.52 and 0.42 respectively.

The Australian masonry standard is unsuccessful in accurately predicting the masonry shear strength, as shown in Figure 5.10. The figure shows that v_{max}/v_n varies from 0.73 to 2.97. The AS 3700 expression over-predicts the shear strength of 13 specimens (about 23% of total), of which 5 specimens have $v_{max}/v_n < 0.75$. When closely studying Figure 5.10a, it is evident that v_{max}/v_n tends to increase with increasing f'_m. This is most likely caused by the absence of the f'_m term in Equation 2-22. In addition, the beneficial effect of vertical reinforcement and axial compressive load is not considered in AS 3700, causing the scatter in Figures 5.10c and 5.10d. Similar to the UBC, failure by the AS 3700 to account for the reduction in masonry shear strength as ductility level increases resulted in the reduced v_{max}/v_n ratio when displacement ductility level increases.

The accuracy of Equation 4-4 in predicting masonry shear strength is presented in Figure 5.11. Comparing these results with that shown in Figure 5.4 indicates a significant reduced scatter of v_{max}/v_n, therefore confirming that masonry shear predictions using Equation 4-4 resulted in improved accuracy than that predicted according to the NZS 4230:1990. By comparing Figures 5.8 and 5.11, it is observed that masonry shear strength prediction according to Equation 4-4 resulted in accuracy similar to that predicted according to NEHRP. Equation 4-4 has an advantage over the NEHRP shear expression because Equation 4-4 addresses masonry shear strength within potential plastic hinge regions. This is achieved by considering the reduction in masonry shear strength as displacement ductility level increases (see Figure 4.1). Normalised plot in Figure 5.11e shows that the influence of displacement ductility level appear to be well represented by Equation 4-4. Equation 4-4 over-predicts the shear strength of 9 specimens, of which 1 had $0.8 < v_{max}/v_n < 0.9$. Normalised plots in Figure 5.11 show that v_{max}/v_n

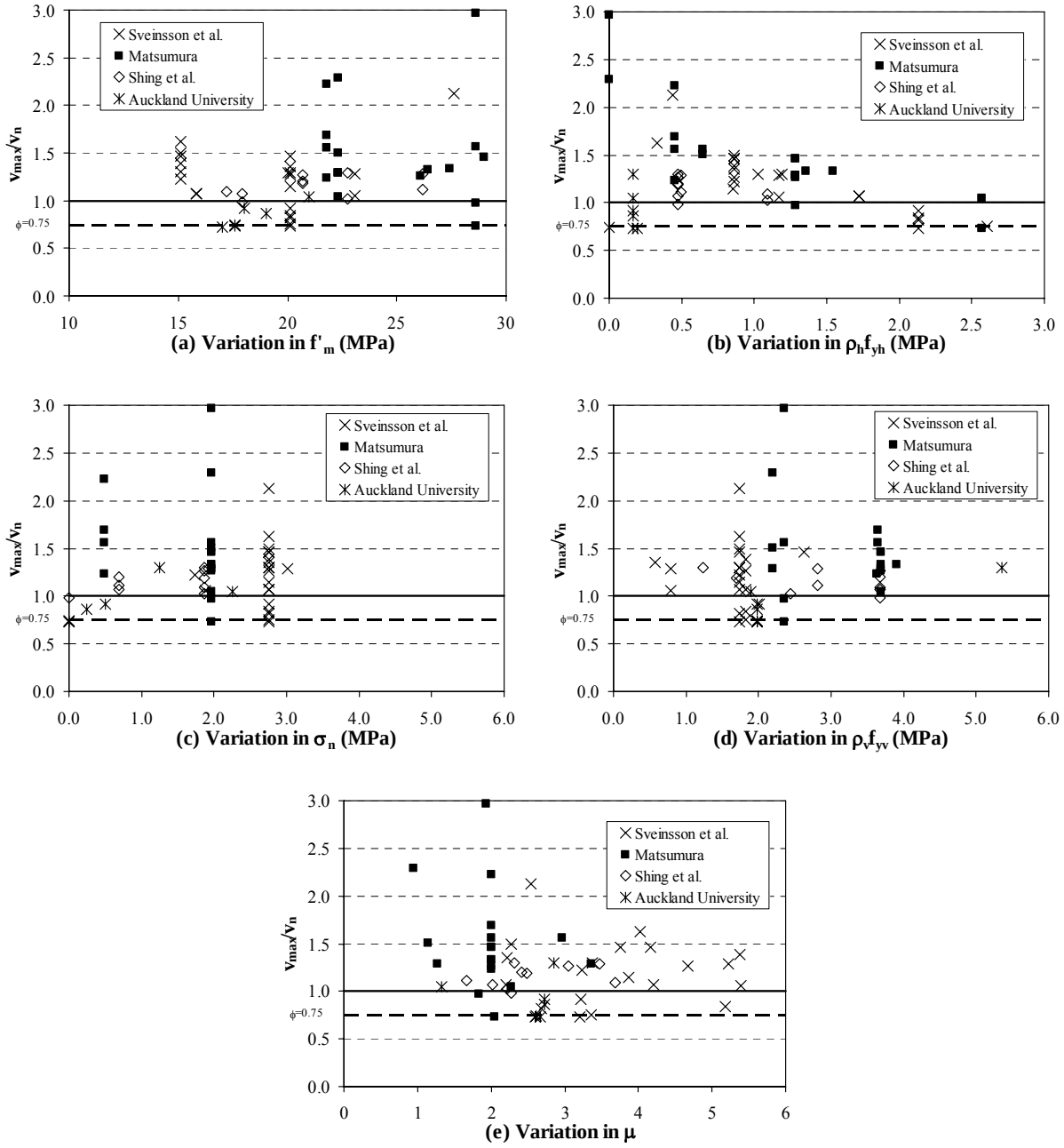

Figure 5.10 Experimental results versus prediction by AS 3700-1998.

varies from 0.84 to 1.56, of which the shear strength of just 1 specimen is under-predicted by Equation 4-4 by more than 50% (i.e. $v_{max}/v_n \geq 1.50$). Finally, shear strength prediction using Equation 4-4 resulted in a mean v_{max}/v_n of 1.17.

In Figure 5.12, predictions using the shear equation of the recently revised New Zealand masonry design standard, NZS 4230:2004, are compared with the experimental database for masonry walls. The normalised plots show that v_{max}/v_n varies from 0.89 to 1.74, with a mean v_{max}/v_n of 1.34. Consequently, the strength reduction factor of $\phi = 0.75$ would effectively provide a lower bound to the experimental data. The influence of ductility level and the other

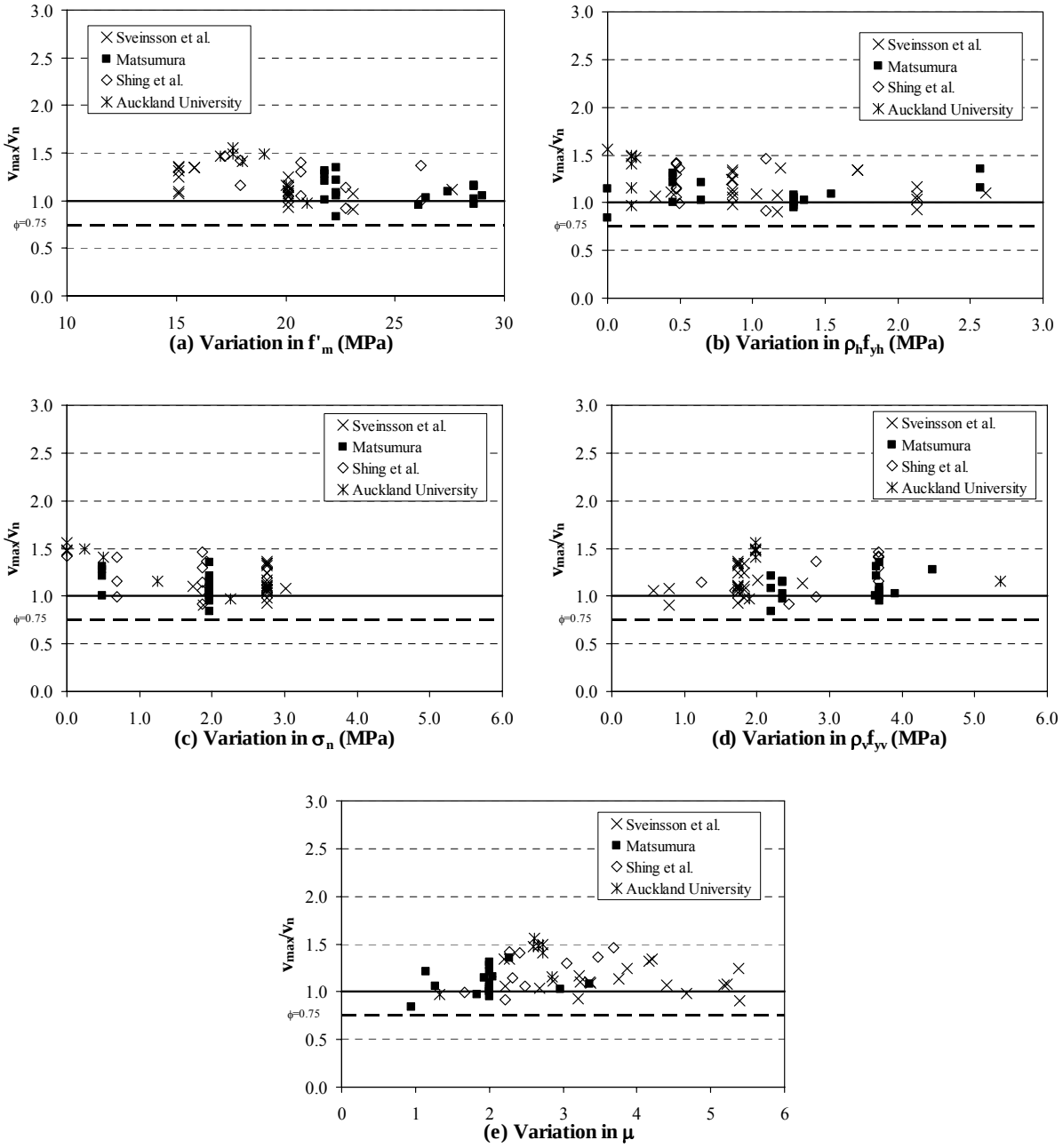

Figure 5.11 Experimental results versus prediction by Equation 4-4.

four parameters presented in the figure appear to be well represented by the newly developed shear equation adopted by NZS 4230:2004. Comparing these results with that shown in Figure 5.4 indicates a significantly improved codified masonry shear equation as scatter of points is significantly narrowed. As shown in Figure 5.12, NZS 4230:2004 over-predicts the shear strength of just 1 specimen, indicating a significantly improvement when compared to those presented in Figures 5.5-5.10. It is shown that strength prediction of the $h_e/L_w = 2.0$ concrete masonry wall tested at the University of Auckland is improved from $v_{max}/v_n = 0.77$ (NEHRP prediction) to $v_{max}/v_n = 1.21$ when the interaction between flexural ductility and masonry shear strength is properly considered in the NZS 4230:2004 shear equation.

Observing closely the results presented in Figure 5.12 (or Table B.2 in Appendix B), it is shown that strength prediction of the five square (h_e/L_w = 1.0) concrete masonry walls tested at the University of Auckland using the NZS 4230:2004 produced improved results when compared to the prediction according to NZS 4230:1990, after the interaction between flexural ductility and masonry shear strength was accurately accounted for in the NZS 4230:2004 shear prediction (recalling that the NZS 4230:1990 prediction presented in Figure 5.5 assumed all walls were within the elastic range). In addition, it is shown that strength prediction using NZS 4230:2004 produced significantly improved strength prediction for the slender (h_e/L_w = 2.0) and squat (h_e/L_w = 0.6) walls, resulting in v_{max}/v_n of 1.21 and 1.00 respectively, as compared to v_{max}/v_n of 1.42 and 2.41 when predicted using NZS 4230:1990.

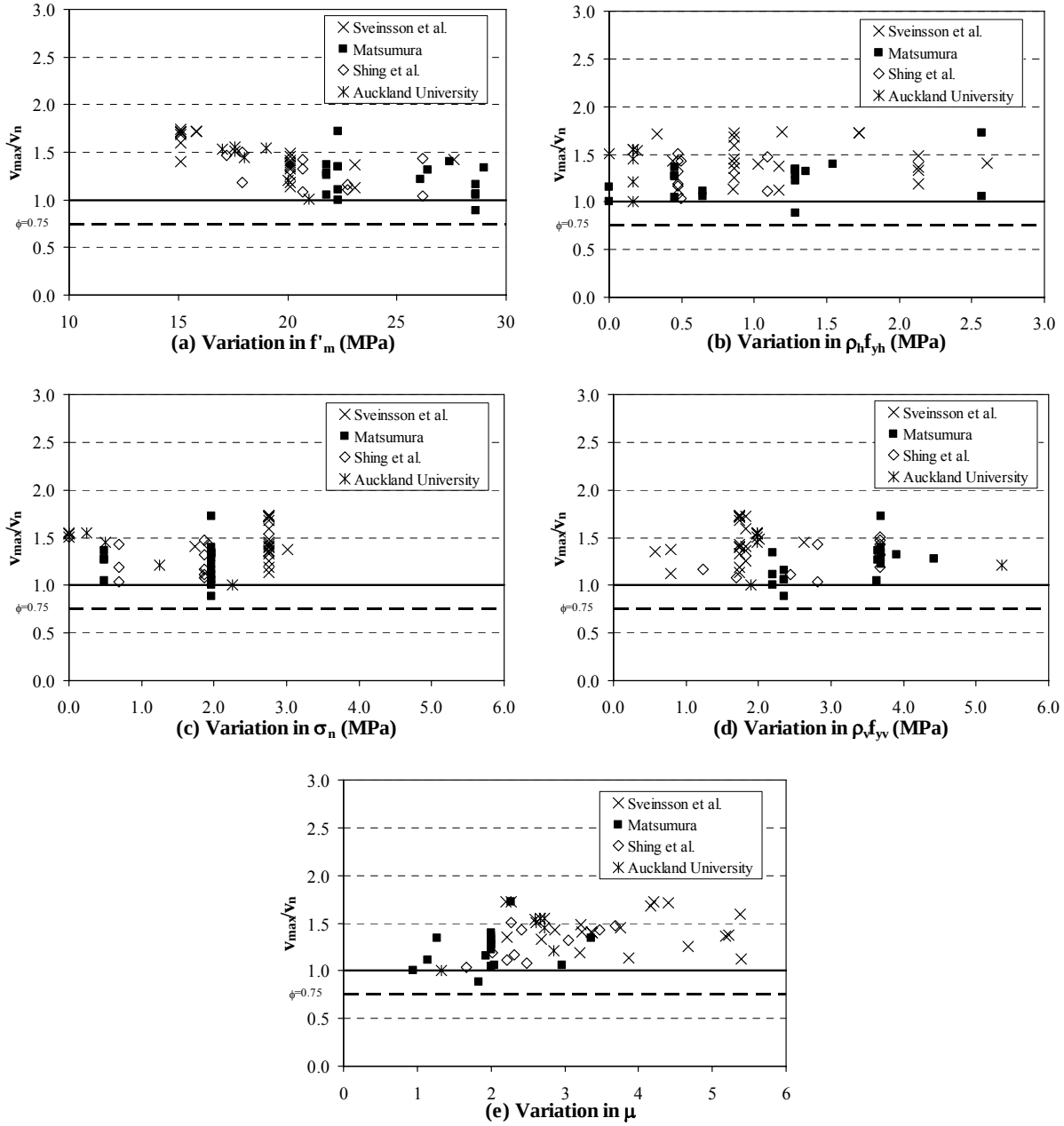

Figure 5.12 Experimental results versus prediction by NZS 4230:2004.

A statistical comparison of the different methods discussed in this section is provided in Table 5.2 in terms of mean and standard deviation for the experimental/predicted shear strength ratios of the 56 fully-grouted concrete masonry walls. It was successfully demonstrated that Equation 4-4 provides significantly improved masonry shear strength prediction than the NZS 4230:1990 shear expressions. In addition, it was also shown that shear prediction according to Equation 4-4 resulted in accuracy very similar to that resulted from the NEHRP prediction. Consequently, it is appropriate to use Equation 4-4 as the basis when developing a masonry shear strength design equation for NZS 4230:2004.

The NZS 4230:2004 shear equation provides significantly improved prediction of masonry shear strength compared to NZS 4230:1990, by reducing the scatter of the v_{max}/v_n ratio. Predictions using the NZS 4230:2004 shear equation produces a mean strength ratio of 1.34 and a standard deviation of 0.22. This standard deviation is more than half of that resulted from the NZS 4230:1990 equation, and similar in value to those resulting from the Shing et al., Matsumura and NEHRP shear expressions. Although the NZS 4230:2004 approach resulted in a slightly higher mean value of v_{max}/v_n compared to those resulting from the Shing et al., Matsumura and NEHRP shear expressions, final determination of the appropriateness of the design approach is dependent on the lower limits to the measured/prediction comparison. As is evident from Figures 5.4-5.12, a strength reduction factor of $\phi = 0.75$ forms a reasonable lower bound to all shear equations, with the exception to the Shing et al. and AS 3700-1998 shear expressions where four and five data points respectively fall below $\phi = 0.75$. Also presented in

Table 5.2 Statistical comparison between shear equations and data, in term of v_{max}/v_n

Shear Equation	v_{max}/v_n				
	Mean	Std dev.	Smallest value	Largest value	95 percentile
NZS 4230:1990	1.69	0.48	1.00	3.78	0.89
Matsumura	1.03	0.16	0.74	1.55	0.76
Shing et al.	1.12	0.25	0.54	1.67	0.70
Anderson & Priestley	1.36	0.40	0.89	2.27	0.70
NEHRP	1.18	0.17	0.77	1.60	0.88
UBC	1.52	0.42	0.89	3.39	0.83
AS 3700-1998	1.26	0.41	0.73	2.97	0.58
Equation 4-4	1.17	0.18	0.84	1.56	0.88
NZS 4230:2004	1.34	0.22	0.89	1.74	0.98

Table 5.2 is the 95 percentile value to represent the ratio of v_{max}/v_n for which 95% of the test result is expected to fall. Of the nine shear equations shown, the 95 percentile value resulting from NZS 4230:2004 is closest to unity, therefore further supporting its appropriateness in accounting for masonry shear strength.

It is noted that the numerical value of standard deviation presented in Table 5.2 cannot be used in statistical analysis because the data points being evaluated do not represent repetitive tests. However, the standard deviation and 95 percentile values presented here can be useful for making comparisons of the predictive accuracy of each shear equation.

Chapter 6

STRUCTURAL TESTING – SERIES B

6.1 INTRODUCTION

In order to compare the standard predicted and the actual wall behaviour, and to ascertain the force-displacement and other behavioural characteristics of partially grout-filled nominally reinforced concrete masonry walls, ten masonry walls of Series B were tested in the Civil Engineering Test Hall at the University of Auckland. The first eight specimens tested in Series B were concrete masonry walls containing openings. These walls had a range of opening geometries and variations in the trimming reinforcement detailing below window openings. The objectives for this part of the research were to study the performance of concrete masonry walls with openings under seismic loading and to validate the adequacy of NZS 4229:1999 in addressing the bracing capacity of these types of masonry walls. The remaining two test specimens were solid built concrete masonry walls (i.e. no opening within the wall) that incorporated a vertical shrinkage control joint at the centre of each wall. These two walls were tested to validate the structural adequacy of the shrinkage control joint detail published in NZS 4229:1999.

6.2 CONSTRUCTION DETAILS

6.2.1 Wall Specifications

The geometries and reinforcement details of the ten single-storey masonry walls are shown in Figures 6.1. All ten walls were partially grout-filled, where only those cells containing reinforcement were grouted, and were constructed to a common height of 2400 mm. None of the ten masonry walls had applied axial compression load. The first eight test specimens shown in Figure 6.1 had variations in trimming reinforcement detailing, including those complying to NZS 4229:1999, and a range of penetration geometries. The vertical reinforcement of the partially grout-filled walls shown in Figure 6.1 was generally spaced at 800 mm centres, with the exception being the 3600 mm long Walls B9 and B10 where vertical bars were located at 100 mm away from the control joints. The horizontal reinforcement in all walls consisted of two D16 reinforcing bars placed in a solid grout-filled bond beam within the top two block

courses and a D16 trimming reinforcing bar placed below a window opening. Refer to Voon and Ingham (2006) for more detailed description of wall constructional details.

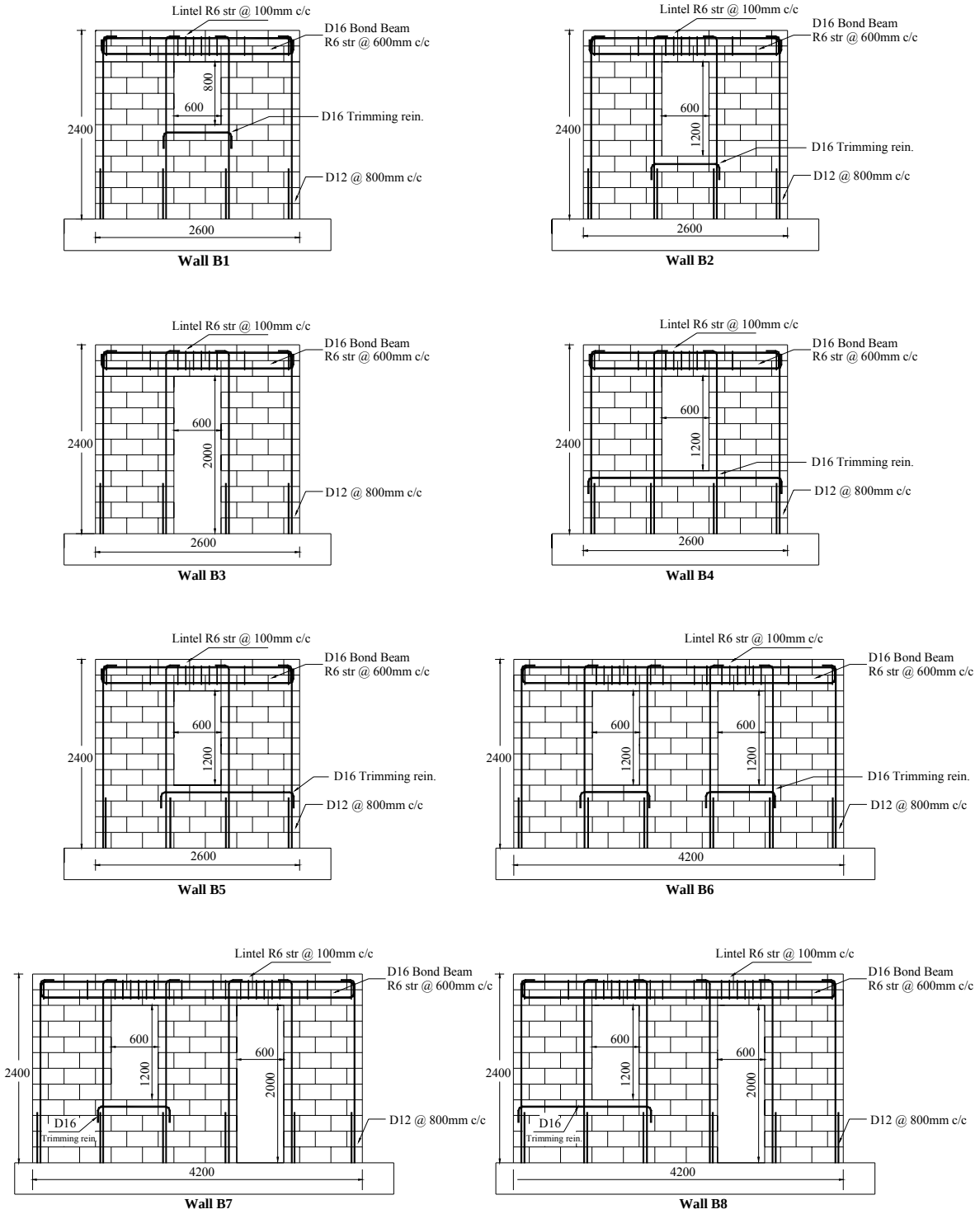

Figure 6.1 Series B - Wall geometries and reinforcing details.

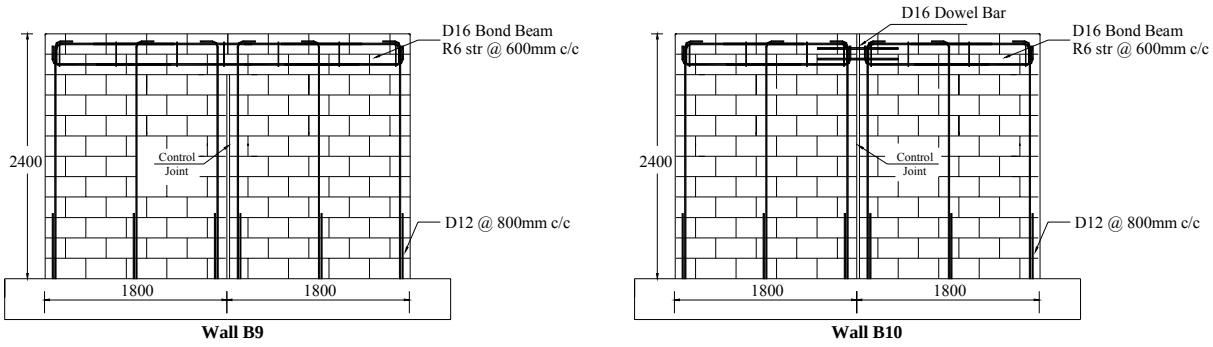

Figure 6.1Series B - Wall geometries and reinforcing details (continued).

Unlike Walls B1-B8, Walls B9 and B10 were solid built (i.e. no penetration) and had a vertical control joint at the centre of each wall. These two walls shared similar constructional details, with the only difference being the detailing of bond beam reinforcement at the control joint position. As shown in Figure 6.1, the control joint of Wall B9 was constructed in accordance with the specification of NZS 4229:1999, where the joint was terminated below the bond beam and the horizontal bond beam reinforcement was continuous through the joint. In the case of Wall B10, the control joint penetrated the full height of the wall and the horizontal bond beam reinforcing bars were terminated at 100 mm away from the joint. Two 800 mm long D16 dowel bars were placed across the control joint to transfer shear. In order to prevent the flow of grout across the control joint at the bond beam layer, a thin polystyrene strip was inserted to form a gap between the two piers, and the D16 dowel bars were then punched through the polystyrene strip. The dowels were greased and placed in a plastic sleeve on one side to avoid bonding to the grout.

6.2.2 Construction Materials

Similar to the constructional procedures described in section 3.2.2, all walls described in Series B were constructed by experienced masons under supervision and consisted of a running bond pattern of standard 15 Series grey precast concrete masonry block units (CMUs) using DRICON^{TM} trade mortar. Open-end bond beam CMUs were used at the bond beam layer to allow the placement of D16 horizontal reinforcing steel. Half end-closer blocks were used at the edge and lintel positions. See Figure 3.2 for block geometries.

Similar to the ten walls tested in Series A, high slump ready-mixed grout using small aggregate was employed to fill all masonry walls described in Series B. SIKA Cavex was added to the grout to avoid formation of voids caused by high shrinkage of the grout. All reinforcing steels used in the construction of these partially grout-filled masonry walls was grade 300 MPa,

consisting of D12 for the vertical reinforcement, D16 for the bond beam reinforcement and R6 for stirrups. The vertical reinforcement was erected as described in section 6.3.1, and the D16 had standard 90^o hooks at both ends.

6.2.3 Material Properties

Prior to wall testing, material testing was carried out to evaluate the key material properties: concrete masonry crushing strength, f'_m, and the yield strength of the reinforcing steel, f_y. The f'_m was determined through masonry prism tests using the procedures described in section 3.2.3, with the mean f'_m values summarised in Table 6.1.

Samples of the D12 and D16 steel reinforcement were subjected to tensile testing using the Avery Universal Testing Machine at the University, see section 3.2.3. Similar to Series A, each type of reinforcing steel used in the Series B walls was from the same batch. Consequently, the average strengths of 305 MPa and 315 MPa were used as the yield strength for the D12 and D16 reinforcing bars in this experimental programme.

6.3 TESTING DETAILS

6.3.1 Test Setup

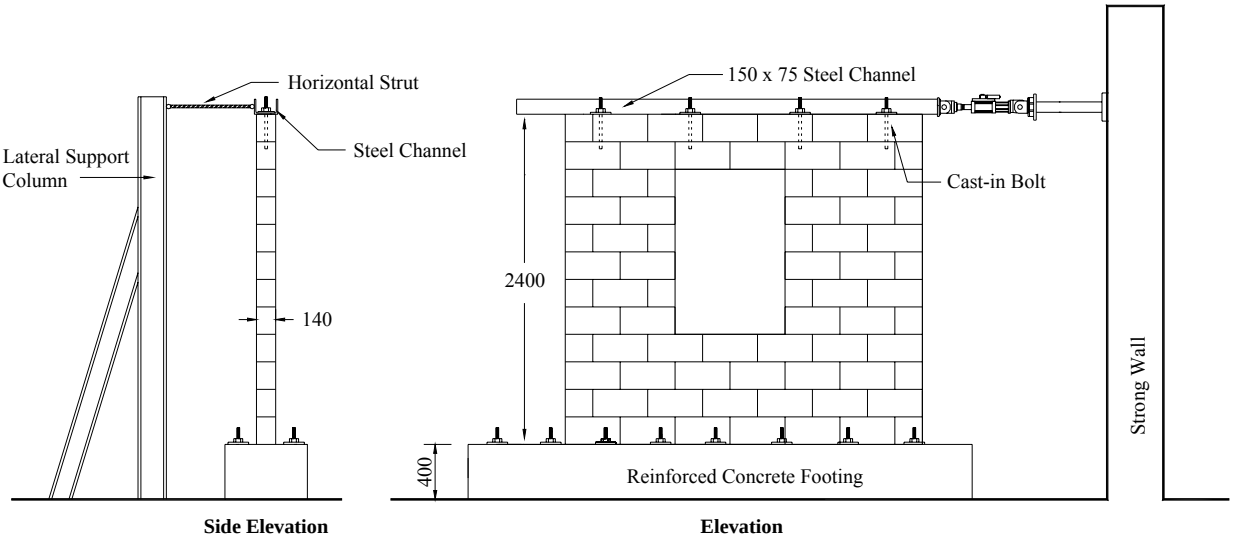

Figure 6.2 Typical test set-up, Series B.

The testing of specimens (except Wall B10, see Voon and Ingham (2006) for detailed description) reported herein was conducted according to the set-up shown in Figure 6.2. The test set-up and method of loading adopted in this experimental programme were designed to

simulate the response that a masonry shear wall would experience during seismic excitation. Although a single-storey wall does not have the complexity of a multi-storey structure, it is advantageous to consider due to the ease of data interpretation. Horizontal cyclic loading was applied to the top of the wall via a 150 x 75 steel channel as shown in Figure 6.2, which was fastened to the top of the bond beam by cast-in bolts. The jack was fastened to the strong wall and the tested wall was stabilised from moving in its out-of-plane direction by two parallel horizontal struts which were positioned perpendicular to the wall and hinged to the channel and a reaction frame. It is recognised that this type of horizontal force transfer is of a cantilevered wall type and therefore may not be representative of all structures.

Due to the presence of full height control joint in Wall B10, the horizontal cyclic load was applied to this wall through the attachment of two jacks, one at each end of the wall. One jack reacted off the strong wall while the other reacted off a steel reaction frame. Both jacks were capable of pushing and pulling and were attached to the top of the wall by two separated pieces of 150x75 steel channels that were fastened to the bond beam by cast-in bolts. The decision for using two jacks was taken so that the bond beams on either ends of the control joint were allowed to "flex", therefore no additional strength was provided by the steel channel to the walls.

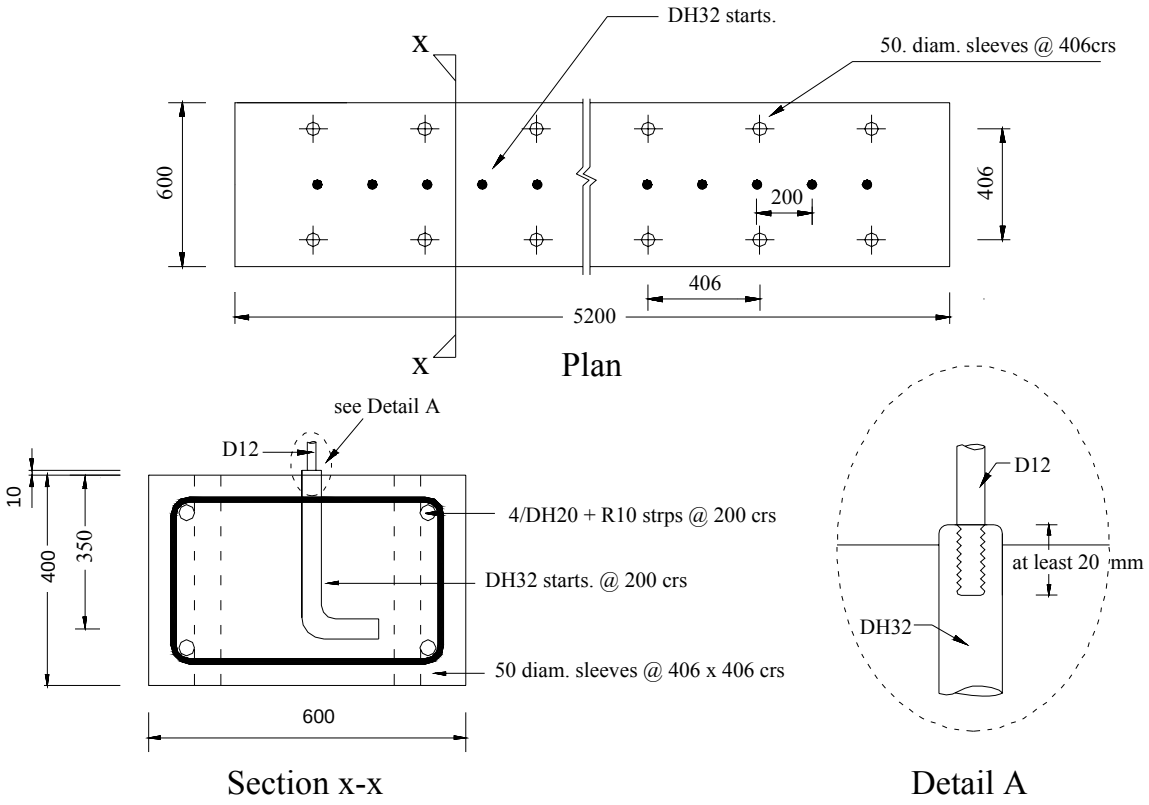

Figure 6.3 Details of concrete footing.

All masonry walls of Series B were constructed on a 5.2 m long re-usable reinforced concrete footing. Similar to the concrete footing described in section 3.3.1, the concrete footing shown in Figure 6.3 had DH32 starter bars spaced at 200 mm centres that were drilled and tapped to accommodate D12 vertical reinforcement. Each of the 650 mm long D12 starters was first tapped at one end, then threaded into the DH32 starters that protruded from the reinforced concrete base, allowing the D12 starter reinforcement to penetrate the wall to a distance of not less than 600 mm. The threading of the D12 into the DH32 starter bars was successfully demonstrated by Brammer (1995) and Davidson (1996) to result in negligible effect on the flexural strength of the nominally reinforced concrete masonry walls. As shown in Figure 6.1, the wall vertical reinforcement was lap-spliced immediately above the foundation, imitating typical construction practice as indicated in Figure 8.1 of NZS 4229:1999. Finally, the concrete footing was stressed down to the laboratory floor with eight high strength steel rods, each loaded to approximately 300 kN so that sufficient shear friction was provided to eliminate any slip between the footings and the floor.

6.3.2 Instrumentation

As shown in Figures 6.4 and 6.5, the arrangement of the measuring instrumentation was similar to that described in section 3.3.2. A load cell to measure the magnitude of the lateral force was placed between the actuator and the steel channel, denoted as [0] in Figure 6.4. Portal displacement transducers, denoted as [1] and [2], measured lateral displacement at the top of the wall while displacements at the window levels were measured by instruments [3] and [4]. Portal displacement transducers [47] – [49] were used to measure sliding of the wall relative to the concrete footing, and transducers [45] and [46] measured the uplift at wall toe positions. Any slip in the steel channel and the concrete footing were measured by transducers [50] and [51] respectively. Further transducers were placed according to the configuration shown in Figure 6.4 to attain the shear and flexural components of deformation.

6.4 WALL STRENGTH PREDICTION

6.4.1 Flexural Strength of Perforated Walls

Prior to testing, the flexural strengths of the masonry walls were evaluated using the bracing capacity values (see Table 2.1) specified by NZS 4229:1999. Furthermore, two analytical methods were also employed to evaluate the wall strengths: strut-and-tie model (Yanez et al., 1991; Wu and Li, 2003) and plastic hinge model (Leiva et al., 1990; Davidson, 1996; Elshafie et al., 2002).

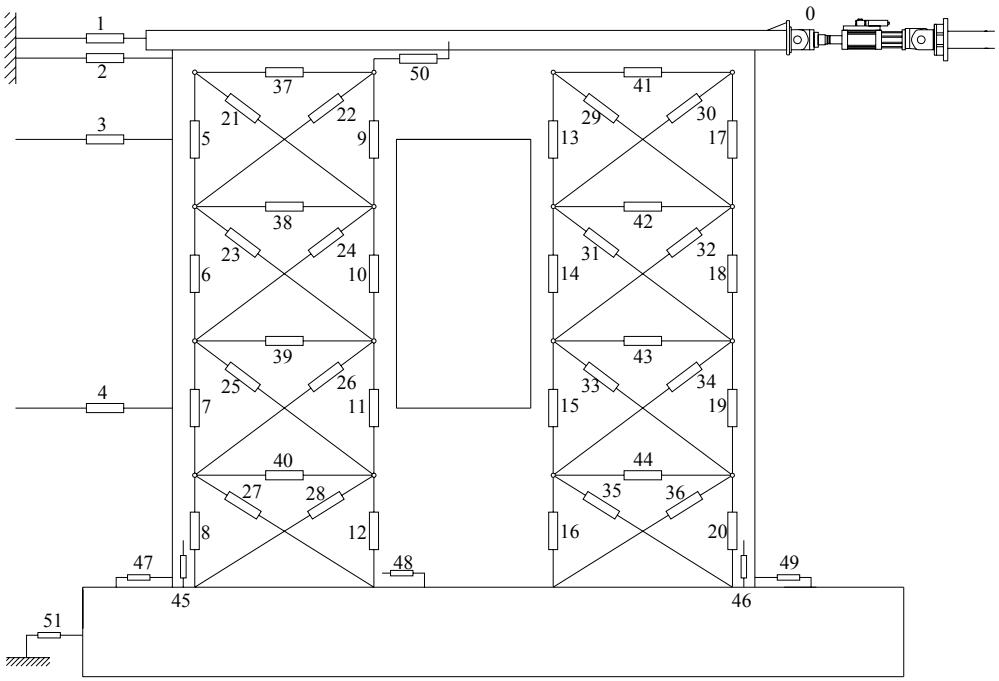

Figure 6.4 Instrumentation for test wall.

Figure 6.5 Instrumentation mounted on wall before testing.

6.4.1.1 NZS 4229:1999 Procedure

The procedure employed in NZS 4229:1999 for proportioning bracing capacity was described in Section 2.5.2. The assumption was that the bracing capacity of a masonry wall having penetrations and/or shrinkage control joints could be determined based on the geometry of individual bracing panels, as identified by the shaded areas shown in Figure 6.6, where the

bracing capacity geometry of each bracing panel is based upon the vertical dimension of the smallest adjacent opening. The total bracing capacity is then assumed to be the sum of the capacities provided by the individual bracing panels of the wall. The evaluated wall strengths using the NZS 4229:1999 specified procedure are identified as F_{code} in Table 6.1. From Table 6.1 it is clearly illustrated that the wall strength decreases as the depth of opening increases. This is because taller bracing panels have less capacity than shorter bracing panels of the same length.

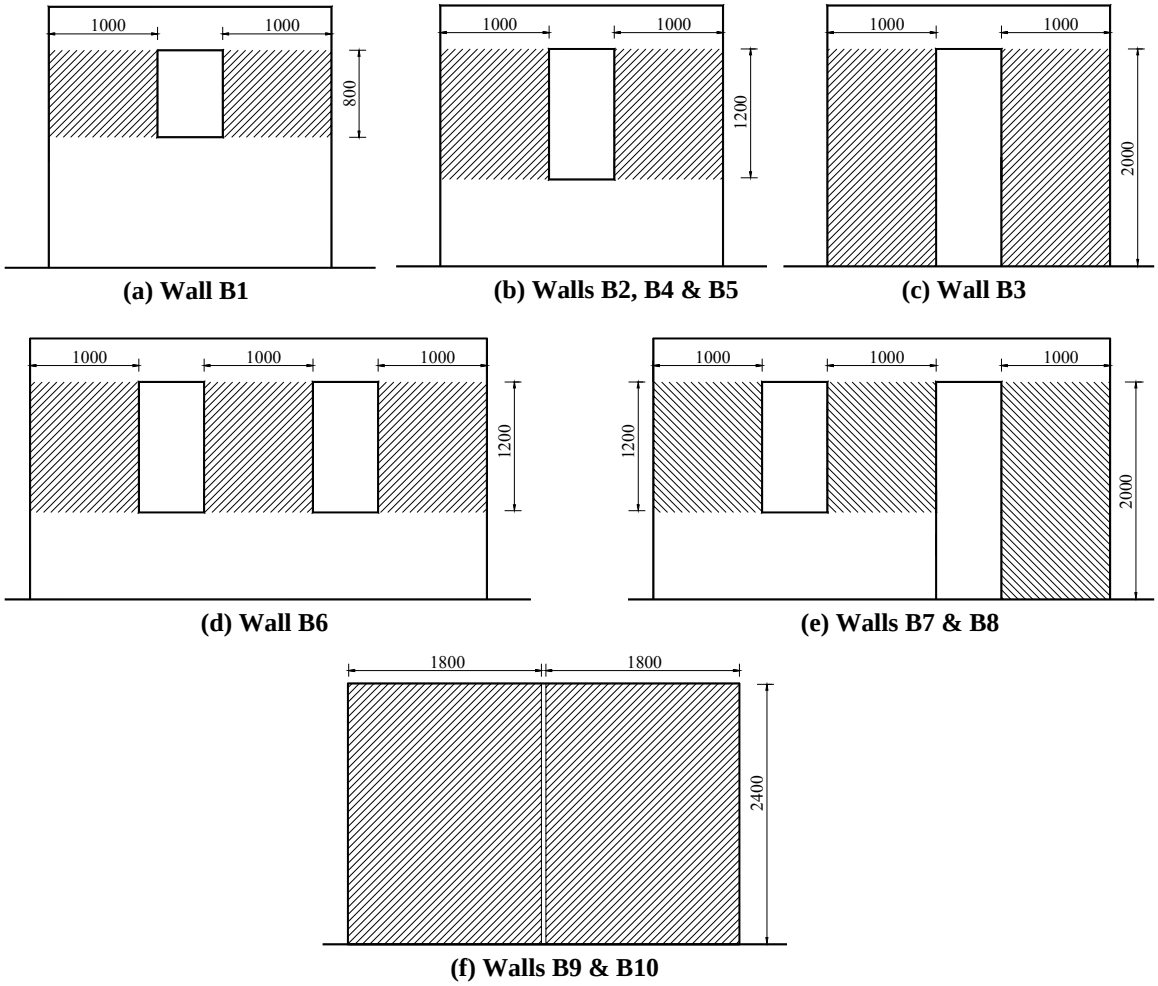

Figure 6.6 Identification of bracing panels.

6.4.1.2 Simple Strut-and-Tie Models

Due to the presence of openings in Walls B1 to B8, Equation 2-1 was deemed to be inappropriate for evaluating the nominal flexural strength of these test specimens. Consequently, two types of strut-and-tie models were employed to evaluate wall strengths. The first type was a simplified strut-and-tie model, which assumed that all panels were pinned at

the bond beam centre and lateral force was applied to the bracing panels from the centre of the bond beam. In addition, the effect of wall self-weights was not considered in this simplified strut-and-tie model in order to ease the analysis process. The resultant strut-and-tie analyses using this simplified procedure are diagrammatically shown in Figures 6.7 and 6.8 for the push and pull directions respectively, where the struts are components indicated by a broader element thickness. It is illustrated in Figure 6.7 that the introduction of extended trimming reinforcement beneath the window in Walls B4 and B5 would result in an increase in wall strength when compared to that predicted for Wall B2. This was due to a change of slope of the strut components in the right hand side panels of Walls B4 and B5. Similarly, the effect of extended trimming reinforcement in the pull direction can be observed by comparing the geometries of the left-most diagonal struts in Walls B4 and B8 with those predicted for Walls B2 and B7 respectively. The evaluated lateral wall strengths using the simplified strut-and-tie analysis is identified as $F_{n,st0}$ in Table 6.1.

For Walls B9 and B10, regardless of the detailing of bond beam horizontal reinforcement, the wall flexural strengths were evaluated (according to the simplified strut-and-tie model) as the sum of strength provided by the individual 1.8 m long cantilever piers. The predicted lateral wall strengths for these two walls are presented in Figures 6.7 and 6.8 for the push and pull directions respectively.

6.4.1.3 Improved Strut-and-Tie Models

A second set of strut-and-tie models considered lateral force that was applied as a single point load at the wall top. These models are referred to here as "improved" to clearly delineate them from the "simple" models previously discussed. The lateral force was then transferred from the wall top to the bond beam centre through a triangular truss, which was subsequently applied to the bracing panels. Unlike the simplified models presented in Figures 6.7 and 6.8, the wall self-weight of 1.6 kN/m^2 was considered to act along the bond beam centre in the second strut-and-tie model. The resultant strut-and-tie analyses using the above mentioned procedure are diagrammatically shown in Figures 6.9 and 6.10 for the push and pull directions respectively, where the strut components are indicated by a broader element thickness. Similar to the simplified strut-and-tie analysis procedure discussed earlier, increase in predicted strengths are illustrated in Figures 6.9 and 6.10 when extended trimming reinforcement are included in walls having the same dimensions and identical penetration geometries. By comparing the strut-and-tie analyses presented in Figures 6.7-6.10, it is clearly shown that the addition of wall self-

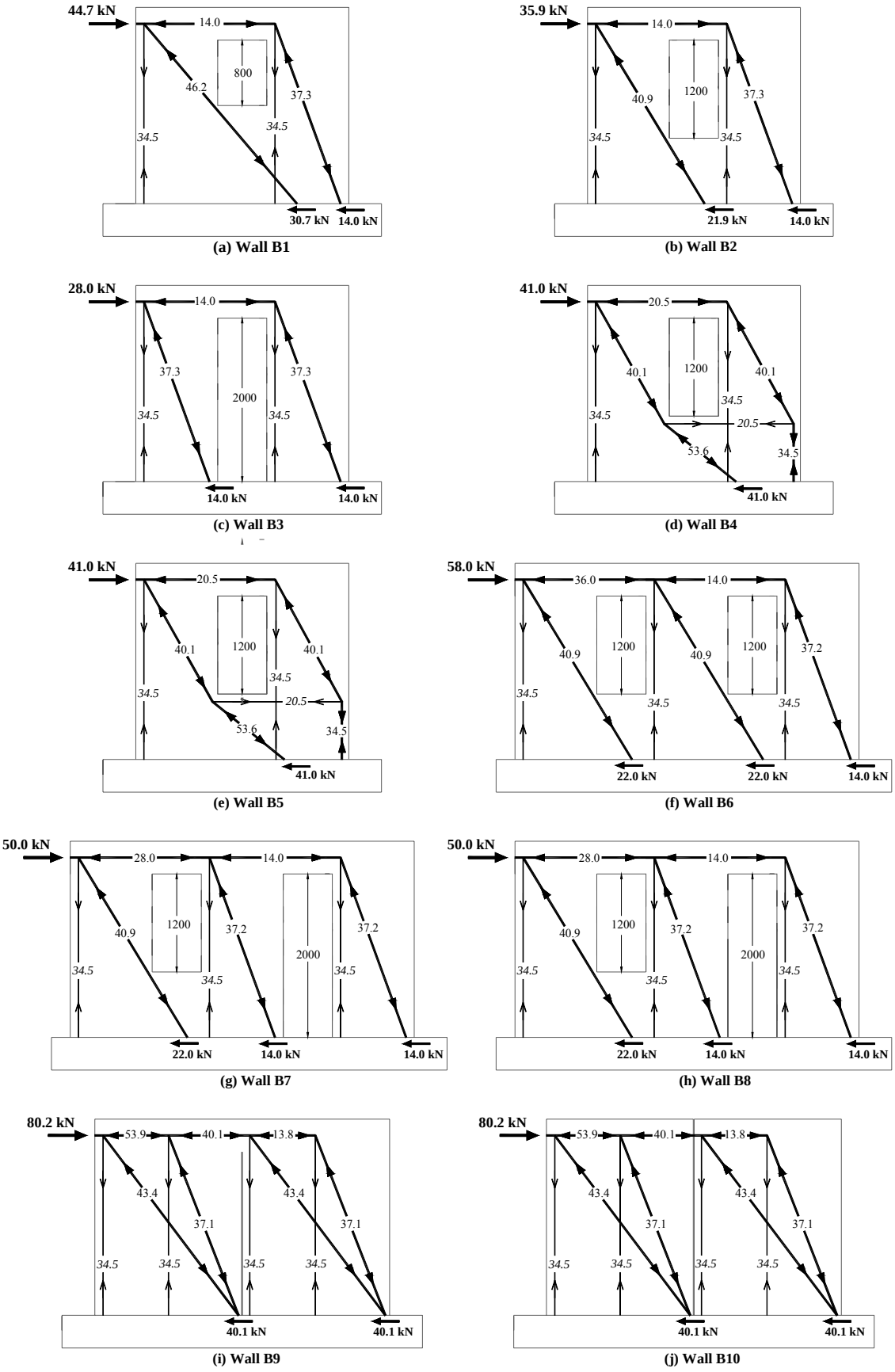

Figure 6.7 Simplified strut-and-tie models in push direction (forces in kN).

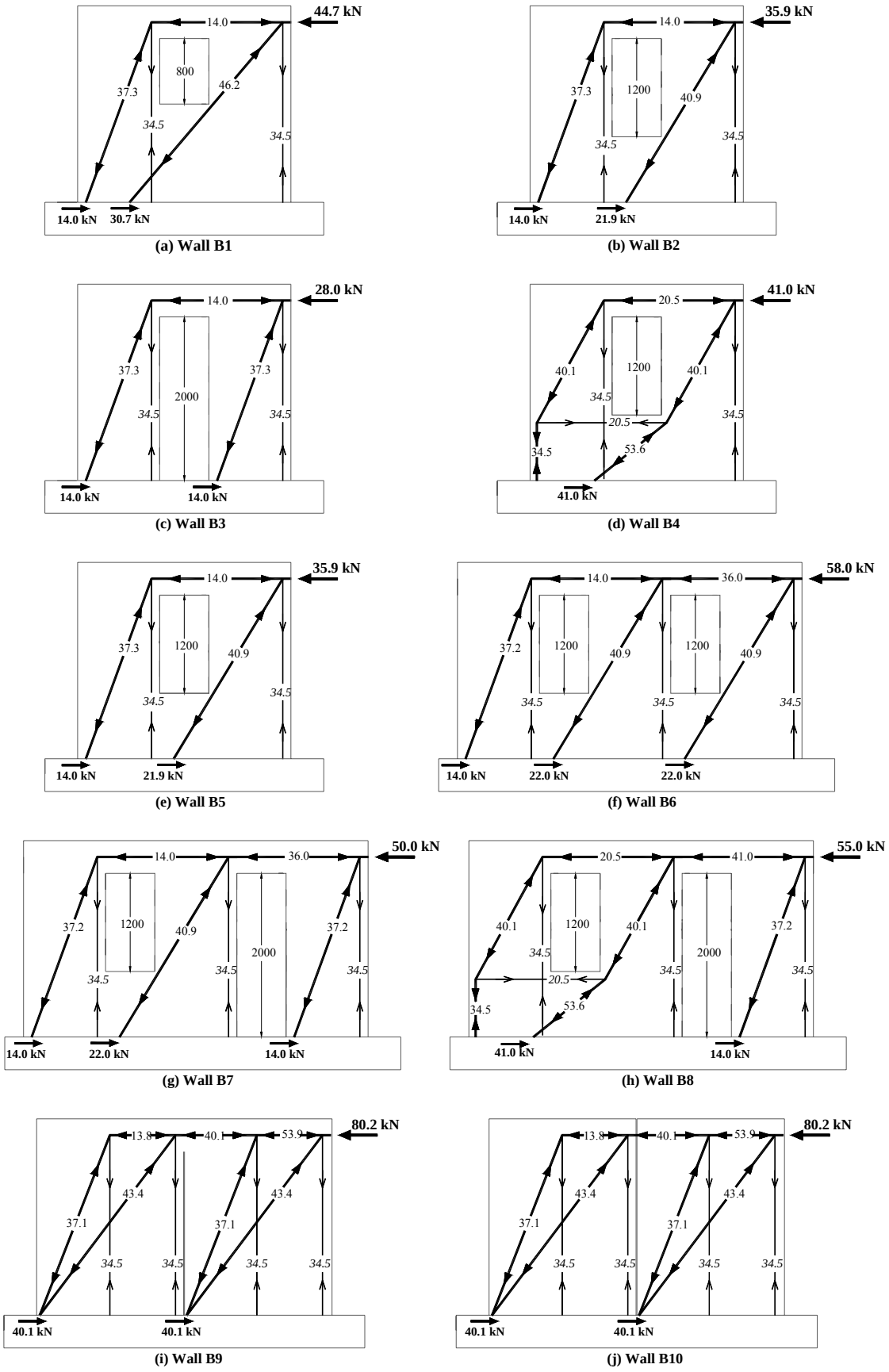

Figure 6.8 Simplified strut-and-tie models in pull direction (forces in kN).

weight in the strut-and-tie analysis resulted in predicted strength increases of 4% to 10% for the 2.6 m long perforated concrete masonry included in this study. For the 4.2 m long masonry walls with two openings, the inclusion of wall self-weight and double bending of the central pier (see Figures 6.9 and 6.10) resulted in significant increase in the predicted strengths by 24% to 46% when compared to those predicted using the simplified strut-and-tie models. The predicted lateral wall strengths using the strut-and-tie models illustrated in Figures 6.9 and 6.10 are identified as $F_{n,st1}$ in Table 6.1.

For Wall B9 that had a control joint constructed in accordance with the NZS 4229:1999 specification, the strut-and-tie models presented in Figures 6.9 and 6.10 accurately accounted for transmission of the applied shear force from the wall top into the bond beam, plus the effect of having the control joint terminate below the bond beam. Consequently, the lateral strength of Wall B9 evaluated using the improved strut-and-tie model was about 38% higher than that predicted using the simplified strut-and-tie method. For Wall B10, the strength predicted using the model presented in Figure 6.9 was similar to that predicted using the simplified strut-and-tie model. Predicted strengths of similar magnitude were generated for this wall because both models considered the 10 mm control joint was sufficient to prevent the proper transfer of shear across the bond beams.

6.4.1.4 Full Plastic Collapse Analysis

The method used here was to assume that a flexural collapse mechanism could form and then calculate the lateral force required to cause this collapse. A number of collapse mechanisms are possible, with that which required the least force being the most likely. Similar to the procedure employed by Davidson (1996), the walls were treated as frames comprising of vertical piers in order to develop the plastic bending moment diagrams shown in Figures 6.11 and 6.12. The flexural strength of pier and lintel were evaluated according to the procedures presented in section 2.3.1 and adopting Brammer's (1995) recommendation of excluding the longitudinal steel adjacent to the neutral axis. Using the described procedures, the pier and lintel strengths were established to be 30.7 kNm and 17.5 kNm respectively when f'_m of 16 MPa was assumed and the masonry self weight was not considered. It is emphasised that the lintel strength was evaluated excluding any possible composite action of the masonry bond beam and the steel channel loading beam.

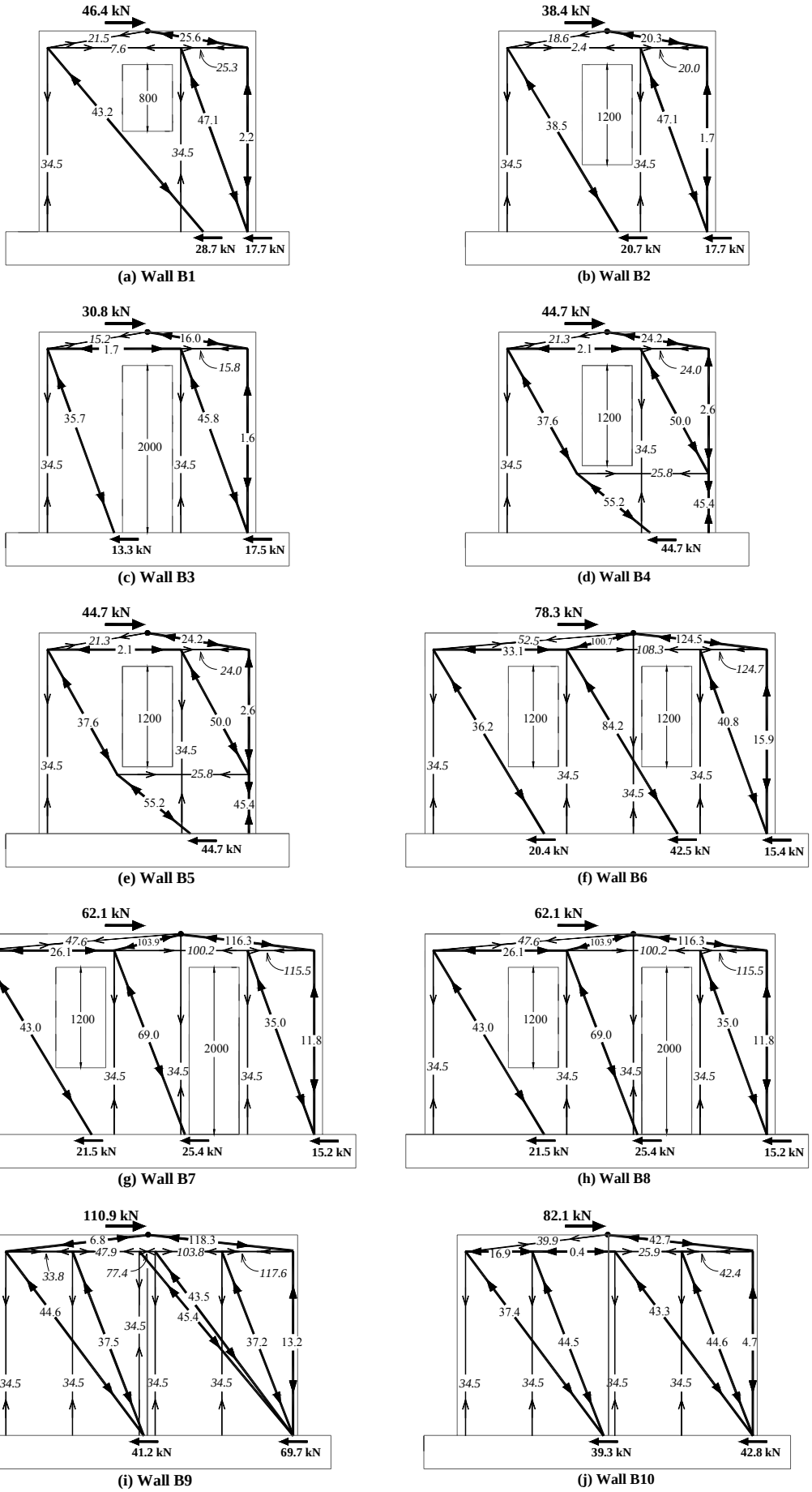

Figure 6.9 Strut-and-tie models in push direction (forces in kN).

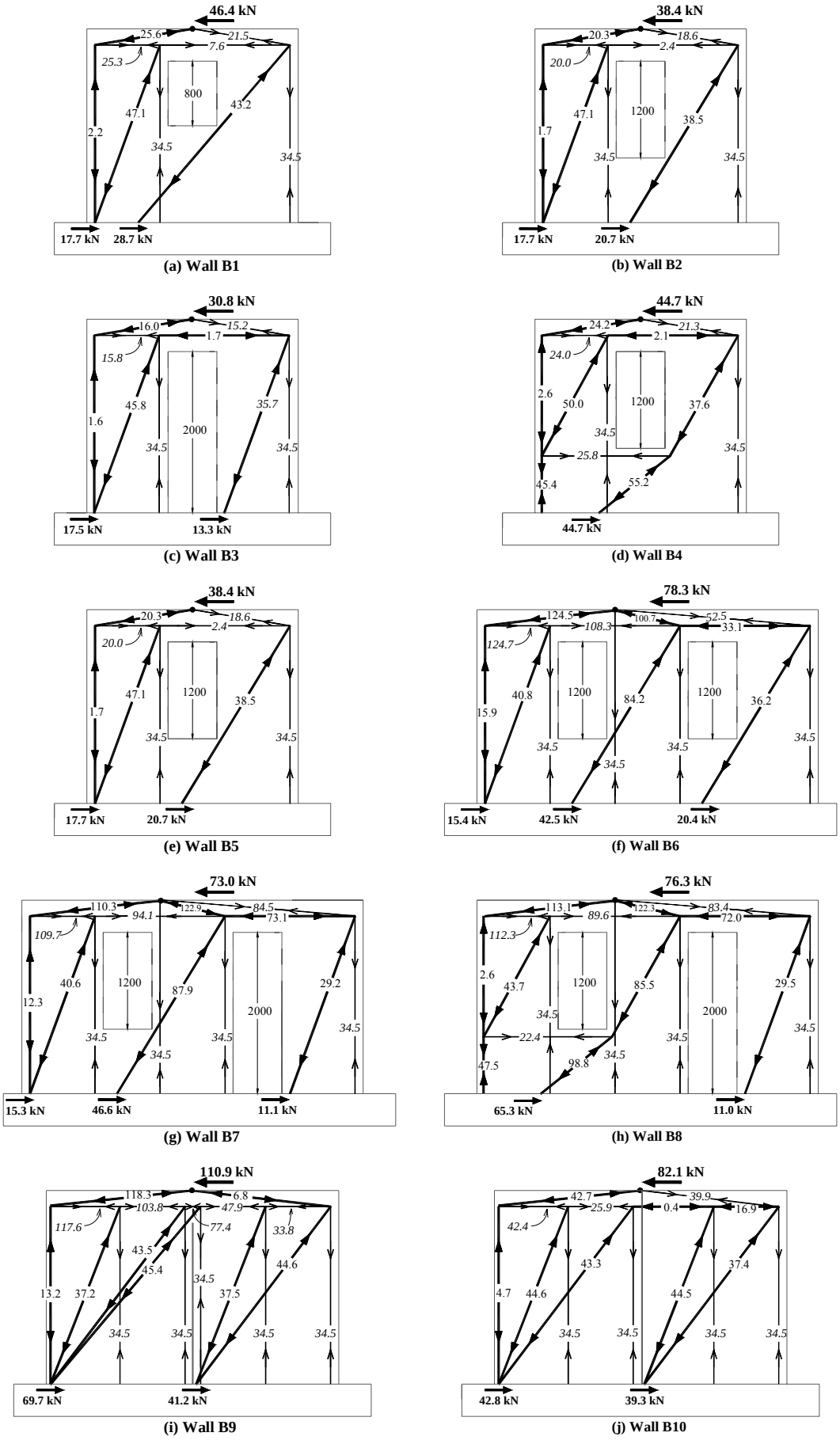

Figure 6.10 Strut-and-tie models in pull direction (forces in kN).

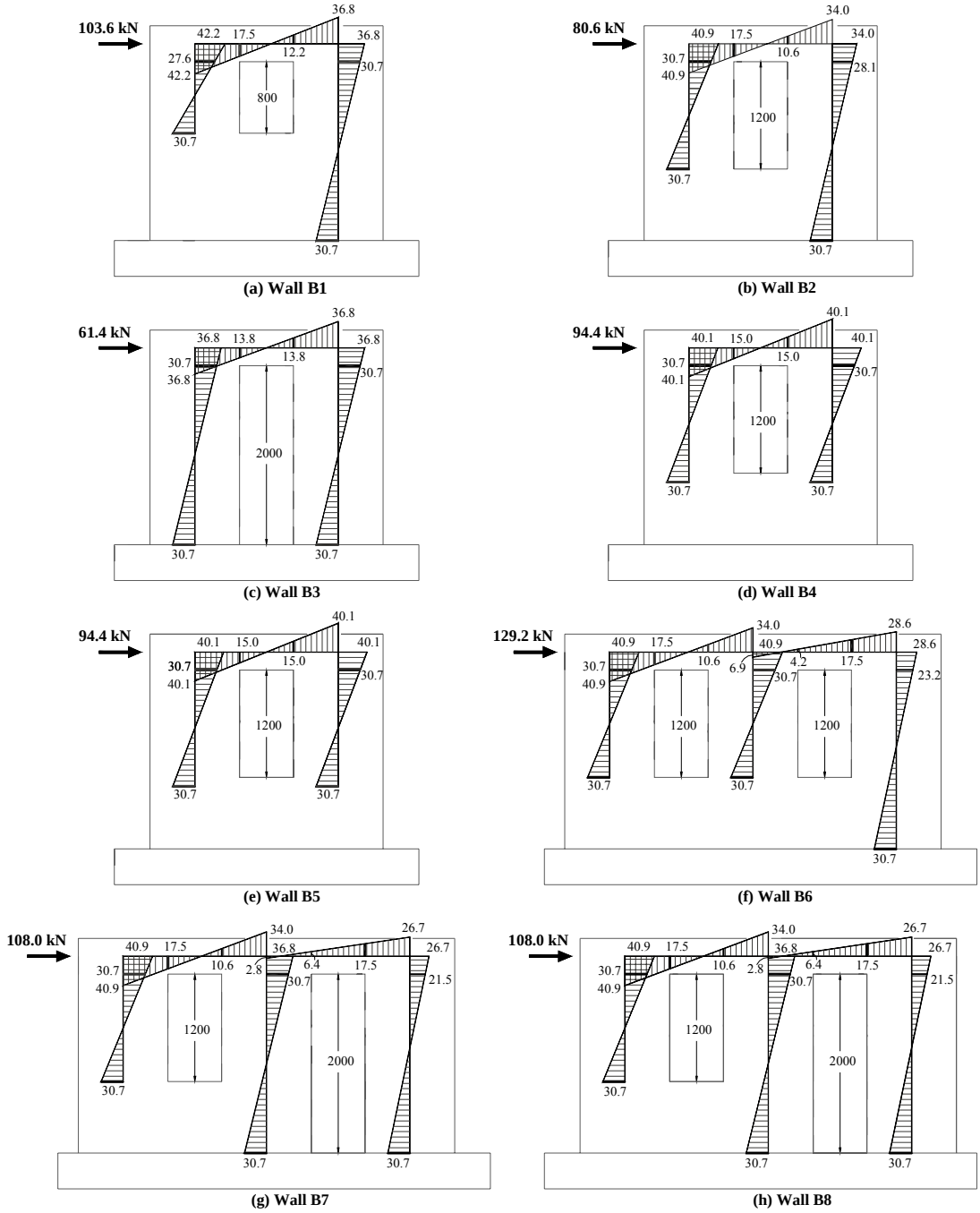

Figure 6.11 Full plastic collapse analyses in push direction (moments in kNm).

By conducting a push-over or plastic collapse analysis, it was found that the flexural strength at the base of each pier was developed, but that the moments at the top of the piers were mostly, but not completely governed by the pier strength. These strength critical member-joint interfaces are identified by the thickened lines shown in Figures 6.11 and 6.12.

An illustration of the wall strength calculation is presented here for Wall B2. For the wall pushed to the right (away from the strong wall) as shown in Figure 6.11, the critical member

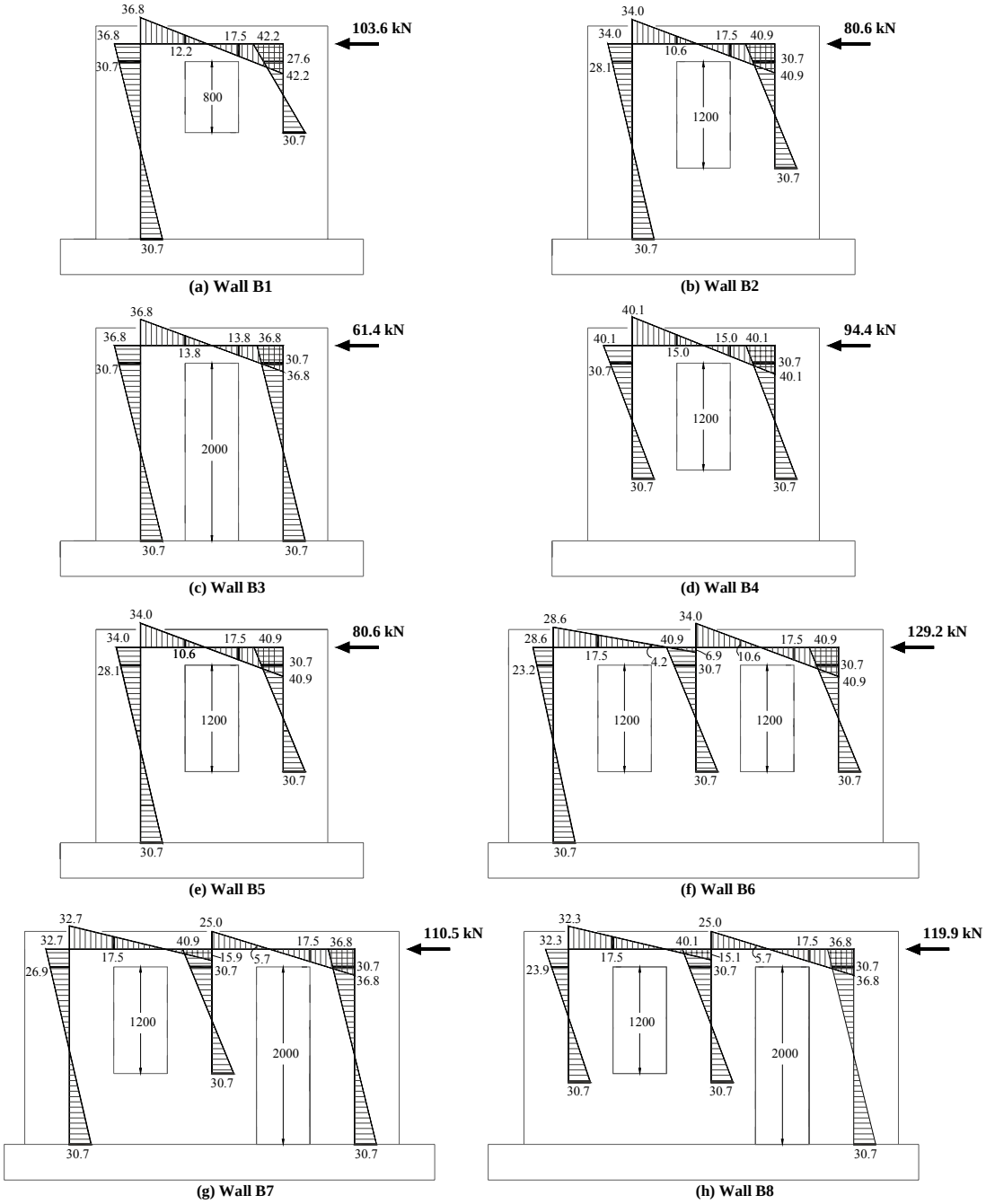

Figure 6.12 Full plastic analyses in pull direction (moments in kNm).

height of the left pier was that of the window opening (1.2 m) and the height of the right pier was that of the door opening (2.0 m). Hence, the base shears of the two piers were as follows:

The left pier	(30.7 + 30.7)/1.2 = 51.2 kN
The right pier	(28.1 + 30.7)/2.0 = 29.4 kN
	Sum = 80.6 kN

Hence, the predicted strength in the push direction was 80.6 kN. However, this lateral strength was calculated neglecting the influence of axial force in each pier. The shear force in the lintel, resulted from the rotational moment, gave rise to axial forces in the outer piers. These shear forces were calculated based upon the slope of the lintel bending moments shown in Figure 6.11 and assuming that these shears acted through the centreline of the piers. Therefore, the axial force in each pier was established to be (40.9 + 34.0)/1.6 = 46.8 kN. This axial force in turn increased or decreased the moment capacity of the two piers by approximately 46.8 x 0.5= 23.4 kNm (note that the 0.5 m was the approximate length of lever arm between the pier centre and masonry compression edge). For the mechanism chosen and the wall displaced to the right, the increase or decrease in wall strength was calculated as follow:

The left pier	-23.4/1.2 = -19.5 kN
The right pier	23.4/2.0 = 11.7 kN

Hence, this resulted in a reduction lateral strength of approximately 7.8 kN. However, it is acknowledged that the influence of such axial loads in the piers on the lateral force resistance is less significant in single-storey structures than in multi-storey buildings. Consequently, this value was not considered in order to ease the analysis process. The evaluated wall strengths using the plastic collapse analysis are identified as $F_{n,fr0}$ in Table 6.1.

6.4.1.5 Modified Plastic Collapse Analysis

The second set of plastic collapse analyses treated the outer piers as isolated cantilever with a height measured from the base of cantilever to the centre of bond beam. As shown in Figures 6.13 and 6.14, this modified analysis method only considered the double bending to occur in the central pier of the 4.2 m long perforated masonry walls. This assumption was taken based on Davidson's (1996) observations that the response of individual piers was effectively independent, therefore supporting the assumption of pin formation in the outer piers' bond beam centre. The strength critical member joint interfaces are identified by the thickened lines shown in Figures 6.13 and 6.14. Similar to the full plastic collapse analyses presented in Figures 6.11 and 6.12, the influence of axial force (resulted from wall self weight and rotational moment in the lintel) was not considered in this modified analysis method. The predicted lateral wall strength using this modified analysis methods are identified as $F_{n,fr1}$ in Table 6.1.

An illustration of the wall strength calculation is presented here for Wall B6. For the wall pushed to the right (away from the strong wall) as shown in Figure 6.13, the critical member height of the left and central piers were from the bond beam centre to the underside of the window (1.4 m) and the height of the right pier was taken from the bond beam centre to the foundation face (2.2 m). Hence, the base shears of the three piers were as follows:

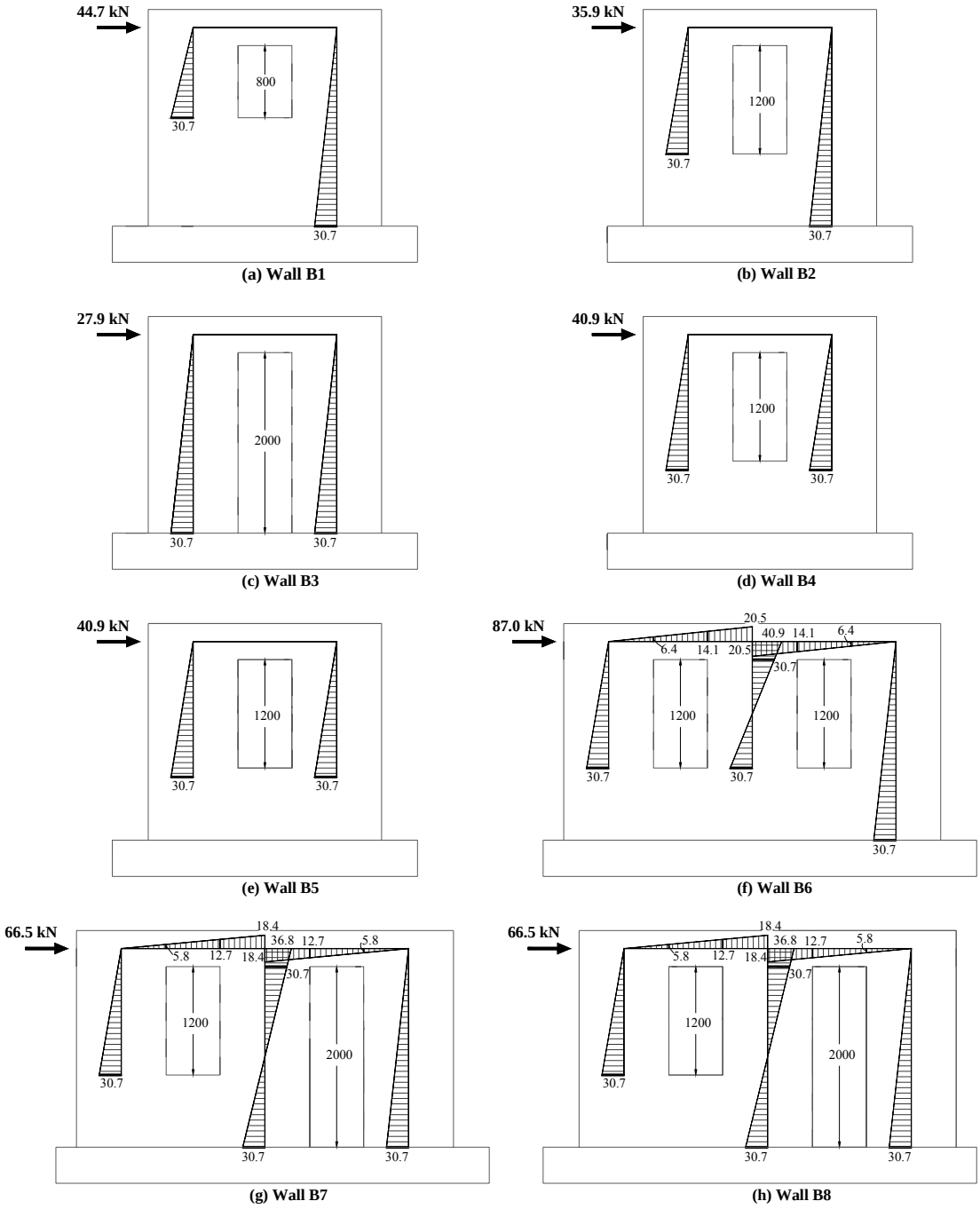

Figure 6.13 Modified plastic collapse analysis in push direction (moments in kNm).

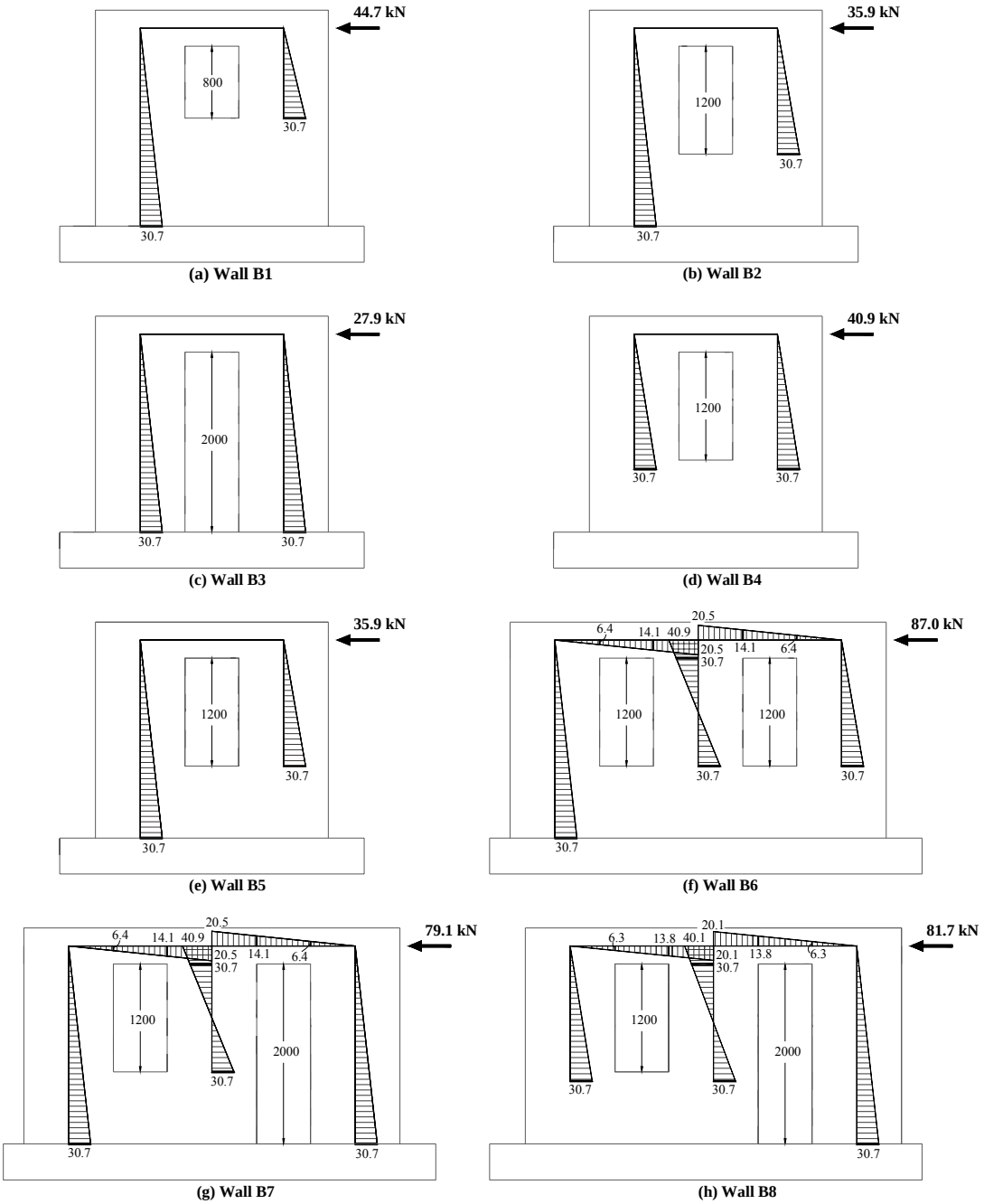

Figure 6.14 Modified plastic analyses in pull direction (moments in kNm).

The left pier	30.7/1.4 = 21.9 kN
The central pier	(40.9 + 30.7)/1.4 = 51.1 kN
The right pier	30.7/2.2 = 14.0 kN
	Sum = 87.0 kN

Hence, the predicted strength in the push direction was 87.0 kN. As anticipated, the $F_{n,fr1}$ values are significantly less than those evaluated according to $F_{n,fr0}$. This is primarily because the outer piers were considered as isolated cantilever in the $F_{n,fr1}$ method, which resulted in

significantly less strength than if the piers were allowed to develop their full flexural strength at both ends.

Similar to other analysis methods discussed earlier, increases in $F_{n,fr1}$ are evaluated when extended trimming reinforcement is included in walls having the same dimensions and identical penetration geometries. In addition, comparison of $F_{n,fr1}$ with the wall strength predictions shown in Figures 6.7-6.10 indicated that the predicted $F_{n,fr1}$ values for the 2.6 m long perforated concrete masonry walls were identical to those predicted according to the simplified strut-and-tie models (i.e. $F_{n,st0}$). For the 4.2 m long concrete masonry walls with two openings, the inclusion of double bending of the central pier resulted in $F_{n,fr1}$ values that were about 33% to 58% more than those predicted according to $F_{n,st0}$. Despite the significantly simplified approach adopted by the modified plastic collapse analysis, the wall strengths predicted according to $F_{n,fr1}$ approximately matched those of the $F_{n,st1}$, with $F_{n,fr1}/F_{n,st1}$ ranges from 0.91 to 1.11 for the perforated concrete masonry walls included in this study.

6.4.2 Flexural strength of wall without opening

For the purpose of strength comparison presented in section 6.7, the flexural strengths of Walls B1-B8 were re-evaluated to provide lateral strengths for the corresponding solid built walls (i.e. no opening). Figure 6.15 presents illustration of the strut-and-tie models for one of the 2.6 m and 4.2 m long walls. In both cases, wall density of 1.6 kN/m^2 was considered. The evaluated wall strengths using the discussed method are identified in Table 6.1 as $F_{n,no\text{-}op}$.

6.4.3 Masonry Shear Strength

Table 6.1 also includes the nominal shear strength values, V_n, calculated using the NZS 4230:2004 specified shear equations described in section 4.3. For masonry walls there is frequently some difficulty in determining the effective section area, $b_w d$, to be used in Equation 4-5. NZS 4230:2004 recommends the use of guidelines illustrated in Figure 2.16. For partially grouted walls the effective section width for shear will be the net thickness of the face-shells. This limitation is necessary to satisfy requirements of continuity of shear flow and to avoid the possibility of vertical shear failure up a continuous ungrouted flue. For concrete masonry units with ungrouted flues, typically b_w = 60 mm.

6.4.4 Predicted Strength Summary

The predicted wall strengths described in sections 6.4.1-6.4.3 are summarised in Table 6.1. Although the masonry shear strengths were higher than the predicted flexural strengths, it was

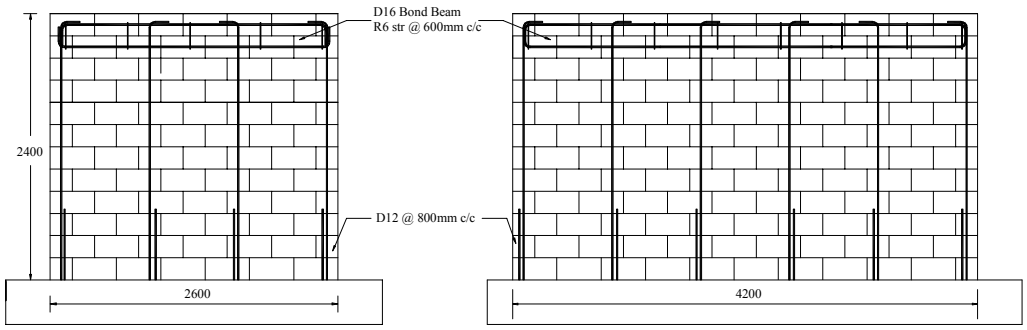

(a) Wall reinforcement details

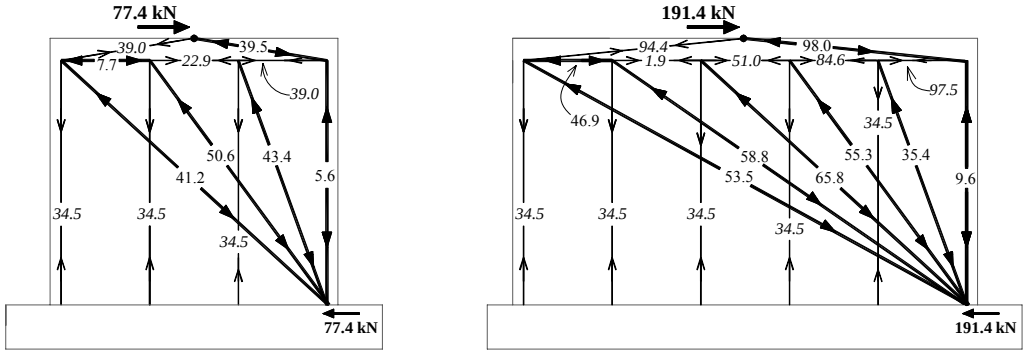

(b) Strut-and-tie models (forces in kN)

Figure 6.15 Strut-and-tie models for masonry walls without opening.

anticipated that all walls would fail in diagonal tension due to partial grouting and the lack of distributed horizontal shear reinforcement. This was preferable to the hinge-sliding mode, where lateral force was resisted only by dowel action of the vertical reinforcement once a crack opened up along the entire length of the wall/foundation interface (Priestley, 1976). While four procedures were used to evaluate the wall predicted strengths, only values within the shaded columns in Table 6.1 were chosen as the assumed nominal lateral wall strengths on the day of testing (refer to Voon and Ingham (2006)). For the 2.6 m long perforated masonry walls and the walls with control joint, the $F_{n,st0}$ values were used instead of the $F_{n,st1}$ since $F_{n,st0}$ had the advantage of being easier to evaluate and they were only 2% to 10% less than $F_{n,st1}$. In addition, it was expected that a full plastic mechanism would not develop in the nominally reinforced perforated masonry walls. Davidson (1996) successfully observed from his study that the response of individual piers was effectively independent, therefore supporting the assumption of pin formation in the outer piers at the bond beam centre. For the masonry walls with double openings, $F_{n,st1}$ was used as the predicted flexural strengths for the 4.2 m long walls. It was expected that double bending of the central pier would significantly increase the lateral strength of the 4.2 m long walls. The $F_{n,fr0}$ and $F_{n,fr1}$ values are useful when compared to the experimentally measured wall strengths presented in sections 6.6 and 6.7. Although the wall strengths predicted according to the modified plastic collapse analysis were successfully shown to closely match those predicted using the strut-and-tie models, only values predicted

using the strut-and-tie methods were used as the assumed nominal wall strengths (on the day of testing) because they had the advantage of providing a comparison between the cracking patterns on the tested walls and the load paths by which the shear forces were shown to transfer to the foundation in the strut mechanisms. However, on any other occasions, it is deemed appropriate to employ the modified plastic collapse analysis as an alternative to strut-and-tie method when analysing the lateral strength capacities of partially grout-filled perforated concrete masonry walls that were constructed according to NZS 4229:1999 specifications.

Table 6.1 Prediction of wall strengths, based upon measured material properties

Wall	$\mathbf{f'_m}$	$\mathbf{F_{n,st0}}$	$\mathbf{F_{n,st1}}$	$\mathbf{F_{n,fr0}}$	$\mathbf{F_{n,fr1}}$	$\mathbf{F_{n,no\text{-}op}}$	$\mathbf{F_{code}}$	$\mathbf{V_n}$
B1	16.2	44.7	46.4	103.6	44.7	77.3	51.8	81.0
B2	12.9	35.9	38.4	80.6	35.9	77.0	37.3	69.1
B3	14.4	28.0	30.8	61.4	27.9	77.1	24.3	73.0
B4	16.5	41.0	44.7	94.4	40.9	77.3	37.3	78.1
B5	18.9	41.0 (push) 35.9 (pull)	44.7 (push) 38.4 (pull)	94.4 (push) 80.6 (pull)	40.9 (push) 35.9 (pull)	77.5	37.3	83.5
B6	16.5	58.0	78.3	129.2	87.0	191.4	55.9	117.2
B7	18.0	50.0	62.1 (push) 73.0 (pull)	108.0 (push) 110.5 (pull)	66.5 (push) 79.1 (pull)	191.6	49.4	122.4
B8	18.0	50.0 (push) 55.0 (pull)	62.1 (push) 76.3 (pull)	108.0 (push) 119.9 (pull)	66.5 (push) 81.7 (pull)	191.6	49.4	122.4
B9	23.8	80.2	110.9	---	---	---	49.8	169.0
B10	23.8	80.2	82.1	---	---	---	49.8	169.0
Units	**MPa**	**kN**	**kN**	**kN**	**kN**	**kN**	**kN**	**kN**

Note:

1. $F_{n,st0}$ is the nominal wall strength predicted according to the simplified strut-and-tie model discussed in section 6.4.1.2.
2. $F_{n,st1}$ is the nominal wall strength predicted according to the improved strut-and-tie model discussed in section 6.4.1.3.
3. $F_{n,fr0}$ is the nominal wall strength predicted according to the full plastic collapse analysis discussed in section 6.4.1.4.
4. $F_{n,fr1}$ is the nominal wall strength predicted according to the modified plastic collapse analysis discussed in section 6.4.1.5.
5. $F_{n,no\text{-}op}$ is the nominal wall strength predicted for the corresponding solid built walls discussed in section 6.4.2.
6. F_{code} is the code specified wall nominal strength.

6.5 TESTING PROCEDURE

The testing procedure adopted was that described by Park (1989), which for more than a decade has been the standard test procedure used in New Zealand to establish available ductility capacity in a manner consistent with New Zealand design standards. The advantage of this method is that the test can proceed without prior knowledge of the actual strength and ductility capacity of the test specimen. Also, Liddell et al. (2000) have found, when testing reinforced concrete beams, that this loading history results in less damage than when using alternative loading histories considering a larger number of cycles at each displacement interval. In addition, Liddell et al. determined that the New Zealand loading history resulted in hysteretic response most similar to that obtained for structures that were subjected to cyclic loading corresponding to earthquake records. The steps in Park's procedure are:

1. Calculate the nominal lateral force (F_n) required to develop the wall flexural strength.
2. Apply a lateral force equal to ¾ of F_n in one direction and record displacement of the wall Δ_a.
3. Unload the wall and repeat step (2) in the reverse direction to obtain Δ_b. Extrapolate straight lines from the origin of the force/displacement plot through the points (¾ F_n, Δ_a) and (-¾ F_n, Δ_b) and find their intersection with the nominal lateral force. This step is illustrated in Figure 6.16. The yield displacement is Δ_y as shown in the figure. The displacement Δ at a ductility value of μ is defined as $\mu*\Delta_y$.
4. Apply lateral force slowly in a sequence so that the top of the wall is displaced to the ductility levels shown in Figure 6.17.

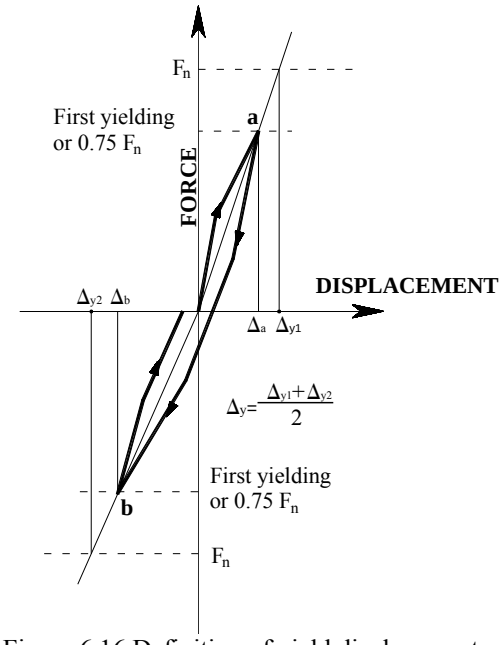

Figure 6.16 Definition of yield displacement.

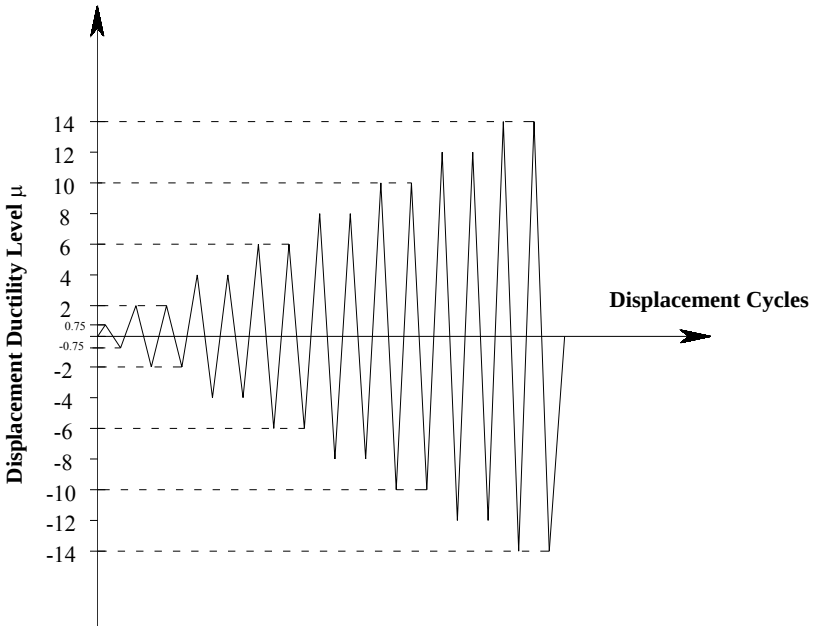

Figure 6.17 Imposed displacement history in terms of ductility.

In New Zealand a practice has evolved over time whereby the available displacement ductility, μ_{av}, of a structural element may be established from laboratory testing. The method has been reported by Park (1989), and is based on the notion that performance is satisfactory if a tested element can sustain four complete (bi-directional) loading cycles to μ_{av}, with less than 20% loss in peak strength. However, as μ_{av} is unknown prior to the test, it is assumed that μ_{av} may adequately be determined from the expression:

$$\mu_{av} = \frac{\sum|\mu_i|}{8} \qquad (6\text{-}1)$$

where $|\mu_i|$ is the absolute magnitude of each ductility semi-cycle during the loading history. As an illustration, two complete cycles in both directions to $\mu = 2$ results in $\sum|\mu_i| = 8$ and a further two complete cycles to $\mu = 4$ results in $\sum|\mu_i| = 24$. Finally, it is noted that NZS 4203:1992 stipulates $\mu \leq 4$ for reinforced concrete masonry, such that accurate determination of ductility capacity above this level was of little relevance.

6.5.1 Miscellaneous

Similar to the procedure described in section 3.5.1, each test wall was inspected for any pre-test cracking or damage prior to the commencement of testing. This procedure was carried out in order to avoid confusion with damage attributed to the applied loading. In addition, cracks due to applied loading were marked during testing and photos were also taken of any significant structural event.

6.5.2 Data Reduction

Instrumentation attached to the wall, as shown in Figure 6.4, allowed the wall deformation to be isolated into the four components. The rocking, sliding and flexural deformation components were evaluated according to the procedures described in section 3.5.2 while the shear deformation component was evaluated according to the procedure described in Appendix C.

6.6 TEST RESULTS

This section of the thesis summarises the behaviour of the ten nominally reinforced partially grout-filled concrete masonry walls and presents the measured force-displacement responses. General wall behaviour is summarised in Table 6.2, where F_{max} corresponds to the maximum wall strength measured in the test, and Δ_y is the evaluated yield displacement of the tested walls. μ_{max} is defined as the displacement ductility level at which maximum strength was measured and μ_{av} is the available displacement ductility factor, which according to Park (1989) is the ductility level at which a test element has sustained less than 20% loss in peak strength after four complete (bi-directional) loading cycles to μ_{av}. For detailed descriptions of the experimental results, refer to Voon and Ingham (2006). The nominal strengths shown on the force-displacement (F-D) curves are without strength reduction factor (i.e. $\phi = 1.0$). In all cases, the first loading excursion was into the positive quadrant.

6.6.1 Force-Displacement Response

The experimentally obtained force-displacement curves for the ten partially grout-filled concrete masonry walls of Series B are presented in Figure 6.18, depicting the lateral displacement at the top of the walls as a function of applied lateral shear force. Due to the lack of horizontal shear reinforcement and the fact that the walls were partially grout-filled, all test walls were observed to fail in diagonal tension mode. This was preferred to the hinge-sliding mode, where lateral force was resisted only by dowel action of the vertical reinforcement once a crack opened up along the entire length of the wall/foundation interface (Priestley, 1976). It is noteworthy that the general nature of the force-displacement responses presented in Figure 6.18 are significantly similar to those reported by Brammer (1995) and Davidson (1996). From the F-D curves illustrated in Figure 6.18, a number of general characteristics of Walls B1-B10 can be identified:

1. The maximum strength was typically developed during the first excursion to $\mu = 4$. Following this, cracking became significant in some walls and strength degradation began.

2. Despite the presence of widely open diagonal cracks, the partially grouted concrete masonry walls detailed in Figure 6.1 exhibited gradual strength and stiffness degradation, and in no case did any wall suffer from sudden failure. This desirable behaviour of the nominally reinforced partially grouted masonry walls with openings was created by the solid filled bond beam at the top of the walls, which caused a frame-type action at latter stage of testing.
3. The force-displacement plots consistently illustrated a pinched shape. This was primarily due to the presence of significant shear deformation in this type of masonry construction. Figure 6.19 depicts a selection of experimentally measured displacement component plots. The results presented in these plots confirm the observations of early horizontal flexural cracks which were then exaggerated by wide open diagonal cracks that extended throughout the wall panels.
4. From the wall cracking pattern diagrammatically shown in Figure 6.20, it is clearly illustrated that the absence of major damage in the solid grout-filled bond beam supported the notion of frame-type action being developed at later stage of the test. This leads to considerable inelastic displacement capacity of the partially grouted masonry walls, where μ_{av} was measured to consistently be above 2.0.
5. Less hysteretic energy was expended during the second cycle to any displacement level, when compared with the first displacement cycle. This is illustrated by the more pinched hysteresis loops of the second cycle.

The μ_{av} values recorded in Table 6.2 show that the largest recorded ductility capacity for the perforated masonry walls corresponded to a wall length of 2600 mm, and reduced significantly for the 4200 mm long perforated masonry walls. It was observed from experimental testing that the 4200 mm long masonry walls displayed greater cracking than the 2600 mm long walls. Consequently, it was deduced that the lower observed ductility rating for the 4200 mm long walls occurred because of the rapid-developing wide cracks that contribute to shear displacement, accelerating initiation of the diagonal tension mode of failure and subsequent strength degradation.

From Figure 6.18a, it was observed that Wall B1 did not achieve the bracing capacity prescribed by NZS 4229:1999 (denoted F_{code}). NZS 4229:1999 over-predicted the lateral strength of this perforated wall by about 3.3% and 5.4% in the respective push and pull directions. However, it is illustrated in Figure 6.18 the conservatism of NZS 4229:1999

increases with the depth of opening, and for a full depth opening (e.g. a door in Wall B3) the NZS 4229:1999 prediction had significant conservatism. Consequently, the preliminary conclusion was therefore that NZS 4229:1999 is only non-conservative for window openings having a depth of less than 1.2 m, though unfortunately this probably accounts for a very large majority of all window openings.

As shown in Figure 6.18i, the maximum strength achieved by Wall B9 was 43% higher than the values of $F_{n,st0}$ obtained from the simple strut-and-tie model shown in Figure 6.7i. This higher strength was due to the solid filled bond beam constructed on top of the control joint. Consequently, the (un-debonded) continuous bond beam caused a frame-type action between

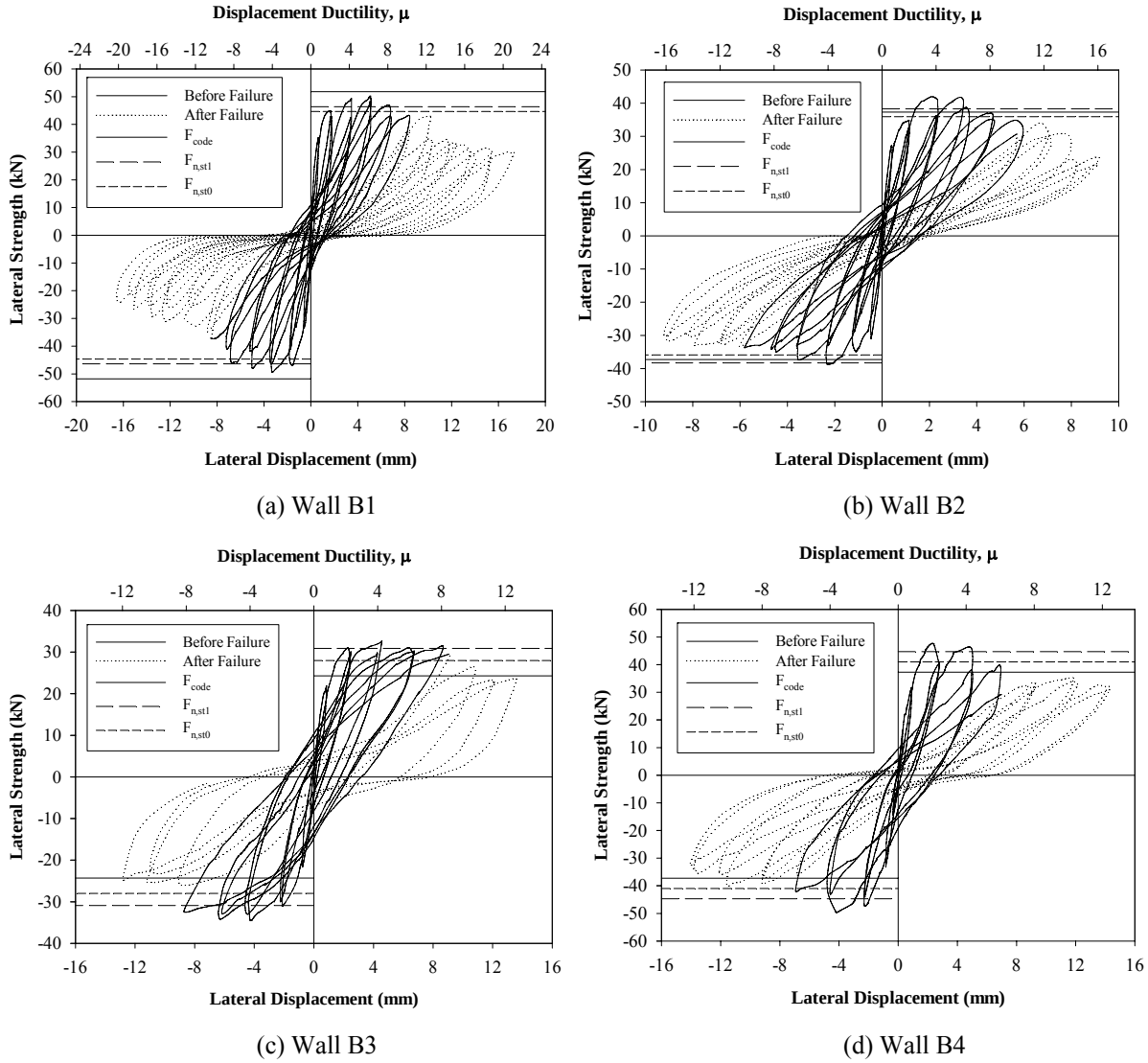

(a) Wall B1 (b) Wall B2

(c) Wall B3 (d) Wall B4

Figure 6.18 Series B, force-displacement histories.

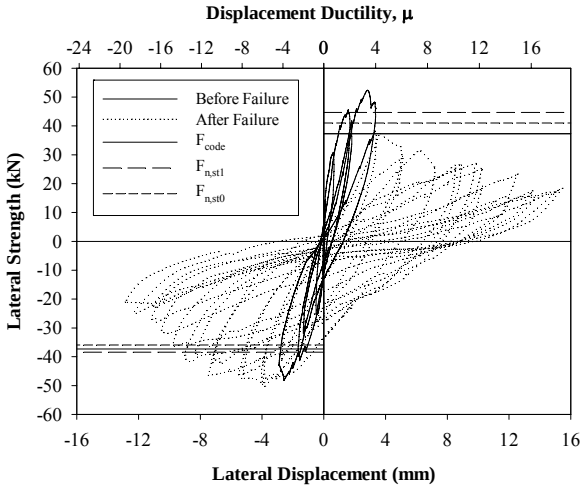

(e) Wall B5

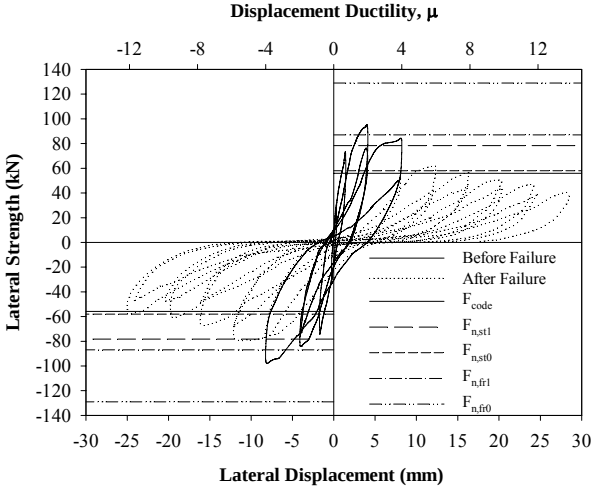

(f) Wall B6

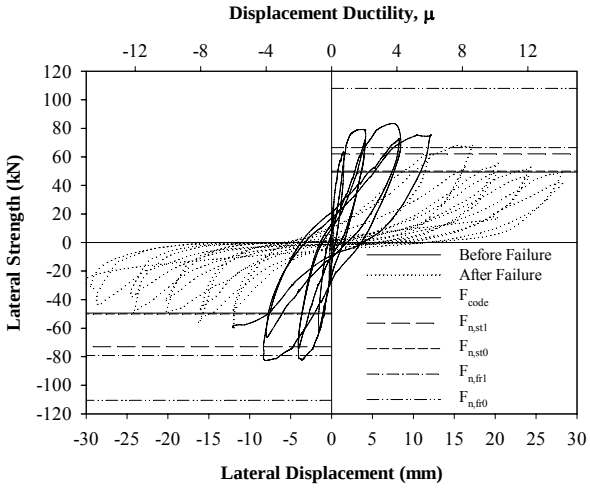

(g) Wall B7

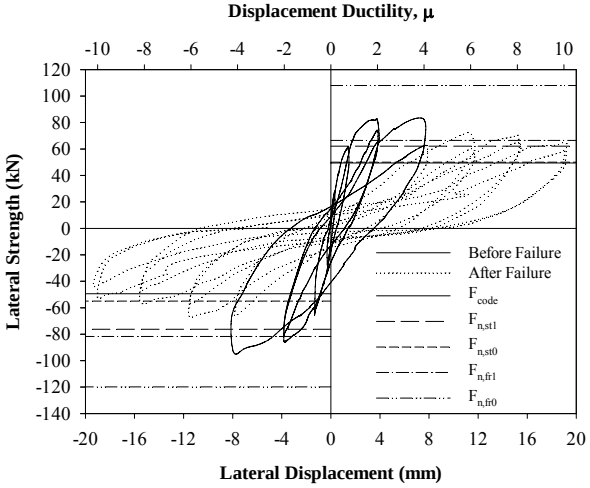

(h) Wall B8

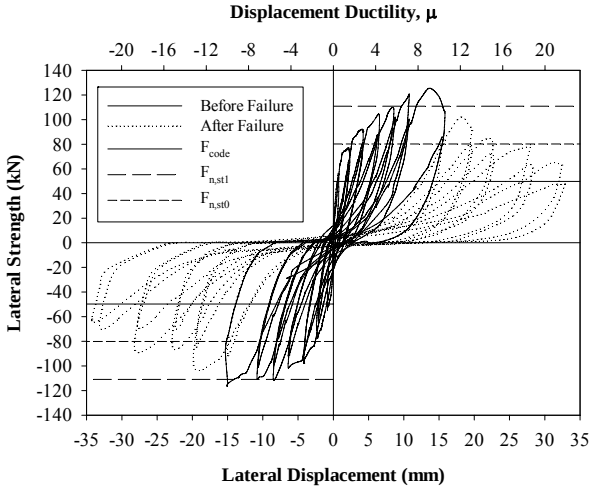

(i) Wall B9

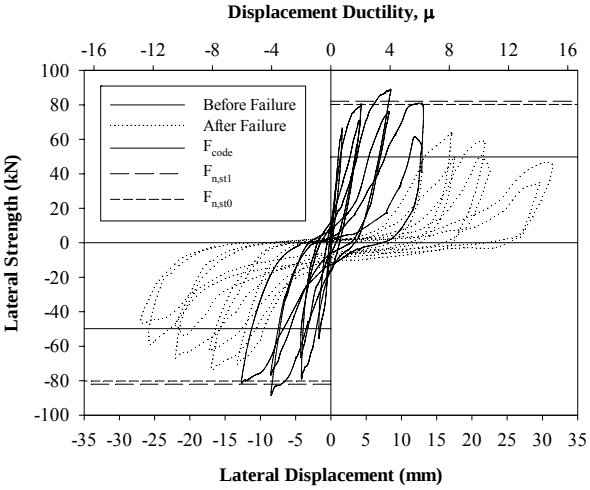

(j) Wall B10

Figure 6.18 Series B, force-displacement histories.

Table 6.2 Summary of test results for the masonry walls.

Wall	Specimen	h_{op}/h_w	f'_m	$F_{n,no\text{-}op}$	F_{max}	$\frac{F_{max}}{F_{n,no-op}}$	Δ_y	μ_{max}	μ_{av}
Current research	B1	0.33	16.2	77.3	+50.2 -49.0	0.65	0.82	+6 -4	>6.0
	B2	0.5	12.9	77.0	+41.2 -38.7	0.54	0.57	±4	>6.0
	B3	0.83	14.4	77.1	+33.3 -34.4	0.45	1.07	±4	>6.0
	B4	0.5	16.5	77.3	+47.4 -48.8	0.63	1.15	+2 -4	4.5
	B5	0.5	18.9	77.5	+52.4 -50.4	0.68	+0.84 -0.66	+4 -6	2.0
	B6	0.5	16.5	191.4	+94.3 -94.6	0.49	1.83	+2 -4	2.0
	B7	0.83*	18.0	191.6	+82.8 -82.5	0.43	1.89	±4	3.8
	B8	0.83*	18.0	191.6	+82.7 -93.2	0.49	1.60	±4	2.0
	B9	0	23.8	105.8	+125.3 -114.6	1.18	1.50	±14	>6.0
	B10	0	23.8	82.1	+89.0 -84.6	1.08	2.10	±4	4.5
Previous	BD1	0	---	75.0	76.5	1.02	1.57	---	5.4
	BD2	0	---	213.1	179.9	0.84	3.60	---	1.0
	DB1	0.83*	---	174.0	89.0	0.51	1.00	---	6.0
Units		---	MPa	kN	kN	---	mm	---	---

Note:

1. * h_{op}/h_w ratio according to the largest opening on the wall
2. BD1 is the 2600 x 2400 x 140 concrete masonry wall tested by Brammer (1995), see Figure 2.18a.
3. BD2 is the 4200 x 2400 x 140 concrete masonry wall tested by Brammer (1995), see Figure 2.18b.
4. DB1 is the 4200 x 2400 x 190 perforated concrete masonry wall tested by Davidson (1996), see Figure 2.19.

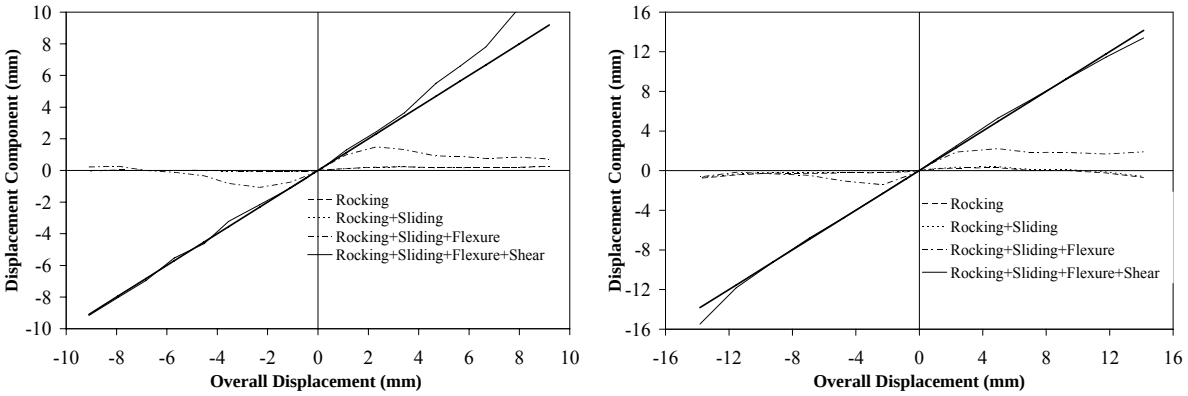

(a) Wall B2 (b) Wall B4

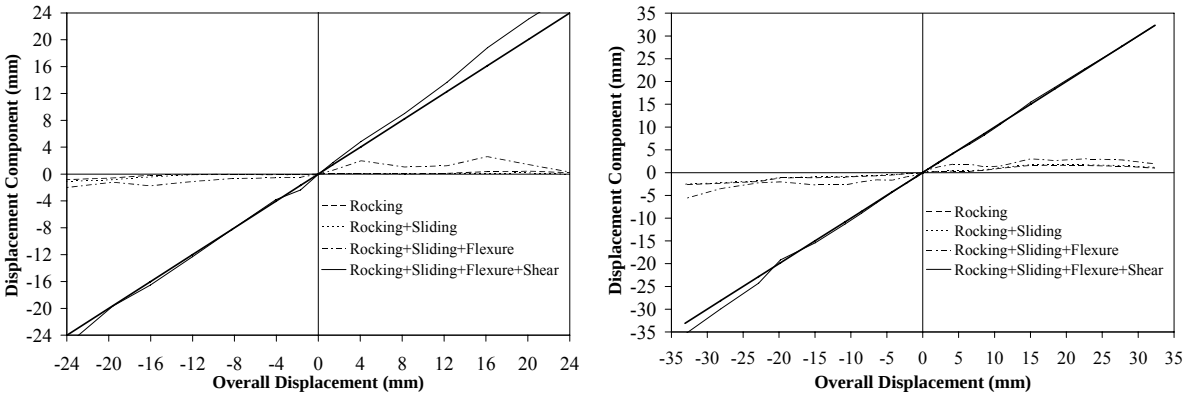

(c) Wall B6 (d) Wall B9

Figure 6.19 Series B, plots of displacement component.

the two piers, therefore allowing partial shear transfer. This notion was supported by the absence of significant structural damage in the bond beam. In addition, double bending of the solid filled bond beam (above the control joint) allowed it to generate some strength and subsequently led to yielding of the D12 reinforcing bar adjacent to the compression edge (as shown by the $F_{n,st1}$ model presented in Figure 6.9i). Furthermore, closing of the control joint at the wall mid-height position at latter stage of testing permitted additional shear transfer between the two piers. The maximum strengths recorded by the wall were 13% and 3% higher than the predicted value of $F_{n,st1}$ in the respective push and pull loading directions.

6.6.2 Damage Pattern

Due to the lack of distributed horizontal shear reinforcement and the fact that the wall was partially grout-filled, all test walls were observed to fail in diagonal tension mode. This type of failure was characterised by the development of early horizontal flexural cracking, which was later superseded by wide open diagonal cracks that extended throughout the wall panels. The cracking patterns for these walls are depicted diagrammatically in Figure 6.20, with the shaded areas indicating masonry crushing. From Figure 6.20, it is illustrated that the diagonal cracking

patterns on the perforated concrete masonry walls aligned well with the load paths by which shear force was transferred to the foundation in the strut mechanisms. This observation supports the use of strut-and-tie analysis as the tool to evaluate the strength of walls with reinforcement details complying with the specifications of NZS 4229:1999. Figures 6.21-6.25 present a selection of photographs to illustrate the condition of some tested wall at end of testing.

In addition, from the wall cracking patterns illustrated in Figure 6.20, it is shown that the absence of major damage in the solid grout-filled bond beam supported the notion of frame-type action being developed at later stage of testing. This leads to considerable inelastic displacement capacity of the partially grout-filled masonry walls and allowing the perforated partially grouted masonry walls to exhibit gradual strength and stiffness degradation. It was observed during experimental testing that the reduced ductility capacity of the 4200 mm long masonry walls coincided with the greater cracking displayed on these walls than those observed on the 2600 mm masonry walls. Consequently, it was deduced that the lower observed ductility rating for the 4200 mm long walls occurred because of the rapid-developing wide cracks that contribute to shear displacement, accelerating initiation of the diagonal tension mode of failure and subsequent strength degradation.

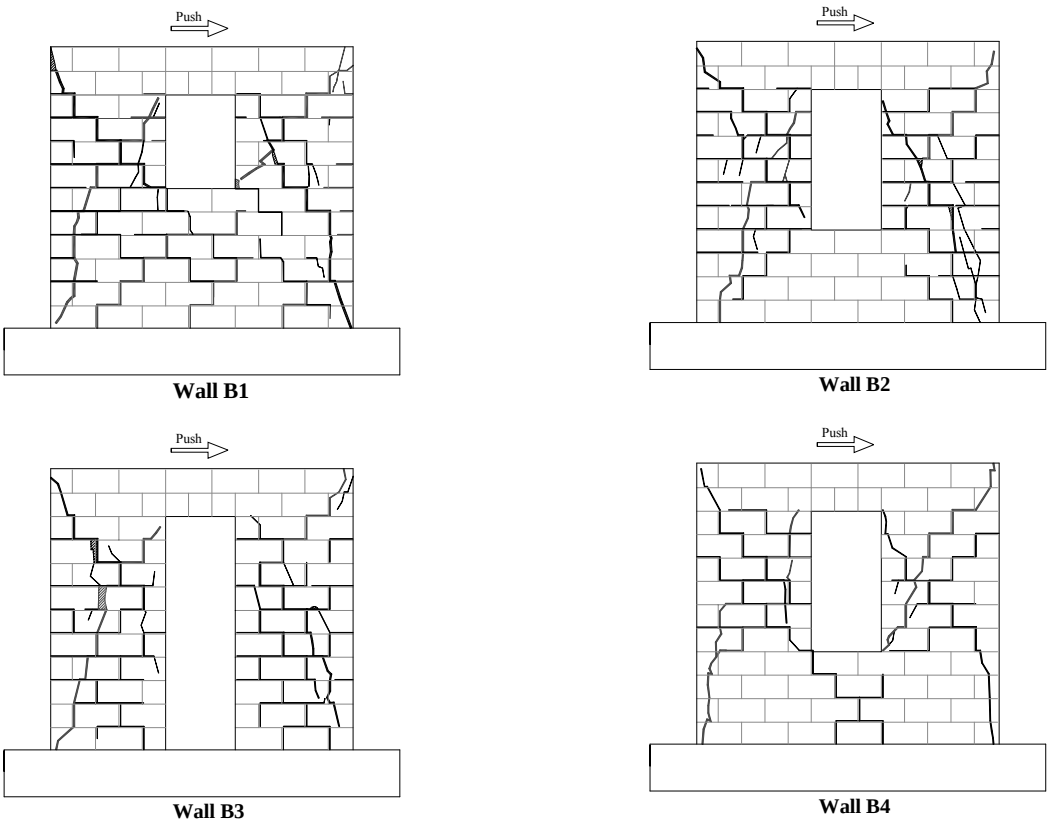

Figure 6.20 Series B, masonry wall cracking patterns at end of testing at end of testing.

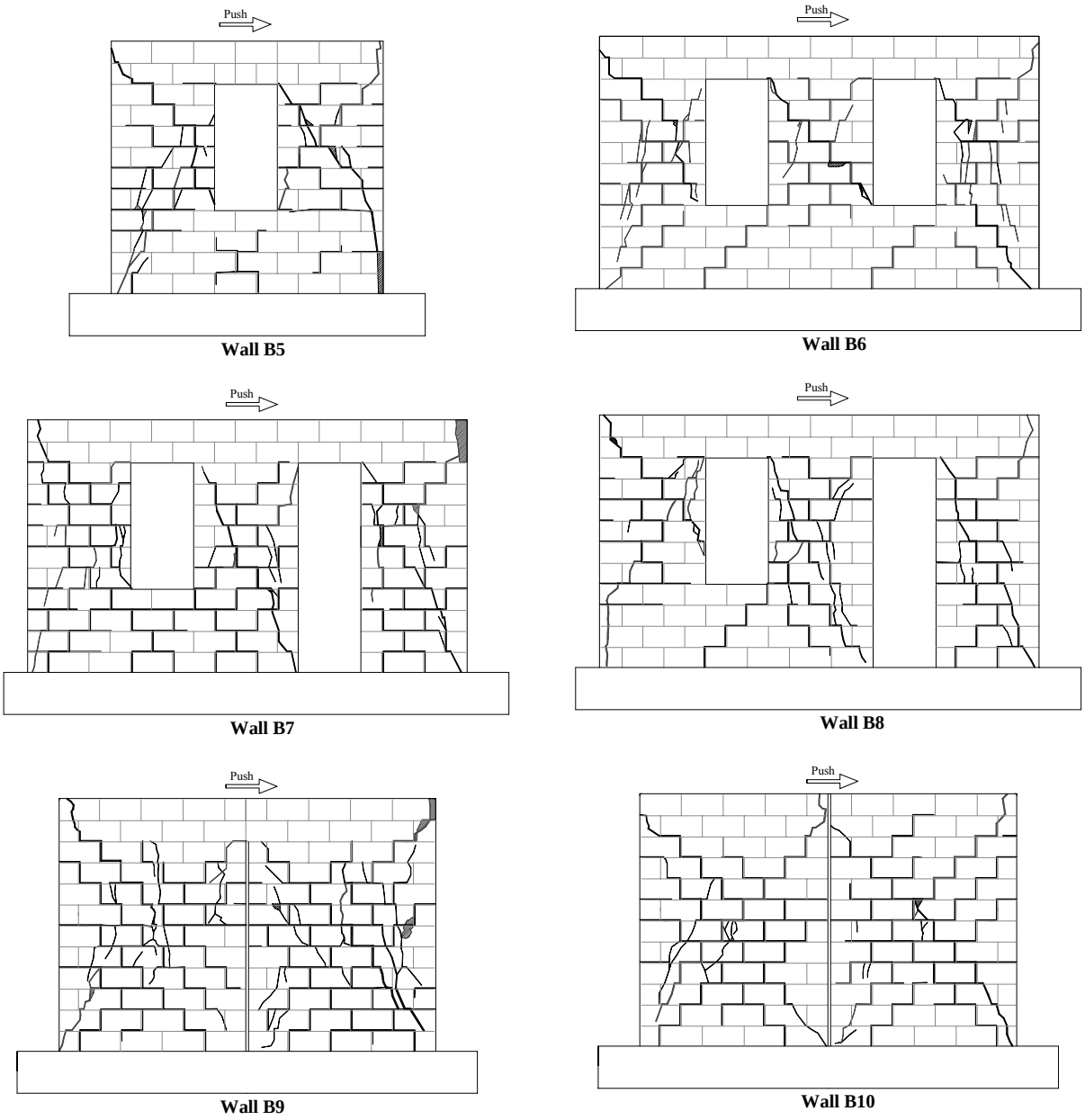

Figure 6.20 Series B, masonry wall cracking patterns at end of testing at end of testing (continued).

6.7 DISCUSSION

The primary objective of the research discussed in this chapter was to validate the adequacy of NZS 4229:1999 in addressing the bracing capacity of masonry walls containing openings. As shown in Figure 6.1, design of the eight perforated masonry wall specimens was conceived to facilitate comparison of wall behaviour between two or more walls with respect to variation of a given design parameter. These eight nominally reinforced partially grouted concrete masonry walls had variations in trimming reinforcement detailing, including those complying with NZS 4229:1999, and a range of penetration geometries. In addition, experimental works previously conducted at the University of Auckland (see Figures 2.18 and 2.19) were included

Figure 6.21 Series B, condition of Wall B2 at end of testing.

Figure 6.22 Series B, condition of Wall B4 at end of testing.

Figure 6.23 Series B, condition of Wall B6 at end of testing.

Figure 6.24 Series B, condition of Wall B8 at end of testing.

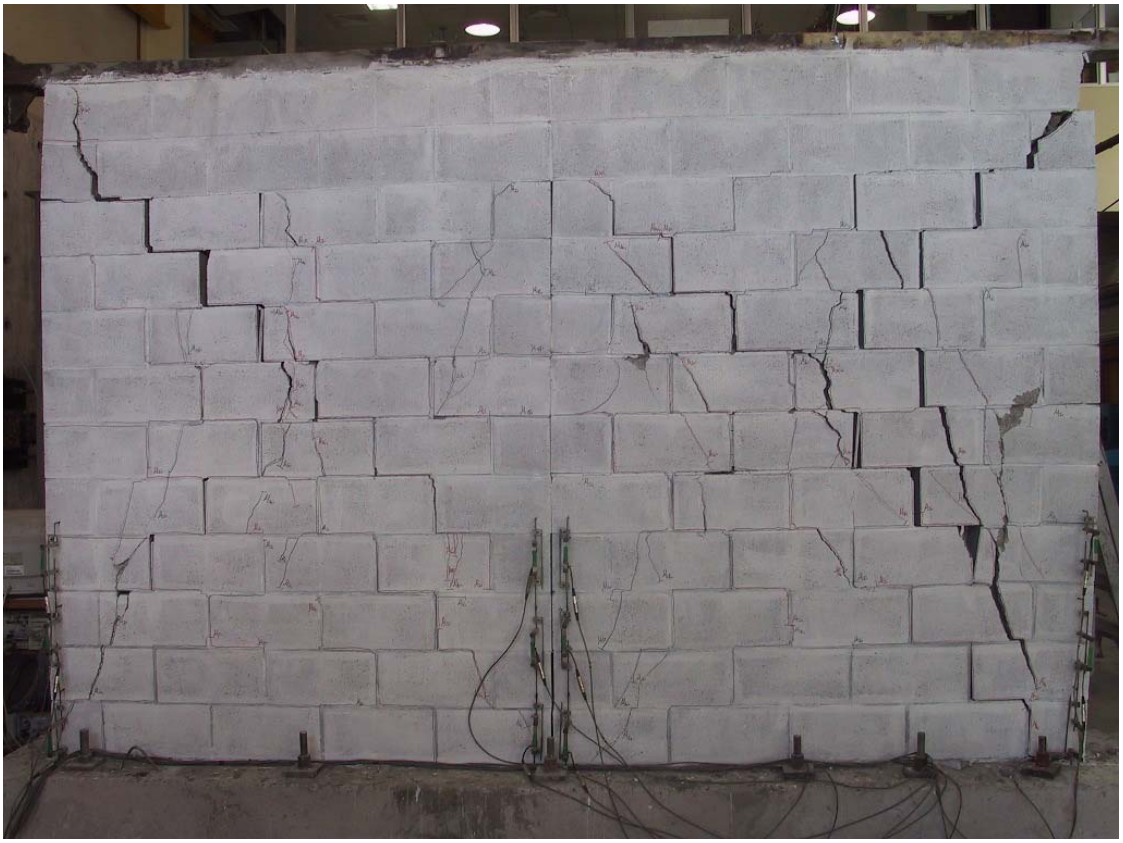

Figure 6.25 Series B, condition of Wall B9 at end of testing.

in this part of the study to supplement the experimental results presented in section 6.6. The two 15 series concrete masonry walls tested by Brammer (1995) are valuable to provide comparison of behaviour between perforated walls and those of solid built walls (i.e. without opening). A parallel issue is the influence which shrinkage control joints have on the bracing capacity of partially grouted concrete masonry walls. NZS 4229:1999 prescribed a procedure to account for shrinkage control joints, but this detail has never been verified through structural testing. Consequently, experimental testing on two partially grout-filled concrete masonry walls was conducted to validate the structural adequacy of the shrinkage control joint detail published in NZS 4229:1999.

The figures in this section are limited to force-displacement (F-D) envelopes. These are curves that relate the peak strength recorded in the first cycle for each displacement ductility level. The F-D envelopes are arranged in groups to show the effect of a particular parameter. A full set of curves for each test is presented in section 6.6.

6.7.1 Depth of Openings

Test results from this study successfully illustrate correlation between the reduction of wall strength and depth of openings (h_{op}) on masonry walls. This is shown in Table 6.2 and Figure 6.26 by the consistent reduction of $F_{max}/F_{n,no\text{-}op}$ ratios when the depth of openings were increased in the 2600 mm and 4200 mm long masonry walls that were constructed according to NZS 4229:1999 specifications. This reduction of wall strength could also be identified in the F-D envelopes presented in Figures 6.27 and 6.29. In Figure 6.27, it is shown that the lateral strength of the 2600 mm long walls reduced from the maximum of 76.5 kN in the case of Wall BD1 (without opening), to 50.2 kN when a window opening of 600 x 800 was included in Wall B1. The same figure also shows further reduction of wall strength to 41.2 kN and 34.4 kN when the depth of openings was increased to 1200 mm and 2000 mm in Walls B2 and B3 respectively. As diagrammatically illustrated in the strut-and-tie models presented in Figure 6.28, the further reduction of strength in Walls B2 and B3 (compared to Wall B1) was because of the steepened diagonal struts on the left piers when the depth of openings increased. While the diagonal strut on the right piers remained unchanged for these three walls, the steepened diagonal struts on the left piers resulted in reduction of horizontal shear components that could be resisted by the left piers, consequently leading to the overall reduction of lateral strength in Walls B2 and B3.

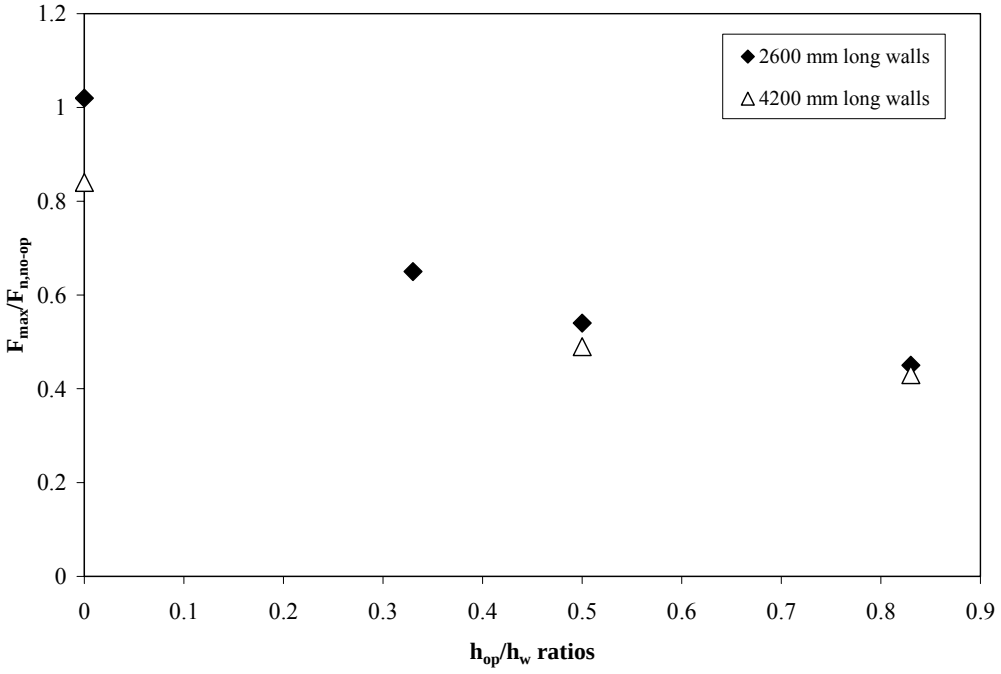

Figure 6.26 Effect of opening for walls constructed according to NZS 4229:1999 specifications.

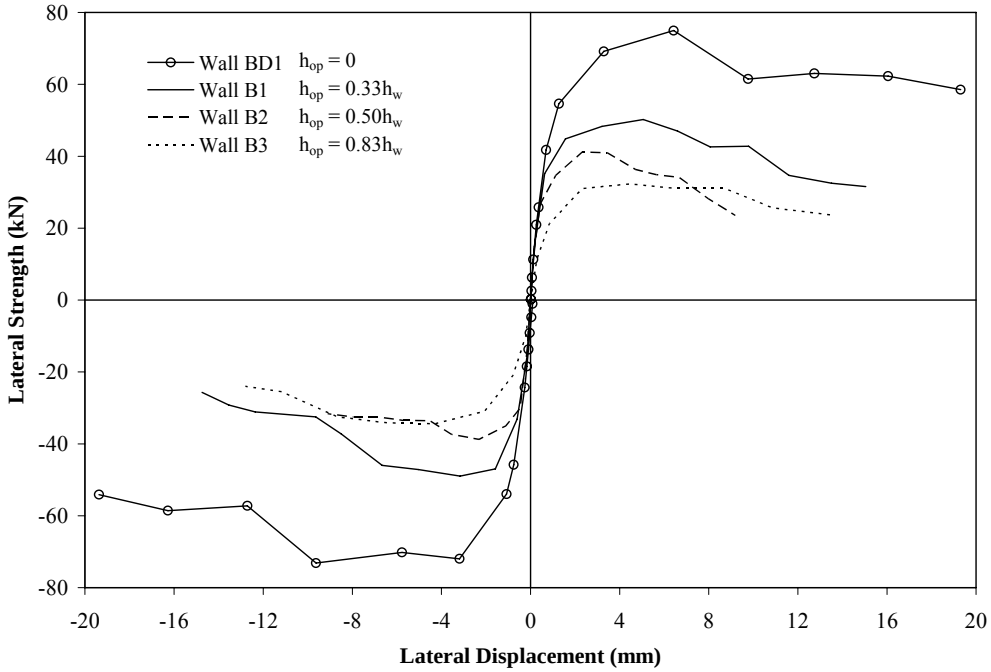

Figure 6.27 Effect of opening on the 2600 mm long walls.

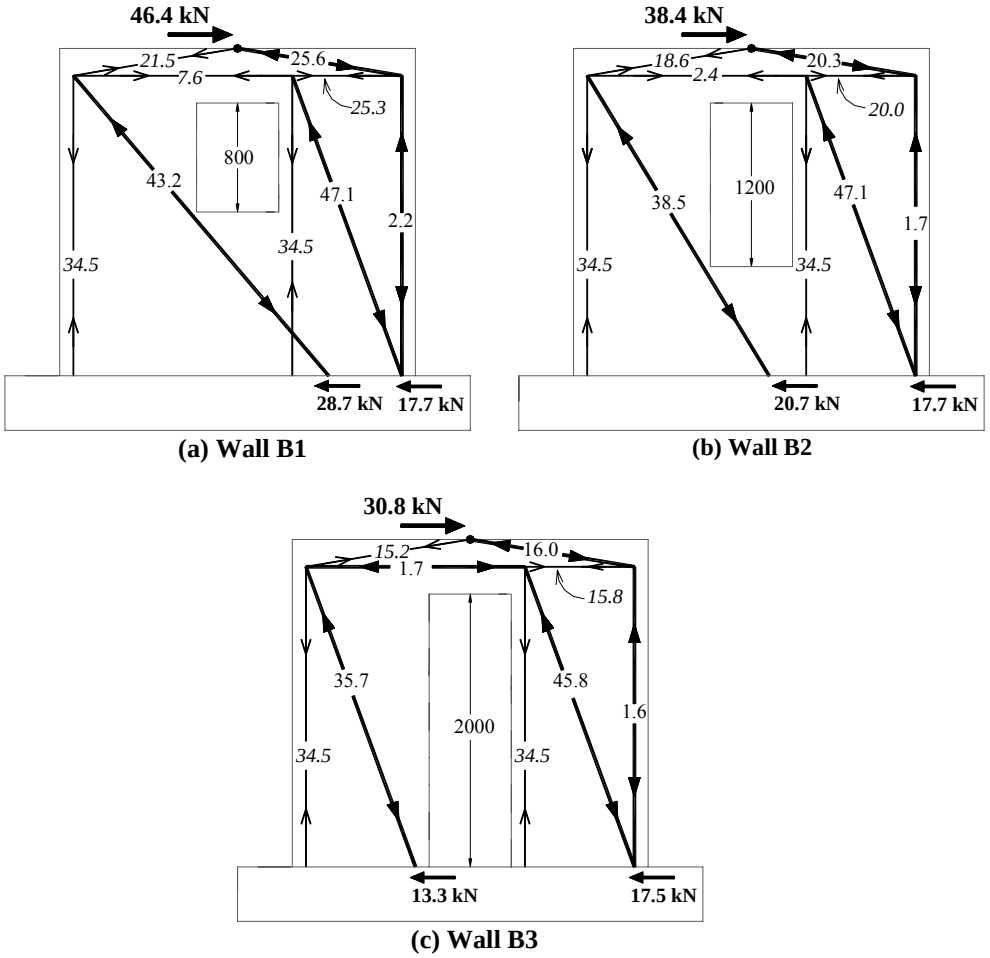

Figure 6.28 Strut-and-tie models in push direction.

Similarly, the reduction of lateral strength in the 4200 mm long walls is also evident in Figure 6.29. As compared to the strength recorded in Wall BD2, it is shown that the wall lateral strength was almost halved when openings were introduced on the 4200 mm long masonry walls. In addition, by comparing the lateral strengths of Walls B6 and B7, it is shown that the introduction of a door opening resulted in the reduction of strength from 94 kN to 83 kN in Wall B7 (about 12% reduction of strength). Note that the test results of Walls B4, B5 and B8 are not included in Figures 6.26 - 6.29 because the detailing of trimming reinforcement in these walls differed from that specified in NZS 4229:1999. The primary objective of Figures 6.26-6.29 is to illustrate the effect of openings on the lateral strength of perforated masonry walls constructed according to NZS 4229:1999 specifications. It is noted in Figure 6.26 that the 4200 mm long masonry wall tested by Brammer (1995), denoted as BD2 in Table 6.2, failed to develop its predicted nominal strength even though it had no openings.

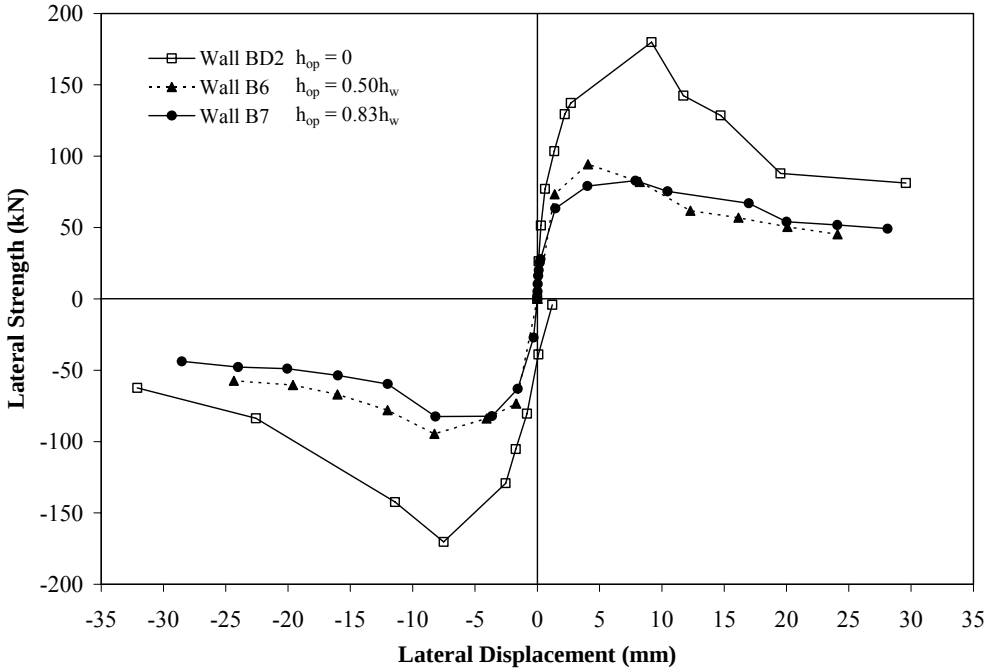

Figure 6.29 Effect of openings on the 4200 mm perforated masonry walls.

6.7.2 Effect of Trimming Reinforcement

The effect of trimming reinforcement on the lateral strength of perforated masonry walls is discussed in this subsection. It was illustrated in section 6.6 that the use of extended D16 trimming reinforcement could affect the wall ultimate strength considerably. This is shown by the increase in magnitude of the $F_{max}/F_{n,no\text{-}op}$ ratios presented in Table 6.2 when the trimming reinforcement was extended below the window openings in the 2600 mm and 4200 mm long masonry walls. This increase of wall strength can also be identified in the F-D envelopes

presented in Figures 6.30 and 6.31. Figure 6.30 shows the force-displacement envelopes for Walls B2, B4 and B5. These three partially grout-filled masonry walls were constructed to identical geometries and consisted of identical longitudinal and bond beam reinforcement, with the only difference being the length of trimming reinforcement used in each wall. The trimming reinforcement in Wall B2 (see Figure 6.1) was detailed according to the specifications of NZS 4229:1999, but Walls B4 and B5 were detailed with extended trimming reinforcement. As shown in Figure 6.1, the trimming reinforcement in Wall B5 was only extended to the outermost vertical reinforcement on one side of the wall, therefore resulting in higher strength being predicted in the push direction than in the pull direction. The force-displacement envelopes in Figure 6.30 clearly illustrate the increase of lateral strength from the maximum of 41.2 kN for Wall B2 to 47.7 kN and 52.4 kN when the trimming reinforcement was extended beneath the window opening in Walls B4 and B5, therefore resulting in strength increases of about 18% and 27% respectively. However, the effect of the extended trimming reinforcement in the pull direction could not be properly observed in Wall B5. Although a lesser strength was predicted in the pull direction for Wall B5, a maximum strength of about 50 kN was recorded despite the absence of extended trimming reinforcement on the left pier. As shown in Table 6.1, this maximum strength in Wall B5 was higher than that recorded in the pull direction for Wall B4, although an extended trimming reinforcement bar was present on the left pier in Wall B4. Consequently, this observation confirms that Wall B5 may have developed strength in its pull direction that was substantially higher than specimens of similar

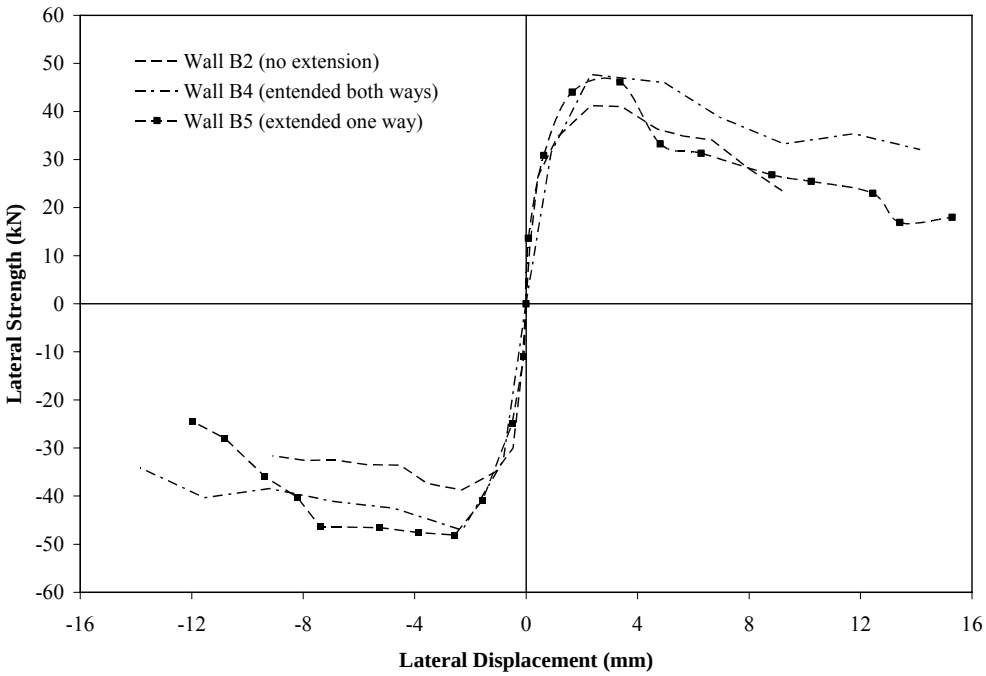

Figure 6.30 Effect of trimming reinforcement on the 2600 mm long perforated masonry walls.

construction. Discarding the experimental result of Wall B5, the effect of trimming reinforcement in increasing wall strength (pull direction) could be undoubtedly demonstrated by the experimental results of Walls B2 and B4. It was shown that a strength increase of about 26% was recorded in Wall B4, as compared to Wall B2, when extended trimming reinforcement was present in the left pier.

Strength increase due to the extended trimming reinforcement in the 4200 mm perforated masonry walls is shown in Figure 6.31. Although the test result reported by Davidson (1996), denoted as BD1, is presented in Figure 6.31, it is not suitable for use as a wall strength comparison. This is because the reinforcing steel used in Davidson's wall construction was inconsistent with the reinforcing steel used in the current study. Davidson employed f_y = 275 MPa reinforcing steel in his wall construction, therefore resulting in a lower wall strength than if f_y = 300 MPa reinforcing steel was used. Figure 6.31 is valuable to show the significantly similar nature of the force-displacement response of the three 4200 mm long perforated masonry walls. This provides further credibility to the performance of partially grout-filled masonry construction. Similar to Figure 6.30, the force-displacement envelopes in Figure 6.31 illustrate an increase in wall pull strength from 82.5 kN for Wall B7 to 93.2 kN when the trimming reinforcement of Wall B8 was extended to the outermost vertical reinforcement in the left pier (see Figure 6.1), resulting in a strength increase of about 12% in the pull direction.

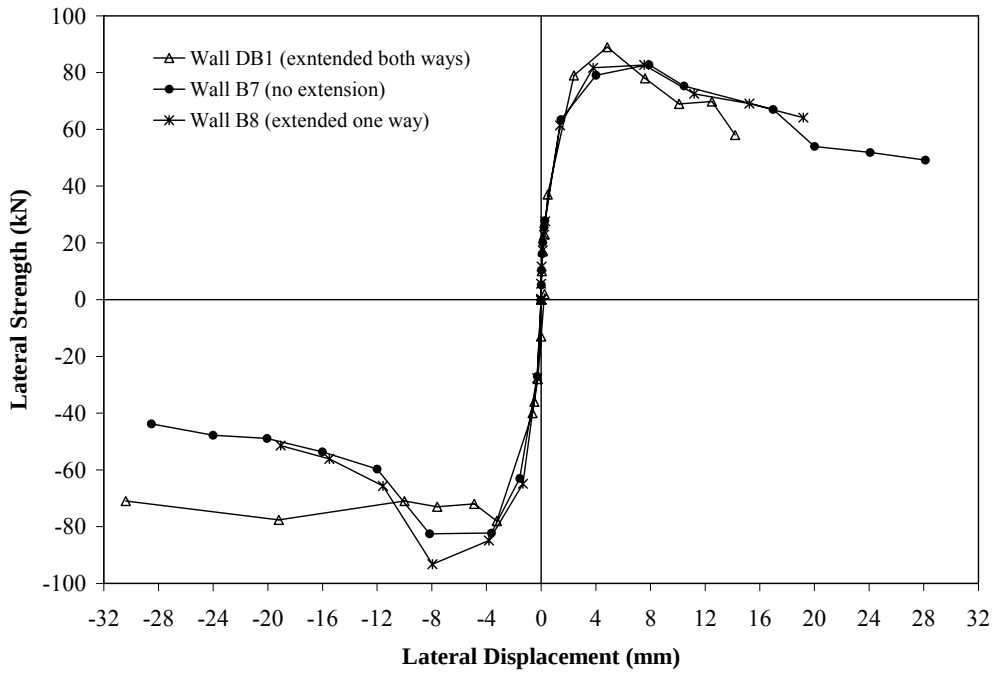

Figure 6.31 Effect of trimming reinforcement on the 4200 mm long perforated masonry walls.

6.7.3 Effect of Shrinkage Control Joint

Figure 6.32 shows the force-displacement envelopes of the two walls containing a shrinkage control joint at wall centre. It is clearly illustrated that the lateral strength of Wall B9, which had a control joint constructed in accordance with the specifications of NZS 4229:1999, exceeded the maximum strength recorded in Wall B10 by about 38%. This higher strength was due to the solid filled bond beam constructed on top of the control joint. Consequently, the (un-debonded) continuous bond beam caused a frame-type action between the two piers, therefore allowing partial shear transfer. This notion was supported by the absence of significant structural damage in the bond beam. In addition, double bending of the solid filled bond beam (above the control joint) allowed it to generate some strength and subsequently led to the yielding of D12 reinforcing bar adjacent to the compression edge (as shown by the $F_{n,st1}$ model presented in Figure 6.9i). Furthermore, closing of the control joint at the wall mid-height position at latter stage of testing permitted additional shear transfer between the two piers. It is also shown in Table 6.2 that the control joint detailed according to the NZS 4229:1999 procedure resulted in a F_{max}/F_{code} ratio of 2.52 for Wall B9, while a F_{max}/F_{code} ratio of 1.79 was measured for Wall B10 that had a control joint extended up the full height of the wall. Consequently, it is concluded that there is additional conservatism in the standard when the control joint is constructed according to the specifications of NZS 4229:1999.

Apart from the difference in strength shown in Figure 6.32, both Walls B9 and B10 shared similar force-displacement responses, with gradual strength and stiffness degradation. Consequently, the results attained from this study successfully demonstrated that the NZS 4229:1999 procedure for accounting for shrinkage control joints has resulted in adequate structural performance.

6.7.4 Wall Strength Prediction

The test results of Walls B1-B5 presented in Table 6.3 clearly demonstrate that the size of openings and the arrangement of trimming reinforcement significantly affect the lateral strength of perforated masonry walls. For the small window opening in Wall B1, the measured strength was slightly less than that prescribed by NZS 4229:1999, resulting in F_{max}/F_{code} = 0.97. However, it was successfully illustrated in section 6.6 that the conservatism of NZS 4229:1999 increases with the depth of opening, and for a full depth opening (e.g. a door in Wall B3) the NZS 4229:1999 prediction had significant conservatism. As shown in Figure

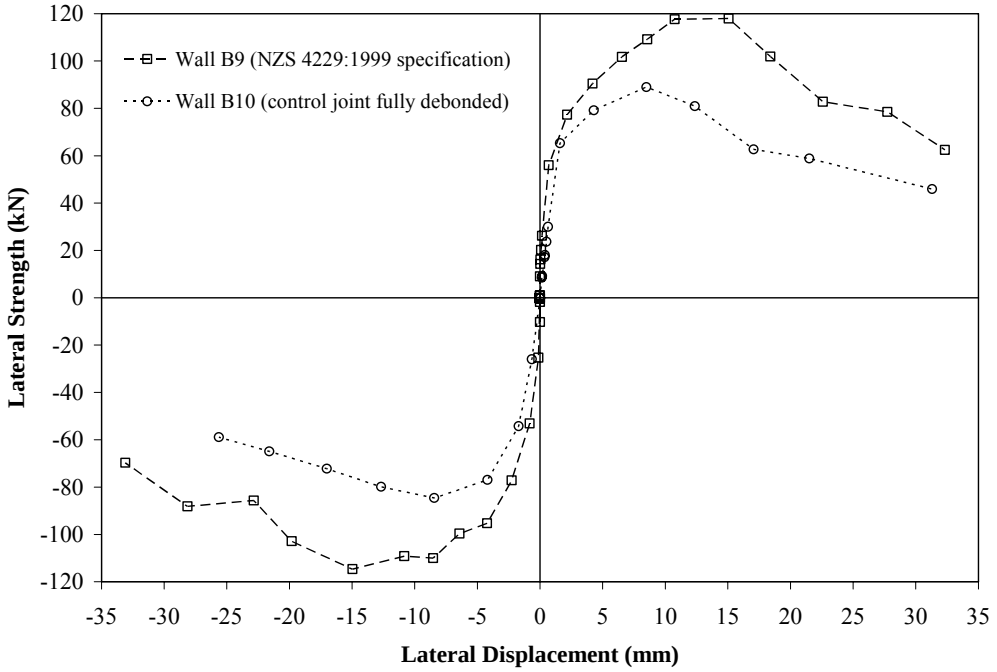

Figure 6.32 Effect of shrinkage control joint on partially grout-filled masonry walls.

6.33, it is illustrated that a 50% increase in the number of piers for the 4200 mm long walls resulted in approximately 100% increase in lateral strength when compared to the strengths recorded for the 2600 mm long walls. It is therefore established that double bending of the central pier significantly increased the lateral strength of perforated walls. Consequently, failure of NZS 4229:1999 to account for the extra strength generated by double bending of the central pier resulted in significant under-prediction of strengths recorded in Walls B6-B8. As shown in Table 6.3, ratios of $0.97 \leq F_{max}/F_{code} \leq 1.40$ and $1.68 \leq F_{max}/F_{code} \leq 1.89$ were observed for the 2600 mm and 4200 mm long perforated walls included in this study. This observation subsequently lead to the preliminary conclusion that NZS 4229:1999 is only non-conservative for walls containing single opening with a depth of less than 1200 mm, but significant conservatism of the standard would result for walls that have more than one opening where the inner piers can undergo double bending.

Comparisons of $F_{max}/F_{n,st0}$, $F_{max}/F_{n,st1}$, $F_{max}/F_{n,fr0}$ and $F_{max}/F_{n,fr1}$ are presented in Table 6.3 and Figure 6.34. It is shown that the simplified strut-and-tie method was reasonably accurate in predicting the lateral strength of the 2600 mm long perforated masonry walls, with $F_{max}/F_{n,st0}$ varying from 1.12 to 1.28 (excluding the experimental result obtained in the pull direction for Wall B5). However, the effectiveness of this method was significantly reduced when

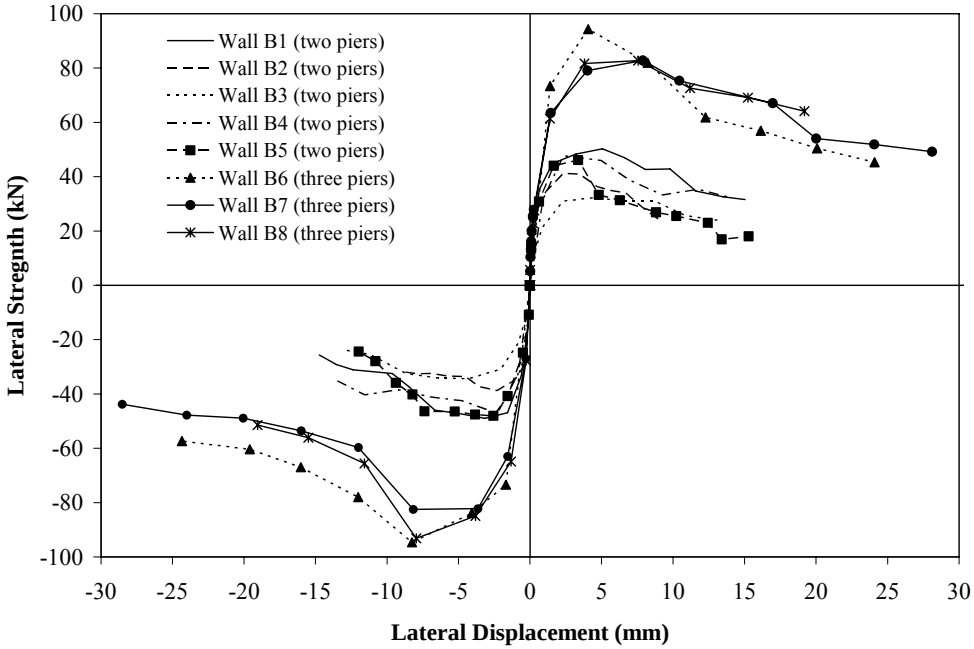

Figure 6.33 Effect of double bending of central pier on wall strength.

predicting the strengths of the 4200 mm long masonry walls included in this study. This was shown by the consistent under-prediction of strengths for Walls B6-B8 by about 60% when the simplified strut-and-tie method was used. Similar to NZS 4229:1999, this under-prediction of wall strength by $F_{n,st0}$ was due to the fact that double bending of the central pier was not accounted for in the simplified strut-and-tie models. When using the improved strut-and-tie method, it is illustrated in Figure 6.34c that significantly improved strength predictions were attained when double bending of the central pier and when wall self-weight were considered in models presented in Figures 6.9 and 6.10, resulted in average $F_{max}/F_{n,st1}$ values of about 1.10 for the 2600 mm long walls (excluding Wall B5 pull direction) and 1.24 for the 4200 mm long masonry walls. The diagonal cracking patterns (see section 6.6) on the perforated walls were observed to align well with the load paths by which shear force was assumed to be transferred to the foundation in the strut mechanism. This observation supports use of the strut-and-tie method as the tool to evaluate the strength of nominally reinforced masonry walls with openings.

The full plastic collapse analysis, as shown by the $F_{max}/F_{n,fr0}$ ratios presented in Figure 6.34d, was shown to significantly over-predict the lateral strengths of all perforated walls included in this study, with $0.48 \leq F_{max}/F_{n,fr0} \leq 0.63$ and $0.73 \leq F_{max}/F_{n,fr0} \leq 0.78$ for the 2600 mm and 4200 mm long walls respectively. It is therefore successfully illustrated that a full plastic mechanism would not develop in the nominally reinforced perforated masonry walls. Consequently, test

results from this study indicated that lateral strength prediction of perforated walls using the full plastic collapse analysis can lead to unsafe design for masonry walls constructed according to specifications of NZS 4229:1999. Finally, the $F_{max}/F_{n,fr1}$ values presented in Table 6.3 and Figure 6.34e show that strength predictions using the modified plastic collapse analysis have resulted in accuracy that closely matches predictions using the improved strut-and-tie models. It is successfully illustrated that significantly improved strength predictions were attained when single bending of the outer piers was considered in the models presented in Figures 6.13 and 6.14, resulted in $1.12 \leq F_{max}/F_{n,fr1} \leq 1.40$ and $1.09 \leq F_{max}/F_{n,fr1} \leq 1.25$ for the respective 2600 mm and 4200 mm long masonry walls.

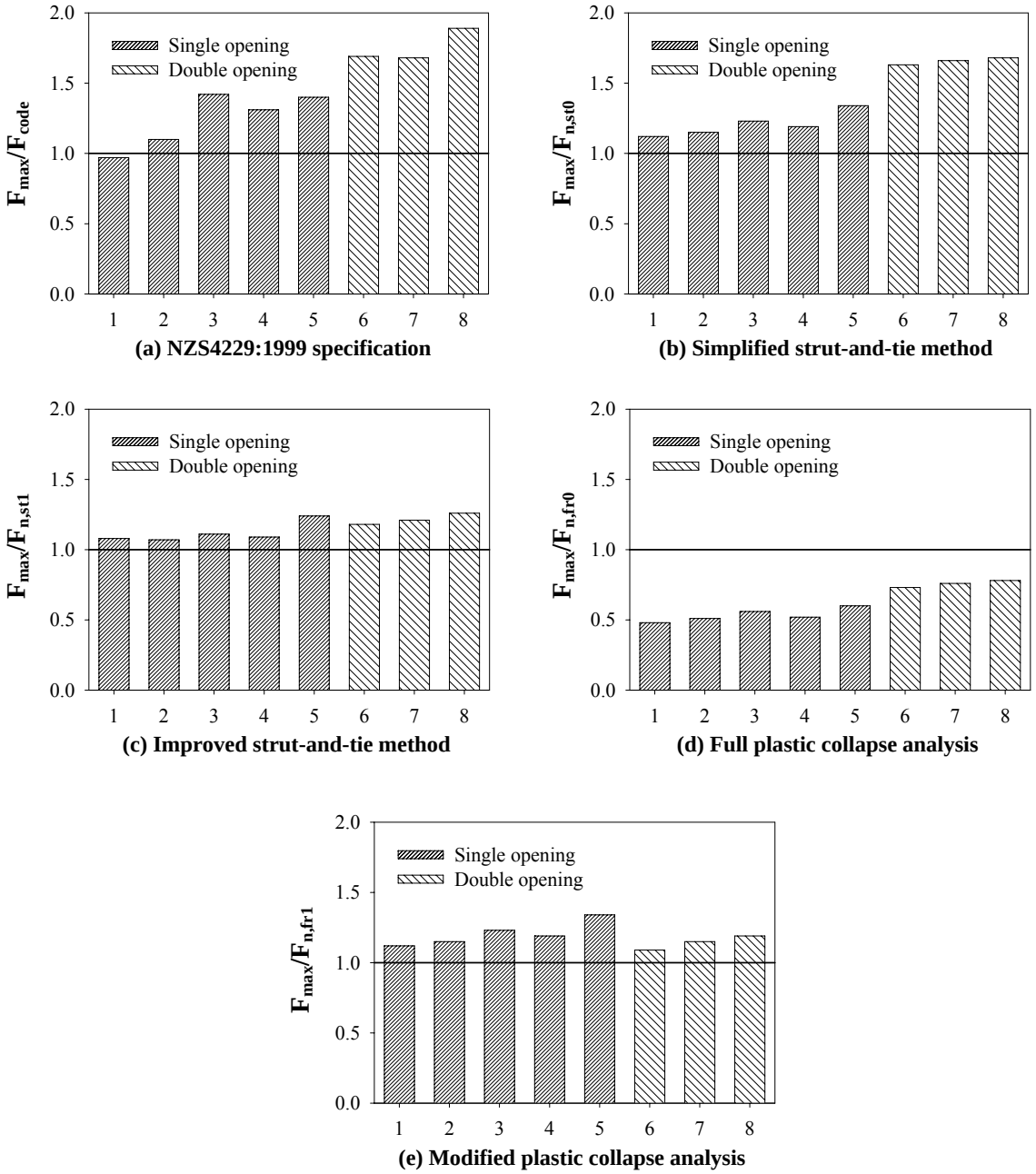

(a) NZS4229:1999 specification

(b) Simplified strut-and-tie method

(c) Improved strut-and-tie method

(d) Full plastic collapse analysis

(e) Modified plastic collapse analysis

Figure 6.34 Accuracy of strength predictions for Walls B1-B8.

Table 6.3 Summary of test results and wall strength predictions

Wall	Specimen	Prediction					Test Result					
		$F_{n,st0}$	$F_{n,st1}$	$F_{n,fr0}$	$F_{n,fr1}$	F_{code}	F_{max}	$\frac{F_{max}}{F_{n,st0}}$	$\frac{F_{max}}{F_{n,st1}}$	$\frac{F_{max}}{F_{n,fr0}}$	$\frac{F_{max}}{F_{n,fr1}}$	$\frac{F_{max}}{F_{code}}$
Current research	B1	44.7	46.4	103.6	44.7	51.8	+50.2 -49.0	1.12	1.08	0.48	1.12	0.97
	B2	35.9	38.4	80.6	35.9	37.3	+41.2 -38.7	1.15	1.07	0.51	1.15	1.10
	B3	28.0	30.8	61.4	27.9	24.3	+33.3 -34.4	1.23	1.11	0.56	1.23	1.42
	B4	41.0	44.7	94.4	40.9	37.3	+47.4 -48.8	1.19	1.09	0.52	1.19	1.31
	B5	+41.0 -35.9	44.7 -38.4	94.4 -80.6	40.9 -35.9	37.3	+52.4 -50.4	1.28* 1.40**	1.17* 1.31**	0.56* 0.63**	1.28* 1.40**	1.40
	B6	58.0	78.3	129.2	87.0	55.9	+94.3 -94.6	1.63	1.21	0.73	1.09	1.69
	B7	50.0	62.1 -73.0	108.0 -110.5	66.5 -79.2	49.4	+82.8 -82.5	1.66	1.33* 1.13**	0.77* 0.75**	1.25* 1.04**	1.68
	B8	50.0 -55.0	62.1 -76.3	108.0 -119.9	66.5 -81.7	49.4	+82.7 -93.2	1.66* 1.69**	1.33* 1.22**	0.77* 0.78**	1.24* 1.14**	1.89
	B9	80.2	110.9	---	---	49.8	+125.3 -114.6	1.56	1.13	---	---	2.52
	B10	80.2	82.1	---	---	49.8	+89.0 -84.6	1.11	1.08	---	---	1.79
Previous	BD1	---	75.0	---	---	46.0	76.5	---	1.02	---	---	1.66
	BD2	---	213.1	---	---	85.6	179.9	---	0.84	---	---	2.10
	DB1	49.5	75.5	111.8	74.9	50.1	89.0	1.80	1.18	0.80	1.19	1.78
	Units	kN	kN	kN	kN	kN	kN	---	---	---	---	----

Note:

1. * indicates push direction.
2. ** indicates pull direction.
3. BD1 is the 2600 x 2400 x 140 concrete masonry wall tested by Brammer (1995), see Figure 2.18a.
4. BD2 is the 4200 x 2400 x 140 concrete masonry wall tested by Brammer (1995), see Figure 2.18b.
5. DB1 is the 4200 x 2400 x 190 perforated concrete masonry wall tested by Davidson (1996), see Figure 2.19.

Based on the values for $F_{max}/F_{n,st0}$, $F_{max}/F_{n,st1}$, $F_{max}/F_{n,fr0}$ and $F_{max}/F_{n,fr1}$ presented in Tables 6.3 and Figure 6.34, it is shown that the simplified strut-and-tie method ($F_{n,st0}$) is only accurate in predicting the lateral strength of perforated walls that have a single opening and the conservatism of $F_{n,st0}$ is significantly increased when two openings are present in a masonry wall. Consequently, test results show the $F_{n,st0}$ method can lead to a non-economic cost design for masonry walls that contain more than one opening, which could subsequently lead to the reduced popularity of masonry as a constructional material. Conversely, the full plastic collapse analysis ($F_{n,fr0}$) was shown to consistently over-predict the strength of all perforated walls included in this study and therefore indicating that this analysis method could lead to unsafe design for partially grout-filled masonry walls constructed according to NZS 4229:1999 specifications.

Of the strength prediction methods discussed in section 6.4.1, the improved strut-and-tie method ($F_{n,st1}$) and modified plastic collapse analysis ($F_{n,fr1}$) were shown to predict the lateral strength of the perforated walls with significantly improved accuracy. This is shown by the average $F_{max}/F_{n,st1}$ ratio of 1.16 and $F_{max}/F_{n,fr1}$ ratio of 1.18 for the eight perforated walls included in this study. Hence, it is strongly recommended that the strength prediction of partially grout-filled perforated masonry walls with reinforcement details similar to those shown in Figure 6.1 be conducted according to the improved strut-and-tie model ($F_{n,st1}$) or the modified plastic collapse analysis ($F_{n,fr1}$). Although the $F_{n,st1}$ method is shown to produce strength prediction accuracy that is slightly better than the $F_{n,fr1}$ method, the $F_{n,st1}$ method would normally require computer software, such as SAP2000 (Computer and Structures, Inc., 2005), in order to quickly produce an accurate answer. Conversely, the modified plastic collapse analysis is significantly easier to perform and can be carried out without the use of complicated computer software. The $F_{n,fr1}$ method can be performed once the capacity of individual member is calculated. Consequently, the modified plastic collapse analysis can be used as an alternative to the strut-and-tie method when analysing the lateral strength capacities of partially grout-filled perforated concrete masonry walls that were constructed according to NZS 4229:1999 specifications.

Chapter 7

POSSIBLE AMENDMENT TO NZS 4229:1999

7.1 INTRODUCTION

Due to the lack of distributed horizontal shear reinforcement, all perforated walls included in this experimental study were observed to fail in a diagonal tension mode. As reported in Chapter 6, the diagonal cracking patterns identified on the walls were observed to align well with the load paths by which shear force is transferred to the foundation in the strut mechanism. Furthermore, vertical compressive cracks similar to vertical struts shown in strut-and-tie models were also identified beneath the trimming reinforcement in Walls B4, B5 and B8. These observations further support the use of strut-and-tie analysis as the tool to evaluate the strength of walls with reinforcement details similar to those specified by NZS 4229:1999. Consequently, crack patterns observed from the wall tests suggested that NZS 4229:1999 incorrectly defines the bracing geometries for walls constructed according to its specification and it might be non-conservative for NZS 4229:1999 to assume that the base of the cantilevered piers on either side of an opening corresponds to the level of the penetration sill, i.e. it is non-conservative for NZS 4229:1999 to define bracing capacity geometry based upon the vertical dimension of the smallest adjacent penetration.

Ingham et al. (2001) reported that NZS 4229:1999 significantly underestimates the capacity of full-height bracing panels. The total bracing capacity of most bracing lines is primarily derived from the capacity of a limited number of large bracing panels. Consequently, any code overestimation of the capacity of small bracing panels, such as that tested in Wall B1, will be readily compensated for. The code-predicted values for the capacity of the complete bracing line can therefore be expected to have considerable conservatism. Nevertheless, failure of NZS 4229:1999 to correctly identify the bracing geometries is of some concern and the matter clearly warrants attention to determine if an amendment to the standard is required.

There are several possible amendments that could be introduced to the standard. These amendments include use of the strut-and-tie method to correctly identify the bracing geometry or adopting bracing panel dimensions based upon the geometry of the largest adjacent wall

openings. Recalling that NZS 4229:1999 is primarily targeted for use by architects and draftspersons, rather than structural engineers, the adoption of strut-and-tie models to identify bracing geometry would increase the complexity of the standard, therefore restricting the effective use of NZS 4229:1999 by non-engineering professions. Also, the adoption of the second mentioned amendment would significantly increase the conservatism of NZS 4229:1999 and result in reduced efficiency of the standard, which would ultimately lead to the perception that reinforced concrete masonry is an expensive form of construction when compared with competing products and systems. Consequently, it is considered that these two amendments may not well suit the primary purpose of NZS 4229:1999. Other possible amendments to the standard, if required, are presented in the following sections.

7.2 EXTENDED TRIMMING REINFORCEMENT

Possible solution is to prescribe an extended trimming reinforcement detail as shown in Figure 7.1a. This amendment has the advantage of requiring minimum education, and therefore could be easily adopted by users of this standard. In addition, as shown by the simplified strut-and-tie model in Figure 7.1b, this amendment would result in bracing geometries that are identical to those currently prescribed by NZS 4229:1999, therefore resulting in the same level of conservatism as the current standard.

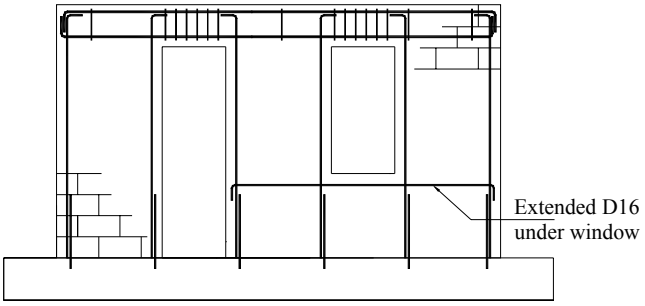

(a) Wall reinforcement detail

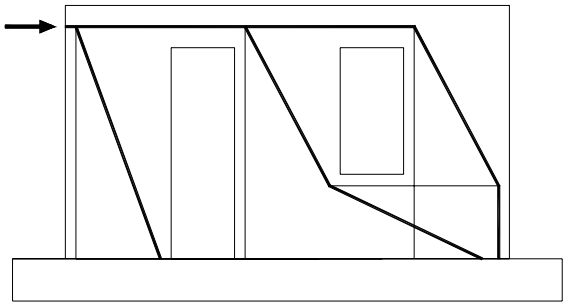

(b) Simplified strut-and-tie model

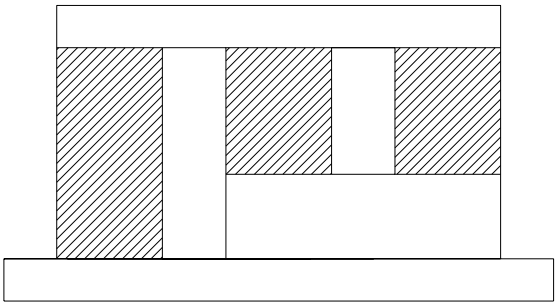

(c) Resulting bracing panels of Figure (b)

Figure 7.1 Proposed amendment to trimming reinforcement.

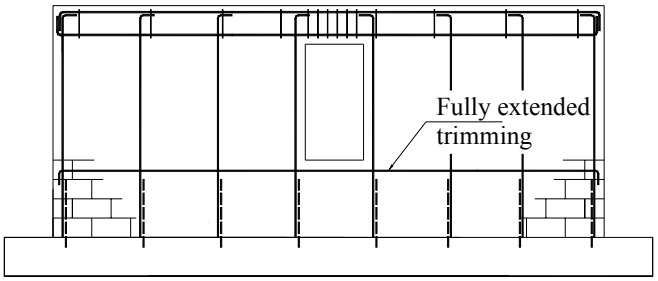

(a) Full extension to trimming reinforcement

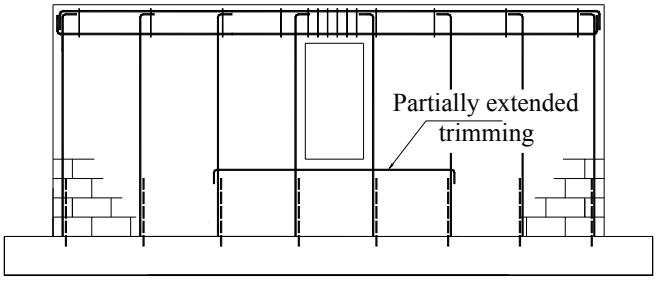

(b) Partial extension to trimming reinforcement

Figure 7.2 Extension to trimming reinforcement.

However, the detailing of trimming reinforcement such as that shown in Figure 7.1a may only be feasible for partially grout-filled masonry walls that have closely spaced penetrations. For a partially filled masonry wall that has a geometry similar to that shown in Figure 7.2, an issue regarding the length of extension to the trimming reinforcement may arise. In order to achieve bracing geometries specified by the standard, the trimming reinforcement, as illustrated in Figure 7.2a, needs to be extended to cover the whole length of the wall. For a partial extension of trimming reinforcement such as that shown in Figure 7.2b, it is unlikely to produce bracing geometries that are significantly different from the bracing geometries of a wall that is reinforced with NZS 4229:1999 specified trimming reinforcement (i.e. no trimming extension). In addition, it is noted that by extending trimming reinforcement such as shown in Figure 7.2, it may make such walls more difficult and more expensive to construct. This is because the construction of such walls may require at least two phases in order to ascertain that full grouting is achieved in masonry core containing the trimming reinforcement. Such a construction procedure may increase the cost of construction and this may potentially reduce the popularity of masonry construction.

7.3 AMENDMENT TO NZS 4229:1999 BRACING CAPACITY

This section examines the degree of non-conservatism of the NZS 4229:1999 prescribed bracing capacity. As discussed in section 6.7.4, it was found that NZS 4229:1999 is only non-

conservative for walls containing a single opening with a depth of less than 1200 mm, with the conservatism significantly increasing when the masonry walls contain more than one opening. Consequently, this section only examines the adequacy of NZS 4229:1999 in prescribing the bracing capacities for masonry walls containing a single opening. This investigation is accomplished by comparing predictions derived using the NZS 4229:1999 prescribed bracing capacities with those predicted using the modified plastic collapse analysis ($F_{n,fr1}$). The $F_{n,fr1}$ method is selected instead of the improved strut-and-tie analysis because the $F_{n,fr1}$ method is significantly easier to perform and it was successfully shown that wall strength predictions using the $F_{n,fr1}$ method closely matched the test results of the perforated masonry walls tested in this study.

As shown in Figure 7.3, the masonry walls included in this investigation had a single opening of varying depth and piers of varying length. In all cases, the walls were considered to be 140 mm thick and of partially grout-filled construction. The D12 longitudinal reinforcement was of f_y = 300 MPa and spaced at a maximum spacing of 800 mm centres, with f'_m = 12.0 MPa being assumed. NZS 4229:1999 recommended that vertical control joints should be placed at not more than 6.0 m centres. Consequently, only perforated masonry walls with length less than or equal to 6.0 m are included in the following investigation. The wall strengths predicted according to the two mentioned methods are summarised in Tables 7.1-7.3. This information is then used to produce normalised plots ($F_{n,fr1}/F_{code}$) in Figure 7.4 to investigate the adequacy of the NZS 4229:1999 prescribed bracing capacities. Consequently, any spread of points below the line of unity demonstrates the tendency to over-predict the wall bracing capacities by NZS 4229:1999. Included in the same tables are the NZS 4229:1999 prescribed bracing capacities for the corresponding walls when they have no opening. These values are identified as $F_{code,no\text{-}op}$ in the tables.

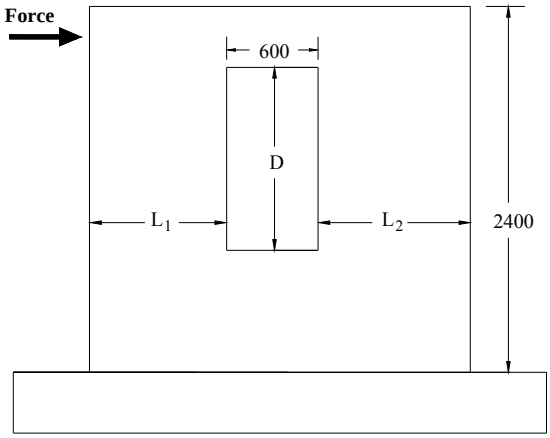

Figure 7.3 Masonry wall with varying pier lengths and opening depth.

From the predicted strengths presented in Tables 7.1-7.3 and Figure 7.4, it is found that the bracing capacities prescribed by the current standard is non-conservative when L_1 is less than 1200 mm long and when the opening is not more than 1000 mm high. As shown by the $F_{n,fr1}/F_{code}$ ratios presented in Tables 7.1-7.3, the conservatism of NZS 4229:1999 increases when the depth of opening and the length of L_1 increase. In addition, it is shown that the standard would remain conservative when L_1 is at least 1200 mm regardless of the size of opening. Consequently, it is deduced from this study that the standard is only non-conservative when the height of a single opening is less than 1200 mm and when one of the adjacent piers is less than 1200 mm in length.

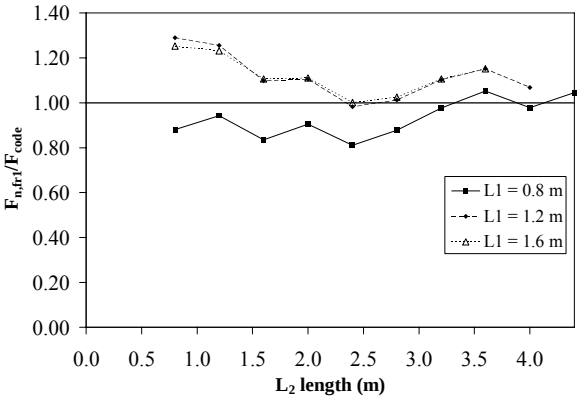

(a) $F_{n,fr1}/F_{code}$, D = 0.8 m

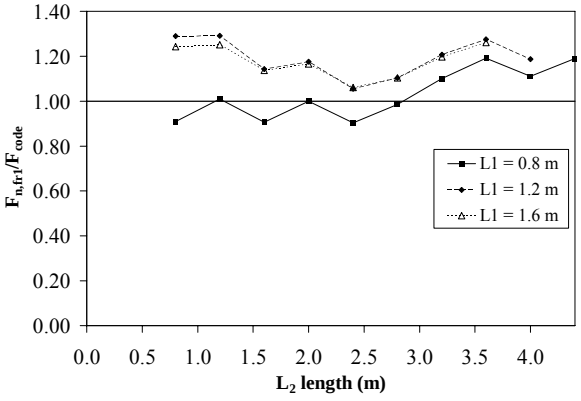

(b) $F_{n,fr1}/F_{code}$, D = 1.0 m

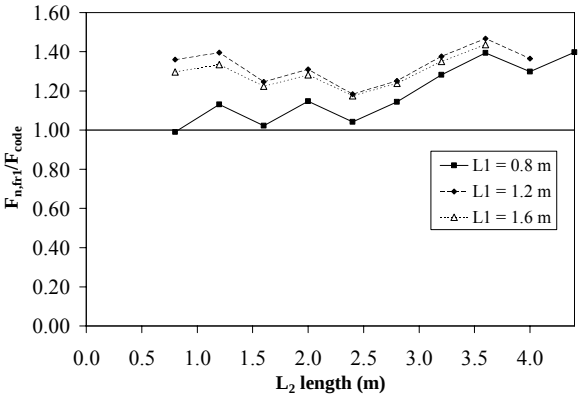

(c) $F_{n,fr1}/F_{code}$, D = 1.2 m

Figure 7.4 Comparison of $F_{n,fr1}$ with F_{code}.

As shown in Tables 7.1-7.3, for a significant number of the walls included in this part of study, the summation of capacity of small bracing panels (F_{code}) is more than the bracing capacity currently prescribed by the standard for the corresponding solid built walls ($F_{code,no\text{-}op}$). Consequently, one possible solution to the current problem is to limit the bracing capacity of any masonry wall containing a single opening of less than 1200 mm deep, to be no more than the capacity currently prescribed by NZS 4229 for the corresponding solid built masonry wall,

i.e. $F_{code} \leq F_{code,no\text{-}op}$. This proposed procedure has the advantage of requiring minimum education without further reducing the bracing capacity values currently prescribed by the standard. A comparison of the $F_{n,fr1}$ predicted wall strength with the standard predicted bracing capacity using the newly proposed procedure is presented in Tables 7.1-7.3 as $F_{n,fr1}/F_{code,amd}$ and diagrammatically illustrated in Figure 7.5. It is shown that the new procedure significantly reduces the over-prediction of strength by NZS 4229:1999.

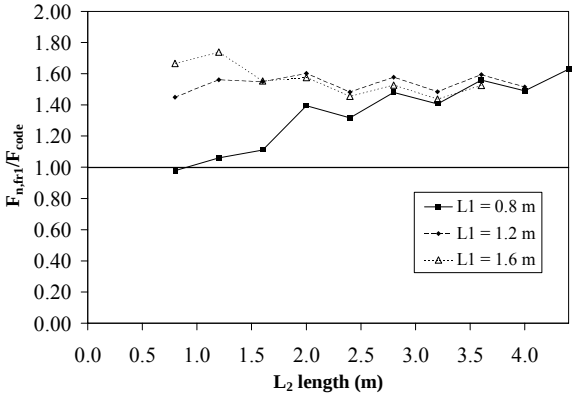

(a) $F_{n,fr1}/F_{code,amd}$, D = 0.8 m

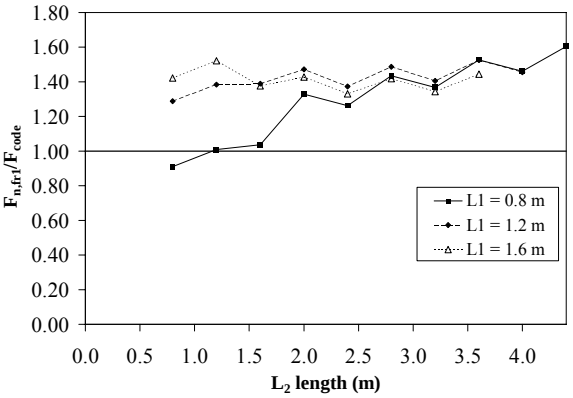

(b) $F_{n,fr1}/F_{code,amd}$ D = 1.0 m

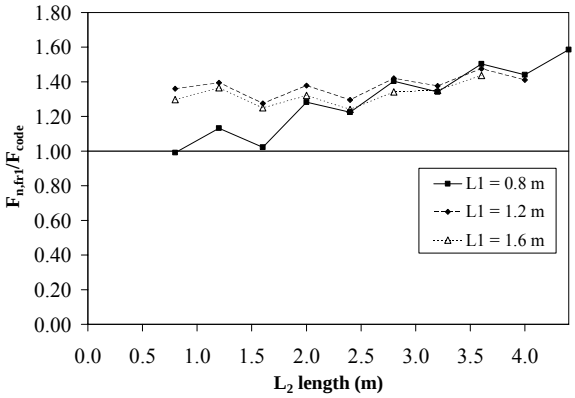

(c) $F_{n,fr1}/F_{code,amd}$ D = 1.2 m

Figure 7.5 Comparison of $F_{n,fr1}$ with $F_{code,amd}$.

7.4 NO AMENDMENT TO NZS 4229:1999

Within a bracing line, a structural wall is divided into bracing panels of various heights and lengths as dictated by wall openings, control joints and wall ends. As shown in Figure 7.6, the total bracing capacity of most bracing lines is primarily derived form the capacity of a limited number of large bracing panels. As previously reported, NZS 4229:1999 significantly underestimates the capacity of full height bracing panels. Consequently, any code overestimation of capacity of small bracing panels, such as that shown in Figure 7.3 will be readily compensated for.

Table 7.1 Strength predictions for walls with 800 mm high single opening

L_1 (m)	L_2 (m)	$F_{n,fr1}$ (kN)	F_{code} (kN)	$F_{code,no-op}$ (kN)	$F_{n,fr1}/F_{code}$	$F_{n,fr1}/F_{code,amd}$
0.8	0.8	33.9	38.5	34.6	0.88	0.98
	1.2	48.8	51.8	46.0	0.94	1.06
	1.6	58.0	69.5	52.3	0.83	1.11
	2	81.8	90.5	58.6	0.90	1.40
	2.4	94.1	116.0	71.5	0.81	1.32
	2.8	126.8	144.5	85.6	0.88	1.48
	3.2	142.2	145.5	101.1	0.98	1.41
	3.6	183.8	174.8	117.9	1.05	1.56
	4	202.4	207.0	135.9	0.98	1.49
	4.4	252.8	242.0	155.3	1.04	1.63
1.2	0.8	66.7	51.8	46.0	1.29	1.45
	1.2	81.6	65.0	52.3	1.26	1.56
	1.6	90.8	82.8	58.6	1.10	1.55
	2.0	114.6	103.8	71.5	1.10	1.60
	2.4	126.9	129.3	85.6	0.98	1.48
	2.8	159.6	157.8	101.1	1.01	1.58
	3.2	175.0	158.8	117.9	1.10	1.48
	3.6	216.6	188.0	135.9	1.15	1.59
	4.0	235.2	220.3	155.3	1.07	1.51
1.6	0.8	87.0	69.5	52.3	1.25	1.66
	1.2	101.9	82.8	58.6	1.23	1.74
	1.6	111.1	100.5	71.5	1.11	1.55
	2.0	134.9	121.5	85.6	1.11	1.58
	2.4	147.2	147.0	101.1	1.00	1.46
	2.8	179.9	175.5	117.9	1.03	1.53
	3.2	195.3	176.5	135.9	1.11	1.44
	3.6	236.9	205.8	155.3	1.15	1.53

Table 7.2 Strength predictions for walls with 1000 mm high single opening

L_1 (m)	L_2 (m)	$F_{n,fr1}$ (kN)	F_{code} (kN)	$F_{code,no-op}$ (kN)	$F_{n,fr1}/F_{code}$	$F_{n,fr1}/F_{code,amd}$
0.8	0.8	30.0	33.0	34.6	0.91	0.91
	1.2	44.9	44.5	46.0	1.01	1.01
	1.6	54.1	59.8	52.3	0.91	1.04
	2	77.9	78.0	58.6	1.00	1.33
	2.4	90.2	100.0	71.5	0.90	1.26
	2.8	122.9	124.8	85.6	0.99	1.44
	3.2	138.3	125.8	101.1	1.10	1.37
	3.6	179.9	151.0	117.9	1.19	1.53
	4	198.5	178.8	135.9	1.11	1.46
	4.4	249.0	209.3	155.3	1.19	1.60
1.2	0.8	57.3	44.5	46.0	1.29	1.29
	1.2	72.3	56.0	52.3	1.29	1.38
	1.6	81.5	71.3	58.6	1.14	1.39
	2.0	105.3	89.5	71.5	1.18	1.47
	2.4	117.6	111.5	85.6	1.05	1.37
	2.8	150.3	136.3	101.1	1.10	1.49
	3.2	165.7	137.3	117.9	1.21	1.41
	3.6	207.2	162.5	135.9	1.28	1.52
	4.0	225.8	190.3	155.3	1.19	1.45
1.6	0.8	74.3	59.8	52.3	1.24	1.42
	1.2	89.2	71.3	58.6	1.25	1.52
	1.6	98.4	86.5	71.5	1.14	1.38
	2.0	122.2	104.8	85.6	1.17	1.43
	2.4	134.5	126.8	101.1	1.06	1.33
	2.8	167.2	151.5	117.9	1.10	1.42
	3.2	182.6	152.5	135.9	1.20	1.34
	3.6	224.1	177.8	155.3	1.26	1.44

Table 7.3 Strength predictions for walls with 1200 mm high single opening

L_1 (m)	L_2 (m)	$F_{n,fr1}$ (kN)	F_{code} (kN)	$F_{code,no-op}$ (kN)	$F_{n,fr1}/F_{code}$	$F_{n,fr1}/F_{code,amd}$
0.8	0.8	27.2	27.5	34.6	0.99	0.99
	1.2	42.1	37.3	46.0	1.13	1.13
	1.6	51.4	50.3	52.3	1.02	1.02
	2	75.1	65.5	58.6	1.15	1.28
	2.4	87.5	84.0	71.5	1.04	1.22
	2.8	120.1	105.0	85.6	1.14	1.40
	3.2	135.6	105.8	101.1	1.28	1.34
	3.6	177.1	127.0	117.9	1.39	1.50
	4	195.7	150.8	135.9	1.30	1.44
	4.4	246.2	176.3	155.3	1.40	1.59
1.2	0.8	50.7	37.3	46.0	1.36	1.36
	1.2	65.6	47.0	52.3	1.40	1.40
	1.6	74.8	60.0	58.6	1.25	1.28
	2.0	98.6	75.3	71.5	1.31	1.38
	2.4	110.9	93.8	85.6	1.18	1.30
	2.8	143.6	114.8	101.1	1.25	1.42
	3.2	159.0	115.5	117.9	1.38	1.38
	3.6	200.5	136.8	135.9	1.47	1.48
	4.0	219.2	160.5	155.3	1.37	1.41
1.6	0.8	65.2	50.3	52.3	1.30	1.30
	1.2	80.1	60.0	58.6	1.33	1.37
	1.6	89.3	73.0	71.5	1.22	1.25
	2.0	113.1	88.3	85.6	1.28	1.32
	2.4	125.4	106.8	101.1	1.17	1.24
	2.8	158.1	127.8	117.9	1.24	1.34
	3.2	173.5	128.5	135.9	1.35	1.35
	3.6	215.0	149.8	155.3	1.44	1.44

The following examples show that considerable conservatism is maintained in the code-predicated values for the capacity of the complete bracing line. A summary of predicted strengths are included in Tables 7.4-7.6. The predicted $F_{n,fr1}$ values for the two loading directions are also included. Again the bracing panels shown in Figure 7.6 are reinforced with D12 vertical reinforcement (f_y = 300 MPa) and spaced at no more than 800 mm apart, with f'_m = 12.0 MPa being assumed.

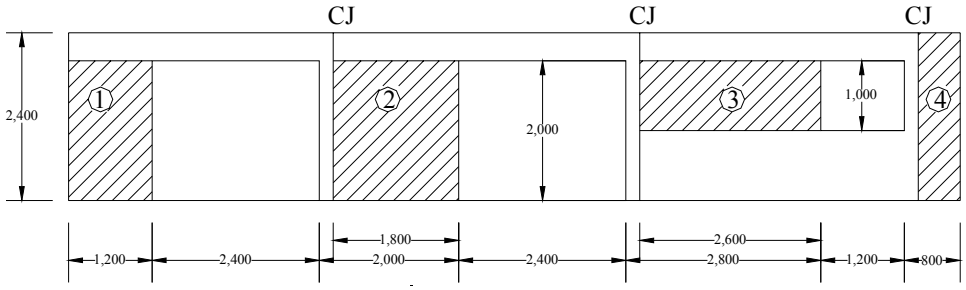

(a) Design example A

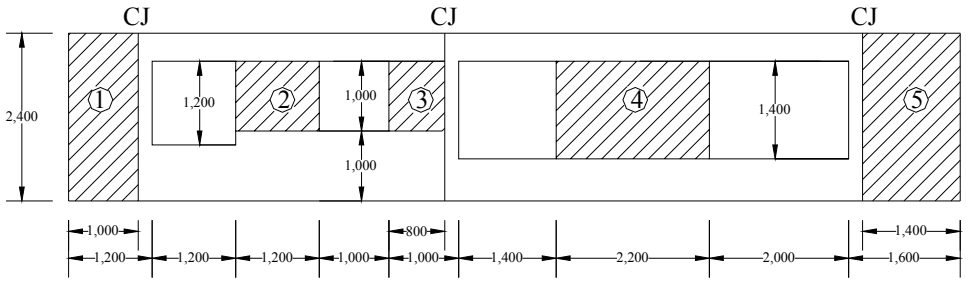

(b) Design example B

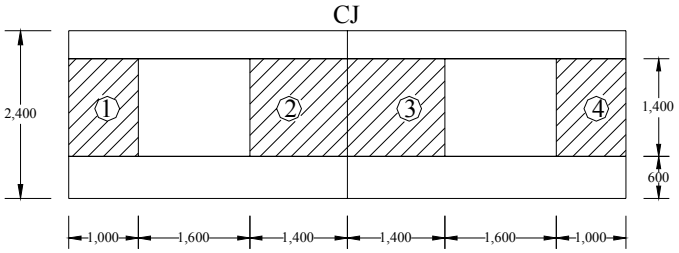

(c) Design example C

Figure 7.6 Bracing panel for design examples.

Table 7.4 Bracing capacity for design example A

Bracing Panel	F_{code} (kN)	$F_{n,fr1}$ (kN)	
		Push	Pull
1	15.3	25.5	25.5
2	29.0	39.4	39.4
3	83.5	129.8	70.8
4	7.8	9.7	9.7
Total	135.5	204.4	145.4

Table 7.5 Bracing capacity for design example B

Bracing Panel	F_{code} (kN)	$F_{n,fr1}$ (kN)	
		Push	Pull
1	10.4	12.6	12.6
2	28.0	46.8	40.1
3	16.5	10.6	19.4
4	54.8	88.8	88.8
5	16.8	27.6	27.6
Total	126.5	186.4	188.5

Table 7.6 Bracing capacity for design example C

Bracing Panel	F_{code} (kN)	$F_{n,fr1}$ (kN)	
		Push	Pull
1	16.6	18.8	13.7
2	26.8	30.1	41.4
3	26.8	41.4	30.1
4	16.6	13.7	18.8
Total	86.8	104.0	104.0

The three design examples successfully illustrated that code overestimation of capacity of small bracing panels, such as Panel 3 in Examples A and B is readily compensated for by the significant underestimation of the bracing capacity of the larger bracing panels. Based on the design examples presented above, it is proposed that an amendment to the NZS 4229:1999 specified bracing capacities may not be necessary.

Chapter 8

CONCLUSIONS

This chapter has three sections, with sections 8.1 and 8.2 reporting the conclusions pertaining to the cyclic load tests on the twenty single storey-height concrete masonry walls described in Chapters 3 and 6 respectively. Section 8.3 lists recommendations for future research on topics associated with the research studies presented in this thesis.

8.1 CONCRETE MASONRY SHEAR STRENGTH

The first part of the scope set out in Chapter 1 was to experimentally determine the in-plane shear strength of ten single storey-height concrete masonry wall panels. The main variables considered in this experimental programme included the amount and distribution of shear reinforcement, level of axial compression stress, type of grouting and wall aspect ratio. The experimental programme described in Chapter 3 supplemented the experimental data already available by specifically investigating the shear strength of walls subjected to low axial compression stresses and low shear reinforcement ratios. From the experimental results presented in Chapter 3, it was established that the shear resistance of reinforced masonry walls is the result of complex mechanisms, such as tension of horizontal shear reinforcement, dowel action of vertical reinforcement, as well as aggregate interlocking along diagonal cracks. However, due to the complexity of these mechanisms, no effective theoretical models have yet been proposed to predict the shear strength of a masonry wall panel. Hence, the nominal shear strength of a reinforced masonry walls is evaluated as a sum of contributions from masonry, shear reinforcement and applied axial compression load during practical calculation.

It was established that axial compression load had a significant influence on the in-plane shear performance of masonry shear walls, mainly because it suppressed the tensile field in a material inherently weak in tension. Consequently, as the axial compression load increased, so did the ability of the walls to provide shear resistance. However, the post-cracking deformation capacities were observed to reduce with increasing axial load. This was because of the increasing brittleness of this failure type as the axial compression stress increased.

It was observed that shear reinforcement not only provided additional shear resistance, but also improved the post-cracking performance of the masonry walls when shear reinforcement was uniformly distributed up the height of the walls. The provision of closely spaced shear reinforcement enabled the distribution of stresses throughout the wall diagonals after the initiation of shear cracking. Accordingly, the initial diagonal cracks did not widen significantly under increasing lateral displacements, but instead new sets of diagonal cracks formed and gradually spread over the wall diagonals, accompanied by higher energy dissipation and more ductile behaviour. The test results also demonstrated that partial grouting significantly reduced masonry shear strength. However, the effect of grouting became less significant when net shear stress was calculated accounting for the cross-sectional area of both the masonry units and grouted cells. In addition, the test results indicated that masonry shear strength decreased inversely in relation to the wall aspect ratio. Finally, the test results presented in section 3.6 clearly illustrated that NZS 4230:1990 was conservative in its treatment of masonry shear strength.

The suitability of the nine shear equations presented in Table 5.1 in predicting the maximum in-plane shear strength of masonry walls was discussed in section 5.3.2. It was successfully shown that NZS 4230:1990 was conservative in its treatment of masonry in-plane shear strength. This was illustrated by the constant under-prediction of shear strength for the 56 test specimens included in the strength prediction study discussed in section 5.3.2. Of the seven existing masonry shear expressions (excluding NZS 4230:2004) presented in Table 5.1, the NEHRP shear expression was found to be commendable, but it does not address masonry shear strength within plastic hinge regions, therefore limiting its use when designing masonry structures in seismic regions. Consequently, a new shear equation is proposed in Chapter 4. Particular emphasis is placed on a model that is capable of representing the interaction between flexural ductility and masonry shear strength in order to account for the reduction in masonry shear capacity as displacement ductility increases. The simple method proposed in this thesis enables the strength enhancement provided by axial compression load to be separated from the masonry component of shear strength, and is considered to result from strut action. In addition, conservative modifications are made to the proposed shear equation to facilitate adoption of the method in the updated version of the New Zealand masonry design standard, NZS 4230:2004.

A statistical comparison of the NZS 4230:2004 shear equation and the other seven masonry shear expressions presented in section 2.4.2 was provided in section 5.3.2 in terms of mean and

standard deviation for the experimental/predicted (v_{max}/v_n) shear strength ratios. It was successfully shown that the NZS 4230:2004 expression provides a significantly improved prediction of shear strength with respect to NZS 4230:1990. As shown in section 5.3.2, predictions using the NZS 4230:2004 shear expression produced a mean v_{max}/v_n of 1.34 and a standard deviation of 0.22. This standard deviation is about half of that resulted from the NZS 4230:1990 shear equation, and similar in value to those resulting from the Shing et al., Matsumura and NEHRP shear expressions. In addition, it was successfully shown that shear strength prediction using the NZS 4230:2004 expression resulted in a v_{max}/v_n ratio of at least 0.89. Consequently, the masonry shear strength reduction factor of $\phi = 0.75$ adopted by the recently revised NZS 4230:2004 would be sufficient to provide a safe lower bound. Furthermore, of the nine masonry shear equations investigated in section 5.3, it was shown that the 95 percentile v_{max}/v_n value of 0.98 resulted from the NZS 4230:2004 prediction is the closest to unity, therefore further confirming its appropriateness in accounting for masonry shear strength by providing substantially greater safety against shear failure.

8.2 BRACING CAPACITY OF PERFORATED MASONRY WALLS

The primary objective of the second part of the research presented in this thesis was to validate the adequacy of NZS 4229:1999 in addressing the bracing capacity of partially grout-filled perforated concrete masonry walls. The design of the ten nominally reinforced partially grout-filled concrete masonry walls described in section 6.2 was conceived to facilitate comparison of wall behaviour between two or more walls with respect to variation of a given design parameter. The following findings are drawn from the cyclic load tests conducted on the ten partially grout-filled masonry walls:

1. It was observed that the perforated partially grouted concrete masonry walls tested at the University of Auckland exhibited gradual strength and stiffness degradation, and in no case did any wall suffer from sudden failure. This desirable behaviour of the nominally reinforced partially grouted masonry walls with openings was attributed to the solid filled bond beam at the top of the walls, which caused frame-type action at latter stages of testing. This leads to considerable inelastic displacement capacity of the partially grouted masonry walls, where μ_{av} was measured to consistently be above 2.0. In addition, it was observed that maximum strength was typically developed during the first excursion to $\mu = 4.0$. Following this, cracking became significant in the masonry walls and strength degradation began.

2. The test results clearly demonstrated that the size of openings significantly affect the lateral strength of the tested walls. It was shown that the reduction of wall strength corresponded to the increased depth of an opening. This reduction of strength was because of the steepened diagonal strut when the depth of openings increase. This in turn leads to a reduction of the horizontal shear component that could be resisted by the masonry piers, which resulted in the overall reduction of lateral strength in the perforated masonry walls.
3. It was successfully demonstrated that extension of the trimming reinforcement below the window had the effect of increasing wall strength. It was also observed that the wall cracking pattern was altered when the trimming reinforcement was extended below the window opening. Diagonal cracks on walls without extended trimming reinforcement were observed to be steeper than those presented on walls with extended trimming reinforcement.
4. The diagonal cracking patterns on the perforated masonry walls were observed to align well with the load paths by which shear force was assumed to be transferred to the foundation in the strut mechanism. This observation supported use of the strut-and-tie method of analysis as the tool to evaluate the strength of nominally reinforced masonry walls with openings.
5. It was established that NZS 4229:1999 fails to correctly identify the geometry of bracing panels of perforated masonry walls. This resulted in the over-prediction of strength of walls containing a small opening. It was shown in the experimental study that the conservatism of NZS 4229:1999 would increase when the depth of opening is increased and when a wall contains more than one opening.
6. Strength prediction using the improved strut-and-tie ($F_{n,st1}$) method and the modified plastic collapse ($F_{n,fr1}$) analysis were found to closely match the experimental results of the perforated walls tested in this study. Strength prediction by the simplified strut-and-tie method was found to closely match the test results of masonry walls with a single opening, but significant underestimation of strength by this method was found for walls with double openings. The full plastic collapse analysis was found to significantly over-predict the strength of all perforated walls included in this study. Consequently, it is strongly recommended that the strength prediction of partially grout-filled perforated masonry walls with reinforcement details similar to those specified by NZS 4229:1999 be conducted according to the $F_{n,st1}$ method or the $F_{n,fr1}$ method. Although the $F_{n,st1}$ method was shown to produce strength prediction accuracy that is slightly better than the $F_{n,fr1}$ method, the $F_{n,st1}$ method would normally require computer software, such as

SAP2000, in order to quickly produce an accurate answer. Conversely, the $F_{n,fr1}$ method is significantly easier to perform and can be carried out without the use of computer software. Hence, the $F_{n,fr1}$ method is considered as an appropriate alternative to the $F_{n,st1}$ method when analyzing the lateral strength capacities of partially grout-filled perforated concrete masonry walls that were constructed according to NZS 4229:1999 specifications.

7. It was successfully demonstrated that the NZS 4229:1999 detail for the shrinkage control joint results in adequate structural performance. In addition, shrinkage control joints constructed in accordance with the NZS 4229:1999 prescription result in a masonry wall that has significantly higher wall strength than a masonry wall that has control joint which penetrates the full height of the wall. This higher strength was due to the solid filled bond beam constructed on top of the joint that subsequently led to a frame-type action between the two piers, therefore allowing partial shear transfer and enabling the wall to exhibit gradual strength and stiffness degradation. In addition, closing of the control joint at the wall mid-height position at latter stage of testing permitted additional shear transfer between the two piers.

8.3 FUTURE RESEARCH

In order to further the rationalisations that could be made to the shear strength provisions in the New Zealand masonry design standard, NZS 4230:2004, and the bracing capacity prescribed by NZS 4229:1999, the following areas of research could be undertaken:

1. The studies reported in Chapters 3 and 6 concentrated on walls with simple geometry. Consequently, further structural testing may be necessary to address the effect of complex geometries, such as Tee-sections and corners, and wall with penetrations for doors and windows. In addition, it is also recommended to perform test on multi-storey structures.
2. In Chapter 3, only reinforced concrete masonry walls were considered. In lieu of the development of prestressed masonry, it is deemed appropriate to investigate the shear strength capacity of unreinforced prestressed masonry walls.
3. The research presented in Chapter 3 focused on the in-plane strength of masonry walls. Consequently, a study of the suitability of the NZS 4230:2004 masonry shear expression to predict the out-of-plane shear strength is required.
4. Only re-usable concrete footings were used in the construction of the test specimens presented in this thesis (except Wall A9). This arrangement required the wall vertical reinforcing bars to be first tapped, then thread into the starters that protruded from the

footing. However, in reality the vertical reinforcement is usually cast into the concrete footing. Consequently, some of the test specimens should be re-tested on purpose-built reinforced concrete footing with cast-in starter bars in order to investigate the effect, if any, of threading on the lateral strength and post elastic performance of masonry walls.

5. The wall specimens reported in Chapters 3 and 6 were performed using a quasi-static cyclic load test procedure. However, in reality an earthquake would only last for a short duration. Consequently, dynamic shake table testing is recommended to be carried out to investigate the performance of masonry walls under such loading condition.
6. Of the twenty wall specimens reported in this thesis, only two had control joints incorporated and these walls did not have any openings. While the wall tests were successful, there remains further need to investigate the influence, if any, of openings on the structural performance of the NZS 4229:1999 specified control joint detail.

Chapter 9

REFERENCES

Anderson, D. L., and Priestley, M. J. N. (1992), "In Plane Shear Strength of Masonry Walls", Proceedings of the 6th Canadian Masonry Symposium, Saskatoon, Saskatchewan, pp. 223-234.

ACI 530/ASCE 5/TMS 402 (2002), "Building Code Requirements for Masonry Structures", Masonry Standard Joint Committee.

Applied Tech. Council. (1981), "Seismic Design Guidelines for Highway Bridges", ATC-6, Berkeley, California.

AS 3700—1998, "Masonry Structures", Standards Association of Australia, Homebush, NSW, Australia.

Beck, J. K., Curtin, W. G., and Shaw, G. (1988), "Design of Reinforced and Prestressed Masonry", Thomas Telford, London.

Brammer, D. R. (1995), "The Lateral Force-Deflection Behaviour of Nominally Reinforced Masonry Walls", ME Thesis, Department of Civil and Resource Engineering, University of Auckland, New Zealand.

Brunner, J. D., and Shing, P. B. (1996), "Shear Strength of Reinforced Masonry Walls", TMS Journal, Vol. 14, No. 1, pp. 65-77.

Cavalheiro, O. P., and Pedroso, G. M. (2000), "Experimental Data on Hollow Block Prisms Using Direct Shear Test", Proceedings of the 12th International Brick/Block Masonry Conference, Madrid, Spain, pp. 433-440.

Chen, Shi-Wen J., Hidalgo, P. A., Mayes, R. L., Clough, R. W., and McNiven, H. D. (1978), "Cyclic Loading Tests of Masonry Single Piers, Volume 2-Height to Width Ratio of 1",

Report No. UCB/EERC-78/28, Earthquake Engineering Research Centre, University of California, Berkeley, CA.

Computer and Structures, Inc. (2005), "SAP2000-Basic Analysis Reference Manual", Berkeley, California, USA.

Crisafulli, F. J., Carr, A. J., and Park, R. (1995), "Shear Strength of Unreinforced Masonry Panels", Proceedings of the Pacific Conference on Earthquake Engineering, Vol. 3, Melbourne, Australia, pp. 77-86.

Davidson, B. J. (1996), "In-Plane Cyclic Loading of Nominally Reinforced Masonry Walls with Openings", New Zealand Concrete Society Conference, Wairakei, New Zealand, pp. 120-129.

Elshafie, H., Hamid, A., and Nasr, E. (2002), "Strength and Stiffness of Masonry Shear Walls with Openings", The Masonry Society Journal, pp. 49-60.

Fattal, S.G., and Todd, D.R. (1991), "Ultimate Strength of Masonry Shear Walls: Prediction vs Test Results," NISTIR 4633, Building and Fire Research Laboratory, Gaithersburg, 40p.

Hansen, K. F., Nykanen, E., and Gottfredsen, F. R. (1998), "Shear Behaviour of Bed Joints at Different Levels of Precompression", Danish Building Research Institute-VTT Building Research, Vol. 12, No. 2, pp. 70-78.

Hart, G. C., Hong, W., and Englekirk, R. (1988), "Structural Component Model of Flexural Walls", Fourth Meeting of the U.S.-Japan Joint Technical Coordination Committee on Masonry Research, San Diego.

Hendry, A. W. (1991), "Reinforced and Prestressed Masonry", Longman Scientific & Technical, England.

Hidalgo, P. A., Mayes, R. L., McNiven, H. D., and Clough, R.W. (1978), "Cyclic Loading Tests of Masonry Single Piers", Volume 1, Report No. UCB/EERC-78/27, Earthquake Engineering Research Centre, University of California, Berkeley, CA.

Hidalgo, P. A., Mayes, R. L., McNiven, H. D., and Clough, R.W. (1979), "Cyclic Loading Tests of Masonry Single Piers", Volume 3, Report No. UCB/EERC-79/12, Earthquake Engineering Research Centre, University of California, Berkeley, CA.

Hiraishi, H. (1985), "Flexural Behaviour of Reinforced Masonry Walls", First Meeting of the U.S.-Japan Joint Technical Coordinating Committee on Masonry Research, Tokyo, Japan.

Hiraishi, H. (1984), "Evaluation of Shear and Flexural Deformation of Flexural Type Shear Walls", Bulletin NZSEE, Vol. 17, No. 2, pp. 135-144.

Ingham, J.M., Davidson, B.J., Brammer, D.R., and Voon, K.C. (2001), "Testing and Codification of Partially Grout-filled Nominally-reinforced Concrete Masonry Subjected to In-plane Cyclic Loads", The Masonry Society Journal, Vol. 19, No. 1, pp. 83-96.

Kaminosono, T., Teshigowara, M., Hiraishi, H., Fujisawa, M., and Nakaoka, A. (1988), "Experimental Study on Seismic Performance of Reinforced Masonry Walls", Proceedings of the 9th World Conference on Earthquake Engineering, Tokyo-Kyoto, Japan, pp. 109-114.

Larbi, A., and Harris, H. (1990), " Seismic Behaviour of Reinforced Block Masonry Shear Walls using 1/3 Scale Direct Models", Proceedings of the 5th North America Masonry Conference, University of Illinois, Urbana-Champaign, pp. 321-332.

Laursen, P. T., and Ingham, J. M. (2000a), "Cyclic In-Plane Structural Testing of Prestressed Concrete Masonry Walls. Phase 1: Simple Wall Configurations. Volume A: Evaluation of Wall Structural Performance", School of Engineering Report No. 599, University of Auckland.

Laursen, P. T., and Ingham, J. M. (2000b), "Cyclic In-Plane Structural Testing of Prestressed Concrete Masonry Walls. Phase 1: Simple Wall Configurations. Volume B: Data Resource", School of Engineering Report No. 600, University of Auckland.

Leiva, G., Merrymann, M., and Klingner, R. E. (1990a), " In-Plane Seismic Resistance of Two-Story Concrete Masonry Coupled Walls", Fifth North American Masonry Conference, University of Illinois, Urbana-Champagne, pp. 333-345.

Leiva, G., Merryman, M., and Klingner, R.E. (1990b), "Design Philosophies for Two-Storey Concrete Masonry Walls with Door and Window Openings", Fifth North American Masonry Conference, University of Illinois, Urbana-Champagne, pp. 287-295.

Leiva, G., and Klingner, R. E. (1994), "Behaviour and Design of Multistory Masonry Walls under In-Plane Seismic Loading", The Masonry Society Journal, Vol. 12, No. 1, pp. 12-24.

Liddell, D., Ingham, J. M., and Davidson, B. J. (2000), "Influence of Loading History on Ultimate Displacement of Concrete Structures", School of Engineering Report No. 597, University of Auckland.

Mann, W. and Muller, H. (1982), "Failure of Shear-Stressed Masonry-An Enlarged Theory, Tests and Application to Shear Walls", Proceedings of the British Ceramic Society, pp. 223-235.

Mason Standards Joint Committee (2002), "Building Code Requirements for Masonry Structures" and "Specification for Masonry Structures", ACI 530-02/ASCE 5-02/ TMS 402-02, USA.

Matsumura, A. (1985), "Effectiveness of Shear Reinforcement in Concrete Masonry Walls", First Joint Technical Coordinating Committee on Masonry Research-U.S.-Japan Coordinated Earthquake Research Programme, Tokyo, Japan.

Matsumura, A. (1987), "Shear Strength of Reinforced Hollow Unit Masonry Walls", Proceedings of the 4th North America Masonry Conference, Paper No. 50, Los Angeles, CA, pp. 50-1—50-16.

Matsumura, A. (1988), "Shear Strength of Reinforced Masonry Walls", Proceedings of the 9th World Conference on Earthquake Engineering, Vol. 7, Tokyo, Japan, pp. 121-126.

Matsumura, A. (1990), "Planar Shear Loading Test on Reinforced Fully Grouted Hollow Clay Masonry Walls", Proceedings of the 5th North America Masonry Conference, University of Illinois, Urbana-Champaign, pp. 347-356.

Mayes, R. L., Omote, Y., and Clough, R. W. (1976a), "Cyclic Shear Tests on Masonry Piers, Volume 1: Test Results", Report No. UCB/EERC-76/8, Earthquake Engineering Research Centre, University of California, Berkeley, CA.

Mayes, R. L., Omote, Y., and Clough, R. W. (1976b), "Cyclic Shear Tests of Masonry Piers, Volume 2, No. EERC 76-16, Earthquake Engineering Research Centre, University of California, Berkeley, CA.

Mörsch, E. (1912), "Der Eisenbeton, seine Theorie und Anwendung", Verlag Konrad Witter, Stuttgart.

NEHRP. (1997), "Recommended Provisions for Seismic Regulations for New Buildings and Other Structures, Part-1 Provisions", Building Seismic Safety Council, Washington, D.C., U.S.A.

NZS 4229:1999, "Concrete Masonry Buildings Not Requiring Specific Engineering Design", Standards Association of New Zealand. Wellington.

NZS 4230P:1985, "Code of Practice for Masonry Design", Standards Association of New Zealand, Wellington.

NZS 4230:1990, "Code of Practice for the Design of Masonry Structures", Standards Association of New Zealand, Wellington.

NZS 4230:Part2:1990, "Commentary on the Design of Masonry Structures", Standards Association of New Zealand, Wellington.

NZS 4230:2004, "Design of Reinforced Concrete Masonry Structures", Standards Association of New Zealand, Wellington.

Okamoto, S., Yamazaki, Y., Kaminosono, T., Teshigawara, M., and Hirashi, H. (1987), "Seismic Capacity of Reinforced Masonry Walls and Beams", Proceedings of the 18th Joint Meeting of the U.S.-Japan Cooperative Program in Natural Resource Panel on Wind and Seismic Effects, NBSIR 87-3540, National Institute of Standards and Technology, Gaithersburg, pp. 307-319.

Page, A. W. (1989), "A Parameter Study of The Behaviour of Masonry Shear Walls", Proceedings of the 5th Canadian Masonry Symposium, Vancouver, pp. 341-352.

Park, R. (1986), "Design of Building Structures of Limited Ductility", Bulletin NZSEE, Vol. 19, No. 4, pp. 285-338.

Park, R. (1989), "Evaluation of Ductility of Structures and Structural Assemblages for Laboratory Testing", Bulletin NZSEE, Vol. 22, No. 3, pp. 155-166.

Paulay, T. and Loeber, P. J. (1974), "Shear Transfer by Aggregate Interlock", Shear in Reinforced Concrete, Volume 1, American Concrete Institute, Detroit, pp. 1-15.

Priestley, M. J. N. (1976), "Cyclic Testing of Heavily Reinforced Concrete Masonry Shear Walls", Department of Civil Engineering, University of Canterbury, New Zealand, Research Report 76-12.

Priestley, M. J. N. (1977), "Seismic Resistance of Reinforced Concrete Masonry Shear Walls with High Steel Percentages", Bulletin NZSEE, Vol. 10, No. 1, pp. 1-16.

Priestley, M. J. N. (1980), "Seismic Design of Masonry Buildings-Background to the Draft Masonry Design Code DZ4210", Bulletin NZSEE, Vol. 13, No. 4, pp. 329-346.

Priestley, M. J. N. (1981), "Ductility of Unconfined Masonry Shear Walls", Bulletin NZSEE, Vol. 14, No.1, pp. 3-11.

Priestley, M. J. N. (1982), "Ductility of Confined Masonry Shear Walls", Bulletin NZSEE, Vol. 5, No. 1, pp. 22-26.

Priestley, M. J. N., and Elder, D.McG. (1982), "Cyclic Loading Tests of Slender Concrete Masonry Shear Walls", Bulletin NZSEE, Vol. 15, No. 1, pp. 3-21.

Priestley, M. J. N., Seible, S., and Calvi, G. M. (1996), "Seismic Design and Retrofit of Bridges", John Wiley and Sons, New York.

Priestley, M. J. N., Verma, R., and Xiao, Y. (1994), "Seismic Shear Strength of Reinforced Concrete Column", Journal of Structural Engineering, Vol. 120, No. 8.

Schultz, A. E. (1996), "Seismic Performance of Partially-Grouted Masonry Shear Walls", Proceedings of the 11th World Conference on Earthquake Engineering, CD-Rom Paper No. 1221, Acapulco, Mexico, pp. 246-256.

Shing, P. B., Brunner, J. D., and Lotfi, H. R. (1993), "Evaluation of Shear Strength of Reinforced Masonry Walls", TMS Journal, Vol. 12, No. 1, pp. 65-77.

Shing, P. B., Klamerua, E., Spaeh, H., and Noland, J. L. (1988), "Seismic Performance of Reinforced Masonry Shear Walls", Proceedings of the 9th World Conference on Earthquake Engineering, Vol. 7, Tokyo, Japan, pp. 103-108.

Shing, P. B., Noland, J. L., Klamerus, E., and Schuller, M. (1989), "Inelastic Behaviour of Concrete Masonry Shear Walls", ASCE Journal of Structural Engineering, Vol. 15, pp. 2204-2225.

Shing, P. B., Noland, J. L., Spaech, H., Klamerus, E., and Schuller, M. (1991), "Response of Single-Storey Reinforced Masonry Shear Walls to In-Plane Lateral Loads", TCCMAR Report 3.1(a)-2.

Shing, P. B., Schuller, M., and Hoskere, V. S. (1990a), "In-Plane Resistance of Reinforced Masonry Shear Walls", ASCE Journal of Structural Engineering, Vol. 116, No. 3, pp. 619-640.

Shing, P. B., Schuller, M., and Hoskere, V. S. (1990b), "Strength and Ductility of Reinforced Masonry Shear Walls", Proceedings of the 5th North America Masonry Conference, University of Illinois, Urbana-Champaign, pp. 309-320.

Singh, S. S. (1998), "The Performance of a Partially Grouted Reinforced Concrete Masonry Wall and Ribraft™ Floor under Simulated Seismic Loading", M.E. Report, Department of Civil Engineering, University of Canterbury.

Sucuoglu, H., and McNiven, H. D. (1991), "Seismic Shear Capacity of Reinforced Masonry Piers", ASCE Journal of Structural Engineering, Vol. 117, No. 7, pp. 2166-2186.

Sveinsson, B. I., Mayes, R. L., and McNiven, H. D. (1985), "Cyclic Loading of Masonry Single Piers", Volume 4, Report No. UCB/EERC-85/15, Earthquake Engineering Research Centre, University of California, Berkeley.

Tomaževič, M. (1999), "Earthquake-Resistance Design of Masonry Buildings", Imperial College Press, London.

Tomaževič, M., Lutman, M., Velechovsky, T., and Zarnic, R. (1986), "Seismic Resistance of Reinforced Masonry Walls, Volume 1: Test Results, Part One", Report ZRMK/IKPI-86/04, Institute for Testing and Research in Material and Structures, Ljubljana, Yugoslavia.

Tomaževič, M., Lutman, M., Velechovsky, T., and Zarnic, R. (1987), "Seismic Resistance of Reinforced Masonry Walls, Volume 2: Test Results, Part two", Report ZRMK/IKPI-87/06, Institute for Testing and Research in Material and Structures, Ljubljana, Yugoslavia.

Tomaževič, M., Lutman, M. (1988), "Seismic Resistance of Reinforced Masonry Walls", Proceedings of the 9th World Conference on Earthquake Engineering, Vol. 6, Tokyo, Japan, pp97-102.

Uniform Building Code. (1997), "International Conference of Building Officials", Volume 2, Whittier, California, April 1997, 492p.

Voon, K. C., and Ingham, J. M. (2001), "Towards Suitable Shear Strength Provisions for inclusion in the New Zealand Masonry Design Standard", Proceedings of the 6th Australasian Masonry Conference, Adelaide, South Australia, pp. 393-402.

Voon, K. C., and Ingham, J. M. (2003). "Shear Strength of Concrete Masonry Walls", School of Engineering Report No. 611, University of Auckland, New Zealand.

Voon, K. C., and Ingham, J. M. (2006), "Bracing Capacity of Partially Grouted Concrete Masonry Walls with Openings", School of Engineering Report No. 629, University of Auckland, New Zealand.

Woodward, K., and Rankin, F. (1985a), "Influence of Block and Mortar Strength on Shear Resistance of Concrete Block Masonry Walls", NBSIR 85-3143, National Bureau of Standards, Gaithersburg, MD.

Woodward, K., and Rankin, F. (1985b), "Influence of Aspect Ratio on Shear Resistance of Concrete Block Masonry Walls", NBSIR 84-2993, National Bureau of Standards, Gaithersburg, MD.

Wu, H., and Li, B. (2003), "Investigating the Load Paths of RC Shear Wall with Openings under Reversed Cyclic Loadings", Pacific Conference on Earthquake Engineering, New Zealand.

Yancey, C. W., Fattal, S. G., and Dikkers, R. D. (1991), "Review of Research Literature on Masonry Shear Walls", NISTIR 4512, National Bureau of Standards, Gaithersburg, MD.

Yanez, F.V., Park, R., and Paulay, T. (1991), "Seismic Behaviour of Reinforced Concrete Structural Walls with Irregular Openings", Pacific Conference on Earthquake Engineering, New Zealand, pp. 3303-3308.

Yokel, F. Y., and Fattal, S. G. (1975), "A Failure Hypothesis for Masonry Shear Walls", NBSIR 75-703, National Bureau of Standards, Gaithersburg, MD.

Yokel, F. Y., and Fattal, S. G. (1976), "Failure Hypothesis for Masonry Shear Walls", ASCE Journal of Structural Engineering, Vol. 102, pp. 515-531.

Zhang, X. D. (1999), "Out-of-Plane Performance of Partially Grouted Reinforced Concrete Masonry Walls under Simulated Seismic Loading", ME Thesis, University of Canterbury.

Appendix A

DESIGN ILLUSTRATION

A.1 Introduction

NZS 4230 is the materials standard specifying design and detailing requirements for masonry structures. The latest version of this document has the full title 'NZS 4230:2004 Design of Reinforced Concrete Masonry Structures'. The purpose of this appendix is to provide additional information and to demonstrate the procedure in which it is intended that the new Standard be used when designing an unconfined concrete masonry wall.

A.2 Moment Capacity of Walls

Moment capacity may be calculated from first principles using a linear distribution of strain across the section, the appropriate magnitude of ultimate compression strain, and the appropriate rectangular stress block. Alternatively, for rectangular-section masonry components with uniformly distributed flexural reinforcement, Tables A.1 to A.4 overpage may be used. These tables list in non-dimensional form the nominal capacity of unconfined and confined concrete masonry walls with either Grade 300 or Grade 500 flexural reinforcement, for different values of the two salient parameters, namely the axial load ratio N_n/f'_mL_wt or N_n/Kf'_mL_wt, and the strength-adjusted reinforcement ratio pf_y/f'_m or pf_y/Kf'_m. Charts, produced from Tables A.1 to A.4, are also plotted which enable the user to quickly obtain a value for pf_y/f'_m or pf_y/Kf'_m given the axial load ratio N_n/f'_mL_wt or N_n/Kf'_mL_wt and the moment ratio $M_n/f'_mL_w^2t$ or $M_n/Kf'_mL_w^2t$. These charts are shown as Figures A.1 to A.4. On the charts, each curve represents a different value for pf_y/f'_m or pf_y/Kf'_m. For points which fall between the curves, values can be established using linear interpolation.

Table A.1 $\frac{M_n}{f'_m L_w^2 t}$ for unconfined wall with f_y = 300 MPa

$\frac{pf_y}{f'_m}$	Axial Load Ratio $\frac{N_n}{f'_m L_w t}$								
	0	0.05	0.10	0.15	0.20	0.25	0.30	0.35	0.40
0.00	0.000	0.0235	0.0441	0.0618	0.0765	0.0882	0.0971	0.1029	0.1059
0.01	0.0049	0.0279	0.0480	0.0652	0.0795	0.0909	0.0995	0.1052	0.1079
0.02	0.0097	0.0322	0.0518	0.0686	0.0826	0.0937	0.1020	0.1075	0.1102
0.04	0.0190	0.0406	0.0593	0.0753	0.0886	0.0992	0.1070	0.1122	0.1146
0.06	0.0280	0.0487	0.0665	0.0818	0.0945	0.1045	0.1120	0.1168	0.1190
0.08	0.0367	0.0566	0.0735	0.0881	0.1002	0.1099	0.1169	0.1215	0.1235
0.10	0.0451	0.0641	0.0804	0.0944	0.1059	0.1152	0.1218	0.1261	0.1279
0.12	0.0534	0.0713	0.0871	0.1005	0.1116	0.1204	0.1267	0.1307	0.1324
0.14	0.0613	0.0783	0.0936	0.1064	0.1171	0.1255	0.1315	0.1353	0.1369
0.16	0.0690	0.0853	0.0999	0.1123	0.1225	0.1306	0.1363	0.1399	0.1414
0.18	0.0762	0.0922	0.1062	0.1181	0.1279	0.1357	0.1411	0.1445	0.1459
0.20	0.0832	0.0989	0.1124	0.1238	0.1332	0.1406	0.1459	0.1491	0.1503

Table A.2 $\frac{M_n}{f'_m L_w^2 t}$ for unconfined wall with f_y = 500 MPa

$\frac{pf_y}{f'_m}$	Axial Load Ratio $\frac{N_n}{f'_m L_w t}$								
	0	0.05	0.10	0.15	0.20	0.25	0.30	0.35	0.40
0.00	0.000	0.0235	0.0441	0.0618	0.0765	0.0882	0.0971	0.1029	0.1059
0.01	0.0049	0.0279	0.0480	0.0652	0.0794	0.0908	0.0993	0.1049	0.1076
0.02	0.0097	0.0322	0.0517	0.0685	0.0824	0.0934	0.1015	0.1068	0.1093
0.04	0.0190	0.0405	0.0591	0.0750	0.0881	0.0984	0.1059	0.1107	0.1128
0.06	0.0280	0.0484	0.0662	0.0813	0.0937	0.1033	0.1103	0.1147	0.1163
0.08	0.0365	0.0561	0.0731	0.0874	0.0992	0.1081	0.1147	0.1186	0.1199
0.10	0.0448	0.0635	0.0797	0.0934	0.1043	0.1129	0.1190	0.1225	0.1234
0.12	0.0528	0.0707	0.0862	0.0992	0.1096	0.1176	0.1233	0.1264	0.1271
0.14	0.0605	0.0777	0.0925	0.1047	0.1147	0.1223	0.1275	0.1303	0.1307
0.16	0.0680	0.0844	0.0986	0.1103	0.1198	0.1269	0.1318	0.1342	0.1344
0.18	0.0752	0.0910	0.1045	0.1157	0.1247	0.1315	0.1359	0.1381	0.1380
0.20	0.0823	0.0974	0.1104	0.1211	0.1297	0.1359	0.1400	0.1420	0.1417

Table A.3 $\frac{M_n}{Kf'_m L_w^2 t}$ for confined wall with f_y = 300 MPa

$\frac{pf_y}{Kf'_m}$	Axial Load Ratio $\frac{N_n}{Kf'_m L_w t}$								
	0	0.05	0.10	0.15	0.20	0.25	0.30	0.35	0.40
0.00	0.000	0.0236	0.0444	0.0625	0.0778	0.0903	0.1000	0.1069	0.1111
0.01	0.0049	0.0280	0.0484	0.0661	0.0810	0.0933	0.1027	0.1095	0.1136
0.02	0.0098	0.0324	0.0523	0.0696	0.0842	0.0962	0.1055	0.1121	0.1161
0.04	0.0191	0.0409	0.0599	0.0766	0.0905	0.1020	0.1108	0.1173	0.1211
0.06	0.0281	0.0491	0.0673	0.0833	0.0967	0.1078	0.1163	0.1224	0.1261
0.08	0.0369	0.0569	0.0746	0.0899	0.1029	0.1135	0.1217	0.1275	0.1311
0.10	0.0454	0.0645	0.0818	0.0964	0.1089	0.1191	0.1271	0.1326	0.1360
0.12	0.0537	0.0720	0.0888	0.1027	0.1149	0.1246	0.1323	0.1377	0.1410
0.14	0.0616	0.0794	0.0956	0.1090	0.1209	0.1302	0.1376	0.1428	0.1459
0.16	0.0692	0.0867	0.1021	0.1152	0.1267	0.1357	0.1428	0.1479	0.1509
0.18	0.0767	0.0939	0.1085	0.1214	0.1324	0.1412	0.1480	0.1530	0.1558
0.20	0.0841	0.1009	0.1149	0.1275	0.1381	0.1466	0.1532	0.1581	0.1608

Table A.4 $\frac{M_n}{Kf'_m L_w^2 t}$ for confined wall with f_y = 500 MPa

$\frac{pf_y}{Kf'_m}$	Axial Load Ratio $\frac{N_n}{Kf'_m L_w t}$								
	0	0.05	0.10	0.15	0.20	0.25	0.30	0.35	0.40
0.00	0.000	0.0236	0.0444	0.0625	0.0778	0.0903	0.1000	0.1069	0.1111
0.01	0.0049	0.0280	0.0484	0.0661	0.0809	0.0932	0.1027	0.1094	0.1135
0.02	0.0098	0.0324	0.0523	0.0696	0.0841	0.0961	0.1054	0.1120	0.1159
0.04	0.0191	0.0408	0.0599	0.0765	0.0904	0.1019	0.1107	0.1171	0.1208
0.06	0.0281	0.0489	0.0673	0.0832	0.0967	0.1076	0.1161	0.1221	0.1257
0.08	0.0369	0.0569	0.0746	0.0898	0.1027	0.1133	0.1214	0.1272	0.1306
0.10	0.0454	0.0646	0.0817	0.0962	0.1088	0.1188	0.1267	0.1322	0.1355
0.12	0.0534	0.0720	0.0887	0.1026	0.1146	0.1243	0.1320	0.1372	0.1403
0.14	0.0614	0.0794	0.0956	0.1089	0.1205	0.1298	0.1372	0.1422	0.1452
0.16	0.0692	0.0866	0.1018	0.1151	0.1262	0.1352	0.1424	0.1472	0.1500
0.18	0.0769	0.0938	0.1083	0.1212	0.1319	0.1406	0.1475	0.1522	0.1549
0.20	0.0843	0.1006	0.1148	0.1273	0.1377	0.1460	0.1527	0.1573	0.1598

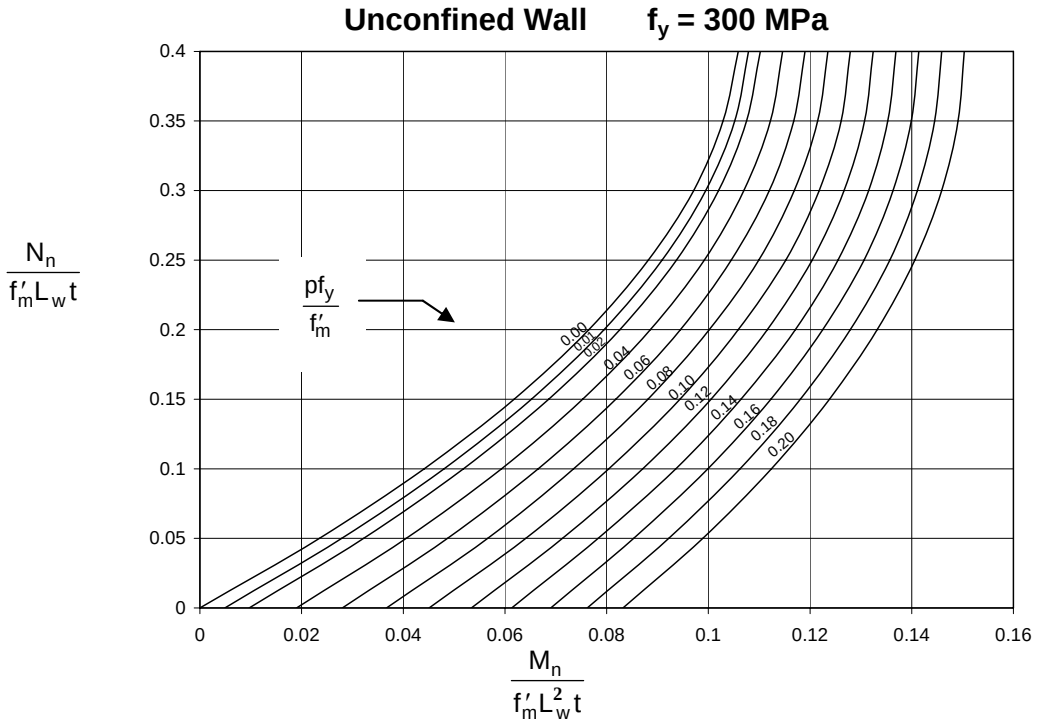

Figure A.1 Flexural strength of rectangular masonry walls with uniformly distributed reinforcement, unconfined wall f_y = 300 MPa.

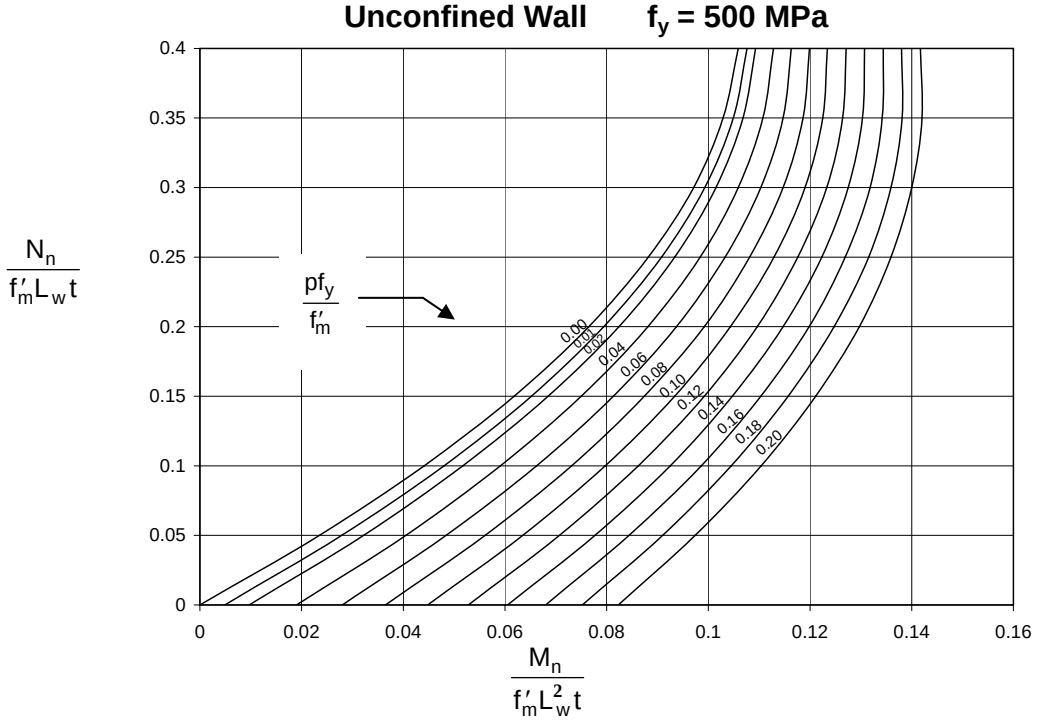

Figure A.2 Flexural strength of rectangular masonry walls with uniformly distributed reinforcement, unconfined wall f_y = 500 MPa.

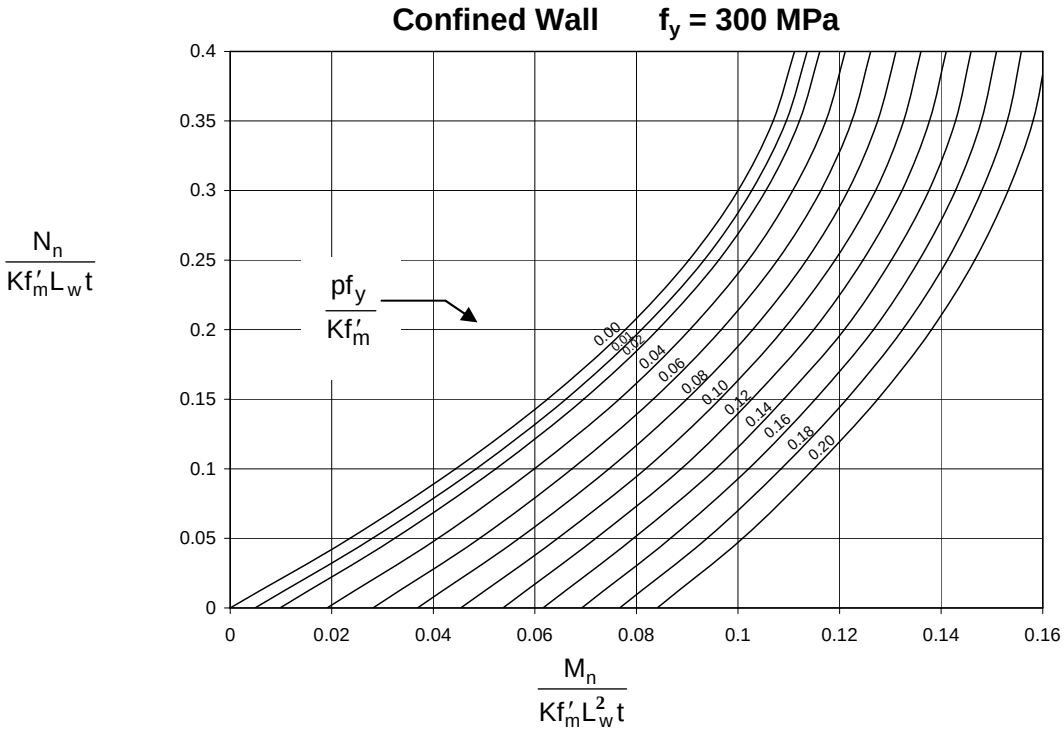

Figure A.3 Flexural strength of rectangular masonry walls with uniformly distributed reinforcement, confined wall f_y = 300 MPa.

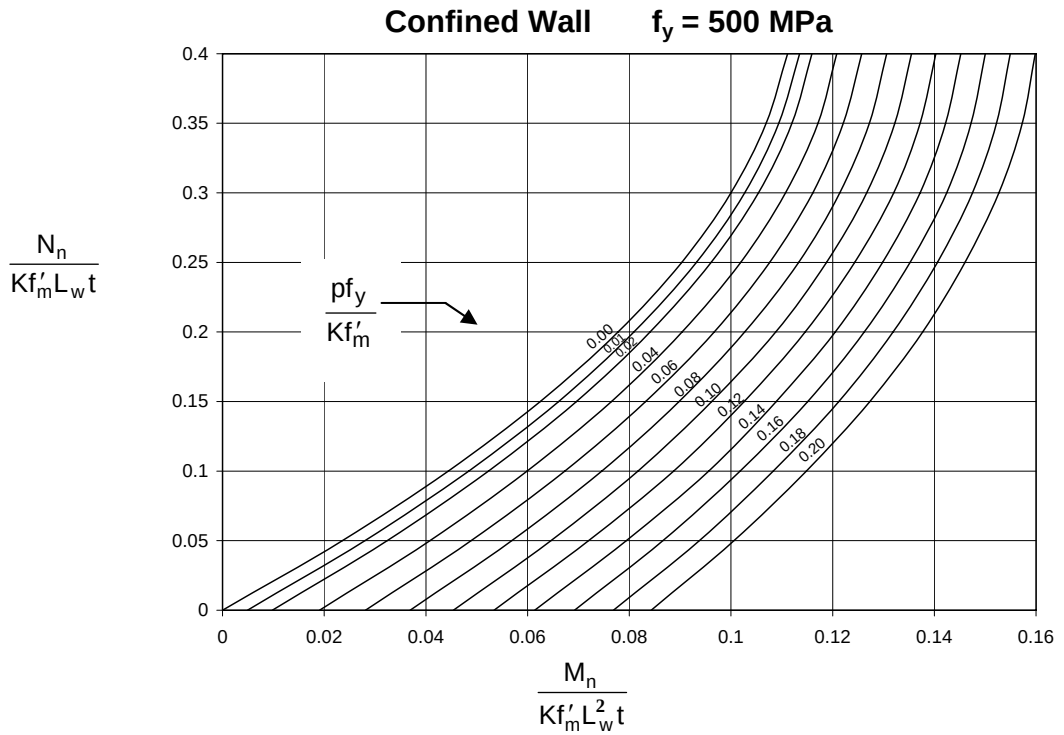

Figure A.4 Flexural strength of rectangular masonry walls with uniformly distributed reinforcement, confined wall f_y = 500 MPa.

A.3 Ductility Considerations

NZS 4230:2004 notes in section 7.4.6 that unless confirmed by a special study, adequate ductility may be assumed when the neutral axis depth of a component is less than an appropriate fraction of the section depth. Section A.2.1 below lists the ratios c/L_w for masonry walls. In addition, an outline of the procedure for conducting a special study to determine the available ductility of cantilevered concrete masonry walls is presented in section A.2.2.

A.3.1 Neutral axis depth

Neutral axis depth may be calculated from first principles, using a linear distribution of strain across the section, the appropriate level of ultimate compression strain and the appropriate rectangular stress block. Alternatively, for rectangular section structural walls, Tables A.5 and A.6 may be used. These list in non-dimensional form the neutral axis depth of unconfined and confined walls with either Grade 300 or Grade 500 flexural reinforcement, for different values of axial load ratio N_n/f'_mL_wt or N_n/Kf'_mL_wt and reinforcement ratio pf_y/f'_m or pf_y/Kf'_m, where p is the ratio of uniformly distributed vertical reinforcement. Charts, produced from Tables A.5 and A.6, are also plotted which enable the user to quickly obtain a value for c/L_w given the axial load ratio N_n/f'_mL_wt or N_n/Kf'_mL_wt and different value of pf_y/f'_m or pf_y/Kf'_m. These charts are shown as Figures A.5 and A.6.

A.3.2 Ductility capacity of cantilevered concrete masonry walls

Section 7.4.6.1 of NZS 4230:2004 provides a simplified but conservative method to ensure that adequate ductility can be developed in masonry walls. The Standard allows the rational analysis developed by Priestley (1981 and 1982) as an alternative to determine the available ductility of cantilevered concrete masonry walls.

Figure A.7 includes dimensionless design charts for the ductility capacity, μ_3 of unconfined concrete masonry walls whose aspect ratio is $A_r = h_e/L_w = 3$. For walls of other aspect ratio, A_r, the ductility capacity can be found from the μ_3 value using Equation A-1:

$$\mu_{A_r} = 1 + \frac{3.3(\mu_3 - 1)\left(1 - \frac{0.25}{A_r}\right)}{A_r} \qquad \text{(A-1)}$$

Table A.5 Neutral axis depth ratio c/L_w (f_y= 300 MPa or 500 MPa): unconfined walls

$\frac{pf_y}{f'_m}$	Axial Load Ratio $\frac{N_n}{f'_m L_w t}$								
	0	0.05	0.1	0.15	0.2	0.25	0.3	0.35	0.4
0	0.0000	0.0692	0.1384	0.2076	0.2768	0.3460	0.4152	0.4844	0.5536
0.01	0.0135	0.0808	0.1481	0.2155	0.2828	0.3502	0.4175	0.4848	0.5522
0.02	0.0262	0.0918	0.1574	0.2230	0.2885	0.3541	0.4197	0.4852	0.5508
0.04	0.0498	0.1121	0.1745	0.2368	0.2991	0.3614	0.4237	0.4860	0.5483
0.06	0.0712	0.1306	0.1899	0.2493	0.3086	0.3680	0.4273	0.4866	0.5460
0.08	0.0907	0.1473	0.2040	0.2606	0.3173	0.3739	0.4306	0.4873	0.5439
0.1	0.1084	0.1626	0.2168	0.2710	0.3252	0.3794	0.4336	0.4878	0.5420
0.12	0.1247	0.1766	0.2286	0.2805	0.3325	0.3844	0.4364	0.4883	0.5403
0.14	0.1397	0.1895	0.2394	0.2893	0.3392	0.3890	0.4389	0.4888	0.5387
0.16	0.1535	0.2014	0.2494	0.2974	0.3453	0.3933	0.4412	0.4892	0.5372
0.18	0.1663	0.2125	0.2587	0.3048	0.3510	0.3972	0.4434	0.4896	0.5358
0.2	0.1782	0.2227	0.2673	0.3118	0.3563	0.4009	0.4454	0.4900	0.5345

Table A.6 Neutral axis depth ratio c/L_w (f_y= 300 MPa or 500 MPa): confined walls

$\frac{pf_y}{Kf'_m}$	Axial Load Ratio $\frac{N_n}{Kf'_m L_w t}$								
	0	0.05	0.1	0.15	0.2	0.25	0.3	0.35	0.4
0	0.0000	0.0579	0.1157	0.1736	0.2315	0.2894	0.3472	0.4051	0.4630
0.01	0.0113	0.0679	0.1244	0.1810	0.2376	0.2941	0.3507	0.4072	0.4638
0.02	0.0221	0.0774	0.1327	0.1881	0.2434	0.2987	0.3540	0.4093	0.4646
0.04	0.0424	0.0953	0.1483	0.2013	0.2542	0.3072	0.3602	0.4131	0.4661
0.06	0.0610	0.1118	0.1626	0.2134	0.2642	0.3150	0.3659	0.4167	0.4675
0.08	0.0781	0.1270	0.1758	0.2246	0.2734	0.3223	0.3711	0.4199	0.4688
0.1	0.0940	0.1410	0.1880	0.2350	0.2820	0.3289	0.3759	0.4229	0.4699
0.12	0.1087	0.1540	0.1993	0.2446	0.2899	0.3351	0.3804	0.4257	0.4710
0.14	0.1224	0.1661	0.2098	0.2535	0.2972	0.3409	0.3846	0.4283	0.4720
0.16	0.1351	0.1774	0.2196	0.2618	0.3041	0.3463	0.3885	0.4307	0.4730
0.18	0.1471	0.1879	0.2288	0.2696	0.3105	0.3513	0.3922	0.4330	0.4739
0.2	0.1582	0.1978	0.2373	0.2769	0.3165	0.3560	0.3956	0.4351	0.4747

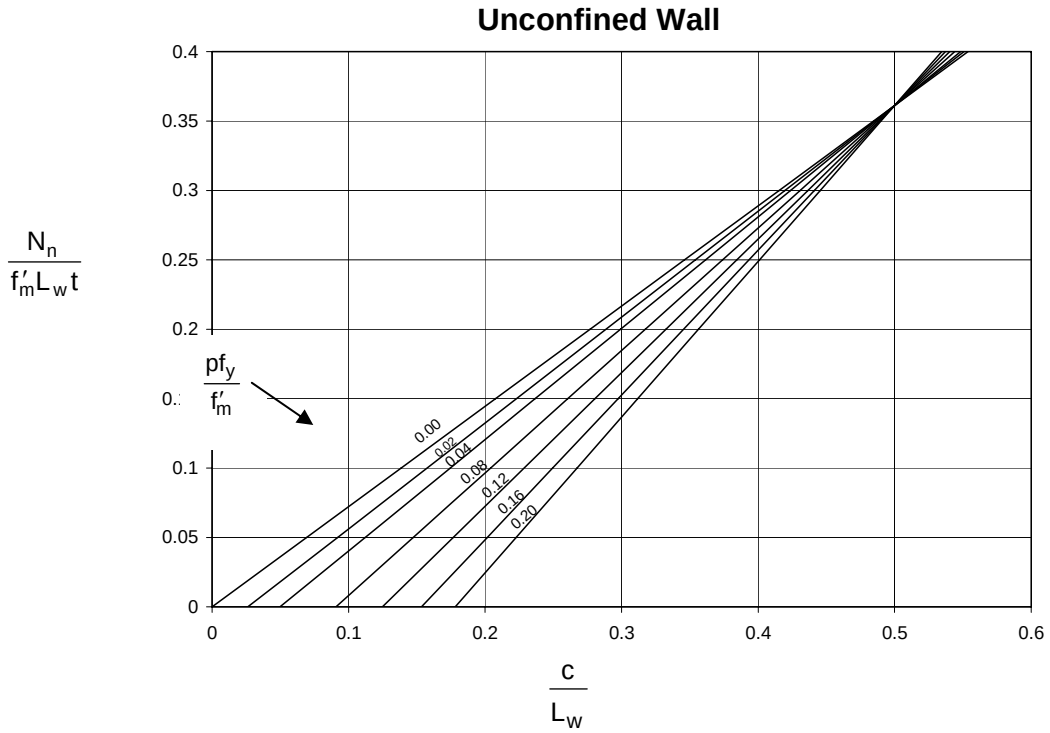

Figure A.5 Neutral axis depth of unconfined rectangular masonry walls with uniformly distributed reinforcement, f_y = 300 MPa or 500 MPa.

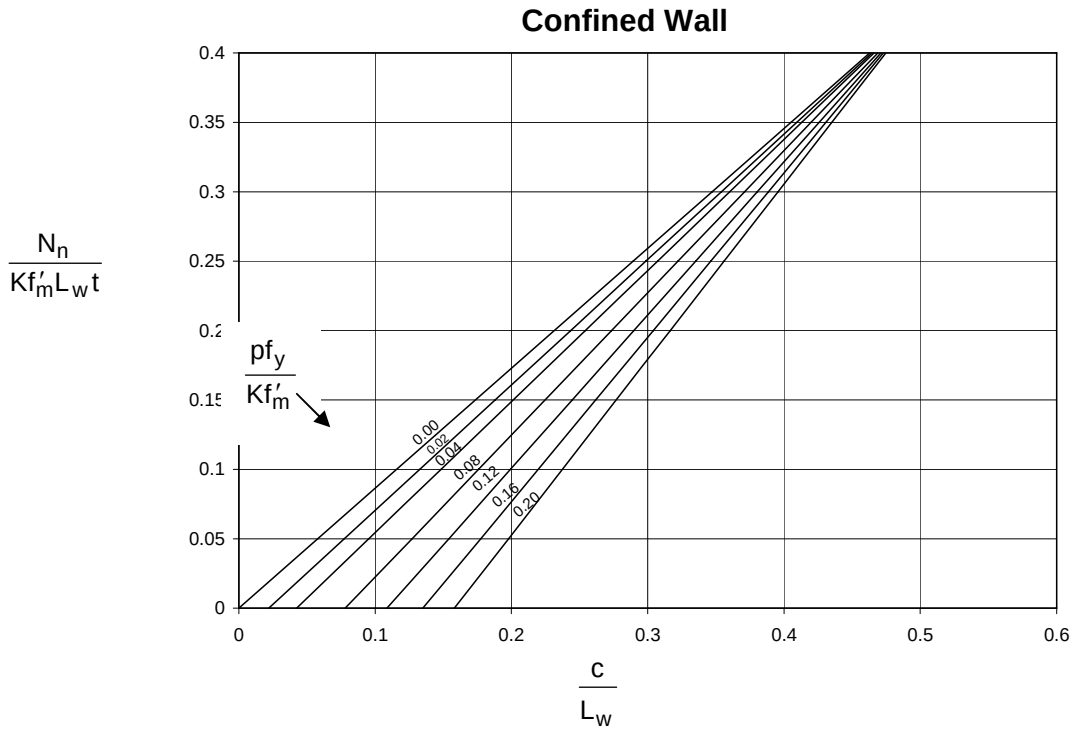

Figure A.6 Neutral axis depth of confined rectangular masonry walls with uniformly distributed reinforcement, f_y = 300 MPa or 500 MPa.

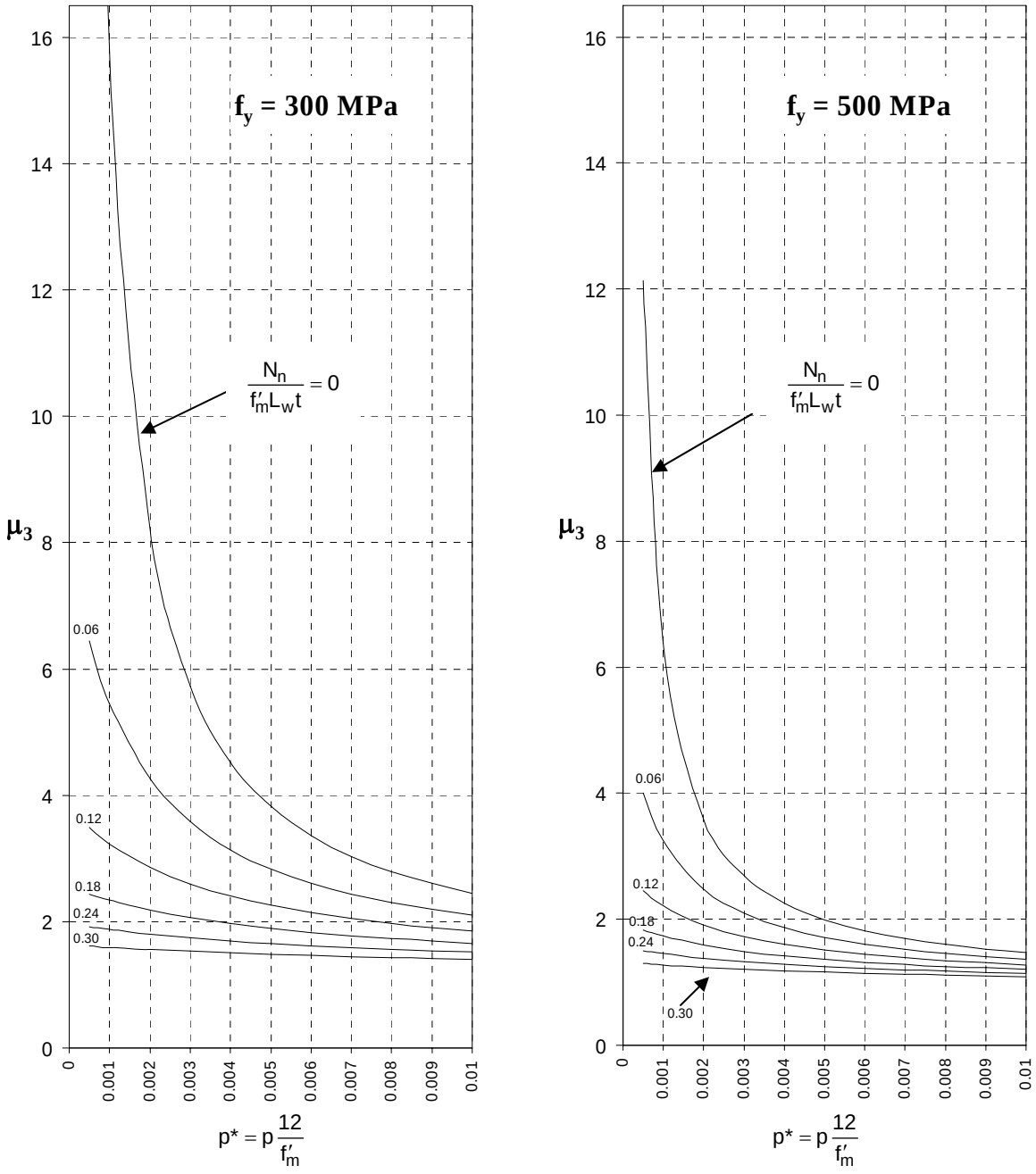

Figure A.7 Ductility of unconfined concrete masonry walls for aspect ratio $A_r = 3$.

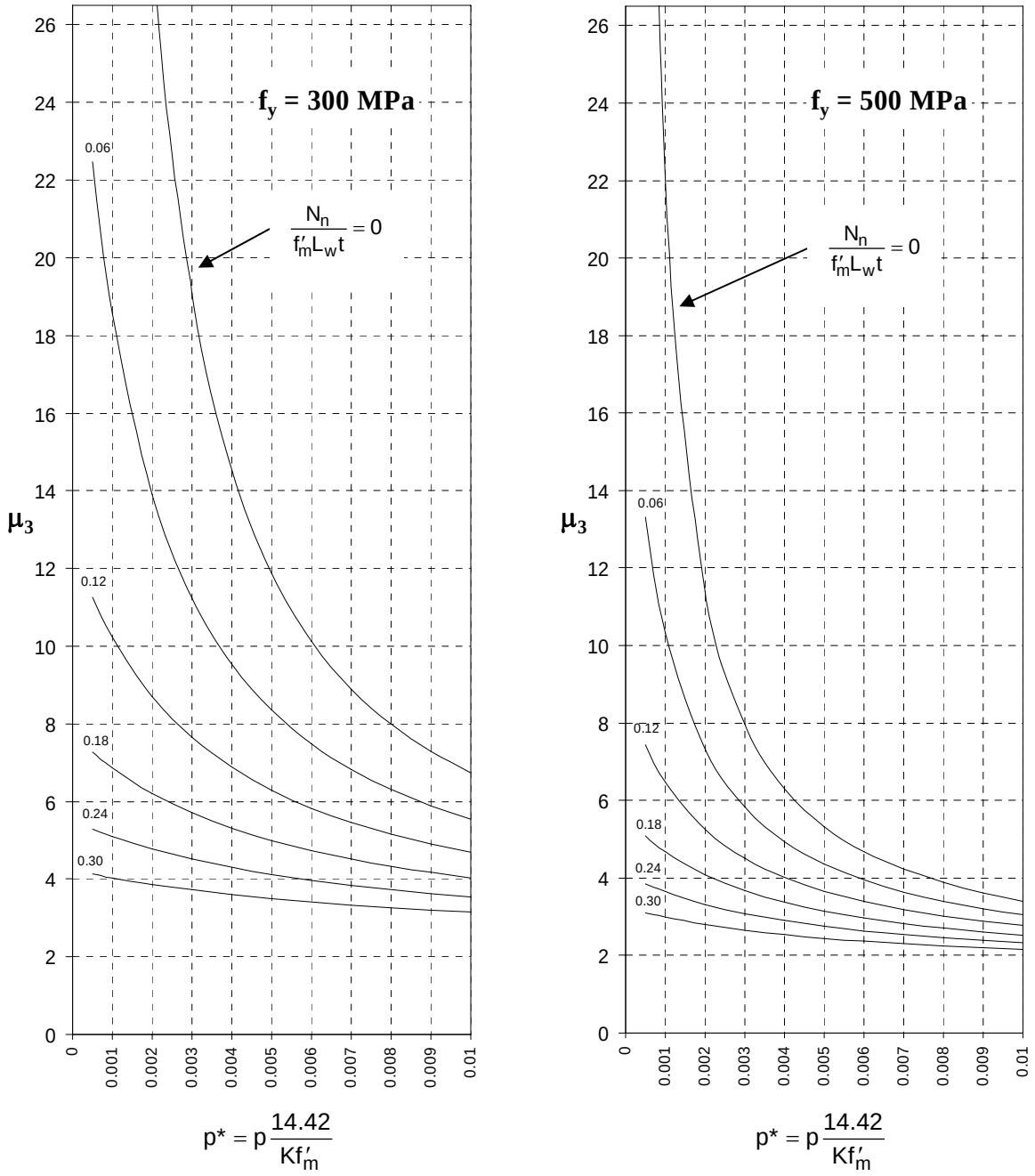

Figure A.8 Ductility of confined concrete masonry walls for aspect ratio $A_r = 3$.

When the ductility capacity found from Figure A.7 and Eqn. A-1 is less than that required, redesign is necessary to increase ductility. The most convenient and effective way to increase ductility is to use a higher design value of f'_m for Type A masonry. This will reduce the axial load ratio $N_n/f'_m A_g$ (where $N_n = N^*/\phi$) and the adjusted reinforcement ratio $p^* = p12/f'_m$ proportionally. From Figure A.7, the ductility will therefore increase.

Where the required increase in f'_m cannot be provided, a second alternative is to confine the masonry within critical regions of the wall. The substantial increase in ductility capacity

resulting from confinement is presented in Figure A.8. A third practical solution is to increase the thickness of the wall.

In Figures A.7 and A.8, the reinforcement ratio is expressed in the dimensionless form p*, where:

$$\text{for unconfined walls:} \quad p^* = \frac{12p}{f'_m}$$

$$\text{for confined walls:} \quad p^* = \frac{14.42p}{Kf'_m}$$

$$\text{and} \quad K = 1 + p_s \frac{f_{yh}}{f'_m}$$

A.3 DESIGN EXAMPLE

The 6 storey concrete masonry shear wall of Figure A.9 is to be designed for the seismic lateral loads shown, which have been based on a ductility factor of $\mu = 4.0$. Design gravity loads of 150 kN, including self weight, act at each floor and at roof level, and the weight of the ground floor and footing are sufficient to provide stability at the foundation level under the overturning moments. Wall width should be 190 mm. Design flexural and shear reinforcement for the wall.

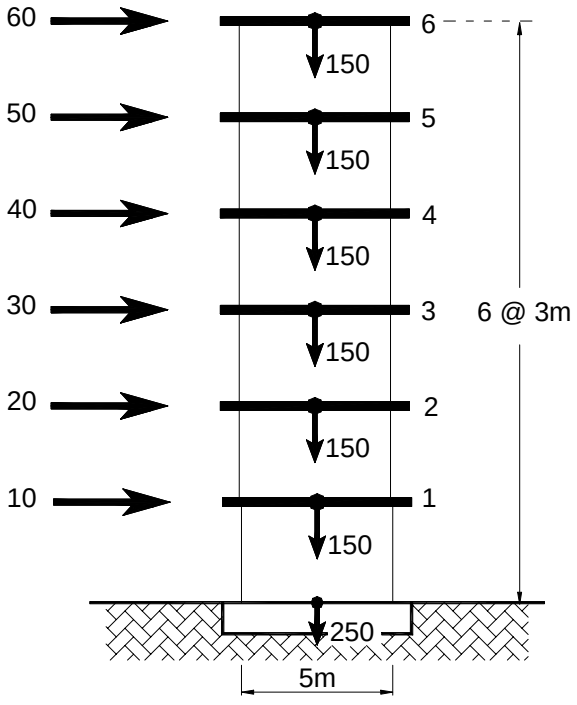

Figure A.9 Ductile cantilever shear wall.

Solution

Initially f'_m = 12 MPa will be assumed. From the lateral loads of Figure A.9, the wall base moment is:

M^* = 3 x (60 x 6 + 50 x 5 + 40 x 4 + 30 x 3 + 20 x 2 + 10)

= 2730 kNm

Require $\phi M_n \geq M^*$

Therefore $M_n \geq \frac{M^*}{\phi}$

$M_n \geq \frac{2730}{0.85}$

≥ 3211 kNm

Axial load at Base

N^* = 6 x 150

= 900 kN

$N_n = \frac{N^*}{\phi} = \frac{900}{0.85} = 1058.8$ kN

Check Dimensional Limitations

Assuming a 200 mm floor slab, the unsupported interstorey height = 2.8 m.

$$\frac{b_w}{L_n} = \frac{190}{2800} = 0.068 \quad < 0.075$$

This is less than the general seismic requirement cited by NZS 4230:2004 (clause 7.4.4.1).

However, from Table A.5,

$c < 0.3\ L_w$ (see Page 187)

Hence the less stringent demand of

$$\frac{b_w}{L_n} \geq 0.05$$

applies here (clause 7.3.3 of NZ 4230:2004) and this is satisfied by the geometry of the wall.

Flexure and Shear Design

Dimensionless Design Parameters

$$\frac{M_n}{f'_m L_w^2 t} = \frac{3211.8\times10^6}{12\times5000^2\times190} = 0.0563$$

and $$\frac{N_n}{f'_m L_w t} = \frac{1058.8\times10^3}{12\times5000\times190} = 0.0929$$

From Figure A.1 and assuming $f_y = 300$ MPa for flexural reinforcement

$$p\frac{f_y}{f'_m} = 0.04$$

Therefore $p = 0.0016$

Check Ductility Capacity

Check this using the ductility chart, Figure A.7

$$p\frac{12}{f'_m} = 0.0016 \qquad \text{and} \qquad \frac{N_n}{f'_m A_g} = 0.0929$$

Figure A.7 gives $\mu_3 = 3.3$

Actual aspect ratio: $A_r = \frac{3\times6}{5} = 3.6$

Therefore from Equation A-1:

$$\mu_{3.6} = 1+\frac{3.3\times(3.3-1)\times\left(1-\frac{0.25}{3.6}\right)}{3.6} = 3.0 < \mu = 4 \text{ required}$$

Thus ductility is inadequate and redesign is necessary

Redesign for f'_m =16 MPa (Note that this will require verification of strength using the procedures reported in Appendix B of NZS 4230:2004).

Now new Dimensionless Design Parameters

$$\frac{N_n}{f'_m A_g} = \frac{1058.8\times10^3}{16\times5000\times190} = 0.0697$$

and $$\frac{M_n}{f'_m L_w^2 t} = \frac{3211.8\times10^6}{16\times5000^2\times190} = 0.0423$$

From Figure A.1 and for f_y = 300 MPa for flexural reinforcement:

$$p\frac{f_y}{f'_m} = 0.028$$

Therefore $p = \frac{0.028 \times 16}{300} = 0.0015$

Check Ductility Capacity

Using Figure A.7, check the available ductility

$$p^* = p\frac{12}{f'_m} = 0.0015 \times \frac{12}{16} = 0.0011$$

$$\frac{N_n}{f'_m A_g} = 0.0697$$

From Figure A.7, $\mu_3 \approx 4.5$

From Equation A-1,

$$\mu_{3.6} = 1 + \frac{3.3 \times (4.5 - 1) \times \left(1 - \frac{0.25}{3.6}\right)}{3.6} = 3.98 \approx 4.0$$

Hence ductility OK

Flexural Reinforcement

For p = 0.0015 reinforcement per 400 mm will be

$$A_s = 0.0015 \times 400 \times 190 = \frac{114 \text{ mm}^2}{400 \text{ mm}}$$

Therefore use <u>D12 @ 400 mm crs</u> (113 mm^2/400 mm).

Shear Design

To estimate the maximum shear force on the wall, the flexural overstrength at the base of the wall, M_o, needs to be calculated:

$M_o = 1.25M_{n,provided}$ (for Grade 300 reinforcement)

f'_m = 16 MPa

$$\frac{N_n}{f'_m L_w t} = 0.070$$

$$p_{provided} = \frac{13 \text{ bars x } 113 \text{ mm}^2}{5000 \times 190} = 0.00155$$

and $$p\frac{f_y}{f'_m} = 0.00155 \times \frac{300}{16} = 0.029$$

From Table A.1:

$$\frac{M_n}{f'_m L_w^2 t} = 0.047$$

Therefore

$M_{n,provided} = 0.047 \text{ x } 16 \text{ x } 5000^2 \text{ x } 190 = 3580 \text{ kNm}$

The overstrength value, $\phi_{o,w}$, is calculated as follow:

$$\phi_{o,w} = \frac{M_o}{M^*} = \frac{1.25M_{n,provided}}{M^*} = \frac{1.25 \times 3580}{2730} = 1.64$$

Dynamic Shear Magnification Factor

For up to 6 storeys:

$$\omega_v = 0.9 + \frac{n}{10}$$

$$= 0.9 + \frac{6}{10} = 1.5$$

Hence, the design shear force at the wall base is:

$V_n = \omega_v \phi_{o,w} V^* = 1.5 \text{ x } 1.64 \text{ x } V^*$

$= 2.46V^*$

$= 2.46 \text{ x } 210$

$= 516.6 \text{ kN}$

Check Maximum Shear Stress

$$v_n = \frac{V_n}{b_w d} = \frac{516.6x10^3}{190x0.8x5000} = 0.68 \text{ MPa}$$

From Table 4.1, the maximum allowable shear stress, v_g, for $f'_m = 16$ MPa is 1.8 MPa. Therefore OK.

Plastic Hinge Region

Within the plastic hinge region, $v_m = 0$. Therefore $v_p + v_s = 0.68$ MPa

and $v_p = 0.9\dfrac{N^*}{b_w d}\tan\alpha$

Note that NZS 4230:2004 specified the vertical extent of the potential plastic hinge region from the critical section in the wall shall be taken as the greatest of:

1. The length of the wall in the plane of forces resisting the seismic load;
2. One sixth the clear height of the wall;
3. 600 mm.

As illustrated in Figure 4.2 (see p80), it is necessary to calculate the compression depth **a** in order to establish tanα.

To establish compression depth **a** using Table A.5:

$$p\frac{f_y}{f'_m} = 0.029 \quad \text{and} \quad \frac{N_n}{f'_m L_w t} = 0.0697$$

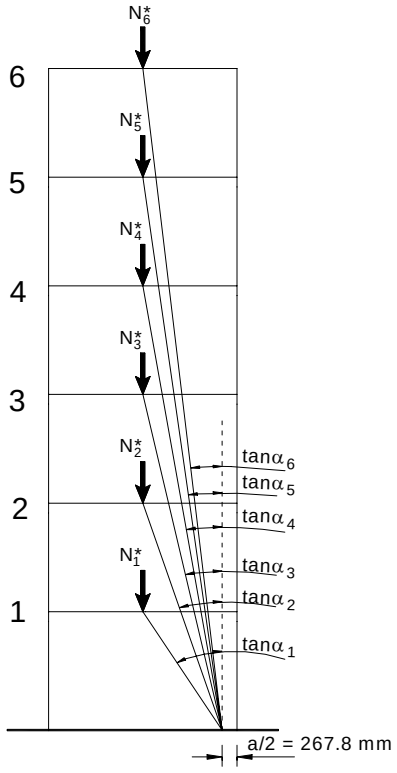

From Table A.5:

$$\frac{c}{L_w} = 0.126$$

Therefore c = 0.126 x 5000

= 630 mm

$\Rightarrow$ a = βc (for unconfined concrete masonry, β = 0.85)

= 0.85 x 630

= 535.5 mm

Figure A.10 Contribution of axial load.

Calculation of tanα

$$\tan\alpha_1 = \frac{2500 - 267.8}{3000} = 0.744$$

$$\tan\alpha_2 = \frac{2500 - 267.8}{6000} = 0.372$$

$$\tan\alpha_3 = \frac{2500 - 267.8}{9000} = 0.248$$

$$\tan\alpha_4 = \frac{2500 - 267.8}{12000} = 0.186$$

$$\tan\alpha_5 = \frac{2500 - 267.8}{15000} = 0.149$$

$$\tan\alpha_6 = \frac{2500 - 267.8}{18000} = 0.124$$

Hence,

$$v_{p1} = 0.9\frac{150\times10^3}{190\times0.8\times5000}\times0.744 = 0.112 \text{ MPa}$$

$$v_{p2} = 0.9\frac{150\times10^3}{190\times0.8\times5000}\times0.372 = 0.066 \text{ MPa}$$

$$v_{p3} = 0.9\frac{150\times10^3}{190\times0.8\times5000}\times0.248 = 0.044 \text{ MPa}$$

$$v_{p4} = 0.9\frac{150\times10^3}{190\times0.8\times5000}\times0.186 = 0.033 \text{ MPa}$$

$$v_{p5} = 0.9\frac{150\times10^3}{190\times0.8\times5000}\times0.149 = 0.026 \text{ MPa}$$

$$v_{p6} = 0.9\frac{150\times10^3}{190\times0.8\times5000}\times0.124 = 0.022 \text{ MPa}$$

$$\Rightarrow \quad v_p = v_{p1} + v_{p2} + v_{p3} + v_{p4} + v_{p5} + v_{p6} = 0.30 \text{ MPa}$$

Therefore, the required shear reinforcement:

$$v_s = v_n - v_p$$
$$= 0.68 - 0.30$$
$$= 0.38 \text{ MPa}$$

$$v_s = C_3 \frac{A_v f_y}{b_w s_h}$$

where C_3 = 0.8 for a wall and the maximum spacing of transverse reinforcement = 200 mm since the wall height exceeds 3 storeys. Try f_y = 300 MPa:

$$0.38 = 0.8 \frac{A_v \times 300}{190 \times 200}$$

A_v = 60.2 mm^2/200 mm vertical spacing

Therefore use R10 @ 200 crs within plastic hinge region = 78.5 mm^2 per 200 mm spacing.

Outside Plastic Hinge Region

For example, immediately above level 2:

V_n = 1.5 x 1.64 x (60 + 50 + 40 + 30)

= 443 kN

Therefore

$$v_n = \frac{443 x 10^3}{b_w d} = 0.58 \text{ MPa}$$

From Equation 4-6:

$$v_m = (C_1 + C_2) v_{bm}$$

where $C_1 = 33 p_w \frac{f_y}{300}$

$$= 33x \frac{13 \text{bars} \times 113}{b_w d} \frac{f_y}{300}$$

$$= 33x \frac{13x113}{190x0.8x5000} \times \frac{300}{300}$$

$$= 0.064$$

and $C_2 = 1.0$ since $h_e/L_w > 1.0$

Therefore $v_m = (C_1 + C_2)v_{bm}$

$$= (0.064 + 1) \times 0.2\sqrt{16}$$

= 0.85 MPa> v_n

Since $v_m > v_n$, only minimum shear reinforcement of 0.07% is required. Take s_h = 400 mm,

A_v = 0.07% x 400 x190 = 53.2 mm^2

Therefore, use R10 @ 400 crs outside plastic hinge region.

Appendix B

PROPERTIES OF AVAILABLE TEST RESULTS

The experimental data sets presented in this section are limited to those of fully grouted concrete and clay brick reinforced masonry walls, which were subjected to reverse cyclic lateral forces and failed in shear. Relevant properties of the tested walls are listed in Table B.1. The data sets selected are (i) tests conducted by Shing et al. (1990), specimen no. 1-10, (ii) tests conducted by Matsumura (1987), specimen no. 11-28, (iii) tests conducted by Sveinsson et al., (1985) specimen no. 29-49, and (iv) tests conducted at the University of Auckland (Voon and Ingham, 2003), specimen no. 50-56. Of the 56 specimens listed in Table B.1, nineteen of them were single-wythe walls constructed with hollow clay brick units, see shaded rows.

Table B.1 Properties of specimens, fully grouted

Specimen no.	Specimen label	h mm	L_w mm	t mm	d mm	s_h mm	ρ_h X10^{-3}	f_{yh} MPa	ρ_{ve} X10^{-3}	ρ_v X10^{-3}	f_{yv} MPa	f'_m MPa	σ_n MPa	v_{max} MPa	μ_{vmax}
1	1-S	1830	1830	143	1727	406	1.22	385.8	1.48	7.41	496.1	20.67	1.86	1.74	3.10
2	2-S	1830	1830	143	1727	406	1.22	385.8	1.48	7.41	496.1	17.91	0	1.35	2.30
3	3-S	1830	1830	143	1727	406	1.22	385.8	1.48	7.41	496.1	17.91	0.69	1.47	2.00
4	4-S	1830	1830	143	1727	406	1.22	385.8	1.48	7.41	496.1	22.36	0.69	1.65	2.40
5	5-S	1830	1830	143	1727	406	1.22	385.8	0.77	3.83	441.3	22.36	1.86	1.63	2.50
6	6-S	1830	1830	143	1727	406	2.22	491.6	1.09	5.43	448.2	23.04	1.86	1.92	2.20
7	7-S	1830	1830	143	1727	406	1.22	385.8	1.09	5.43	228.2	23.04	1.86	1.78	2.30
8	8-S	1830	1830	143	1727	406	2.22	491.6	1.48	7.41	496.1	17.07	1.86	2.05	3.70
9	9-S	1830	1830	137	1727	406	1.28	385.8	1.14	5.68	496.1	26.18	1.93	1.79	3.50
10	10-S	1830	1830	137	1727	406	1.28	385.8	1.14	5.68	496.1	26.18	0.69	1.56	4.44
11	1-M	1800	1590	150	1500	400	1.18	385	4.26	9.43	385	21.8	0.49	1.60	2*
12	2-M	1800	1190	150	1100	400	1.18	385	4.34	9.46	385	21.8	0.49	1.72	2*
13	3-M	1800	1190	150	1100	400	1.18	385	4.34	9.46	385	21.8	0.49	1.87	2*
14	4-M	1800	790	150	700	400	1.18	385	5.41	11.48	385	21.8	0.49	1.61	2*
15	5-M	1800	1190	190	1095	400	0	385	2.54	5.71	385	22.3	1.96	1.70	0.95
16	6-M	1800	1190	190	1095	400	1.67	385	2.54	5.71	385	22.3	1.96	1.89	1.14
17	7-M	1800	1190	190	1095	400	3.34	385	2.54	5.71	385	22.3	1.96	2.28	3.36
18	8-M	1800	1190	190	1095	400	3.34	385	4.48	9.59	385	22.3	1.96	2.29	1.27
19	9-M	1800	1190	190	1095	400	6.68	385	4.48	9.59	385	22.3	1.96	2.93	2.28
20	10-M	1800	1190	190	1095	400	3.34	385	4.48	9.59	385	29	1.96	2.59	2*
21	11-M	1800	1190	190	1095	400	3.34	385	4.48	9.59	385	26.1	1.96	2.24	2*
22	12-M	1800	1190	190	1095	400	4.00	385	4.48	9.59	385	27.4	1.96	2.63	2*

* This wall was assumed to develop it maximum shear strength at $\mu = 2.0$.

Table B.1 Properties of specimens, fully grouted (continued)

Specimen no.	Specimen label	h mm	L mm	t mm	d mm	s_h mm	ρ_h X10^{-3}	f_{yh} MPa	ρ_{ve} X10^{-3}	ρ_v X10^{-3}	f_{yv} MPa	f'_m MPa	σ_n MPa	v_{max} MPa	μ_{vmax}
23	13-M	1800	1190	190	1095	400	3.53	385	4.73	10.13	385	26.4	1.96	2.43	2*
24	14-M	1800	1190	190	1095	400	3.34	385	4.48	9.59	385	31.4	1.96	2.59	2*
25	15-M	1700	1110	190	1005	378	0	385	2.72	6.12	385	28.6	1.96	2.18	1.94
26	16-M	1700	1110	190	1005	378	1.67	385	2.72	6.12	385	28.6	1.96	1.95	2.97
27	17-M	1700	1110	190	1005	378	3.34	385	2.72	6.12	385	28.6	1.96	1.71	1.83
28	18-M	1700	1110	190	1005	378	6.68	385	2.72	6.12	385	28.6	1.96	2.04	2.04
29	1-B	1422	1219	194	1143	284	2.87	406.5	0.85	1.69	465.1	23.1	1.88	1.95	5.39
30	2-B	1422	1219	194	1143	284	2.87	406.5	0.85	1.69	465.1	23.1	3.01	2.38	5.23
31	3-B	1422	1219	143	1143	284	3.94	437.5	2.22	4.44	390.7	15.8	2.76	2.46	4.21
32	4-B	1422	1219	143	1143	284	3.94	437.5	0.74	4.44	410	15.8	2.76	2.46	2.20
33	5-B	1422	1219	143	1143	474	1.97	437.5	2.22	4.44	390.7	15.1	2.76	2.36	4.90
34	6-B	1422	1219	143	1143	474	1.97	437.5	0.74	4.44	410	15.1	2.76	2.23	5.38
35	7-B	1422	1219	143	1143	203	0.75	437.5	2.22	4.44	390.7	15.1	2.76	1.92	4.41
36	8-B	1422	1219	143	1143	399	2.72	437.5	2.22	4.44	390.7	15.1	2.76	2.43	6.26
37	9-B	1422	1219	143	1143	474	1.97	437.5	2.22	4.44	390.7	15.1	1.74	1.96	3.23
38	10-B	1422	1219	143	1143	474	1.97	437.5	2.22	4.44	390.7	15.1	2.76	2.40	2.27
39	11-B	1422	1219	143	1143	474	1.95	437.5	2.22	4.44	390.7	20.1	2.76	1.84	3.87
40	12-B	1422	1219	143	1143	237	4.87	437.5	2.22	4.44	390.7	20.1	2.76	1.92	3.2
41	13-B	1422	1219	143	1143	474	1.97	437.5	2.22	6.74	390.7	20.1	2.76	2.35	3.75
42	14-B	1422	1219	143	1143	237	4.87	437.5	1.15	4.59	437.5	20.1	2.76	2.40	3.22
43	15-B	1422	1219	143	1143	474	1.97	437.5	0.74	4.44	410	20.1	2.76	2.03	4.68
44	16-B	1422	1219	143	1143	237	4.87	437.5	0.74	4.44	410	20.1	2.76	2.20	5.18
45	17-B	1422	1219	143	1143	474	1.97	437.5	2.22	1.48	390.7	20.1	2.76	2.18	2.21
46	18-B	1422	1219	143	1143	237	4.87	437.5	2.22	4.44	390.7	20.1	2.76	2.14	2.68
47	19-B	1422	1219	143	1143	284	2.50	410	2.22	4.44	390.7	20.1	2.76	2.25	3.38
48	20-B	1422	1219	143	1143	129	6.25	416.9	2.22	4.44	410	20.1	2.76	2.27	3.36
49	21-B	1422	1219	143	1143	203	1.00	437.5	2.22	4.44	390.7	27.6	2.76	2.69	2.86
50	1-A	1800	1800	140	1700	400	0.50	325	1.25	6.23	318	17.6	0	0.83	2.67
51	2-A	1800	1800	140	1700	1800	0	325	1.25	6.23	318	17.6	0	0.74	2.61
52	3-A	1800	1800	140	1700	800	0.62	310	1.25	6.23	318	17	0	0.84	2.60
53	4-A	1800	1800	140	1700	400	0.50	325	1.25	6.23	318	18.5	0.5	1.04	2.73
54	5-A	1800	1800	140	1700	400	0.50	325	1.25	6.23	318	18.5	0.25	0.98	2.73
55	6-A	3600	1800	140	1700	400	0.51	325	1.90	9.70	550	24.3	0.25	0.82	2.85
56	7-A	1800	3000	140	2900	400	0.51	325	0.75	5..90	318	24.3	0.25	1.39	1.33

* This wall was assumed to develop it maximum shear strength at $\mu = 2.0$.

Experimental results are compared to shear strength predictions using the shear expressions listed in Table 5.1, accurately accounting for the correct parameters appropriate for each test result. In all cases, predicted strengths are based on measured material properties rather than nominal values. The predicted strength (v_m, v_p, v_s and the sum v_n) and the actual shear strength (v_{max}) determined from the experimental results of the fifty six specimens are listed in Table B.2. Also included in Table B.2 is the v_{max}/v_n ratios.

Table B.2 Predicted strength of fully grouted masonry walls

Specimen no.	Specimen label	v_m (MPa)									v_p (MPa)								
		NZS 4230: 1990	Matsumura	Shing et al.	Anderson & Priestley	NEHPR	UBC	AS3700	Equation 4-4	NZS 4230:2004	NZS 4230: 1990	Matsumura	Shing et al.	Anderson & Priestley	NEHPR	UBC	AS3700	Equation 4-4	NZS 4230:2004
1	1-S	0.58	1.09	1.12	0.52	0.85	0.45	1.00	0.35	0.35	0.00	0.31	0.18	0.47	0.47	0.00	0.00	0.66	0.66
2	2-S	0.38	1.01	1.04	0.88	0.79	0.42	1.00	0.59	0.60	0.00	0.00	0.00	0.00	0.00	0.00	0.00	0.00	0.00
3	3-S	0.55	1.01	1.04	1.01	0.79	0.42	1.00	0.68	0.68	0.00	0.11	0.06	0.17	0.17	0.00	0.00	0.26	0.26
4	4-S	0.55	1.13	1.16	0.90	0.88	0.47	1.00	0.61	0.61	0.00	0.11	0.07	0.17	0.17	0.00	0.00	0.25	0.25
5	5-S	0.58	0.93	0.96	0.86	0.88	0.47	1.00	0.48	0.50	0.00	0.31	0.19	0.47	0.47	0.00	0.00	0.71	0.71
6	6-S	0.58	1.05	1.05	1.03	0.90	0.48	1.00	0.62	0.63	0.00	0.31	0.19	0.47	0.47	0.00	0.00	0.70	0.70
7	7-S	0.58	1.05	0.93	0.97	0.90	0.48	1.00	0.51	0.53	0.00	0.31	0.19	0.47	0.47	0.00	0.00	0.70	0.70
8	8-S	0.58	0.99	1.02	0.16	0.77	0.41	1.00	0.11	0.11	0.00	0.31	0.17	0.47	0.47	0.00	0.00	0.64	0.59
9	9-S	0.58	1.13	1.16	0.16	0.96	0.51	1.00	0.20	0.20	0.00	0.32	0.21	0.48	0.48	0.00	0.00	0.73	0.73
10	10-S	0.55	1.13	1.16	0.61	0.96	0.51	1.00	0.89	0.91	0.00	0.11	0.08	0.17	0.17	0.00	0.00	0.28	0.28
11	1-M	0.50	1.43	1.14	1.12	1.17	0.71	0.93	0.93	0.90	0.00	0.08	0.05	0.12	0.12	0.00	0.00	0.33	0.33
12	2-M	0.50	1.15	1.14	1.12	1.04	0.58	0.74	0.85	0.83	0.00	0.08	0.05	0.12	0.12	0.00	0.00	0.25	0.25
13	3-M	0.50	1.15	1.14	1.12	1.04	0.58	0.74	0.85	0.83	0.00	0.08	0.05	0.12	0.12	0.00	0.00	0.25	0.25
14	4-M	0.50	0.85	1.22	1.12	0.78	0.47	0.36	0.81	0.81	0.00	0.08	0.05	0.12	0.12	0.00	0.00	0.16	0.16
15	5-M	0.58	0.98	1.01	1.13	1.05	0.58	0.74	1.05	1.03	0.00	0.32	0.20	0.49	0.49	0.00	0.00	0.99	0.99
16	6-M	0.58	0.98	1.01	1.13	1.05	0.58	0.74	1.05	1.03	0.00	0.32	0.20	0.49	0.49	0.00	0.00	0.99	0.99
17	7-M	0.58	0.98	1.01	0.36	1.05	0.58	0.74	0.24	0.24	0.00	0.32	0.20	0.49	0.49	0.00	0.00	0.99	0.99
18	8-M	0.58	1.17	1.16	1.13	1.05	0.58	0.74	1.18	1.15	0.00	0.32	0.20	0.49	0.49	0.00	0.00	0.98	0.98
19	9-M	0.58	1.17	1.16	0.97	1.05	0.58	0.74	0.74	0.72	0.00	0.32	0.20	0.49	0.49	0.00	0.00	0.98	0.98
20	10-M	0.58	1.33	1.33	1.29	1.20	0.66	0.74	0.99	0.96	0.00	0.32	0.23	0.49	0.49	0.00	0.00	0.97	0.97
21	11-M	0.58	1.26	1.26	1.23	1.13	0.63	0.74	0.93	0.91	0.00	0.32	0.22	0.49	0.49	0.00	0.00	0.95	0.95
22	12-M	0.58	1.29	1.29	1.26	1.16	0.65	0.74	0.96	0.93	0.00	0.32	0.22	0.49	0.49	0.00	0.00	0.96	0.96
23	13-M	0.58	1.29	1.29	1.23	1.14	0.63	0.74	0.96	0.93	0.00	0.32	0.22	0.49	0.49	0.00	0.00	0.95	0.95
24	14-M	0.58	1.38	1.38	1.34	1.24	0.69	0.74	1.03	1.00	0.00	0.32	0.24	0.49	0.49	0.00	0.00	0.98	0.98
25	15-M	0.58	1.10	1.16	0.64	1.18	0.64	0.73	0.90	0.88	0.00	0.31	0.23	0.49	0.49	0.00	0.00	1.00	1.00
26	16-M	0.58	1.10	1.16	0.33	1.18	0.64	0.73	0.45	0.44	0.00	0.31	0.23	0.49	0.49	0.00	0.00	1.00	1.00
27	17-M	0.58	1.10	1.16	0.64	1.18	0.64	0.73	0.94	0.93	0.00	0.31	0.23	0.49	0.49	0.00	0.00	1.00	1.00
28	18-M	0.58	1.10	1.16	0.63	1.18	0.64	0.73	0.85	0.84	0.00	0.31	0.23	0.49	0.49	0.00	0.00	1.00	1.00
29	1-B	0.58	0.88	0.88	0.00	1.19	0.72	0.92	0.00	0.00	0.00	0.31	0.20	0.47	0.47	0.00	0.00	1.30	1.30
30	2-B	0.58	0.88	0.88	0.00	1.19	0.72	0.92	0.00	0.00	0.00	0.49	0.31	0.75	0.75	0.00	0.00	1.96	1.50
31	3-B	0.58	0.97	0.81	0.00	0.98	0.60	0.92	0.00	0.00	0.00	0.45	0.24	0.69	0.69	0.00	0.00	1.69	0.97
32	4-B	0.58	0.70	0.82	0.86	0.98	0.60	0.92	0.61	0.60	0.00	0.45	0.24	0.69	0.69	0.00	0.00	1.58	0.91
33	5-B	0.58	0.95	0.79	0.00	0.96	0.58	0.92	0.00	0.00	0.00	0.45	0.23	0.69	0.69	0.00	0.00	1.67	0.91
34	6-B	0.58	0.68	0.80	0.00	0.96	0.58	0.92	0.00	0.00	0.00	0.45	0.23	0.69	0.69	0.00	0.00	1.55	0.85
35	7-B	0.58	0.95	0.79	0.00	0.96	0.58	0.92	0.00	0.00	0.00	0.45	0.23	0.69	0.69	0.00	0.00	1.66	0.91
36	8-B	0.58	0.95	0.79	0.00	0.96	0.58	0.92	0.00	0.00	0.00	0.45	0.23	0.69	0.69	0.00	0.00	1.66	0.91
37	9-B	0.58	0.95	0.79	0.36	0.96	0.58	0.92	0.25	0.25	0.00	0.29	0.15	0.44	0.44	0.00	0.00	1.14	0.99
38	10-B	0.58	0.95	0.79	0.81	0.96	0.58	0.92	0.57	0.56	0.00	0.45	0.23	0.69	0.69	0.00	0.00	1.67	0.91

Table B.2 Predicted strength of fully grouted masonry walls (continued)

Specimen no.	Specimen label	v_m (MPa)									v_p (MPa)								
		NZS 4230: 1990	Matsumura	Shing et al.	Anderson & Priestley	NEHPR	UBC	AS3700	Equation 4-4	NZS 4230:2004	NZS 4230: 1990	Matsumura	Shing et al.	Anderson & Priestley	NEHPR	UBC	AS3700	Equation 4-4	NZS 4230:2004
39	11-B	0.58	1.09	0.91	0.03	1.11	0.67	0.92	0.05	0.05	0.00	0.45	0.27	0.69	0.69	0.00	0.00	1.77	1.29
40	12-B	0.58	1.09	0.91	0.22	1.11	0.67	0.92	0.30	0.30	0.00	0.45	0.27	0.69	0.69	0.00	0.00	1.77	1.29
41	13-B	0.58	1.09	1.00	0.07	1.11	0.67	0.92	0.10	0.10	0.00	0.45	0.27	0.69	0.69	0.00	0.00	1.70	1.24
42	14-B	0.58	0.90	0.94	0.21	1.11	0.67	0.92	0.30	0.30	0.00	0.45	0.27	0.69	0.69	0.00	0.00	1.69	1.23
43	15-B	0.58	0.79	0.92	0.00	1.11	0.67	0.92	0.00	0.00	0.00	0.45	0.27	0.69	0.69	0.00	0.00	1.67	1.21
44	16-B	0.58	0.79	0.92	0.00	1.11	0.67	0.92	0.00	0.00	0.00	0.45	0.27	0.69	0.69	0.00	0.00	1.67	1.21
45	17-B	0.58	1.09	0.80	0.48	1.11	0.67	0.92	0.61	0.61	0.00	0.45	0.27	0.69	0.69	0.00	0.00	1.77	1.29
46	18-B	0.58	1.09	0.91	0.36	1.11	0.67	0.92	0.50	0.50	0.00	0.45	0.27	0.69	0.69	0.00	0.00	1.77	1.29
47	19-B	0.58	1.09	0.91	0.17	1.11	0.67	0.92	0.24	0.23	0.00	0.45	0.27	0.69	0.69	0.00	0.00	1.77	1.29
48	20-B	0.58	1.09	0.92	0.17	1.11	0.67	0.92	0.24	0.24	0.00	0.45	0.27	0.69	0.69	0.00	0.00	1.77	1.29
49	21-B	0.58	1.28	1.07	0.36	1.30	0.79	0.92	0.51	0.50	0.00	0.45	0.31	0.69	0.69	0.00	0.00	1.86	1.86
50	1-A	0.38	0.96	0.88	0.67	0.78	0.42	1.00	0.42	0.40	0.00	0.00	0.00	0.00	0.00	0.00	0.00	0.00	0.00
51	2-A	0.38	0.96	0.88	0.70	0.78	0.42	1.00	0.48	0.41	0.00	0.00	0.00	0.00	0.00	0.00	0.00	0.00	0.00
52	3-A	0.38	0.94	0.86	0.69	0.77	0.41	1.00	0.41	0.41	0.00	0.00	0.00	0.00	0.00	0.00	0.00	0.00	0.00
53	4-A	0.50	0.98	0.90	0.66	0.80	0.43	1.00	0.40	0.39	0.00	0.08	0.05	0.13	0.13	0.00	0.00	0.20	0.20
54	5-A	0.44	0.98	0.90	0.66	0.80	0.43	1.00	0.41	0.39	0.00	0.04	0.02	0.06	0.06	0.00	0.00	0.10	0.10
55	6-A	0.44	0.81	1.39	0.68	0.92	0.49	0.50	0.53	0.52	0.00	0.04	0.03	0.06	0.06	0.00	0.00	0.05	0.05
56	7-A	0.44	1.30	1.02	1.18	1.21	0.74	1.20	1.12	1.11	0.00	0.04	0.03	0.06	0.06	0.00	0.00	0.17	0.17

Table B.2 Predicted strength of fully grouted masonry walls (continued)

Specimen no.	Specimen label	v_s (MPa)									v_n (MPa)								
		NZS 4230: 1990	Matsumura	Shing et al.	Anderson & Priestley	NEHPR	UBC	AS3700	Equation 4-4	NZS 4230:2004	NZS 4230: 1990	Matsumura	Shing et al.	Anderson & Priestley	NEHPR	UBC	AS3700	Equation 4-4	NZS 4230:2004
1	1-S	0.38	0.28	0.31	0.22	0.24	0.47	0.38	0.33	0.30	0.95	1.67	1.61	1.21	1.51	0.92	1.38	1.34	1.32
2	2-S	0.38	0.26	0.31	0.22	0.24	0.47	0.38	0.36	0.30	0.76	1.27	1.35	1.10	1.03	0.89	1.38	0.95	0.90
3	3-S	0.38	0.26	0.31	0.22	0.24	0.47	0.38	0.34	0.30	0.93	1.39	1.42	1.40	1.20	0.89	1.38	1.28	1.24
4	4-S	0.38	0.29	0.31	0.22	0.24	0.47	0.38	0.33	0.30	0.93	1.54	1.55	1.29	1.29	0.94	1.38	1.18	1.16
5	5-S	0.38	0.29	0.31	0.22	0.24	0.47	0.38	0.36	0.30	0.95	1.53	1.46	1.55	1.57	0.94	1.38	1.55	1.51
6	6-S	0.87	0.45	0.73	0.51	0.55	1.09	0.87	0.76	0.70	1.45	1.80	1.97	2.01	1.59	1.57	1.87	2.08	1.73
7	7-S	0.38	0.29	0.31	0.22	0.24	0.47	0.38	0.35	0.30	0.95	1.65	1.43	1.65	1.59	0.95	1.38	1.56	1.53
8	8-S	0.87	0.38	0.73	0.51	0.55	1.09	0.87	0.65	0.70	1.45	1.68	1.91	1.14	1.37	1.37	1.87	1.40	1.40
9	9-S	0.40	0.32	0.33	0.23	0.25	0.49	0.40	0.38	0.32	0.97	1.77	1.71	0.88	1.68	1.00	1.40	1.31	1.25
10	10-S	0.40	0.32	0.33	0.23	0.25	0.49	0.40	0.40	0.32	0.94	1.57	1.57	1.02	1.37	1.00	1.40	1.57	1.50
11	1-M	0.36	0.47	0.29	0.21	0.23	0.45	0.36	0.34	0.29	0.87	1.97	1.48	1.46	1.52	1.17	1.30	1.59	1.52
12	2-M	0.36	0.46	0.23	0.21	0.23	0.45	0.36	0.33	0.29	0.87	1.69	1.43	1.45	1.39	1.03	1.11	1.43	1.37
13	3-M	0.36	0.46	0.23	0.21	0.23	0.45	0.36	0.33	0.29	0.87	1.69	1.43	1.45	1.39	1.03	1.11	1.43	1.37
14	4-M	0.36	0.44	0.12	0.20	0.23	0.45	0.36	0.30	0.29	0.87	1.37	1.39	1.44	1.13	0.92	0.72	1.26	1.17
15	5-M	0.00	0.00	0.00	0.00	0.00	0.00	0.00	0.00	0.00	0.58	1.30	1.21	1.62	1.54	0.58	0.74	2.03	1.70
16	6-M	0.51	0.55	0.32	0.30	0.32	0.64	0.51	0.44	0.41	1.09	1.85	1.53	1.92	1.83	1.22	1.26	1.56	1.70
17	7-M	1.03	0.78	0.86	0.59	0.64	1.29	1.03	0.88	0.82	1.60	2.07	2.07	1.44	1.83	1.83	1.77	2.11	1.70
18	8-M	1.03	0.78	0.86	0.59	0.64	1.29	1.03	0.87	0.82	1.60	2.26	2.23	2.21	1.83	1.83	1.77	2.17	1.70
19	9-M	2.06	1.10	1.73	1.18	1.29	2.57	2.06	1.60	1.65	1.92	2.58	3.09	2.65	1.83	1.83	2.80	2.17	1.70
20	10-M	1.03	0.89	0.86	0.59	0.64	1.29	1.03	0.88	0.82	1.60	2.53	2.42	2.37	2.08	1.95	1.77	2.48	1.94
21	11-M	1.03	0.84	0.86	0.59	0.64	1.29	1.03	0.85	0.82	1.60	2.42	2.34	2.31	1.98	1.92	1.77	2.35	1.84
22	12-M	1.23	0.94	1.04	0.71	0.77	1.54	1.23	1.02	0.99	1.81	2.55	2.55	2.45	2.02	2.02	1.98	2.41	1.88
23	13-M	1.09	0.87	0.91	0.63	0.68	1.36	1.09	0.89	0.87	1.66	2.47	2.42	2.35	1.99	1.99	1.83	2.36	1.85
24	14-M	1.03	0.92	0.86	0.59	0.64	1.29	1.03	0.90	0.82	1.60	2.62	2.48	2.43	2.17	1.98	1.77	2.58	2.02
25	15-M	0.00	0.00	0.00	0.00	0.00	0.00	0.00	0.00	0.00	0.58	1.41	1.39	1.13	1.67	0.64	0.73	1.90	1.88
26	16-M	0.51	0.61	0.29	0.29	0.32	0.64	0.51	0.46	0.41	1.09	2.02	1.68	1.11	1.99	1.29	1.25	1.91	1.85
27	17-M	1.03	0.86	0.81	0.58	0.64	1.29	1.03	0.92	0.82	1.60	2.27	2.20	1.71	2.06	1.93	1.76	1.76	1.93
28	18-M	2.06	1.22	1.62	1.16	1.29	2.57	2.06	1.72	1.65	1.92	2.63	3.01	2.28	2.06	2.06	2.79	1.76	1.93
29	1-B	0.93	0.77	0.75	0.55	0.58	1.17	0.93	0.85	0.75	1.51	1.95	1.83	1.02	2.04	1.89	1.85	2.16	1.73
30	2-B	0.93	0.77	0.75	0.55	0.58	1.17	0.93	0.78	0.75	1.51	2.14	1.94	1.30	2.04	1.89	1.85	2.21	1.73
31	3-B	1.38	0.77	1.11	0.81	0.86	1.72	1.38	0.97	1.10	1.92	2.19	2.15	1.50	1.69	1.69	2.30	1.83	1.43
32	4-B	1.38	0.77	1.11	0.81	0.86	1.72	1.38	0.87	1.10	1.92	1.92	2.16	2.36	1.69	1.69	2.30	1.83	1.43
33	5-B	0.69	0.53	0.42	0.40	0.43	0.86	0.69	0.49	0.55	1.27	1.93	1.44	1.09	1.65	1.44	1.61	1.79	1.40
34	6-B	0.69	0.53	0.42	0.40	0.43	0.86	0.69	0.43	0.55	1.27	1.67	1.45	1.09	1.65	1.44	1.61	1.79	1.40
35	7-B	0.26	0.33	0.23	0.15	0.16	0.33	0.26	0.22	0.21	0.84	1.73	1.26	0.84	1.65	0.91	1.18	1.79	1.12
36	8-B	0.95	0.63	0.65	0.56	0.60	1.19	0.95	0.65	0.76	1.53	2.03	1.68	1.25	1.65	1.65	1.87	1.79	1.40
37	9-B	0.69	0.53	0.42	0.40	0.43	0.86	0.69	0.56	0.55	1.27	1.77	1.36	1.20	1.65	1.44	1.61	1.79	1.40
38	10-B	0.69	0.53	0.42	0.40	0.43	0.86	0.69	0.49	0.55	1.27	1.93	1.44	1.90	1.65	1.44	1.61	1.79	1.40

Table B.2 Predicted strength of fully grouted masonry walls (continued)

Specimen no.	Specimen label	v_s(MPa)									v_n (MPa)								
		NZS 4230: 1990	Matsumura	Shing et al.	Anderson & Priestley	NEHPR	UBC	AS3700	Equation 4-4	NZS 4230:2004	NZS 4230: 1990	Matsumura	Shing et al.	Anderson & Priestley	NEHPR	UBC	AS3700	Equation 4-4	NZS 4230:2004
39	11-B	0.68	0.61	0.42	0.40	0.43	0.85	0.68	0.55	0.55	1.26	2.16	1.60	1.12	1.91	1.52	1.60	1.48	1.61
40	12-B	1.70	0.97	1.45	1.00	1.07	2.13	1.70	1.34	1.36	1.92	2.51	2.63	1.90	1.91	1.91	2.62	2.06	1.61
41	13-B	0.69	0.61	0.42	0.40	0.43	0.86	0.69	0.52	0.55	1.27	2.16	1.69	1.16	1.91	1.53	1.61	2.06	1.61
42	14-B	1.70	0.97	1.45	1.00	1.07	2.13	1.70	1.24	1.36	1.92	2.32	2.66	1.90	1.91	1.91	2.62	2.06	1.61
43	15-B	0.69	0.61	0.42	0.40	0.43	0.86	0.69	0.51	0.55	1.27	1.85	1.61	1.09	1.91	1.53	1.61	2.06	1.61
44	16-B	1.70	0.97	1.45	1.00	1.07	2.13	1.70	1.21	1.36	1.92	2.21	2.64	1.69	1.91	1.91	2.62	2.06	1.61
45	17-B	0.69	0.61	0.42	0.40	0.43	0.86	0.69	0.56	0.55	1.27	2.16	1.49	1.58	1.91	1.53	1.61	2.06	1.61
46	18-B	1.70	0.97	1.45	1.00	1.07	2.13	1.70	1.34	1.36	1.92	2.51	2.63	2.04	1.91	1.91	2.62	2.06	1.61
47	19-B	0.82	0.67	0.66	0.48	0.51	1.03	0.82	0.69	0.66	1.40	2.22	1.84	1.34	1.91	1.70	1.74	2.06	1.61
48	20-B	2.08	1.07	2.00	1.22	1.30	2.61	2.08	1.72	1.67	1.92	2.62	3.19	2.08	1.91	1.91	3.00	2.06	1.61
49	21-B	0.35	0.51	0.31	0.21	0.22	0.44	0.35	0.34	0.28	0.93	2.25	1.69	1.25	2.21	1.22	1.27	2.42	1.89
50	1-A	0.13	0.15	0.11	0.08	0.08	0.17	0.13	0.14	0.11	0.52	1.11	0.99	0.75	0.87	0.58	1.13	0.56	0.50
51	2-A	0.00	0.00	0.00	0.00	0.00	0.00	0.00	0.00	0.00	0.38	0.96	0.88	0.70	0.78	0.42	1.00	0.48	0.41
52	3-A	0.15	0.16	0.09	0.09	0.10	0.19	0.15	0.16	0.12	0.54	1.10	0.95	0.78	0.87	0.60	1.15	0.57	0.53
53	4-A	0.13	0.16	0.11	0.08	0.08	0.17	0.13	0.14	0.11	0.64	1.22	1.06	0.86	1.01	0.59	1.13	0.74	0.69
54	5-A	0.13	0.16	0.11	0.08	0.08	0.17	0.13	0.14	0.11	0.58	1.18	1.03	0.80	0.95	0.59	1.13	0.66	0.59
55	6-A	0.13	0.18	0.11	0.08	0.08	0.17	0.13	0.13	0.11	0.58	1.03	1.53	0.82	1.07	0.66	0.63	0.71	0.68
56	7-A	0.13	0.18	0.13	0.08	0.08	0.17	0.13	0.14	0.11	0.58	1.53	1.18	1.33	1.35	0.91	1.33	1.43	1.39

Table B.2 Predicted strength of fully grouted masonry walls (continued)

Specimen no.	v_{max}/v_n								
	NZS 4230: 1990	Matsumura	Shing et al.	Anderson & Priestley	NEHPR	UBC	AS3700	Equation 4-4	NZS 4230:2004
1	1.83	1.04	1.08	2.54	1.15	1.89	1.27	1.30	1.32
2	1.78	1.06	1.00	1.64	1.32	1.51	0.98	1.42	1.50
3	1.59	1.06	1.04	1.28	1.23	1.65	1.07	1.16	1.19
4	1.79	1.08	1.07	1.95	1.28	1.76	1.20	1.41	1.43
5	1.71	1.07	1.12	0.90	1.04	1.73	1.19	1.05	1.08
6	1.32	1.06	0.97	0.90	1.20	1.22	1.02	0.92	1.11
7	1.87	1.08	1.25	0.97	1.12	1.88	1.30	1.14	1.16
8	1.42	1.22	1.08	2.10	1.50	1.50	1.10	1.46	1.47
9	1.84	1.01	1.05	1.45	1.06	1.79	1.28	1.37	1.43
10	1.65	0.99	0.99	1.53	1.13	1.55	1.12	0.99	1.04
11	1.85	0.81	1.08	1.10	1.05	1.37	1.23	1.00	1.05
12	1.99	1.02	1.21	1.19	1.24	1.67	1.56	1.21	1.26
13	2.16	1.11	1.31	1.29	1.35	1.81	1.69	1.31	1.37
14	1.86	1.18	1.16	1.12	1.43	1.75	2.23	1.28	1.37
15	2.95	1.31	1.41	1.05	1.11	2.92	2.29	0.84	1.00
16	1.73	1.02	1.23	0.98	1.03	1.54	1.50	1.21	1.11
17	1.42	1.10	1.10	1.58	1.25	1.25	1.29	1.08	1.34
18	1.43	1.01	1.03	1.03	1.25	1.25	1.29	1.05	1.35
19	1.53	1.14	0.95	1.11	1.60	1.60	1.05	1.35	1.72
20	1.61	1.02	1.07	1.09	1.24	1.33	1.46	1.05	1.34
21	1.40	0.93	0.96	0.97	1.13	1.17	1.26	0.95	1.22
22	1.46	1.03	1.03	1.07	1.30	1.30	1.33	1.09	1.40
23	1.46	0.98	1.01	1.04	1.22	1.22	1.33	1.03	1.31
24	1.61	0.99	1.04	1.07	1.20	1.31	1.46	1.01	1.28
25	3.78	1.55	1.57	1.92	1.30	3.39	2.97	1.15	1.16
26	1.79	0.97	1.16	1.75	0.98	1.52	1.56	1.02	1.05
27	1.06	0.75	0.78	1.00	0.83	0.89	0.97	0.97	0.89
28	1.06	0.78	0.68	0.89	0.99	0.99	0.73	1.16	1.06
29	1.29	1.00	1.07	1.92	0.95	1.03	1.05	0.90	1.13
30	1.57	1.11	1.22	1.83	1.16	1.26	1.28	1.08	1.37
31	1.28	1.12	1.14	1.64	1.45	1.45	1.07	1.35	1.72
32	1.28	1.28	1.14	1.04	1.45	1.45	1.07	1.35	1.72
33	1.86	1.22	1.63	2.15	1.43	1.63	1.47	1.32	1.68
34	1.76	1.34	1.54	2.04	1.35	1.55	1.39	1.25	1.60

Table B.2 Predicted strength of fully grouted masonry walls (continued)

Specimen no.	v_{max}/v_n								
	NZS 4230: 1990	Matsumura	Shing et al.	Anderson & Priestley	NEHPR	UBC	AS3700	Equation 4-4	NZS 4230:2004
35	2.28	1.11	1.52	2.27	1.16	2.10	1.62	1.07	1.71
36	1.59	1.20	1.45	1.95	1.47	1.47	1.30	1.36	1.74
37	1.55	1.11	1.45	1.64	1.19	1.36	1.22	1.10	1.40
38	1.90	1.24	1.67	1.27	1.45	1.67	1.50	1.35	1.72
39	1.46	0.85	1.15	1.64	0.96	1.21	1.15	1.24	1.14
40	1.00	0.76	0.73	1.01	1.00	1.00	0.73	0.93	1.19
41	1.86	1.09	1.39	2.02	1.23	1.53	1.46	1.14	1.46
42	1.25	1.03	0.90	1.26	1.26	1.26	0.91	1.16	1.49
43	1.61	1.10	1.26	1.86	1.07	1.33	1.27	0.99	1.26
44	1.15	1.00	0.83	1.31	1.16	1.16	0.84	1.07	1.37
45	1.72	1.01	1.46	1.38	1.14	1.42	1.36	1.06	1.35
46	1.12	0.85	0.81	1.05	1.12	1.12	0.82	1.04	1.33
47	1.61	1.02	1.22	1.68	1.18	1.33	1.30	1.09	1.40
48	1.18	0.87	0.71	1.09	1.19	1.19	0.76	1.10	1.41
49	2.91	1.20	1.59	2.15	1.22	2.20	2.13	1.11	1.42
50	1.61	0.75	0.84	1.11	0.96	1.43	0.74	1.49	1.66
51	1.93	0.77	0.84	1.06	0.94	1.77	0.74	1.56	1.79
52	1.56	0.76	0.89	1.07	0.97	1.39	0.73	1.47	1.58
53	1.63	0.85	0.98	1.21	1.03	1.75	0.92	1.41	1.50
54	1.70	0.83	0.95	1.23	1.03	1.65	0.87	1.49	1.65
55	1.42	0.80	0.54	1.00	0.77	1.25	1.30	1.16	1.21
56	2.41	0.91	1.18	1.05	1.03	1.54	1.04	0.97	1.00

Appendix C

SHEAR DISPLACEMENT COMPONENT

The objective of decomposition of panel deformation is to calculate and identify the dominant displacement components. The components of displacement are calculated from the test data obtained during testing. This test data was attained from the measuring instrumentation attached to the wall face, and the typical arrangement of the instrumentation is shown in Figure 3.11. This appendix describes calculation of the shear displacement component.

Having measured the relative displacements between points of a panel section on the wall face denoted A, B, C and D, as shown in Figure C.1(a), it is possible to extract the shear displacement component from the deformation in the panel section. The total shear displacement of the wall can be evaluated by summation of shear deformation of each panel section. The method used in this report for the extraction of the shear displacement component is based on Hiraishi (1984) and Brammer (1995).

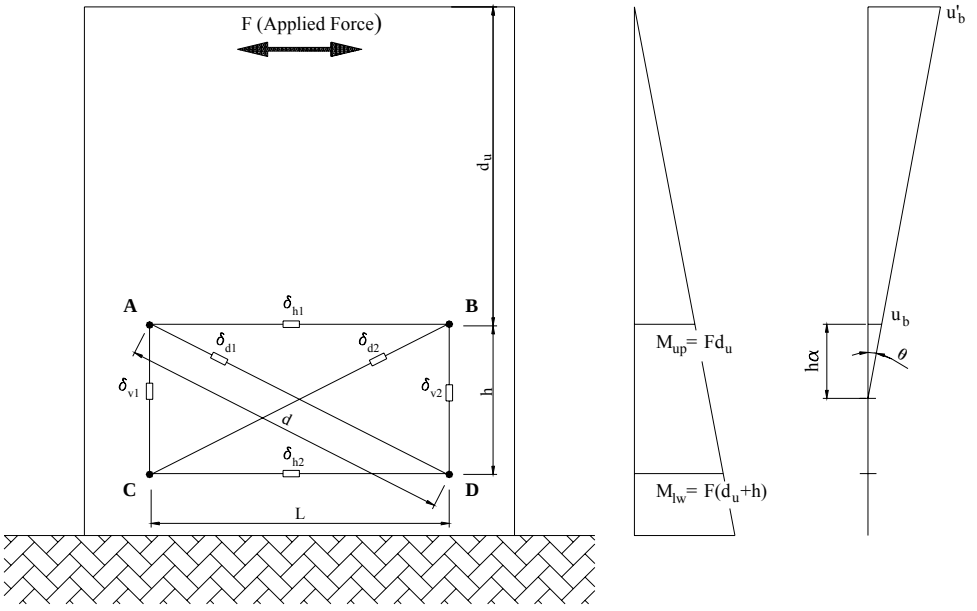

(a) Wall panel section (b) Moment distribution (c) Panel flexural deformation

Figure C.1 Wall panel section.

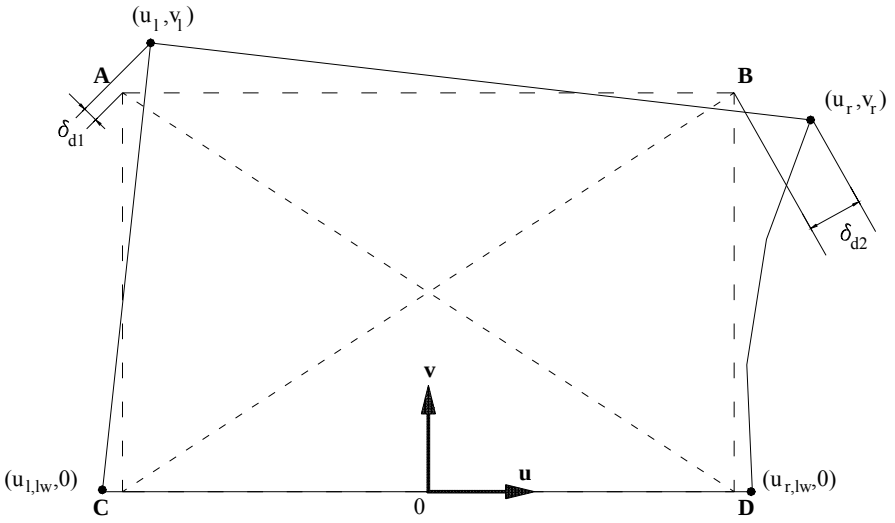

Figure C.2 Nodal displacement of a panel section.

The deformation of a panel section is illustrated in Figure C.2. It is assumed that the two upper points, A and B, may translate horizontally by u_l and u_r, and vertically by the amounts v_l and v_r. The lower points, C and D, are assumed to translate only horizontally by the amount $u_{l,lw}$ and $u_{r,lw}$. The subscripts 'l' and 'r' refer to the left and right hand sides respectively, while the subscript 'lw' refers to the lower points. The adopted sign convention is for positive displacements to be to the right and upwards. As shown in Figure C.1, δ_{d1} and δ_{d2} are the elongations of the respective diagonal, while elongations of the horizontal elements are termed δ_{h1} and δ_{h2}, and elongations of the vertical elements are termed δ_{v1} and δ_{v2}. The dimensions of the panel are defined by the length, L, the height, H, and the diagonal length, d. The termed d_u is used to defined the position of the panel bracing with respect to the top of the wall, see Figure C.1(a).

As shown in Figure C.3, the panel section deformation, represented by u_l, u_r, v_l, v_r, $u_{l,lw}$ and $u_{r,lw}$, is assumed to consist of the three components: shear, flexure and elongation. In this figure, the u and v represent the horizontal and vertical deformation components respectively. The subscripts 's', 'b' and 'e' represent the shear, flexural and elongation deformation components respectively.

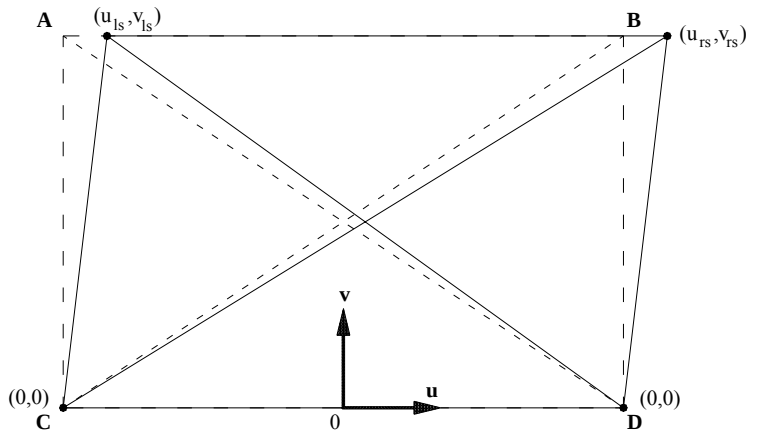

(a) Shear deformation

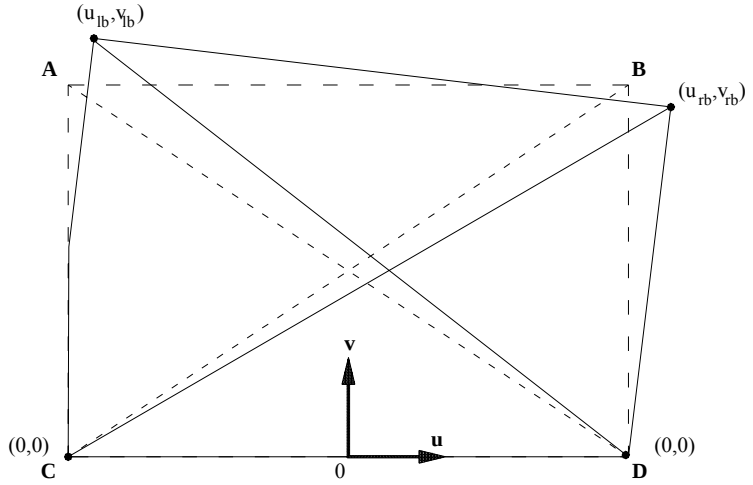

(b) Flexural deformation

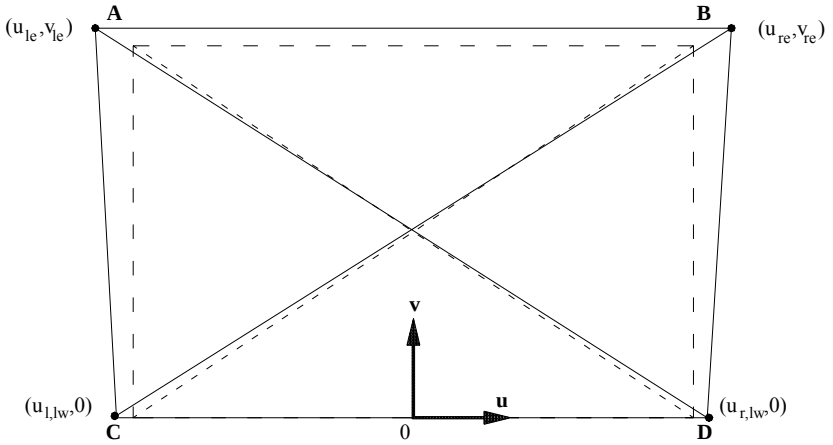

(c) Extension deformation

Figure C.3 Components of panel deformation.

The primarily purpose of the following derivation is to calculate the horizontal displacement at the top of the wall due to shear deformation, U_s, by relating the measured elongation (δ's) to individual displacement components: u's and v's. The following relations are assumed:

1. The left and right horizontal shear deformation components are equal.
2. The left and right horizontal flexural deformation components are equal.
3. The left and right horizontal extension components are equal but of opposite side.
4. The vertical shear deformation components are zero.
5. The upper left and right vertical extension deformation components are equal.

The above assumption can be represented as follow:

a) $u_{ls} = u_{rs} = u_s$

b) $u_{lb} = u_{rb} = u_b$

c) $u_{re} = -u_{le} = \frac{1}{2} u_e$ (C-1)

d) $u_{re,lw} = -u_{le,lw} = \frac{1}{2} u_{e,lw}$

e) $v_{le} = v_{re} = v_e$

The relationships between these displacements and those shown in Figure C.3 are as follows:

a) $u_l = u_s + u_b - \frac{1}{2} u_e$

b) $u_r = u_s + u_b + \frac{1}{2} u_e$

c) $u_{l,lw} = -\frac{1}{2} u_{e,lw}$ (C-2)

d) $u_{r,lw} = \frac{1}{2} u_{e,lw}$

e) $v_l = v_{lb} + v_e$

f) $v_r = v_{rb} + v_{ve}$

The measured relative deformations can be expressed in terms of the global deformations by the following geometric relationships:

a) $\delta_{d1} = \frac{L}{d}\left(u_{r,lw} - u_l\right) + \frac{L}{h} v_l$

b) $\delta_{d2} = \frac{L}{d}\left(u_r - u_{l,lw}\right) + \frac{L}{h} v_r$ (C-3)

c) $\delta_{h1} = -u_l + u_r$

d) $\delta_{h2} = -u_{l,lw} + u_{r,lw}$

e) $\delta_{v1} = v_l$ (C-3)

f) $\delta_{v2} = v_r$

Substituting Equation C-2 into C-3:

a) $$\delta_{d1} = \frac{L}{d}\left(-u_s - u_b + \frac{1}{2}u_e + \frac{1}{2}u_{e,lw}\right) + \frac{L}{h}\left(v_{lb} + v_e\right)$$

b) $$\delta_{d2} = \frac{L}{d}\left(u_s + u_b + \frac{1}{2}u_e + \frac{1}{2}u_{e,lw}\right) + \frac{L}{h}\left(v_{rb} + v_e\right)$$

c) $\delta_{h1} = u_e$ (C-4)

d) $\delta_{h2} = u_{e,lw}$

e) $\delta_{v1} = v_{lb} + v_e$

f) $\delta_{v2} = v_{rb} + v_e$

From Equation C-4 it seems that the equation is under-determined since the equations are describing the relationship between 6 known measured relative displacements (δ's) and unknown panel deformation components (u's and v's). Inserting Equations C-4(c) and (d) into Equations C-4(e) and (f), and then subtracting C-4(e) from C-4(f) gives:

$$\delta_{d2} - \delta_{d1} = \frac{L}{d}\left(2u_s + 2u_b\right) + \frac{L}{h}\left(\delta_{v2} - \delta_{v1}\right) \quad \text{(C-5)}$$

Rearranging Equation C-5:

$$u_s = \frac{d}{2L}\left(\delta_{d2} - \delta_{d1}\right) + \frac{h}{2L}\left(\delta_{v1} - \delta_{v2}\right) - u_b \quad \text{(C-6)}$$

Equation C-6 can be solved by defining an equation relating the flexural deformation component to the measured relative displacement. This is displayed in Equation C-7:

$$u_b = \theta h \alpha \quad \text{(C-7)}$$

where:

$$\theta = \frac{\delta_{v1} - \delta_{v2}}{L}$$

Equation C-7 states that the flexural deformation is equal to the rotation at the top of the panel section multiplied by the panel section height and by α. When taking α as 2/3, the equation captures the exact flexural displacement of an elastic prismatic cantilever with a concentrated

horizontal force applied at the top, with θ representing the rotation of the top of the wall. However, for reinforced concrete masonry and reinforced concrete walls, the parameter α is generally higher than 2/3 since the wall flexural cracking tends to concentrate rotation towards the bottom of the wall, therefore resulting in higher hα and higher u_b.

In this study, the flexural deflection u_b for a section of wall was calculated from the measured rotation that occurs within the section under study. This rotation is calculated from the bending moment diagram. The bending moment at the top (M_{up}) and the bottom (M_{lw}) of a panel section are known to vary linearly according to the vertical location as shown in Figure C-1(b).

The moment (M)-curvature (φ) relationship for an elastic section is given by:

$$M = \varphi EI \tag{C-8}$$

where E and I are the modulus of elasticity and inertia moment. As the curvature is a linear function of the moment, the total rotation of the panel section between d_u and d_u+h can be calculated from the average bending moment:

$$\theta = \frac{h\left(M_{up} + M_{lw}\right)}{2EI} \tag{C-9}$$

The panel flexural deformation, u_b, is evaluated by integration of curvature along the height of the panel section with the following result:

$$u_b = \frac{h^2}{EI}\left(\frac{M_{lw}}{3} + \frac{M_{up}}{6}\right) = \theta h\left(\frac{d_u + \frac{2h}{3}}{2d_u + h}\right) \text{ where } \alpha = \frac{d_u + \frac{2h}{3}}{2d_u + h} \tag{C-10}$$

The α given in Equation C-10 is defined with respect to the top of the investigated panel section.

u_b can be evaluated by incorporating Equation C-7:

$$u_b = \frac{h\left(\delta_{v1} - \delta_{v2}\right)}{L}\left(\frac{d_u + \frac{2h}{3}}{2d_u + h}\right) \tag{C-11}$$

Subsequently, the shear deformation for the panel section can be evaluated by substituting Equation C-11 into Equation C-6:

$$u_s = \frac{d}{2L}\left(\delta_{d2} - \delta_{d1}\right) + \frac{h}{2L}\left(\delta_{v1} - \delta_{v2}\right) - \frac{h\left(\delta_{v1} - \delta_{v2}\right)}{L}\left(\frac{d_u + \frac{2h}{3}}{2d_u + h}\right) \qquad \text{(C-12)}$$

Rearranging Equation C-12 to give:

$$u_s = \frac{d}{2L}\left(\delta_{d2} - \delta_{d1}\right) - \frac{h^2}{6\left(2d_u + h\right)}\frac{\left(\delta_{v1} - \delta_{v2}\right)}{L} \qquad \text{(C-13)}$$

The total shear displacement, U_s, is given by the sum of the shear deformations from the individual panel sections:

$$U_s = \sum u_s \qquad \text{(C-14)}$$

In addition, the total flexural displacement can be evaluated as follows. The flexural deformation of the investigated panel section (see Figure C.1(c)) with respect to the top of the wall, u'_b, is evaluated as:

$$u'_b = \theta\left(\alpha h + d_u\right) = \frac{\left(\delta_{v1} - \delta_{v2}\right)}{L}\left(h\frac{d_u + \frac{2h}{3}}{2d_u + h} + d_u\right) \qquad \text{(C-15)}$$

The total flexural displacement, U_b, is the summation of flexural deformation from individual panel section:

$$U_b = \sum u'_b \qquad \text{(C-16)}$$